

ABSTRACT

WANG, KAI. Multiscale Multi-Pollutant Air Quality Modeling: Incorporation of Dust Treatments into CMAQ and Application for Criteria and Hazardous Air Pollutants. (Under the direction of Drs. Yang Zhang and Sharon Phillips.)

In this study, the U.S. EPA's CMAQ modeling system is applied, evaluated, and further developed and improved via two specific studies: the U.S. EPA's International Transport and Climatic Effects of Air Pollutants (ICAP) study and the 2002 multiple-pollutant (MP) modeling platform study. The objectives are to improve and demonstrate the capability of CMAQ in multiscale MP air quality modeling analyses and enhance the understanding of the chemical and physical interactions among criteria air pollutants (CAPs) and hazardous air pollutants (HAPs).

CMAQ v4.4 is first applied to study the intercontinental transport of air pollution across the Pacific region. Simulated meteorology captures the synoptic pattern. Most of the fine particulate matter ($PM_{2.5}$) components are overestimated over the U.S. and most of gases are underestimated over East Asia. Simulated nitrogen dioxide (NO_2) and carbon monoxide (CO) columns agree well with satellite observations. Aerosol optical depths (AOD) and tropospheric ozone (O_3) residuals are underpredicted. The simulated horizontal fluxes and process analyses show that the transport in the lower free troposphere followed by a large scale subsidence over the U.S. provides a major Asian pollution export pathway for most pollutants, while the transport in the planetary boundary layer also plays an important role, especially for CO, O_3 , $PM_{2.5}$, and sulfate (SO_4^{2-}).

The CMAQ modeling system is further developed by implementing two online-dust emission schemes and nine dust-related heterogeneous reactions, updating the thermodynamic module to ISORROPIA II, and accounting for the thermodynamic

partitioning of crustal species (referred to as CMAQ-Dust). CMAQ-Dust produces consistent spatial distributions of dust emissions with previous studies and captures the dust outbreak events for the same 2001 April ICAP dust episode. The total dust emission is estimated to be 111.4 Tg during this episode. The inclusion of crustal species tends to reduce the concentration of PM_{2.5} over the polluted areas due to the decrease of nitrate (NO₃⁻) and ammonium (NH₄⁺). The heterogeneous uptake on dust particles tends to decrease the concentrations of O₃ by up to 9% and SO₂ by 30% over the dust source regions. Compared with the simulation without dust, the model performance for PM₁₀ and AOD is greatly improved due to the dust treatments.

The MP modeling platform with CMAQ v4.6 is evaluated over the nested 36/12 km U.S. domains to demonstrate the capability of CMAQ in reproducing the long-term trends of both ambient CAPs and HAPs. A comprehensive model performance evaluation for the full year 2002 is performed. CMAQ performance varies species by species, with generally better performance for CAPs. The seasonal performance is fairly good for O₃, PM_{2.5}, SO₄²⁻, NH₄⁺, and mercury (Hg) wet deposition and moderately good for elemental carbon (EC), formaldehyde (HCHO), acetaldehyde, benzene, and particulate lead. Large model biases are found for NO₃⁻, organic carbon (OC), and most of other HAPs species. CMAQ performs well for column NO₂, moderately well for column CO, O₃, and HCHO, and poorly for AOD. Reasons for the discrepancies include uncertainties in emissions, gas/aerosol chemistry treatments and meteorology, inaccurate boundary conditions at higher altitudes, lack of model treatments such as mineral dust or plume-in-grid process, as well as limitations and errors in surface measurements and satellite retrievals. Process analysis results show that CMAQ can predict O₃ chemistry indicators very well. Overall, this study shows a

comparable and improved performance for most of species comparing to previous studies that used older versions of CMAQ and emission inputs.

Multiscale Multi-Pollutant Air Quality Modeling: Incorporation of Dust Treatments into
CMAQ and Application for Criteria and Hazardous Air Pollutants

by
Kai Wang

A dissertation submitted to the Graduate Faculty of
North Carolina State University
in partial fulfillment of the
requirements for the degree of
Doctor Philosophy

Marine, Earth, and Atmospheric Sciences

Raleigh, North Carolina

2011

APPROVED BY:

Dr. Nicholas Meskhidze

Dr. Carey J. Jang

Dr. Sharon B. Phillips
Co-Chair of Advisory Committee

Dr. Lingjuan Wang

Dr. Yang Zhang
Chair of Advisory Committee

BIOGRAPHY

Kai Wang was born in Shenyang, Liaoning Province, China, where he finished his primary, middle, and high schools. In 1998, Kai was admitted to Peking University, one of the best universities in China. During his four-year undergraduate study at Peking University, he developed a fond interest in atmospheric sciences and received several prestigious scholarships and awards. Upon receiving his B.S. degree in 2002, he was admitted as an M.S. student to Graduate School of Peking University with an honor of exam waiver. He participated in several national and international field campaigns during his graduate study at Peking University. In June 2005, he received his M.S. degree in Atmospheric Sciences. In the fall of 2005, he joined the Air Quality Forecasting Lab in the Department of Marine, Earth, and Atmospheric Sciences, North Carolina State University to pursue his Ph.D. degree. He also worked as an intern at the OAQPS of the U.S. EPA from 2006 to 2009. His research mainly focuses on several topics including the study of the inter-continental transport of Asian air pollutants over the Pacific region using CMAQ, development of dust emissions and dust-related heterogeneous chemistry in CMAQ modeling system and the application of a multi-pollutant version of CMAQ into the U.S. EPA's 2002 modeling platform. During his study at NCSU, he received several national level awards/fellowships including the travel awards to the Workshop on Agricultural Air Quality, the third place best student oral presentation at the 12th conference on Atmospheric Chemistry/90th AMS Annual Meeting, and a fellowship award from the NCAR's Advanced Study Program. He is also a student member for American Geophysical Union and American Meteorological Society.

ACKNOWLEDGEMENTS

Toward the end of my 24-year training in schools, I would sincerely acknowledge many people and organizations for their support and guidance. I would first like to acknowledge my committee members, Drs. Yang Zhang, Sharon B. Phillips, Carey J. Jang, Nicholas Meskhidze, and Lingjuan Wang for their guidance and scientific inputs. Most importantly, I would like to thank Dr. Zhang for the research opportunities she gave to me. Her great efforts and patience in training me to be competitive and professional has greatly improved my research ability during my Ph.D. study and I believe that will benefit me throughout my career life. Special thanks are also due to Drs. Carey J. Jang and Sharon B. Phillips, whom I had been working with for more than three years during my internship at the U.S. EPA. Their inspiration and encouragements are always some of the best memories during my Ph.D. study. I would also like to thank Dr. Jerry Davis for being the substitute member for my defense.

Thanks are also due to the following people who provided scientific contributions and support in alphabetical order, including Mr. Wyatt Appel, Mr. Steve Howard, Ms. Tanya Otte, and Dr. Shao-Cai Yu from the Atmospheric Modeling and Analysis Division of the U.S. EPA, Mr. Patrick Dolwick and Mr. Norm Possiel from the Office of Air Quality Planning and Standards of the U.S. EPA, Dr. Jack Fishman from the NASA Langley Research Center, Drs. Ji-Ming Hao and Ke-Bin He from Tsinghua University, China, Drs. Gary Howell and Eric Sills from the High Performance and Grid Computing Center at NCSU, Dr. Mark Z. Jacobson from Stanford University, Dr. Takigawa Masayuki from the Frontier Research Center for Global Change, Japan, Dr. Athanasios Nenes from Georgia Institute of

Technology, Dr. Hilary E. Snell and Mr. Krish Vijayaraghavan from AER Inc., Drs. Daniel Tong and Binyu Wang from the NOAA/ERL/ARL, and Ms. Shiang-Yuh Wu from the Department of Air Quality and Environmental Management, Clark County, Nevada.

In addition, I also want to thank the project sponsors for my research including the U.S. EPA (the ICAP project and STAR grant program #R833376), the U.S. NSF (Career Award Atm-0348819), the U.S. NASA (Award No. NNG04GJ90G), and the U.S. Department of Agriculture (National Research Initiative Competitive Grant No. 2008-35112-18758).

I am particularly grateful to all the current and former members of the Air Quality Forecasting Lab during my stay at NCSU, including Xin-Yu Wen, Jian-Ping Huang, Xiao-Ming Hu, Yao-Sheng Chen, Ping Liu, Ying Pan, Xiao-Huan Liu, Li-Tao Wang, Shuai Zhu, Nan Zhang, Ashley Penrod, Timothy Glotfelty, Wei Wang, Xuyan Liu, Jia Xing, Ming-Tung Chuang, Xin-Yi Dong, Kristen Olsen, Joshua Hemperly, Mike Burr, Evelyn Frazier, Chris Misenis, Ashley Queen, Srinath Krishnan and many others.

Finally, I want to thank my wife, Wei, who has been always there supporting me and sharing my happiness and sadness. Without her, I cannot make all this happen. I am also deeply indebted to my parents, who provide their endless love and support throughout my entire education.

TABLE OF CONTENTS

| | |
|---|----|
| LIST OF TABLES | ix |
| LIST OF FIGURES | xi |
| LIST OF ACRONYMS | xx |
| 1. INTRODUCTION | 1 |
| 1.1 Background | 1 |
| 1.2 Objectives and Proposed Approaches | 2 |
| REFERENCES | 6 |
| 2. LITERATURE REVIEW | 8 |
| 2.1 Intercontinental Transport of Air Pollutants | 8 |
| 2.2 Modeling of Mineral Dust and Dust-Related Chemistry in the Atmosphere | 11 |
| 2.2.1 Dust Flux Schemes | 12 |
| 2.2.2 Heterogeneous Chemistry Associated with Dust | 13 |
| 2.2.3 Inorganic Aerosol Thermodynamic Module and the Role of Crustal Species | 16 |
| 2.3 Multiscale Multi-Pollutant Air Quality Modeling | 17 |
| REFERENCES | 21 |
| 3. STUDY OF TRANS-PACIFIC TRANSPORT USING CMAQ | 42 |
| 3.1. Introduction | 42 |
| 3.2. Model Configurations, Evaluation Protocols, and Observational Databases | 43 |
| 3.2.1 Model Setup and Inputs | 43 |
| 3.2.2 Model Evaluation Protocols and Available Measurements | 45 |

| | |
|---|-----|
| 3.3 Meteorological Predictions | 50 |
| 3.3.1 Continental U.S. | 51 |
| 3.3.2 China | 53 |
| 3.4 Chemical Predictions at Surface | 54 |
| 3.4.1 Continental U.S. | 54 |
| 3.4.2 China and Japan | 58 |
| 3.5 Vertical/Column Predictions | 59 |
| 3.6. Mechanistic Examination of Trans-Pacific Transport | 63 |
| 3.6.1 Horizontal/Vertical Transport | 63 |
| 3.6.2 Process Analysis | 66 |
| 3.7 Impact of Asian Pollution Export on the U.S. | 70 |
| REFERENCES | 74 |
| | |
| 4. IMPLEMENTATION OF ONLINE DUST EMISSIONS AND DUST-RELATED CHEMISTRY INTO CMAQ AND INITIAL APPLICATION TO THE ICAP EPISODE.. | 127 |
| 4.1 Incorporation of Mineral Dust Treatments into CMAQ | 128 |
| 4.1.1 Online Dust Emission Module | 128 |
| 4.1.2 Dust-Related Heterogeneous Chemistry | 133 |
| 4.1.3 Incorporation of ISORROPIA II and Crustal Species Treatments into CMAQ | 134 |
| 4.1.3.1 Incorporation of ISORROPIA II into CMAQ | 134 |
| 4.1.3.2 Study of Effects of Crustal Materials on Gas/Particle Partitioning Using Box Models of ISORROPIA v1.7, ISORROPIA II, and | |

| | |
|---|-----|
| 5.2.2.1 Ozone | 214 |
| 5.2.2.2 PM _{2.5} and its Composition | 218 |
| 5.2.3 Hazardous Air Pollutants at the Surface | 230 |
| 5.2.3.1 Mercury | 230 |
| 5.2.3.2 Other Air Toxic Compounds | 233 |
| 5.2.4 Column Variables | 237 |
| 5.2.4.1 Column Mass of Gases | 237 |
| 5.2.4.2 AOD | 245 |
| 5.3 Process Analysis | 247 |
| 5.3.1 IPR Analysis | 248 |
| 5.3.2 IRR Analysis | 252 |
| REFERENCES | 255 |
| 6. SUMMARY | 301 |
| 6.1 Summary | 301 |
| 6.2 Limitations and Future Work | 309 |

LIST OF TABLES

| | |
|--|-----|
| Table 2.1. Similarities and differences of several major dust flux schemes..... | 40 |
| Table 3.1. Summary of observational databases used in model evaluation for 2001..... | 89 |
| Table 3.2. Performance statistics for meteorological predictions over the U.S. in January, April, July, and October, 2001..... | 90 |
| Table 3.3. Performance statistics for meteorological predictions over China in January, April, July, and October, 2001..... | 91 |
| Table 3.4. Performance statistics for chemical predictions over the U.S. in January, April, July, and October, 2001..... | 92 |
| Table 3.5. Performance statistics for O ₃ , SO ₂ , NO ₂ , and PM ₁₀ in Beijing, China in January, April, July, and October, 2001..... | 94 |
| Table 3.6. Performance statistics for chemical predictions over Japan in January, April, July, and October, 2001..... | 95 |
| Table 3.7. Performance statistics for column predictions over the ICAP domain in January, April, July, and October, 2001..... | 96 |
| Table 3.8. The monthly-average 24-hr total export of O ₃ , NO _x , NO _y , and PM _{2.5} out of the PBL over different sub-domains in January, April, July, and October, 2001..... | 97 |
| Table 3.9. The monthly average 24-hr total import of O ₃ , NO _x , NO _y , and PM _{2.5} from Asia into the PBL over the U.S. in April 2001 using two different methods..... | 97 |
| Table 4.1. Reactions and uptake coefficients considered in this study..... | 174 |
| Table 4.2. Major characteristics of ISORROPIA II and EQUISOLV II..... | 175 |
| Table 4.3. The configurations of WRF/CMAQ v4.7-Dust used in the model simulation.... | 176 |

| | |
|---|-----|
| Table 4.4. Performance statistics for meteorological predictions over the U.S. and China from MM5 and WRF simulations in April 2001..... | 177 |
| Table 4.5. Performance statistics for chemical predictions over the U.S. from simulations BASELINE, DUST, and CMAQv4.4 in April 2001..... | 179 |
| Table 4.6. Performance statistics for chemical predictions over Asia from simulations BASELINE, DUST, and CMAQv4.4 in April 2001..... | 180 |
| Table 4.7. Performance statistics for column predictions over the ICAP domain from simulations BASELINE, DUST, and CMAQv4.4 in April 2001..... | 181 |
| Table 5.1. Summary of observational databases used in the model evaluation..... | 277 |
| Table 5.2. Seasonal model performance statistics for criteria air pollutants over different sub- regions in 2002..... | 278 |
| Table 5.3. Seasonal model performance statistics for selected hazardous air pollutants over the 36-km CONUS domain in 2002..... | 282 |
| Table 5.4. Seasonal performance statistics for column predictions over the 36 km CONUS domain in 2002..... | 283 |

LIST OF FIGURES

| | |
|---|-----|
| Figure 2.1. Chemical linkage illustrating relationships across CAPs and HAPs. Note that this diagram is a highly-condensed one that does not capture numerous heterogeneous processes and complex chemical pathways. Key atmospheric species that are involved in many reactions across pollutant categories include O ₃ and hydroxyl radical (OH). Primary PM emissions are not included (adopted from Scheffe et al., 2007; note that other pollutants not defined in the text include semi-VOC (SVOC), alkyl peroxy (RO ₂), sulfuric acid (H ₂ SO ₄), and hydroperoxyl radical (HO ₂)) | 41 |
| Figure 3.1. Modeling domain for the ICAP trans-Pacific transport study..... | 98 |
| Figure 3.2. Spatial distributions of NMBs between observations and MM5 simulations for temperature at 2-m (T2), RH at 2-m (RH2), and weekly total precipitation (Precip.) over the U.S. for January, April, July, and October 2001..... | 99 |
| Figure 3.3. Spatial distributions of NMBs between NCDC observational data and MM5 simulations for temperature at 2-m (T2), water vapor mixing ratio at 2-m (QV2), and 24-hr precipitation (Precip.) over China for January, April, July, and October 2001..... | 102 |
| Figure 3.4. Spatial distribution of NMBs for simulated max 8-hr O ₃ concentration at the (a) CASTNET and (b) AIRS-AQS and SEARCH sites in July 2001..... | 105 |

Figure 3.5. The daily variation of domain mean concentration, ME, and MB for max 1-hr and 8-hr O₃ over the CASTNET, AIRS-AQS, and SEARCH sites in July 2001..... 106

Figure 3.6. The normalized mean biases of simulated daily PM_{2.5} concentrations at the IMPROVE (circle), STN (square), and SEARCH (triangle) monitoring sites for January, April, July, and October 2001..... 107

Figure 3.7. The normalized mean bias of simulated monthly PM_{2.5} and its components at the IMPROVE, STN, and CASTNET monitoring sites for April 2001..... 108

Figure 3.8. Daily variation of concentrations of (a) SO₂, (b) max 1-hr O₃, (c) NO₂, and (d) PM₁₀ at Beijing for January, April, July, and October 2001..... 109

Figure 3.9. Spatial distribution of CO column from MOPITT satellite observations and CMAQ simulation for January, April, and October, 2001. No MOPITT data are available for July, 2001..... 110

Figure 3.10. Spatial distribution of NO₂ column from GOME satellite observations and CMAQ simulation for January, April, July, and October, 2001..... 111

Figure 3.11. Spatial distribution of TORs from TOMS/SBUV satellite observations and CMAQ simulation for January, April, July, and October, 2001..... 112

Figure 3.12. Spatial distribution of AODs from MODIS satellite observations and CMAQ simulation for January, April, July, and October, 2001..... 113

Figure 3.13. Horizontal fluxes of O₃, SO₂, NO_x, NH₃, CO, HCHO, and PAN (from top to bottom), super-imposed with the wind fields, at surface layer and the

| | |
|---|-----|
| layer with altitude of ~5 km for April 2001..... | 114 |
| Figure 3.14. Horizontal fluxes of PM _{2.5} , SO ₄ ²⁻ , NO ₃ ⁻ , NH ₄ ⁺ , BC, OC, and other inorganic aerosols (from top to bottom), super-imposed with the wind fields, at surface layer and the layer with an altitude of ~5 km for April 2001.... | 115 |
| Figure 3.15. X-Z cross-sections of average horizontal fluxes of O ₃ , SO ₂ , NO _x , NH ₃ , CO, HCHO, PAN, PM _{2.5} , SO ₄ ²⁻ , NO ₃ ⁻ , NH ₄ ⁺ , BC, OC, and other inorganic aerosols between 25-50° N for April 2001..... | 116 |
| Figure 3.16. Accumulative IPRs for O ₃ for different sub-domains for January, April, July, and October 2001..... | 119 |
| Figure 3.17. Accumulative IPRs for PM _{2.5} for different sub-domains for January, April, July, and October 2001..... | 122 |
| Figure 3.18. IPR differences between baseline and sensitivity simulations for O ₃ and PM _{2.5} for different sub-domains for April 2001..... | 125 |
| Figure 3.19. Absolute and relative contributions of different (a) gaseous species and (b) PM _{2.5} components over the western U.S. and eastern U.S. due to Asian anthropogenic emissions (AAEs) for April 2001..... | 126 |
| Figure 4.1. Comparisons of different volatile species and variables between simulations of ISORROPIA v1.7, ISORROPIA II (with and without crust), EQUISOLV II (with and without crust) at the Hong Kong site..... | 182 |
| Figure 4.2 Comparisons of different volatile species and variables between simulations of ISORROPIA v1.7, ISORROPIA II (with and without crust), EQUISOLV II (with and without crust) at Angiola and Fresno..... | 185 |

Figure 4.3 Flow chart of the physical and chemical drivers in CMAQ..... 188

Figure 4.4. The monthly-mean dust emission rates generated by the Westphal and Zender schemes used in MM5/CMAQ v4.4..... 189

Figure 4.5. Spatial distribution of NMBs between observations and MM5 simulation (left panel) and WRF simulation (right panel) for temperature at 2 m (T2), water vapor mixing ratio at 2 m (Q2), and 24-h total precipitation (Precip.) over China for April 2001..... 190

Figure 4.6. Spatial distribution of NMBs between observations and MM5 simulation (left panel) and WRF simulation (right panel) for temperature at 2 m (T2), relative humidity at 2 m (RH2), and weekly total precipitation (Precip.) over the U.S. for April 2001..... 191

Figure 4.7. The predicted monthly-mean dust emission rates generated by (a) Zender and (b) Westphal schemes, (c) and (d) for fine and (e) and (f) for coarse dust concentrations at surface and ~5 km from the Zender scheme in CMAQ-Dust..... 192

Figure 4.8. Spatial distribution of column variables (from left to right: CO, TOR, NO₂) from satellite observations (1st row), CMAQ v4.4 (2nd row), BASELINE simulation (3rd row) and DUST simulation (4th row) in April 2001..... 193

Figure 4.9. Spatial distribution of AOD from satellite observations (1st row), CMAQ v4.4 (2nd row), BASELINE simulation (3rd row) and DUST simulation (4th row) in April 2001..... 194

Figure 4.10. Spatial distribution of differences between simulations with crustal species (CRUST_ONLY) and without crustal species (DUST_EMIS_ONLY) for surface layer SO₂, HNO₃, and NH₃ in April 2001..... 195

Figure 4.11. Spatial distribution of differences between simulations with crustal species (CRUST_ONLY) and without crustal species (DUST_EMIS_ONLY) for surface layer PM_{2.5}, fine-mode SO₄²⁻, fine-mode NO₃⁻, fine-mode NH₄⁺, fine-mode Cl⁻, coarse-mode SO₄²⁻, coarse-mode NO₃⁻, and coarse-mode NH₄⁺ in April 2001..... 196

Figure 4.12. Spatial distribution of differences between simulations with heterogeneous chemistry (DUST) and without heterogeneous chemistry (CRUST_ONLY) for surface layer O₃, NO_x, SO₂, HNO₃, NO₃, N₂O₅, HO_x, and H₂O₂ in April 2001..... 197

Figure 4.13. Spatial distribution of differences between simulations with heterogeneous chemistry (DUST) and without heterogeneous chemistry (CRUST_ONLY) for surface layer PM_{2.5}, fine-mode SO₄²⁻, NO₃⁻, and NH₄⁺, and coarse-mode SO₄²⁻, NO₃⁻, NH₄⁺, and PM..... 198

Figure 4.14. Spatial distribution of differences between simulations DUST_HIGHY and CRUST_ONLY for surface layer NO_x, NO₃, N₂O₅, and NO₃⁻ (a-d) and differences between simulations DUST and DUST_ISO1.7 for fine-mode NO₃⁻ and coarse-mode NO₃⁻ (e-f) in April 2001..... 199

Figure 4.15. Spatial distribution of differences between simulations with dust treatment (DUST) and without dust treatment (NO_DUST) for surface layer

(left panel) and the layer with ~5 km altitude (right panel) O_3 , NO_x , SO_2 , HNO_3 , HO_x , and H_2O_2 in April 2001..... 200

Figure 4.16. Spatial distribution of differences between simulations with dust treatment (DUST) and without dust treatment (NO_DUST) for surface layer (left panel) and the layer with ~5 km altitude (right panel) $PM_{2.5}$, fine-mode SO_4^{2-} , NO_3^- , and NH_4^+ , and coarse-mode SO_4^{2-} , NO_3^- , NH_4^+ , and PM in April 2001..... 203

Figure 4.17. Absolute and relative contributions of different (a) gaseous species and (b) $PM_{2.5}$ components over the western U.S. and eastern U.S. due to AAEs between simulations DUST and DUST_CUT for April 2001..... 206

Figure 5.1. The CMAQ modeling domain: the black, red, and blue boxes denote domains over the 36-km continental U.S., the 12-km western U.S., the 12-km eastern U.S., respectively (Figure adopted from U.S. EPA, 2008)..... 284

Figure 5.2. Comparison of the simulated and observed O_3 concentrations at the AIRS-AQS monitoring sites during O_3 season (i.e., May to September) in 2002. (a) Scatter plot of daily max 8-h O_3 with a cut off value of 40 ppb (the 1:1, 1.5:1 and 1:1.5 lines are shown for reference); (b) box plot of diurnal variation of median (the cross symbol denotes AQS and the triangle symbol denotes CMAQ) and inter-quartile ranges (light and dark shading denote AQS and CMAQ, respectively) for hourly average O_3 ; Spatial distributions of (c) NMB and (d) NME for daily max 8-h O_3 ; (e) Median and inter-quartile range of MB binned by observed concentrations of daily max 8-h O_3 . The

numbers above the X axis indicate the number of simulated/observed data pairs for each bin; (f) the same as (e), but for RMSE..... 285

Figure 5.3. Spatial plots of NMBs for SO_4^{2-} (a and b), NO_3^- (c and d), and NH_4^+ (e and f), OC (g and h), EC (i and j), and $\text{PM}_{2.5}$ (k and l) for winter (left panel) and summer (right panel) 2002..... 286

Figure 5.4. Comparison of the simulated and observed $\text{PM}_{2.5}$ concentrations at the IMPROVE and STN sites in 2002. Monthly box plot for total $\text{PM}_{2.5}$ concentrations with 25% and 75% quartiles and median values over (a) the IMPORVE sites and (b) the STN sites in 2002 (triangle and dark shading denote CMAQ, square and light shading denote observations, and numbers over each bar represent the numbers of observations); Stacked bar charts of total mass concentrations of $\text{PM}_{2.5}$ and its major components over the STN sites for (c) winter and (d) summer in 2002. The percentages indicate the contribution of each species to the total $\text{PM}_{2.5}$ mass..... 289

Figure 5.5. Spatial plots of NMBs for Hg wet deposition (top), formaldehyde (middle), and acetaldehyde (bottom) for winter (left panel) and summer (right panel) 2002..... 290

Figure 5.6. Monthly box plot for (a) Hg wet deposition, (b) HCHO, (c) ALD2, (d) benzene, (e) butadiene_13, and (f) particulate lead with 25% and 75% quartiles and median values in 2002 (triangle and dark shading denote CMAQ, square and light shading denote observations, and numbers over

| | |
|---|-----|
| each bar represents the numbers of observations)..... | 291 |
| Figure 5.7. Spatial distributions of seasonal TOR from TOMS/SBVU and CMAQ over the 36-km CONUS domain and 12-km EUS for 2002..... | 292 |
| Figure 5.8. Spatial distributions of seasonal tropospheric CO columns from MOPITT and CMAQ over the 36-km CONUS domain and 12-km EUS for 2002.. | 293 |
| Figure 5.9. Spatial distributions of seasonal tropospheric NO ₂ columns from GOME and CMAQ over the 36-km CONUS domain and 12-km EUS for 2002.. | 294 |
| Figure 5.10. Spatial distributions of seasonal tropospheric HCHO columns from GOME and CMAQ over the 36-km CONUS domain and 12-km EUS for 2002..... | 295 |
| Figure 5.11. Spatial distributions of seasonal AODs from MODIS and CMAQ over the 36-km CONUS domain and 12-km EUS for 2002..... | 296 |
| Figure 5.12. The monthly-mean contributions of individual processes to the concentrations of selected criteria air pollutants: (a) NO _x (b) O ₃ , (c) NO ₃ ⁻ , and (d) PM _{2.5} over different sub-regions in January (left panel) and July (right panel) 2002..... | 297 |
| Figure 5.13. The monthly-mean contributions of individual processes to the concentrations of selected hazardous air pollutants (a) Hg(II) (b) PHg, (c) formaldehyde (HCHO), and (d) lead PM _{2.5} over sub-regions in January (left panel) and July (right panel) 2002..... | 298 |

Figure 5.14. The monthly-mean spatial distributions of (a) OH reacted with anthropogenic VOCs and (b) OH reacted with biogenic VOCs in the first layer in January (left panel) and July (right panel) 2002..... 299

Figure 5.15. The monthly-mean spatial distributions of photochemical indicators of (a) surface layer $P_{H_2O_2}/P_{HNO_3}$ and (b) column HCHO/NO₂ predicted by CMAQ and (c) column HCHO/NO₂ observed by GOME satellite (blank denotes missing values) in January (left panel) and July (right panel) 2002..... 300

LIST OF ACRONYMS

| Acronym | Definition |
|-----------------------------|--|
| 3-D | Three dimensional |
| σ_{sp} | Scattering coefficient |
| σ_{ap} | Specific absorption coefficient |
| Δz_i | Layer thickness |
| σ_{sp}^{BC} | Scattering coefficient for black carbon |
| σ_{sp}^{Na} | Scattering coefficient for chloride |
| σ_{sp}^{CM} | Scattering coefficient for coarse masses |
| σ_{sp}^{FS} | Scattering coefficient for fine-mode soils |
| σ_{sp}^{Na} | Scattering coefficient for sodium |
| $\sigma_{sp}^{NH_4}$ | Scattering coefficient for ammonium |
| $\sigma_{sp}^{NO_3}$ | Scattering coefficient for nitrate |
| σ_{sp}^{OC} | Scattering coefficient for organic carbon |
| $\sigma_{sp}^{SO_4}$ | Scattering coefficient for sulfate |
| $\alpha_{ap}^{hydrophobic}$ | Specific absorption coefficient for hydrophobic black carbon |
| $\alpha_{ap}^{hydrophilic}$ | Specific absorption coefficient for hydrophilic black carbon |
| α_{ap}^i | Specific absorption coefficient for species <i>i</i> |
| AAE | Asian anthropogenic emissions |

| | |
|------------------|---|
| ACE-Asia | the Aerosol Characterization Experiment-Asia |
| ACM | Asymmetric Convective Model |
| ACM2 | Asymmetric Convective Model version 2 |
| ADJC | Mass adjustment term |
| AERO | Aerosol chemistry |
| AERO3 | Aerosol module in CMAQ version 3 |
| AERO4 | Aerosol module in CMAQ version 4 |
| AERO5 | Aerosol module in CMAQ version 5 |
| AERONET | the Aerosol Robotic network |
| AIRS-AQS | the Aerometric Information Retrieval System - Air Quality Subsystem |
| ALD2 | acetaldehyde |
| AMET | the Atmospheric Model Evaluation Tool |
| AQM | air quality model |
| AOD | Aerosol optical depth |
| BEIS | the Biogenic Emissions Inventory System |
| BELD | the Biogenic Emissions Land Cover Database |
| BIRA/KNMI | the Belgian Institute for Space Aeronomy/Royal Netherlands Meteorological Institute |
| BRAVO | the Big Bend Regional Aerosol and Visibility Observational Study |
| Ca ²⁺ | Calcium |
| CAA | Clean Air Act |
| CAIR | the Clean Air Interstate Rule |
| CAMx | the Comprehensive Air quality Model with extensions |

| | |
|-----------------|--|
| CAPs | Criteria air pollutants |
| CASTNET | Clean Air Status and Trends Network |
| CBM-IV | Carbon-Bond Mechanism-IV |
| CB05 | Carbon-Bond Mechanism version 2005 |
| Cl ⁻ | Chlorine particle |
| CLDS | Cloud physics |
| CHEM | Gas-phase chemistry |
| CMAQ | U.S. EPA Model-3 Community Multi-scale Air Quality modeling system |
| CMU | the Carnegie-Mellon University (CMU) equilibrium approach |
| CO | Carbon monoxide |
| CONUS | Continental U.S. |
| CRPAQS | the California Regional PM10/PM2.5 Air Quality Study |
| CTM | Chemical transport model |
| DDEP | Dry deposition |
| DU | Dobson Unit |
| E_i | Emission rates |
| EBI | the Euler Backward Iterative solver |
| ECMWF | the European Center for Medium-Range Weather Forecasts |
| EMIS | Emissions |
| EUS | the Eastern U.S. |
| F_d | the Vertical dust mass flux |
| FDDA | Four-dimensional data assimilation |

| | |
|--------------------------------|---|
| GCTM | Global chemistry transport model |
| GEIA | the Global Emissions Inventory Activity |
| GEOS-Chem | Goddard Earth Observing System-Chemistry model |
| GFDL | the Geophysical Fluid Dynamics Laboratory |
| GISS | Goddard Institute for Space Studies |
| GOCART | the Georgia Tech/Goddard Global Ozone Chemistry Aerosol Radiation and Transport model |
| GOME | Global Ozone Mapping Experiment |
| HAPs | Hazardous air pollutants |
| HCHO | formaldehyde |
| Hg | Mercury |
| Hg ⁰ | Elemental Hg |
| Hg (II) | divalent gaseous Hg |
| HCl | hydrochloric acid |
| HK | Hong Kong |
| HKUST | the HK University of Science and Technology |
| HNO ₃ | Nitric acid |
| HO ₂ | Hydroperoxyl radical |
| HO _x | OH + HO ₂ |
| H ₂ O ₂ | Hydrogen peroxide |
| HORZ | Horizontal transport |
| H ₂ SO ₄ | Sulfuric acid |

| | |
|------------|--|
| IMPROVE | the Interagency Monitoring of Protected Visual Environments |
| ICAP | International Transport and Climatic Effects of Air Pollutants |
| ICON | Initial conditions |
| IPR | the Integrated Process Rate analysis |
| IRR | the Integrated Process Rate analysis |
| K_x | Eddy or turbulent diffusivity at x direction |
| K_y | Eddy or turbulent diffusivity at y direction |
| K_z | Eddy or turbulent diffusivity at z direction |
| K^+ | Potassium |
| L_{chem} | Chemical loss rates |
| LFT | Lower free troposphere |
| LRT | Long range transport |
| MAQSIP | the Multiscale Air Quality Simulation Platform |
| MB | Mean bias |
| MCIP | Meteorology-Chemistry Interface Processor |
| MDN | the Mercury Deposition Network |
| Mg^{2+} | Magnesium |
| MM5 | the PSU/NCAR Mesoscale Model Generation 5 |
| MODIS | the MODerate resolution Imaging Spectroradiometer |
| MOPITT | the Measurements of Pollution in the Troposphere |
| MOUDI | Micro-Orifice Uniform Deposit Impactor |
| MOZART-2 | the Model of Ozone and Related Chemical Tracers version 2 |

| | |
|---|---|
| MP | Multiple-pollutant |
| N ₂ O ₅ | Dinitrogen pentoxide |
| N.A. | North America |
| Na ⁺ | Sodium |
| NAAQS | National Ambient Air Quality Standard |
| NADP | the National Acid Deposition Program |
| NATA | National Air Toxics Assessment |
| NATTS | the National Air Toxics Trends Stations |
| NCAR | National Center for Atmospheric Research |
| NCDC | the National Climate Data Center |
| NCEP | the National Centers for Environmental Prediction |
| NEI | National Emission Inventory |
| NEMCC | the National Environmental Monitoring Centre of China |
| NH ₃ | Ammonia |
| NH ₄ ⁺ | Ammonium |
| NH ₄ NO ₃ | Ammonium nitrate |
| (NH ₄) ₂ SO ₄ | Ammonium sulfate |
| NIES | the National Institute for Environmental Studies |
| NMB | Normalized Mean Bias |
| NME | Normalized Mean Error |
| NO | Nitric oxide |
| NO ₂ | Nitrogen dioxide |

| | |
|------------------------------|--|
| NO _x | Nitrogen oxides |
| NO ₃ | Nitrate radical |
| NO ₃ ⁻ | Nitrate |
| NOAA | the National Oceanic and Atmospheric Administration |
| O ₃ | Ozone |
| OH | Hydroxyl radical |
| O _x | Odd oxygen |
| OC | Organic compound |
| OM | Organic matter |
| P_{chem} | Chemical production rates |
| PA | Process Analysis |
| PAN | Peroxyacetylnitrate |
| PBL | Planetary Boundary Layer |
| PM | Particulate matter |
| PHg | Particulate Hg |
| PM _{2.5} | Particulate matter with an aerodynamic diameter less than or equal to 2.5 μm |
| PM ₁₀ | Particulate matter with an aerodynamic diameter less than or equal to 10 μm |
| PM _{coarse} | Coarse-mode PM |
| POA | Primary organic aerosol |
| Precip. | Precipitation |
| PSU | Penn State University |

| | |
|-------------------------------|---|
| Q_s | the Horizontal dust mass flux |
| QV2 | Water vapor mixing ratio at 2 m |
| R | Correlation Coefficient |
| RADM | the Regional Acid Deposition Model |
| RADM2 | the Regional Acid Deposition Mechanism version 2 |
| RH2 | Relative Humidity at 2-m height |
| RMSE | Root Mean Squared Error |
| RRTM | the rapid and accurate radiative transfer model |
| SAPRC99 | the Statewide Air Pollution Research Center Mechanism 1999 version |
| SBUV | the Solar Backscattered Ultraviolet |
| SCIAMACHY | the Scanning Imaging Absorption Spectrometer for Atmospheric Chartography |
| SEARCH | the Southeastern Aerosol Research and Characterization |
| SMOKE | Sparse Matrix Operator Kernel Emissions modeling system |
| SO ₂ | Sulfur dioxide |
| SO ₄ ²⁻ | Sulfate |
| SOA | Secondary organic aerosol |
| SPM | Suspended Particle Matter |
| STATSGO | the U.S. State Soil Geographic database |
| STE | stratosphere-troposphere exchange |
| STEM | the Sulfur Transport Eulerian Model |
| STN | the Speciation Trends Network |
| T2 | 2-m temperature |

| | |
|----------|---|
| TC | Total carbon |
| TOR | Tropospheric ozone residuals |
| TRACE-P | the Transport and Chemical Evolution over the Pacific |
| TEOM | Tapered element oscillating |
| TOMS | the Total Ozone Mapping Spectrometer |
| TRI | Toxics Release Inventory |
| u^* | Surface friction velocity |
| u^*_t | Surface threshold friction velocity |
| U_{10} | 10-m U component of wind speed |
| UFT | Upper free troposphere |
| U.S. EPA | the United States Environmental Protection Agency |
| USGS | the U.S. Geological Survey |
| V_{10} | 10-m V component of wind speed |
| VERT | Vertical transport |
| VOC | Volatile Organic Compound |
| WCB | Warm conveyor belts |
| WD | Wind direction |
| WRAP | the Western Regional Air Partnership |
| WRF | the Weather Research and Forecast model |
| WPS | WRF Preprocessing System |
| WS | Wind speed |
| WSM | WRF Single Moment |

| | |
|-----|-------------------|
| WUS | the western U.S. |
| YSU | Yonsei University |

CHAPTER 1. INTRODUCTION

1.1 Background

Three dimensional (3-D) air quality models (AQMs) are powerful tools that simulate atmospheric processes, such as transport, diffusion, transformation, and removals of various pollutants after their release into the atmosphere. Earlier AQMs have been developed to address the specific issues of air pollutants, such as urban ozone (O_3), regional acid deposition, particles or toxics problems, separately (e.g., Schere and Possiel, 1984; Chang et al., 1987; U.S. EPA, 1992; Scheffe and Morris, 1993). Most of AQMs have conventionally been conducted within a single pollutant framework, which mainly focuses on either criteria air pollutants (CAPs), especially O_3 and particulate matter (PM) with aerodynamic diameter less than or equal to $2.5 \mu\text{m}$ ($PM_{2.5}$) or hazardous air pollutants (HAPs) at urban or regional scales (Seigneur et al., 2003; Mather et al., 2005). However, increasing attention has recently been given to the multiscale multi-pollutant (MP) models due to their ability to integrate across source emissions, atmospheric chemistry and physics, meteorology, and deposition processes at scales ranging from urban to hemispheric, in a flexible and modular framework that permits a detailed comparison of the adequacy of alternative process algorithms, and to evaluate scientific understanding of new process formulations (Mather et al., 2005). Pollutants in the atmosphere undergo numerous transport processes and transformation pathways that control their composition and distributions. The ability to characterize or understand the behavior of one particular pollutant often hinges on the chemical interactions with other pollutants. For example, the emissions of precursors such as volatile organic compounds (VOCs), nitrogen oxides (NO_x), and sulfur dioxide (SO_2) all influence the

formation of O₃, PM_{2.5}, and HAPs through a series of complex reaction pathways involving numerous chemical species. Thus, modeled control scenarios of those pollutant precursors to reduce O₃ levels may cause an exacerbation of other air pollutants, such as PM_{2.5} or air toxics, under a variety of conditions. Proper modeling of the complex ambient atmosphere requires that a broad range of multiple temporal and spatial scales of multiple-pollutant interactions be considered simultaneously.

The U.S. Environmental Protection Agency (EPA)'s Community Multi-scale Air Quality (CMAQ) modeling system (Binkowski and Roselle, 2003; Byun and Schere, 2006) provides such capabilities ("one atmosphere" analysis) to meet this requirement and will be used in the following proposed research work. CMAQ is a 3-D air quality model that simulates chemical formation and transport with meteorological inputs, generated offline from a mesoscale meteorological model such as the PSU/NCAR mesoscale model (MM5) and Weather Research & Forecasting Model (WRF).

1.2 Objectives and Proposed Research

The overall objectives of my Ph.D. research are to apply, evaluate, and further develop and improve the CMAQ modeling system via two specific studies: the U.S. EPA's International Transport and Climatic Effects of Air Pollutants (ICAP) study and the 2002 MP modeling platform study. The specific objectives are:

- (1) Continue and advance research from the previous ICAP study through process analysis (PA), sensitivity simulations, and the use of satellite data for model evaluation to further understand the magnitude, mechanism, and impacts of Asian pollution export and provide a mechanistic examination of its occurrence and impact on the U.S. air quality;

- (2) Incorporate an online dust emission module together with dust-related heterogeneous chemistry and aerosol thermodynamics into CMAQ to study the role of dust in affecting photochemical cycles, aerosol predictions, and Asian pollution export;
- (3) Perform a comprehensive evaluation of chemical predictions for both CAPs and HAPs for 2002 baseline 36-km and 12-km simulations in the 2002 MP platform and identify possible reasons for model biases;
- (4) Apply PA tool into the 2002 MP platform with the 2005 Carbon Bond (CB05) mechanism to better understand the interactions among multiple pollutants through various chemical and physical processes.

This research is expected to gain a better understanding of the chemical and physical interactions among CAPs, Hg, none-Hg toxics, and dust particles. This work will also be part of an effort to develop and demonstrate the capability of multiscale MP air quality modeling analyses as part of a comprehensive air quality management process.

The first component of my Ph.D. research is to further develop the MP modeling platform. The model development work include: incorporate an online dust emission module together with dust-related heterogeneous chemistry into CMAQ; update the default inorganic thermodynamic aerosol module, ISORROPIA v1.7, in CMAQ to ISORROPIA II and add the crustal species (e.g., calcium (Ca^{2+}), potassium (K^+), and magnesium (Mg^{2+})) treatment into CMAQ. Dust emissions will be first calculated on-line in CMAQ by incorporating existing dust emission parameterizations from literatures. Various factors such as land use data, soil types, soil moisture, precipitation, snow cover, and vegetation coverage will be considered when determining dust emissions. Dust particles generated by the on-line emission module

will be split into fine and coarse modes. Crustal species will be prescribed as a function of dust concentrations that vary with time/location and allowed to participate in the aerosol thermodynamic equilibrium. Surface uptake of chemical species on the surface of dust will be considered through the inclusion of heterogeneous chemistry associated with dust particles. CMAQ with the dust treatments will be tested through applying to the U.S. EPA's 2001 April ICAP dust episode in Chapter 4. Several simulations for the representative month (e.g., April) are performed to investigate the influences of dust on chemical predictions. For example, simulations with dust emissions only and with both dust emissions and heterogeneous chemistry will illustrate the role of heterogeneous chemistry in affecting photochemical cycles, PM formation, and aerosol optical properties (e.g., aerosol optical depth (AOD)). Simulations with and without crustal material will be conducted to demonstrate the importance of crustal material in $PM_{2.5}$ formation through changing aerosol inorganic thermodynamic equilibrium.

The second component of my research is to focus on the application and evaluation of CMAQ v4.6 for the 2002 MP platform using both 36-km and 12-km horizontal grid resolutions. The observational data used for the evaluation include both surface monitoring networks and satellite data (see details in Chapter 5). Model results will be analyzed to identify likely causes for model biases in the baseline simulations. The PA will be then applied in CMAQ v4.6 to the 2005 version Carbon Bond (CB05) mechanism within the 2002 MP modeling platform. CB05 is the default gas-phase mechanism in CMAQ4.6. The extension of PA to CMAQ-CB05 in this work enables an assessment of CMAQ-CB05 performance and understand the interactions among pollutants. In applying PA for CB05,

both integrated process rate (IPR) and integrated reaction rate (IRR) are updated in CMAQ v4.6 to reflect the changes in CB05 as compared with the Carbon Bond mechanism IV (CB-IV). The family species and the process parameters for IPRs are redefined and all the calculations of integrated reaction rates are modified based on reactions and species treated in CB05.

REFERENCES

- Schere, K. L., and N. C. Possiel (1984), U.S. EPA (Environmental Protection Agency) Regional Oxidant Model – background and overview, U.S. Environmental Protection Agency, Washington, D.C., EPA/600/D-84/155 (NTIS PB84201680).
- Scheffe, R. D., and R. E. Morris (1993), A review of the development and application of the Urban Airshed model, *Atmos. Environ.*, 27B, 23-29.
- Chang, J. S., Brost R. A., Isaksen I. S. A., Madronich S., Middleton P., Stockwell W. R., and Walcek C. J. (1987), A three-dimensional Eulerian acid deposition model: physical concepts and formulation, *J. Geophys. Res.*, 92, 14681-14700.
- U.S. EPA (1992), *User's Guide for the Industrial Source Complex (ISC2) Dispersion Models, Volume II - Description of Model Algorithms*. Office of Air Quality Planning and Standards, EPA-450/4-92-008b.
- Seigneur C., B. Pun, K. Lohman, and S.-Y. Wu (2003), Regional modeling of the atmospheric fate and transport of benzene and diesel particles, *Environ. Sci. Technol.*, 37, 5236-5246.
- Binkowski, F. S., and S. J. Roselle (2003), Models-3 community multiscale air quality (CMAQ) model aerosol component, 1. Model description, *J. Geophys. Res.*, 108, 4183, doi:10.1029/2001JD001409.
- Byun, D. W., and K. L. Schere (2006), Review of the governing equations, computational algorithms, and other components of the models-3 Community Multi-scale Air Quality (CMAQ) modeling system, *Appl. Mech. Rev.*, 59, 51-77.

Mather, R et al. (2005), Multiscale air quality simulation platform: Initial applications and performance for tropospheric ozone and particulate matter, *J. Geophys. Res.*, *110*, D13308, doi:10.1029/2004JD004918.

CHAPTER 2. LITERATURE REVIEW

2.1 Intercontinental Transport of Air Pollutants

Over the past decade, the intercontinental transport of air pollutants has become an increasingly important issue. There is mounting evidence that the background concentrations of major pollutants (e.g., ozone (O₃) and particulate matter (PM)) in North America can increase to a significant level that could offset the national and local control efforts (Jacob et al., 1999; Fiore et al., 2003a). For instance, Jacob et al. (1999) indicated that the long-range transport of Asian pollutants could increase the background surface O₃ concentrations by 2-6 ppb in the western United States (U.S.), which will offset up to 25% of O₃ control efforts in this region. These pollutants will not only impair public health and environment, but also have potentially significant impacts on climate change (Akimoto, 2003; IPCC, 2007). East Asia, as the most populous region with the largest developing economy in the world, has become the most important contributor of anthropogenic emissions across the Pacific Rim (Bey et al., 2001). North America (N.A.), as a downwind region of East Asia, is a major receptor of the trans-Pacific transport of Asian air pollution. A number of air pollution episodes in the U.S., especially the northwestern and western U.S., have been reported to be associated with trans-Pacific transport events (Husar et al., 2001; McKendry et al., 2001; Jaffe et al., 1999, 2003b; Bertschi et al., 2004).

During the last two decades, numerous ground, aircraft, and satellite-based measurements (e.g., Andreae, et al., 1988; Parrish et al., 1992, 2004; Jaffe et al., 1999, 2003a, 2008; Husar et al., 2001; Mckendry et al., 2001; VanCurren, 2003; Allen et al., 2004; Bertschi et al., 2004; Seinfeld et al., 2004) have shown evidence of trans-Pacific transport of

Asian air pollutants. They found that the transport maximizes in springtime and is most efficient in the lower free troposphere (LFT). Under certain weather conditions, Asian emissions can be transported to N.A. in 5-8 days (Jaffe et al., 1999; Husar et al., 2001). A number of global models have recently been employed to study the impacts of Asian pollution outflow on N.A. These models include the Harvard-Goddard Institute for Space Studies (GISS) global three-dimensional (3-D) model of tropospheric chemistry (Jacob et al., 1999); the Goddard Earth Observing System-Chemistry model (GEOS-CHEM) (Jaeglé et al., 2003; Fiore et al., 2003a; Goldstein et al., 2004; Heald et al., 2006; Fairlie et al., 2007); the Georgia Tech/Goddard Global Ozone Chemistry Aerosol Radiation and Transport model (GOCART) (Chin et al., 2003, 2007); the Geophysical Fluid Dynamics Laboratory (GFDL) global chemistry transport model (GCTM) (Yienger et al., 2000), and the Model of Ozone and Related Chemical Tracers version 2 (MOZART-2) (Horowitz et al., 2003; Fiore et al., 2008; Liu et al., 2008). These modeling studies reported two types of influence of trans-Pacific transport: (1) the enhancement of the background concentrations; and (2) high pollution “episodes” (e.g., the Asian dust storm episodes). For example, Berntsen et al. (1999) reported that the maximum enhancements of carbon monoxide (CO), peroxyacetylnitrate (PAN), and O₃ during strong Asian outflow events can be up to 42 ppb, 75 ppt, and 7.5 ppb, respectively. There are several limitations for these global modeling studies including their use of a relatively-coarse grid resolution (e.g., 4° lat × 5° lon or 2° lat × 2.5° lon), simplified gas-phase chemical mechanisms, and no or simplified aerosol treatments (Fiore et al., 2003b; Liao et al., 2003; and Park et al., 2004). In addition, most of these modeling studies have largely focused on gaseous species (e.g., CO, O₃, and its precursors)

and a few aerosol species (e.g., sulfate or carbonaceous aerosols).

Previous field and modeling studies have shown that there are two main pathways for Asian pollution export to N.A. in spring: (1) the westerly transport in the LFT over the Pacific ocean due to wave cyclones and/or prefrontal lifting of pollution from the surface to high altitudes associated with the warm conveyor belts (WCB), followed by a large scale subsidence over N.A. (Liu et al., 2003; Stohl et al., 2002; Jaffe et al., 2003b; Bey et al., 2001); (2) planetary boundary layer (PBL) outflow behind the front capped at about 2 km (Jacob et al., 2003; Liu et al., 2003). Generally, the transport in the PBL takes a longer time than that in the LFT due to higher wind speeds in LFT (Jaffe et al., 2003a). The peak concentrations of Asian pollutants are typically within the PBL (0-2 km), but the highest westerly outflow occurs in the LFT (Bey et al., 2001; Liu et al., 2003).

Recently, the U.S. Environmental Protection Agency (EPA)'s Model-3 Community Multiscale Air Quality (CMAQ) modeling system (Binkowski and Roselle, 2003; Byun and Schere, 2006) has been applied by Wang (2006) to simulate trans-Pacific transport of major gaseous and aerosol species such as O₃ and PM with aerodynamic diameter less than or equal to 2.5 μm (PM_{2.5}) and the results have shown that CMAQ can capture and reproduce the long range transport pathway of Asian air pollutants very well. CMAQ is a comprehensive Eulerian 3-D model driven by meteorological inputs, generated offline from mesoscale meteorological models such as the 5th generation Pennsylvania State University (PSU) / National Center for Atmospheric Research (NCAR) mesoscale model (MM5; Grell et al., 1994). It has been extensively used in regional and urban scale air quality studies over regions in N. A. (Zhang et al., 2004; Eder and Yu, 2006; Zhang et al., 2006a, b, c, 2007; Wu

et al., 2008a, b), Europe (Aulinger et al., 2007; Matthias et al., 2008), and Asia (M. Zhang et al., 2003, 2006). Compared with most global models, CMAQ includes more detailed gas-phase chemical mechanisms and comprehensive treatments for aerosol chemistry and microphysics that are designed for urban/regional scale simulations. CMAQ simulations are typically conducted at a horizontal grid resolution that is much finer than those used in most global model studies.

2.2 Modeling of Mineral Dust and Dust Related Chemistry in the Atmosphere

Both the natural and anthropogenic aerosols are known to play significant roles in many air pollution issues such as human health problems, climate change, atmospheric visibility, stratospheric ozone depletion, acid deposition, and photochemical smog. The role of natural aerosols on air quality and climate is as significant as that of the anthropogenic aerosols, not only because of their very high global mass loading (natural aerosols are probably 4 to 5 times larger than anthropogenic ones on a global scale according to Satheesh and Moorthy (2005)), but also because of their contribution to the long-range transport. Among the natural aerosols, mineral dust or soil dust is one of the major tropospheric aerosol components (IPCC, 2007). The direct and indirect atmospheric radiative forcing by mineral dust has been considered to be one of the largest uncertainties in climate and chemistry transport models. Therefore, modeling mineral dust emissions, transport and chemistry plays an important role in both studying the dust storm episodes (e.g., Asian dust storms) and better understanding of their considerable impacts on the intercontinental transport and climate.

2.2.1 Dust Flux Schemes

As it is well known, a number of environmental factors may affect dust emissions. Generally, dust emissions are favored by strong winds associated with large-scale disturbances or convective activity. Dust mobilization is often inhibited by surface-covering elements such as vegetation, snow cover, and rocks. It is also constrained by soil conditions such as high soil moisture and high salinity. With these factors, active mineral dust-producing surfaces are normally confined to bare ground or sparsely vegetated ground in arid and semiarid regions with strong winds (Tanaka, 2007; Yue et al., 2009).

The parameterizations of dust fluxes in various dust models often take into consideration of the aforementioned factors, though the formulation and weights of various parameters are diverse or even quite different. Zender et al. (2003) provided a brief review of the dust mobilization/flux schemes in current global models and according to them, there exist three distinct classes of dust emission flux schemes: simple, complex, and intermediate. In the simple class, the dust emission is parameterized in terms of the third or fourth power of the wind speed or wind friction speed and the emitted dust is then redistributed empirically based on an assumption of size distribution (Westphal et al., 1987; Tegen and Fung, 1994; Mahowald et al., 1999). Under this assumption, different sizes of particles have the same emission rates. This class is the simplest one and does not need very detail microphysical information (e.g., the soil particle size distribution over different source regions). In the complex class, a complete microphysical speciation of the erodible environment is used to predict the size-resolved saltation mass flux and resulting sandblasted dust emissions (Marticorena and Bergametti, 1995; Shao, 2001). In this case, different sizes of particles

have different dust emission rates. Although the complex class may provide the most accurate estimation of dust emissions, many input parameters/information for these fully microphysical schemes are not available globally, especially for large-scale simulations. Nevertheless this class of schemes has shown some promising results in regional simulations (Marticorena and Bergametti, 1995). In the intermediate class, the schemes use microphysical parameterizations wherever possible, but make simplified assumptions to produce large scale/global simulations (Ginoux et al., 2001; Zender et al., 2003). Additionally, all the above schemes have been verified by a number of lab or field experiments and the simulated dust emissions can generally reproduce many of available observations. Table 2.1 summarizes the main characteristics of several major dust flux schemes mentioned above.

2.2.2 Heterogeneous Chemistry Associated with Dust

Numerous modeling studies of dust storms have been made in the past decade. Although these studies were able to reproduce many important observations and demonstrate characteristic transport patterns of dust storms (e.g., Westphal et al., 1987; Tegen and Fung, 1994; Marticorena and Bergametti, 1995; Mahowald et al., 1999; Ginoux et al., 2001; Shao, 2001; Uno et. al 2003; Zender et al., 2003), there still exist large uncertainties and discrepancies for various dust emission and transport models. The uncertainties are mainly from different model treatments for dust blowing up or uplifting processes, the estimated amounts of dusts reaching the remote areas in dust storm events, and the variations in the size distribution during long-range transport; and the discrepancies are mainly due to the different treatments in dust emission schemes, meteorological conditions (e.g., soil textures, soil

wetness, and land use data), and atmospheric transport models. There is a limitation for a lot of those dust transport models developed in the early stage, which is the change of chemical composition during the dust transport processes cannot be simulated due to the lack of dust related chemistry treatments such as the heterogeneous uptake of gases on dust particles.

In recent years, increasing attentions have been given to the research on studying the chemical composition and processes associated with dust particles. More and more experimental (Goodman et al., 2000; Underwood et al., 2001; Li et al., 2006; Song et al., 2007; Ndor et al., 2008, 2009; Wagner et al., 2008; Li et al., 2010; McNaughton et al., 2010; Tang et al., 2010) and modeling studies have (Zhang et al., 1994; Dentener et al., 1996; Zhang and Carmichael, 1999; Underwood et al., 2001; Bian and Zender, 2003; Bauer et al., 2004; Liao and Seinfeld, 2005; Tie et al., 2005; Pozzoli et al., 2008a, b; Manktelow et al., 2010) demonstrated the significance of heterogeneous chemistry on the surface of mineral dust particles in altering the concentration of atmospheric gaseous and aerosol compositions. For example, Zhang et al. (1994) reported that the heterogeneous reaction on the surface of mineral dust can reduce nitrogen oxides (NO_x) levels by up to 50%, hydroperoxyl radical (HO_2) concentrations by 20-80%, and O_3 production rates by up to 25% with the dust level of $0\text{-}500 \mu\text{g m}^{-3}$ by using a box model constructed from a regional scale chemical transport model, Sulfur Transport and Emissions Model (STEM) II (Carmichael et al., 1991). Dentener et al. (1996) found that the interactions of dinitrogen pentoxide (N_2O_5), O_3 , and HO_2 radicals with dust are expected to affect photochemical oxidants cycle and cause O_3 decreases up to 10% near the dust sources with dust concentrations $> 300 \mu\text{g m}^{-3}$ by using a global scale model, Moguntia (Zimmermann, 1988). Li et al. (2006) showed that the

atmospheric sulfur dioxide (SO₂) loss by the heterogeneous reaction on dust is comparable to loss by the gas phase oxidation under high dust conditions (i.e., the number concentrations of dust are from ~8-56 cm⁻³) by using the Diffuse Reflectance Infrared Fourier Transform Spectroscopy (DRIFTS). Pozzoli et al. (2008a) also found that the heterogeneous chemistry significantly reduced the regional and global distributions of a number of key gases such as O₃ by 18-23% over the trans-Pacific region and nitric acid (HNO₃) by 15% globally by using a global model.

Theoretically, the heterogeneous uptake or pathway for various gaseous species on dust particles can be described in four main steps (Hodzic et al., 2006). The first step corresponds to the gas-phase diffusion towards the particle surface. In the second step, the molecules of gases are transferred into the particulate phase. This step depends on the accommodation coefficient α that represents the probability of the adsorption of the gas molecules by the particle surface through gas-surface collision. In the third step, the reactions may occur in the bulk phase with a kinetic reaction rate constant k . Finally, the desorption of some gaseous products will occur. The net effects of the above steps 2 and 3 can be described by uptake coefficient, γ , which is defined as the fraction of collisions with a particle that leads to irreversible loss of certain gas species on the particulate surface (Zhang and Carmichael, 1999). The uptake coefficient γ can be influenced by gas-phase diffusion, Henry's law of saturation, aqueous-phase chemistry, and surface chemistry (Zhang and Carmichael, 1999). The uptake coefficient γ is the most important parameter in heterogeneous chemistry simulation and will be discussed further in Chapter 4.

2.2.3 Inorganic Aerosol Thermodynamic Module and the Role of Crustal Species

Particulate matter is predominately composed of inorganic species (e.g., sulfate (SO_4^{2-}), nitrate (NO_3^-), ammonia (NH_4^+), dust, and crustal materials), organic species (e.g., organic carbon (OC)), water, and trace metals, which covers a very broad size range from a few nanometers to tens of micrometers. The chemical composition and formation mechanisms of PM are much different for different size sections (Seinfeld and Pandis, 2006). The knowledge of the physical and chemical properties, composition, and processes of the aerosol particles is of great importance. Among various aerosol processes, gas/particle mass transfer process plays an important role in determining aerosol mass concentration and composition (Seinfeld and Pandis, 2006). Accurately modeling the gas/particle mass transfer will improve our understanding of aerosol behavior and its impacts on air quality and climate change. In the past two decades, many inorganic aerosol modules have been developed to simulate the composition and phase state of PM. Most of them assume a thermodynamic equilibrium between gas and aerosol phases for condensable species. These include: EQUIL (Bassett and Seinfeld, 1983), MARS (Saxena et al., 1986), SEQUILIB (Pilinis and Seinfeld, 1987), AIM and AIM2 (Wexler and Seinfeld, 1991; Clegg et al., 1992, 1998), SCAPE and SCAPE2 (Kim et al., 1993a, b), EQUISOLV and EQUISOLV II (Jacobson et al., 1996; Jacobson, 1999), ISORROPIA and ISORROPIA II (Nenes et al., 1998, 1999; Fountoukis and Nenes, 2007), GFEMN (Ansari and Pandis, 1999a, b) and MESA (Zaveri, 2005a, b). These modules have been extensively used in determining emissions control strategies (Kumar et al., 1998), understanding of PM formations (Zhang et al., 2000), analysis of ambient measurements (Fridlind and Jacobson, 2000; Campbell et al., 2002), and directly simulating

PM in large-scale chemical transport models (Meng et al., 1998; Rodriguez and Dabdub, 2004). A comprehensive review and performance evaluation of some of these modules have also been conducted in several studies (e.g., Ansari and Pandis, 1999b; Zhang et al., 2000).

Among the above modules, only a few of them (i.e., SCAPE2, EQUISOLV II, and ISORROPIA II) treat the crustal species (e.g., calcium (Ca^{2+}), potassium (K^+), and magnesium (Mg^{2+})). It has been shown that the consideration of crustal materials in predicting the partitioning of NO_3^- and NH_4^+ , especially in areas where mineral dust comprises a significant portion of aerosols, is very important and can potentially improve model predictions (Jacobson, 1999; Moya et al., 2002; Fountoukis and Nenes, 2007).

To the author's best knowledge, there are very few models that can simulate the dust emissions, dust related heterogeneous chemistry, and crustal species associated with dust particles all together in a single model framework. The attempt to incorporate all the aforementioned dust treatments into CMAQ model is expected to enhance CMAQ's capability in simulating photochemical cycles, aerosol predictions, and the long range transport of air pollutants during dust storm episodes.

2.3 Multiscale Multi-Pollutant Air Quality Modeling

The U.S. EPA's CMAQ modeling system was developed in order to support both air quality regulatory assessments by regulation offices as well as scientific studies by research institutions (Binkowski and Roselle, 2003; Byun and Schere, 2006). CMAQ has been extensively and successfully applied over a wide range of meteorological conditions and geographical areas in order to address air quality issues related to criteria air pollutants (CAPs) such as O_3 and $\text{PM}_{2.5}$ during the past decades (M. Zhang et al., 2003, 2006; Y. Zhang

et al., 2004, 2006a, b, c, 2007, 2009a, b; Eder and Yu, 2006; Tesche et al., 2006; Appel et al., 2007, 2008; Aulinger et al., 2007; Matthias et al., 2008; Queen et al., 2008a, b, c; Wu et al., 2008; Wang et al., 2009a; X.-H. Liu et al., 2010a, b; Liu and Zhang, 2011, P. Liu et al., 2011). However, increasing attention has recently been given to multi-pollutants (MPs), including both criteria and hazardous air pollutants (HAPs) in a single modeling framework for both air quality management and research (Roselle et al., 2007; Scheffe et al., 2007). It is well known that the formation and fate of many pollutants are closely linked in the atmosphere through complex atmospheric gas-phase chemistry and aerosol processes (as illustrated in Figure 2.1). The ability to characterize the behavior of one particular pollutant often hinges on the chemical interactions of other pollutants. There is a growing awareness that CAPs and HAPs controls should be considered together because there are many areas in the U.S. with air quality issues of more than one pollutant including O₃, PM_{2.5}, and/or HAPs (Scheffe et al., 2007). Proper modeling of this complex MP system requires that a broad range of multiple temporal and spatial scales of multiple pollutant interactions be considered simultaneously. To address this issue and further advance the “one-atmosphere” modeling capability of CMAQ, an MP version of CMAQ has been developed by the U.S. EPA to predict O₃, PM_{2.5}, mercury (Hg), and other HAPs (or air toxics) in a single model setup.

Recently, the U.S. EPA Air Quality Modeling Group (AQMG) has undertaken a series of model application and evaluation efforts across multiple pollutants and over multiple scales (urban, regional, and intercontinental) using CMAQ. They have conducted a comprehensive study based on the EPA’s 2001 modeling platform. Currently, EPA has expanded the 2001 modeling platform to the new 2002 MP modeling platform by

incorporating air toxics including mercury (Hg) and other 38 HAPs, based on CMAQ version 4.6. HAPs or air toxics are the pollutants known to cause serious health effects on human, such as respiratory, cardiovascular, neurological, immune, and other organ system problems and adverse environmental issues (Cook et al., 2007). There are currently 188 air toxics, identified and regulated under the 1990 Clean Air Act (CAA). Among them, nearly 100 of the organic chemicals are VOCs and some of those HAPs are common aromatic and halogenated VOCs (Kelly et al., 1994). HAPs are emitted from a variety of sources, including large manufacturing facilities such as chemical production plants, combustion facilities such as waste incinerators, small commercial operations such as dry cleaners, and both onroad and nonroad mobile sources such as highway vehicles and farming or construction equipments (Rosenbaum et al., 1999). In contrast to CAPs under the CAA, such as O₃ and PM_{2.5}, for which the National Ambient Air Quality Standards (NAAQS) regulate their high levels, HAPs are normally controlled by individual source-specific standards for a large number of industrial sources or through nonroad diesel and onroad mobile source rules set by state or local air toxics monitoring programs (Luecken and Cimorelli, 2008). Moreover, the availability of measurement data for most HAPs is very limited and mainly focuses on the urban areas, as compared with CAPs (Kelly et al., 1994; Rosenbaum et al., 1999; McCarthy et al., 2006). In recent years, the U.S. EPA has launched several programs (e.g., National Air Toxics Assessment (NATA)), in order to gain a better understanding of the impacts of air toxics emissions on public health and environment and eventually to strengthen the nation's air quality management system (U.S. EPA, 2005). Among various nationwide activities included in those programs, the 2002 multiscale MP air quality

modeling platform has been considered as a key one, since it has the ability to integrate across the complex chemical and physical processes for MPs and to provide more comprehensive and scientific supports for all the regulatory strategies and air quality management.

REFERENCES

- Akimoto, H. (2003), Global air quality and pollution, *Science*, *302*, 1716-1719.
- Allen, D., K. Pickering, and M. Fox-Rabinovitz (2004), Evaluation of pollutant outflow and CO sources during TRACE-P using model-calculated, aircraft-based, and measurements of Pollution in the Troposphere (MOPITT)-derived CO concentrations, *J. Geophys. Res.*, *109*, D15S03, doi:10.1029/2003JD004250.
- Andreae, M., O., H. Berresheim, and T. W. Andreae (1988), Vertical distribution of dimethyl sulfide, sulfur dioxide, aerosol ions and radon over the northeast pacific ocean, *J. Atmos. Chem.*, *6*, 149– 173.
- Ansari, A. S., and S. N. Pandis (1999a), Prediction of multicomponent inorganic atmospheric aerosol behavior, *Atmos. Environ.*, *33*, 745-757.
- Ansari, A. S., and S. N. Pandis (1999b), An analysis of four models predicting the partitioning of semi-volatile inorganic aerosol components, *Aero. Sci. Tech.*, *31*, 129-153.
- Appel, K. W., A. B. Gilliland, G. Sarwar, and R. C. Gilliam (2007), Evaluation of the community multiscale air quality (CMAQ) model version 4.5: Sensitivities impacting model performance; Part I – Ozone, *Atmos. Environ.*, *41*, 9603-9615.
- Appel, K. W., P. V. Bhave, A. B. Gilliland, G. Sarwar, and S. J. Roselle (2008), Evaluation of community multiscale air quality (CMAQ) model version 4.5: Sensitivities impacting model performance; Part II – particulate matter, *Atmos. Environ.*, *42*, 6057-6066.

- Aulinger, A., V. Matthias, and M. Quante (2007), Introducing a partitioning mechanism for PAHs into the community multiscale air quality modeling system and its application to simulating the transport of benzo(a)pyrene over Europe, *J. Appl. Meteor. Climatol.*, *46*, 1718-1730.
- Bassett, M. E., and J. H. Seinfeld (1983), Atmospheric equilibrium model of sulfate and nitrate aerosol, *Atmos. Environ.*, *17*, 2237 – 2252.
- Bauer, S. E., Y. Balkanski, M. Schulz, D. A. Hauglustaine, and F. Dentener (2004), Global modeling of heterogeneous chemistry on mineral aerosol surfaces: Influence on tropospheric ozone chemistry and comparison to observations, *J. Geophys. Res.*, *109*, D02304, doi:10.1029/2003JD003868.
- Berntsen, T. K., S. Karlsdottir, and D. A. Jaffe (1999), Influence of Asian emissions on the composition of air reaching the North Western United States, *Geophys. Res. Lett.*, *26*(14), 2171-2174.
- Bertschi, I. T., D. A. Jaffe, L. Jaeglé, H. U. Price, and J. B. Dennison (2004), PHOBEA/ITCT 2002 airborne observations of transpacific transport of ozone, CO, volatile organic compounds, and aerosols to the northeast Pacific: Impacts of Asian anthropogenic and Siberian boreal fire emissions, *J. Geophys. Res.*, *109*, D23S12, doi:10.1029/2003JD004328.
- Bey, I., D. J. Jacob, J. A. Logan, and R. M. Yantosca (2001), Asian chemical outflow to the Pacific in spring: origins, pathways, and budgets, *J. Geophys. Res.*, *106*, 23097–23113.

- Bian, H., and C. S. Zender (2003), Mineral dust and global tropospheric chemistry: Relative roles of photolysis and heterogeneous uptake, *J. Geophys. Res.*, *108*, 4672, doi:10.1029/2002JD003143.
- Binkowski, F. S., and S. J. Roselle (2003), Models-3 community multiscale air quality (CMAQ) model aerosol component, 1. Model description, *J. Geophys. Res.*, *108*, 4183, doi:10.1029/2001JD001409.
- Byun, D. W., and K. L. Schere (2006), Review of the governing equations, computational algorithms, and other components of the models-3 Community Multi-scale Air Quality (CMAQ) modeling system, *Appl. Mech. Rev.*, *59*, 51-77.
- Campbell, S. W., M. C. Evans, and N. D. Poor (2002), Predictions of size-resolved aerosol concentrations of ammonium, chloride and nitrate at a bayside site using EQUISOLV II, *Atmos. Environ.*, *36*, 4299-4307.
- Carmichael, G. R., L. K. Peters, and K. Saylor (1991), The Stem-II regional scale acid deposition and photochemical oxidation model-I. An overview of model development and applications, *Atmos. Environ.*, *25A*, 2077-2090.
- Chin, M., P. Ginoux, R. Lucchesi, B. Huebert, R. Weber, T. Anderson, S. Masonis, B. Blomquist, A. Bandy, and D. Thornton (2003), A global aerosol model forecast for the ACE-Asia field experiment, *J. Geophys. Res.*, *108* (D23), 8654, doi:10.1029/2003JD003642.
- Chin, M., T. Diehl, P. Ginoux, and W. Malm (2007), Intercontinental transport of pollution and dust aerosols: Implications for regional air quality, *Atmos. Chem. Phys.*, *7*, 5501-5517.

- Choi, Y.-J., and H. J. S. Fernando (2008), Implementation of a windblown dust parameterization into MODELS-3/CMAQ: Application to episodic PM events in the US/Mexico border, *Atmos. Environ.*, 42, 6039-6046.
- Clegg, S. L., K. S. Pitzer, and P. Brimblecombe (1992), Thermodynamics of multicomponent, miscible, ionic solutions. II. Mixture including unsymmetrical electrolytes, *J. of Phys. Chem.*, 96, 9470-9479.
- Clegg, S. L., P. Brimblecombe, and A. S. Wexler (1998), A thermodynamic model of the system $H^+ - NH_4^+ - Na^+ - SO_4^{2-} - NO_3^- - Cl^- - H_2O$ at 298.15 K, *J. of Phys. Chem.*, 102, 2155-2171.
- Cook, R., et al. (2007), Impact of underestimating the effects of cold temperature on motor vehicle start emissions of air toxics in the United States, *J. Air & Waste Manage. Assoc.*, 57, 1469-1479.
- Dentener, F. J., G. R. Carmichael, Y. Zhang, J. Lelieveld, and P. J. Crutzen (1996), Role of mineral aerosol as a reactive surface in the global troposphere, *J. Geophys. Res.*, 101, 22,869– 22,889.
- Eder, B., and S. Yu (2006), A performance evaluation of the 2004 release of Models-3 CMAQ, *Atmos. Environ.*, 40, 4811-4824.
- Fairlie, T. D., D. J. Jacob, and R. J. Park (2007), The impact of transpacific transport of mineral dust in the United States, *Atmos. Environ.*, 41, 1251-1266.
- Fiore, A., D. J. Jacob, H. Liu, R. M. Yantosca, T. D. Fairlie, and Q. Li (2003a), Variability in surface ozone background over the United States: Implications for air quality policy, *J. Geophys. Res.*, 108(D24), 4787, doi:10.1029/2003JD003855.

- Fiore, A., D. J. Jacob, R. Mathur, and R. V. Martin (2003b), Application of empirical orthogonal functions to evaluate ozone simulations with regional and global models, *J. Geophys. Res.*, *108* (D14), 4431, 10.1029/2002JD003151.
- Fiore, A. M., J. J. West, L. W. Horowitz, V. Naik, and M. D. Schwarzkopf (2008), Characterizing the tropospheric ozone response to methane emission controls and the benefits to climate and air quality, *J. Geophys. Res.*, *113*, D08307, doi:10.1029/2007JD009162.
- Fountoukis, C. and A. Nenes (2007), ISORROPIA II: a computationally efficient thermodynamic equilibrium model for K^+ - Ca^{2+} - Mg^{2+} - NH_4^+ - SO_4^{2-} - NO_3^- - Cl^- - H_2O aerosols, *Atmos. Chem. Phys.*, *7*, 4639-4659.
- Fridlind, A. M., and M. Z. Jacobson (2000), A study of gas-aerosol equilibrium and aerosol pH in the remote marine boundary layer during the First Aerosol Characterization Experiment (ACE 1), *J. Geophys. Res.*, *105*, 17325-17340.
- Ginoux, P., M. Chin, I. Tegen, J. M. Prospero, B. Holben, O. Dubovik, and S. Lin (2001), Sources and distributions of dust aerosols simulated with the GOCART model, *J. Geophys. Res.*, *106*(D17), 22055-22074.
- Goldstein, A. H., D. B. Millet, M. McKay, L. Jaeglé, L. Horowitz, O. Cooper, R. Hudman, D. J. Jacob, S. Oltmans, and A. Clarke (2004), Impact of Asian emissions on observations at Trinidad Head, California, during ITCT 2K2, *J. Geophys. Res.*, *109*, D23S17, doi:10.1029/2003JD004406.

- Goodman, A. L., G. M. Underwood, and V. H. Grassian (2000), A laboratory study of the heterogeneous reaction of nitric acid on calcium carbonate particles, *J. Geophys. Res.*, *105*, 29,053–29,064.
- Grell, G., J. Dudhia, and D. Stauffer (1994), A description of the fifth-generation Penn State/NCAR Mesoscale model (MM5) NCAR Tech. Note NCAR/TN-398+STR, National Center for Atmospheric Research, Boulder, Colorado.
- Heald, C. L., D. J. Jacob, R. J. Park, B. Alexander, T. D. Fairlie, and R. M. Yantosca (2005), Transpacific transport of Asian anthropogenic aerosols and its impact on surface air quality in the United States, *J. Geophys. Res.*, *111*, D14310, doi:10.1029/2005JD006847.
- Hodzic, A, B. Bessagnet, and R. Vautard (2006), A model evaluation of coarse-mode nitrate heterogeneous formation on dust particles, *Atmos. Environ.*, *40*, 4158-4171.
- Horowitz, L. W., et al. (2003), A global simulation of tropospheric ozone and related tracers: Description and evaluation of MOZART, version 2, *J. Geophys. Res.*, *108*(D24), 4784, doi:10.1029/2002JD002853.
- Husar, R. B., et al. (2001), Asian dust events of April 1998, *J. Geophys. Res.*, *106*, 18,317–18,330.
- IPCC (2007), Climate Change 2007: The Physical Science Basis, Contribution of Working Group I to the Fourth Assessment Report of the Intergovernmental Panel on Climate Change [Solomon, S., et al. (eds.)], Cambridge University Press, Cambridge, United Kingdom and New York, NY, USA.

- Jacob, D. J., J. A. Logan, and P. P. Murti (1999), Effect of rising Asian emission on surface ozone in the United States. *Geophys. Res. Lett.*, *26*, 2175–2178.
- Jacob, D., J. Crawford, M. Kleb, V. Connors, R. Bendura, J. Raper, G. Sachse, J. Gille, and L. Emmons (2003), The transport and chemical evolution over the Pacific (TRACE-P) mission: Design, execution, and overview of first results, *J. Geophys. Res.*, *108*(D20), 8781, doi:10.1029/2002JD003276.
- Jacobson, M. Z. (1999), Studying the effects of calcium and magnesium on size-distributed nitrate and ammonium with EQUISOLV II, *Atmos. Environ.*, *33*, 3635-3649.
- Jacobson, M. Z., A. Tabazadeh, and R. P. Turco (1996), Simulating equilibrium within aerosols and nonequilibrium between gases and aerosols, *J. Geophys. Res.*, *101*, 9079-9091.
- Jaeglé, L., D. A. Jaffe, H. U. Price, P. Weiss-Penzias, P. I. Palmer, M. J. Evans, D. J. Jacob, and I. Bey (2003), Sources and budgets for CO and O₃ in the northeastern Pacific during the spring of 2001: Results from the PHOBEA-II Experiment, *J. Geophys. Res.*, *108*, D20, 8802, doi:10.1029/2002JD003121.
- Jaffe, D. A., et al. (1999), Transport of Asian air pollution to North America, *Geophys. Res. Lett.*, *26*, 711–714.
- Jaffe, D. A., I. McKendry, T. Anderson, and H. Price (2003a), Six ‘new’ episodes of trans-Pacific transport of air pollutants. *Atmos. Environ.*, *37*, 391–404.
- Jaffe, D. A., J. Snow, and O. Cooper (2003b), The 2001 Asian dust events: Transport and impact on surface aerosol concentrations in the U.S., *Eos*, *84*(46), 501–516.

- Kelly, T., R. Mukund, C. Spicer, and A. Pollack (1994), Concentrations and transformations of hazardous air pollutants, *Environ. Sci. Technol.*, *28*, 378A-387A.
- Kim, Y. P., J. H. Seinfeld, and P. Saxena (1993a), Atmospheric gas-aerosol equilibrium I. Thermodynamic model, *Aero. Sci. Tech.*, *19*, 157-181.
- Kim, Y. P., J. H. Seinfeld, and P. Saxena (1993b), Atmospheric gas-aerosol equilibrium II. Analysis of common approximations and activity coefficients calculation methods, *Aero. Sci. Tech.*, *19*, 181-198.
- Kumar, N., F. W. Lurmann, S. N. Pandis, and A. S. Ansari (1998), Final Report: analysis of atmospheric chemistry during 1995 integrated monitoring study. Final Report Prepared for the California Air Resources Board, Sacramento, CA, by Sonoma Technology Inc., Santa Rosa, CA.
- Li, H. J., T. Zhu, D. F. Zhao, Z. F. Zhang, and Z. M. Chen (2010), Kinetics and mechanisms of heterogeneous reaction of NO₂ on CaCO₃ surfaces under dry and wet conditions, *Atmos. Chem. Phys.*, *10*, 463–474.
- Li, L., Z. M. Chen, Y. H. Zhang, T. Zhu, J. L. Li, and J. Ding (2006), Kinetics and mechanism of heterogeneous oxidation of sulfur dioxide by ozone on surface of calcium carbonate, *Atmos. Chem. Phys.*, *6*, 2453-2464.
- Liao, H., and J. H. Seinfeld (2005), Global impacts of gas-phase chemistry-aerosol interactions on direct radiative forcing by anthropogenic aerosols and ozone, *J. Geophys. Res.*, *110*, D18208, doi:10.1029/2005JD005907.

- Liao, H., P. J. Adams, S. H. Chung, J. H. Seinfeld, L. J. Mickley, and D. J. Jacob (2003), Interactions between tropospheric chemistry and aerosols in a unified general circulation model, *J. Geophys. Res.*, *108*, 4001, doi:10.1029/2001JD001260.
- Liu, H., D. J. Jacob, I. Bey, R. M. Yantosca, B. N. Duncan, and G. W. Sachse (2003), Transport pathways for Asian pollution outflow over the Pacific: Interannual and seasonal variations. *J. Geophys. Res.*, *108*(D20), 8786, doi:10.1029/2002JD003102.
- Liu, J., D. L. Mauzerall, and L. W. Horowitz (2008), Source-receptor relationship between East Asian sulfur dioxide emissions and Northern Hemisphere sulfate concentrations, *Atmos. Chem. Phys.*, *8*, 3721-3733.
- Liu, M., and D. L. Westphal (2001), A study of the sensitivity of simulated mineral dust production to model resolution, *J. Geophys. Res.*, *106*, 18099-18112.
- Liu, P. and Y. Zhang (2011), Use of a process analysis tool for diagnostic study on fine particulate matter predictions in the U.S. Part I: Model evaluation using surface, aircraft, and satellite data, *Atmos. Pollu. Res.*, *2*(1), 49-60, doi: 10.5094/APR.2011.007.
- Liu, P., Y. Zhang, S.C. Yu, and K. L. Schere (2011), Use of a process analysis tool for diagnostic study on fine particulate matter predictions in the U.S. Part II: Process analyses and sensitivity simulations, *Atmos. Pollu. Res.*, *2*(1), 61-71, doi: 10.5094/APR.2011.008.
- Liu, X.-H., Y. Zhang, S.-H. Cheng, J. Xing, Q. Zhang, D. G. Streets, C. J. Jang, W.-X. Wang, and J.-M. Hao (2010a), Understanding of regional air pollution over China using CMAQ: Part I Performance evaluation and seasonal variation, *Atmos. Environ.*, *44*(20), 2415-2426.

- Liu, X.-H., Y. Zhang, J. Xing, Q. Zhang, K. Wang, D. G. Streets, C. J. Jang, W.-X. Wang, and J.-M. Hao (2010b), Understanding of regional air pollution over China using CMAQ: Part II. Process analysis and ozone sensitivity to precursor emissions, *Atmos. Environ.*, *44*(20), 3719-3727.
- Luecken, D. J., and A. J. Cimorelli (2008), Codependencies of reactive air toxic and criteria pollutants on emission reductions, *J. Air & Waste Manage. Assoc.*, *58*, 693-701.
- Mahowald, N., K. Kohfeld, M. Hansson, Y. Balkanski, S. P. Harrison, I. C. Printice, M. Schulz, and H. Rodhe (1999), Dust sources and deposition during the last glacial maximum and current climate: A comparison of model results with paleodata from ice cores and marine sediments, *J. Geophys. Res.*, *104*, 15,895-15,916.
- Manktelow, P. T., K. S. Carslaw, G. W. Mann, and D. V. Spracklen (2010), The impact of dust on sulfate aerosol, CN and CCN during an East Asian dust storm, *Atmos. Chem. Phys.*, *10*, 365–382.
- Marticorena, B., and G. Bergametti (1995), Modeling the atmospheric dust cycle: 1. Design of a soil-derived dust emission scheme, *J. Geophys. Res.*, *100*(D8), 16,415-16,430.
- Matthias, V., A. Aulinger, and M. Quante (2008), Adapting CMAQ to investigate air quality pollution in North Sea coastal regions, *Env. Mod. and. Sof.*, *23*, 356-368.
- McCarthy, M. C., H. R. Hafner, and S. A. Montzka (2006), Background concentrations of 18 air toxics for North America, *J. Air & Waste Manage. Assoc.*, *56*, 3-11.
- McKendry, I. G., J. P. Hacker, R. Stull, S. Sakiyam, D. Mignacca, and K. Reid (2001), Long-range transport of Asian dust to the Lower Fraser Valley, British Columbia, Canada, *J. Geophys. Res.*, *106*, 18,361-18,370.

- McNaughton et al. (2009), Observations of heterogeneous reactions between Asian pollution and mineral dust over the Eastern North Pacific during INTEX-B, *Atmos. Chem. Phys.*, *9*, 8283–8308.
- Meng, Z., D., Dabdub, and J. H. Seinfeld (1998), Size-resolved and chemically resolved model of atmospheric aerosol dynamics, *J. Geophys. Res.*, *103*, 3419-3435.
- Moya, M., S. N. Pandis, and M. Z. Jacobson (2002), Is the size distribution of urban aerosols determined by thermodynamic equilibrium?: An application to Southern California, *Atmos. Environ.*, *36*, 2349-2365.
- Ndour, M., B. D'Anna, C. George, O. Ka, Y. Balkanski, J. Kleffmann, K. Stemmler, and M. Ammann (2008), Photoenhanced uptake of NO₂ on mineral dust: Laboratory experiments and model simulations, *Geophys. Res. Lett.*, *35*, L05812, doi:10.1029/2007GL032006.
- Ndour, M., P. Conchon, B. D'Anna, O. Ka, and C. George (2009), Photochemistry of mineral dust surface as a potential atmospheric renoxification process, *Geophys. Res. Lett.*, *36*, L05816, doi:10.1029/2008GL036662.
- Nenes, A., C. Pilinis, and S. N. Pandis (1998), ISORROPIA: a new thermodynamic equilibrium model for multiphase multicomponent marine aerosols, *Aquatic Geochemistry* *4*, 123-152.
- Nenes, A., C. Pilinis, and S. N. Pandis (1999), Continued development and testing of a new thermodynamic aerosol module for urban and regional air quality models. *Atmos. Environ.*, *33*, 1553-1560.

- Park, R. J., D. J. Jacob, B. D. Field, R. M. Yantosca, and M. Chin (2004), Natural and trans-boundary pollution influences on sulfate-nitrate-ammonium aerosols in the United States: implications for policy, *J. Geophys. Res.*, *109*, D15204, 10.1029/2003JD004473.
- Parrish, D. D., C. J. Hahn, E. J. Williams, R. B. Norton, F. C. Fehsenfeld, H. B. Singh, J. D. Shetter, B. W. Gandrud, and B. A. Ridley (1992), Indications of photochemical histories of Pacific air masses from measurements of atmospheric trace species at Point Arena, California, *J. Geophys. Res.*, *97*(D14), 15,883-15901.
- Parrish, D. D., Y. Kondo, O. R. Cooper, C. A. Brock, D. A. Jaffe, M. Trainer, T. Ogawa, G. Hübler, and F. C. Fehsenfeld (2004), Intercontinental Transport and Chemical Transformation 2002 (ITCT 2K2) and Pacific Exploration of Asian Continental Emission (PEACE) experiments: An overview of the 2002 winter and spring intensives. *J. Geophys. Res.*, *109*, D23S01, doi:10.1029/2004JD004980.
- Pilinis, C., and J. H. Seinfeld (1987), Continued development of a general equilibrium model for inorganic multicomponent atmospheric aerosols, *Atmos. Environ.*, *21*, 2453-2466.
- Pozzoli, L., I. Bey, S. Rast, M. G. Schultz, P. Stier, and J. Feichter (2008a), Trace gas and aerosol interactions in the fully coupled model of aerosol-chemistry-climate ECHAM5-HAMMOZ: 1. Model description and insights from the spring 2001 TRACE-P experiment, *J. Geophys. Res.*, *113*, D07308, doi:10.1029/2007JD009007.
- Pozzoli, L., I. Bey, S. Rast, M. G. Schultz, P. Stier, and J. Feichter (2008b), Trace gas and aerosol interactions in the fully coupled model of aerosol-chemistry-climate ECHAM5-HAMMOZ: 2. Impact of heterogeneous chemistry on the global aerosol distributions, *J. Geophys. Res.*, *113*, D07309, doi:10.1029/2007JD009008.

- Queen, A., Y. Zhang, R. Gilliam, and J. Pleim (2008), Examining the sensitivity of MM5-CMAQ predictions to explicit microphysics schemes and horizontal grid resolutions, Part I—Database, evaluation protocol, and precipitation predictions, *Atmos. Environ.*, *42*, 3842-3855.
- Queen, A. and Y. Zhang (2008), Examining the sensitivity of MM5-CMAQ predictions to explicit microphysics schemes and horizontal grid resolutions, Part II— PM concentrations and wet deposition predictions, *Atmos. Environ.*, *42*, 3856-3868.
- Queen, A. and Y. Zhang (2008), Examining the sensitivity of MM5-CMAQ predictions to explicit microphysics schemes and horizontal grid resolutions, Part III— The impact of horizontal grid resolution, *Atmos. Environ.*, *42*, 3869-3881.
- Rodriguez, M. A., and D. Dabdub (2004), IMAGES-SCAPE2: A modeling study of size- and chemically resolved aerosol thermodynamics in a global chemical transport model, *J. Geophys. Res.*, *109*, D02203.
- Roselle, R., D. J. Luecken, W. T. Hutzell, O. R. Bullock, G. Sarwar, and K. L. Schere (2007), Development of a multipollutant version of the Community Multiscale Air Quality (CMAQ) modeling system, presentation at the 6th annual CMAQ conference, Chapel Hill, NC, October 1-3.
- Rosenbaum, A. S., D. A. Axelrad, T. J. Woodruff, Y. H. Wei, M. P. Ligoeki, and J. P. Cohen (1999), National estimates of outdoor air toxics concentrations, *J. Air & Waste Manage. Assoc.*, *49*, 1138-1152.
- Satheesh, S. K., and K. K. Moorthy (2005), Radiative effects of natural aerosols: A review, *Atmos. Environ.*, *39*, 2089-2110.

- Saxena, P., A. B. Hudischewskyj, C. Seigneur, and J. H. Seinfeld (1986) A comparative study of equilibrium approaches to the chemical characterization of secondary aerosols, *Atmos. Environ.*, *20*, 1471-1483.
- Scheffe, R., B. Hubbell, T. Fox, V. Rao, and W. Pennell (2007), The Rationale for a multipollutant, multimedia air quality management framework, *EM*, May, 14-20.
- Seinfeld, J. H., and S. N. Pandis (2006), *Atmospheric Chemistry and Physics: From Air Pollution to Climate Change*, 2nd ed., Wiley, New York.
- Seinfeld, J. H., et al. (2004), ACE-ASIA: Regional climatic and atmospheric chemical effects of Asian dust and pollution, *Bull. Amer. Meteor. Soc.*, *85*(3), 367-380.
- Shao, Y. (2001), A model for mineral dust emission, *J. Geophys. Res.*, *106*, 20,239-20,254.
- Song, C. H., C. M. Kim, Y. J. Lee, G. R. Carmichael, B. K. Lee, and D. S. Lee (2007), An evaluation of reaction probabilities of sulfate and nitrate precursors onto East Asian dust particles, *J. Geophys. Res.*, *112*, D18206, doi:10.1029/2006JD008092.
- Stohl, A., S. Eckhardt, C. Forster, P. James, and N. Spichtinger (2002), On the pathways and timescales on intercontinental air pollution transport, *J. Geophys. Res.*, *107*(D23), 4684, doi:10.1029/2001JD001396.
- Tanaka, T. (2007), Global dust budget, in *Encyclopedia of Earth*, edited by H. Hanson.
- Tang, M. J., J. Thieser, G. Schuster, and J. N. Crowley (2010), Uptake of NO₃ and N₂O₅ to Saharan dust, ambient urban aerosol and soot: a relative rate study, *Atmos. Chem. Phys.*, *10*, 2965–2974.
- Tegen, I., and I. Fung (1994), Modeling of mineral dust in the atmosphere: Source, transport, and optical thickness, *J. Geophys. Res.*, *99*(D11), 22,897-22,914.

- Tesche, T. W., R. Morris, G. Tonnesen, D. McNally, J. Boylan, and P. Brewer (2006), CMAQ/CAMx annual 2002 performance valuation over the eastern US, *Atmos. Environ.*, *40*, 4906-4919.
- Tie, X., S. Madronich, S. Walters, D. P. Edwards, P. Ginoux, N. Mahowald, R. Zhang, C. Lou, and G. Brasseur (2005), Assessment of the global impact of aerosols on tropospheric oxidants, *J. Geophys. Res.*, *110*, D03204, doi:10.1029/2004JD005359.
- U.S. EPA (2005), Technical support document for the Clean Air Interstate Rule: Air quality modeling, Office of Air Quality Planning and Standards, Research Triangle Park, NC, Docket No. OAR-2005-0053-2151.
- Underwood, G. M., C. H. Song, M. Phadnis, G. R. Carmichael, and V. H. Grassian (2001), Heterogeneous reactions of NO₂ and HNO₃ on oxides and mineral dust: A combined laboratory and modeling study, *J. Geophys. Res.*, *106*, 18,055– 18,066.
- Uno I., et al. (2003), Regional chemical weather forecasting system CFORS: Model descriptions and analysis of surface observations at Japanese island stations during the ACE-Asia experiment, *J. Geophys. Res.*, *108*(D23), 8668, doi:10.1029/2002JD002845.
- VanCuren, R. A. (2003), DELTA Group, Asian aerosols in North America: Extracting the chemical composition and mass concentration of the Asian continental aerosol plume from long-term aerosol records in the western United States, *J. Geophys. Res.*, *108*(D20), 4623, doi:1029/2003JD003459.
- Wagner, C., F. Hanisch, N. Holmes, H. de Coninck, G. Schuster, and J. N. Crowley (2008), The interaction of N₂O₅ with mineral dust: aerosol flow tube and Knudsen reactor studies, *Atmos. Chem. Phys.*, *8*, 91–109.

- Wang, B. (2006), Intercontinental and regional modeling of air pollutants transport over the Pacific regions, Ph.D. thesis, 183 pp., North Carolina State University, Raleigh.
- Wang, K., Y. Zhang, C. Jang, S. Phillips, and B. Wang (2009a), Modeling intercontinental air pollution transport over the trans-Pacific Region in 2001 using community multiscale air quality (CMAQ) model, *J. Geophys. Res.*, *114*, D04307, doi:10.1029/2008JD010807.
- Westphal, D. L., O. B. Toon, and T. N. Carlson (1987), A two-dimensional numerical investigation of the dynamics and microphysics of Saharan dust storms, *J. Geophys. Res.*, *92*(D3), 3027-3049.
- Wexler, A. S., and J. H. Seinfeld (1991), Second-generation inorganic aerosol model, *Atmos. Environ.*, *25A*, 2731-2748.
- Wu, S.-Y., S. Krishnan, Y. Zhang, and V. Aneja (2008a), Modeling atmospheric transport and fate of ammonia in North Carolina, Part I. Evaluation of meteorological and chemical predictions, *Atmos. Environ.*, *42*, 3419–3436.
- Wu, S.-Y., J.-L., Hu, Y. Zhang, and V. P. Aneja (2008b), Modeling atmospheric transport and fate of ammonia in North Carolina, Part II. Effect of ammonia emissions on fine particulate matter formation, *Atmos. Environ.*, *42*, 3437–3451.
- Yienger, J. J., M. Galanter, T. A. Holloway, M. J. Phadnis, S. K. Guttikunda, G. R. Carmichael, W. J. Moxim, and H. Levy II (2000), The episodic nature of air pollution transport from Asia to North America, *J. Geophys. Res.*, *105*, 26,931– 26,946.

- Yue, X., H. Wang, Z. Wang, and K. Fan (2009), Simulation of dust aerosol radiative feedback using the Global Transport Model of Dust: 1. Dust cycle and validation, *J. Geophys. Res.*, *114*, D10202, doi:10.1029/2008JD010995.
- Zaveri, R. A., R. C. Easter, and A. S. Wexler (2005a), A computationally efficient multicomponent equilibrium solver for aerosols (MESA), *J. Geophys. Res.*, *110*, D24203, doi:10.1029/2004JD005618.
- Zaveri, R. A., R. C. Easter, and A. S. Wexler (2005b), A new method for multicomponent activity coefficients of electrolytes in aqueous atmospheric aerosols, *J. Geophys. Res.*, *110*, D02201, doi:10.1029/2004JD004681.
- Zender, C. S., H. Bian, and D. Newman (2003), Mineral Dust Entrainment and Deposition (DEAD) model: Description and 1990s dust climatology, *J. Geophys. Res.*, *108(D14)*, 4416, doi:10.1029/2002JD002775.
- Zhang, M., et al. (2003), Large-scale structure of trace gas and aerosol distributions over the western Pacific Ocean during the Transport and Chemical Evolution Over the Pacific (TRACE-P) experiment, *J. Geophys. Res.*, *108(D21)*, 8820, doi:10.1029/2002JD002946.
- Zhang, M., I. Uno, R. Zhang, Z. Han, Z. Wang, and Y. Pu (2006), Evaluation of the Models-3 Community Multi-scale Air Quality (CMAQ) modeling system with observations obtained during the TRACE-P experiment: Comparison of ozone and its related species, *Atmos. Environ.*, *40*, 4874-4882.
- Zhang, Y., and G.R. Carmichael (1999), The Role of mineral aerosol in tropospheric chemistry in East Asia - a model study, *Jrn. Appl. Meteor.*, *38(3)*, 353-366.

- Zhang, Y., Y. Sunwoo, V. Kotamarthi, and G. R. Carmichael (1994), Photochemical oxidant processes in the presence of dust: An evaluation of the impact of dust on particulate nitrate and ozone formation, *J. Appl. Meteorol.*, *33*, 813– 824.
- Zhang, Y., C. Seigneur, J. H. Seinfeld, M. Jacobson, S. L. Clegg, and F. S. Binkowski (2000), A comparative review of inorganic aerosol thermodynamic equilibrium modules: similarities, differences, and their likely causes, *Atmos. Environ.*, *34*, 117-137.
- Zhang, Y., B. Pun, S.-Y. Wu, K. Vijayaraghavan, and C. Seigneur (2004), Application and evaluation of two air quality models for particulate matter for a Southeastern U.S. episode, *J. Air & Waste Manage. Assoc.*, *54*, 1478-1493.
- Zhang, Y., P. Liu, B. Pun, and C. Seigneur (2006a), A comprehensive performance evaluation of MM5-CMAQ for the Summer 1999 Southern Oxidants Study episode- Part I: Evaluation protocols, databases, and meteorological predictions, *Atmos. Environ.*, *40*, 4825-4838.
- Zhang, Y., P. Liu, A. Queen, C. Misenis, B. Pun, and C. Seigneur (2006b), A comprehensive performance evaluation of MM5-CMAQ for the Summer 1999 Southern Oxidants Study episode-Part II: Gas and aerosol predictions, *Atmos. Environ.*, *40*, 4839-4855.
- Zhang, Y., P. Liu, B. Pun, and C. Seigneur (2006c), A comprehensive performance evaluation of MM5-CMAQ for the Summer 1999 Southern Oxidants Study episode- Part III: Diagnostic and mechanistic evaluations, *Atmos. Environ.*, *40*, 4856-4873.
- Zhang, Y., J.-P. Huang, D. K. Henze, and J. H. Seinfeld (2007), The role of isoprene in secondary organic aerosol formation on a regional scale, *J. Geophys. Res.*, *112*, D20207, doi:10.1029/2007JD008675.

Zhang, Y., K. Vijayaraghavan, X.-Y. Wen, H. E. Snell, and M. Z. Jacobson (2009a), Probing into regional O₃ and PM pollution in the U.S., Part I: A 1-year CMAQ simulation and evaluation using surface and satellite data, *J. Geophys. Res.* *114*, D22304, doi:10.1029/2009JD011898.

Zhang, Y., X.-Y. Wen, K. Wang, K. Vijayaraghavan, and M. Z. Jacobson (2009b), Probing into regional O₃ and PM pollution in the U.S., Part II: An examination of formation mechanisms through a process analysis technique and sensitivity study, *J. Geophys. Res.* *114*, D22305, doi:10.1029/2009JD011900.

Zimmermann, P. H. (1988), Moguntia: A handy global tracer model in *Air Pollution Modeling and its Applications*, vol. VI, edited by H. van Dop, Plenum, New York.

Table 2.1. Similarities and differences of several major dust flux schemes.

| | Simple | | Intermediate | | Advanced |
|---------------------------------------|---|-----------------------------------|---|--|--|
| Example References | Westphal et al., 1987; Liu and Westphal, 2001 | Choi and Fernando, 2008 | Ginoux et al., 2001 | Zender et al., 2003 | Marticorena and Bergametti, 1995 |
| Flux calculation * | Vertical flux; u_*^3 and u_*^4 | Vertical flux; u_*^3 or u_*^4 | Horizontal flux; u_{10}^3 and u_t | Horizontal flux and vertical flux; u_*^3 and u_{*t} | Horizontal flux and vertical flux; u_*^3 and u_{*t} |
| Factors affecting threshold velocity | Constant | Soil texture and moisture | Soil particle size, density, and moisture | Soil particle size, density, moisture, and surface roughness | Soil particle size, density, moisture, and surface roughness |
| Flux dependence on the particle sizes | No | No | Yes, different size bins | Yes, but assume a constant | Yes, continuous for any size |
| Size distribution | 30 bins | Modal | 7 bins | 3 or 4 bins | Continuous to any size |
| Topographic consideration | No | No | Yes | Yes | No |
| Erodible flux fraction consideration | Yes; based on land types | Yes; based on land types | Yes; based on soil texture | Yes; based on roughness length | Yes; based on roughness length |
| Host 3-D Models [§] | COAMPS | CMAQ | GOCART | GEOS-Chem | N/A |

* u_* : the surface friction velocity; u_{*t} : the threshold surface friction velocity; u_{10} : the mean 10 m velocity; u_t : the threshold 10 m velocity.

[§]COAMPS: the Navy's operational Coupled Ocean/Atmosphere Mesoscale Prediction System model; CMAQ: the Community Multiscale Air Quality Model; GOCART: the Georgia Tech/Goddard Global Ozone Chemistry Aerosol Radiation and Transport model; GEOS-Chem: the global 3-D model of atmospheric composition driven by the Goddard Earth Observing System (GEOS).

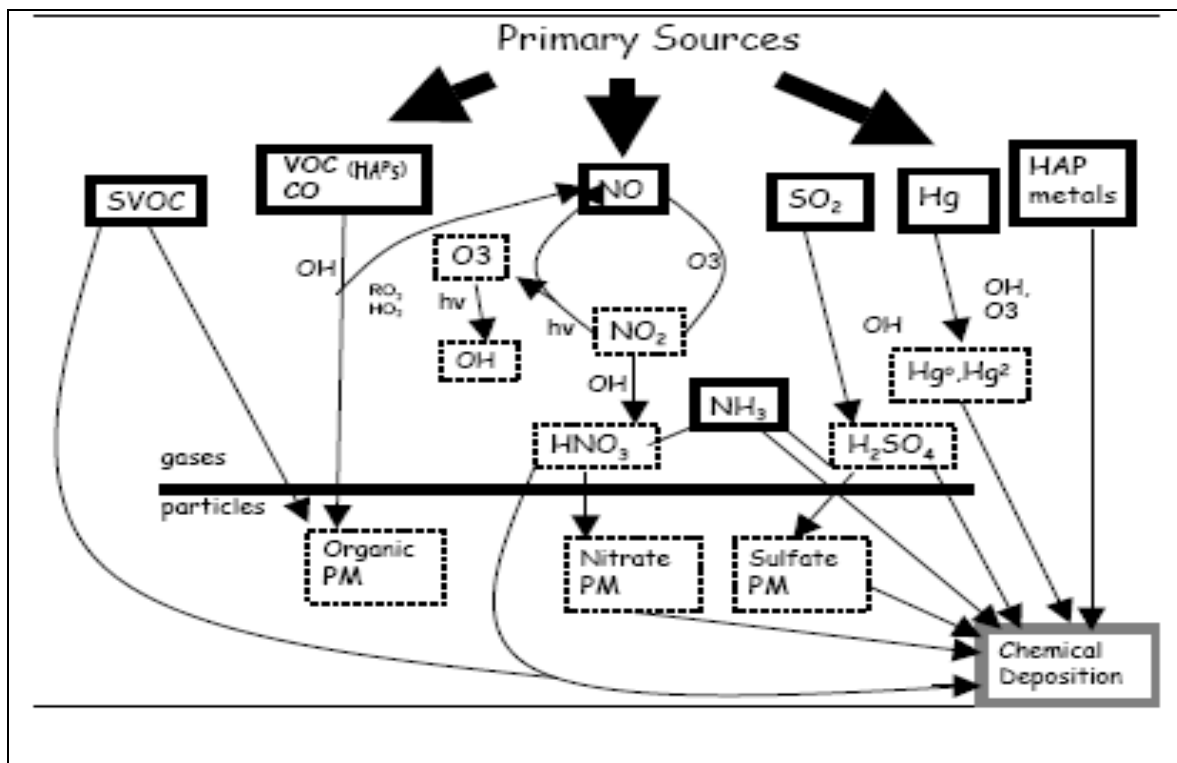


Figure 2.1. Chemical linkages illustrating relationships across CAPs and HAPs. Note that this diagram is a highly-condensed one that does not capture numerous heterogeneous processes and complex chemical pathways. Key atmospheric species that are involved in many reactions across pollutant categories include O_3 and hydroxyl radical (OH). Primary PM emissions are not included (adopted from Scheffe et al., 2007; note that other pollutants not defined in the text include semi-VOC (SVOC), alkyl peroxy (RO_2), sulfuric acid (H_2SO_4), and hydroperoxyl radical (HO_2)).

CHAPTER 3. STUDY OF TRANS-PACIFIC TRANSPORT USING CMAQ

3.1. Introduction

In this section, the U.S. EPA's CMAQ modeling system (Binkowski and Roselle, 2003; Byun and Schere, 2006) is applied to simulate trans-Pacific transport of major gaseous and aerosol species such as O_3 and $PM_{2.5}$ to understand their formation and transport mechanisms as well as impacts on regional air quality over N.A. This study is part of the U.S. EPA's ICAP project. The ICAP project was initiated in 2001 to better quantify the intercontinental transport of air pollutants and to provide scientifically-sound information for the development of integrated air quality and climate control strategies (ICAP, 2005). As introduced in Chapter 2, CMAQ is a comprehensive Eulerian 3-D model driven by meteorological inputs, generated offline from mesoscale meteorological models such as MM5 (Grell et al., 1994). Additionally, detailed process analysis (PA) tool embedded in CMAQ is applied to provide insights into the relative contributions of atmospheric processes for major air pollutants. CMAQ simulations are conducted for the year of 2001, during which frequent intercontinental transport and dust storms events were observed, especially in spring. The model performance of meteorological and chemical predictions is evaluated with available ground, aircraft, and satellite observational data. The magnitudes, mechanisms/pathways, and impacts of Asian pollution export are examined through PA and sensitivity simulations.

3.2. Model Configurations, Evaluation Protocols, and Observational Databases

3.2.1 Model Setup and Inputs

CMAQ version 4.4 is applied to the trans-Pacific domain of ICAP with a 108-km horizontal grid resolution. CB-IV gas-phase mechanism and aerosol module AERO3 are used. PA embedded in CMAQ is an analytical technique (Zhang et al., 2005c) to estimate the relative contribution of various atmospheric processes (e.g., transport and chemistry) to the formation and fate of air pollutants. CMAQ includes two types of PA: Integrated Process Rates (IPRs) and Integrated Reaction Rates (IRRs) (Byun and Ching, 1999). The IPRs determine the relative contributions of individual physical processes and the net effect of chemistry on model predictions, where the major processes include transport, emission, chemistry, aerosol and cloud processes, and deposition. The IRRs track individual chemical pathways, permitting a detailed study of the chemical transformation of various species of interest and their relative importance (Jeffries and Tonnesen, 1994; Jang et al., 1995a, 1995b). The baseline simulations with PA are conducted for four representative months (i.e., January, April, July, and October) in 2001. The model domain covers most of continental Asia and North America, northern Pacific Ocean and western Atlantic Ocean with 180×74 horizontal grid cells, as shown in Figure 3.1. The vertical resolution includes 16 layers from the surface to approximately 100 hPa (at ~16 km) with a finer spacing within the PBL. The 16 layers correspond to sigma levels of 0.995, 0.988, 0.980, 0.970, 0.956, 0.938, 0.893, 0.839, 0.777, 0.702, 0.582, 0.500, 0.400, 0.300, 0.200, and 0.000. The first model layer height is set to be ~35 m above the ground level (AGL).

The meteorological field is generated by the MM5 version 3.6 with four-dimensional

data assimilation (FDDA). MM5 simulations are initialized using several different data sources including the U.S. Geological Survey (USGS) land use data, the European Center for Medium-Range Weather Forecasts (ECMWF) Tropical Ocean-Global Atmosphere (TOGA) data, and surface observations, and rawinsonde observations (ICAP, 2005). The physical options used include the Pleim-Xiu PBL and land surface parameterization schemes (Xiu and Pleim, 2001; Pleim and Xiu, 2003); a mixed-phase explicit moisture scheme (Reisner et al., 1998); the Kuo cumulus cloud parameterization scheme (Kuo and Raymond, 1980); and a simple radiation scheme (Dudhia 1989). The MM5 hourly outputs are converted to CMAQ compatible meteorological inputs with the Meteorology-Chemistry Interface Processor (MCIP) version 2.2.

The emission inputs for CMAQ are generated using the Sparse Matrix Operator Kernel Emissions (SMOKE) model version 1.4 by integrating estimated emissions from diverse sources and regions. The emission data for U.S. is based on the National Emissions Inventory (NEI) 1999 version 1 including point, area, and mobile (on-road and nonroad) sources. The emission inventory for Mexico is prepared from the Big Bend Regional Aerosol and Visibility Observational Study (BRAVO) 1999 database that also includes point, area, and mobile sources. For Canada, the 1995 area and mobile (on-road and non-road) source inventory is used. The emission data for the offshore (i.e., the Gulf of Mexico) sources are from the 1992 inventory of the U.S. (federal) point sources located over most of the western Gulf (ICAP, 2005). The emission inventory in Asia is generated from the Transport and Chemical Evolution over the Pacific (TRACE-P) and the Aerosol Characterization Experiment-Asia (ACE-Asia) data (Streets et al., 2003), which includes 10

different anthropogenic emission sectors: aviation, biomass burning, domestic biofuels, domestic fossil fuels, industry, point sources, power, shipping, transportation, and others. The biogenic emissions for the domain are prepared using the Biogenic Emissions Inventory System (BEIS) version 3.9 with Biogenic Emissions Land cover Database version 3 (BELD3) data. Emissions from continuously emitting volcanoes are also included based on the Global Emissions Inventory Activity (GEIA).

The boundary conditions (BCONs) and initial conditions (ICONS) for the trans-Pacific domain are prepared using a global chemical transport model, GEOS-CHEM ($2^\circ \times 2.5^\circ$ horizontal spacing and a temporal resolution of 3-hour) (Bey et al., 2001; Park et al., 2004). A 15-day spin-up period (January 1-15, 2001) is used to minimize the influence of ICONs that are generated by the global GEOS-CHEM simulation (Fiore et al., 2003a). The four 1-month baseline simulations with PA are analyzed to quantify the amount of export, identify the key contributing processes/reactions for key pollutants, and study associated seasonality. A sensitivity simulation without Asian anthropogenic emissions (AAEs) has also been conducted for April to investigate the impact of AAEs to U.S. during the strong Asian air pollution export season.

3.2.2 Model Evaluation Protocol and Available Measurements

Model evaluation is conducted in terms of spatial distributions, temporal variations, vertical profiles, and column abundances. A set of traditional statistic metrics (e.g., Seigneur et al., 2000; Zhang et al., 2006a) developed based on the protocols from U.S. EPA (2001, 2007) are used. The statistical measures used here include the correlation coefficient (R), the normalized mean bias (NMB), and the normalized mean error (NME).

The model results are evaluated with available ground, aircraft, and satellite-based measurements, as summarized in Table 3.1. Over the U.S., the meteorological, gaseous, and aerosol measurements are taken from several routine monitoring networks including the Clean Air Status and Trends Network (CASTNET), the Interagency Monitoring of Protected Visual Environments (IMPROVE), the Speciation Trends Network (STN), the Aerometric Information Retrieval System (AIRS)-Air Quality System (AQS), the Southeastern Aerosol Research and Characterization study (SEARCH), and the National Acid Deposition Program (NADP). While most of the CASTNET sites are rural sites largely located in the eastern U.S., the majority of the IMPROVE sites are located in national parks and remote sites in the western U.S. and most of the STN sites are found in urban areas. A detailed description of the networks, including sampling protocols, standard operating procedures, and data quality/uncertainties, can be found in Eder and Yu (2006) and Zhang et al. (2006a).

Over Asia, several ground-based datasets over China and Japan are used for model evaluation. These include the hourly or 3-hour meteorological data (i.e., 2-m temperature (T2), 2-m water vapor mixing ratio (QV2), wind speed and wind direction at 10-m (WS10 and WD10, respectively), and 24-hr precipitation at ~400 sites from the National Climate Data Center (NCDC) of NOAA (<http://cdo.ncdc.noaa.gov/CDO/cdo>) over China; the daily-average concentrations of sulfur dioxide (SO₂), nitrogen dioxide (NO₂), and particulate matter with aerodynamic diameter less than or equal to 10 μm (PM₁₀), and max 1-hr concentrations of CO and O₃ at 8 sites from the National Environmental Monitoring Centre of China (NEMCC; <http://www.sepa.gov.cn/english/airqualityinfo.htm>), which were post-processed by Tsinghua University, Beijing; and the monthly-average concentrations of SO₂,

nitric oxide (NO), NO₂, CO, and Suspended Particle Matter (SPM; with aerodynamic diameter less than and equal to 7.0 μm) over ~1000 sites in Japan from the National Institute for Environmental Studies (NIES). The aircraft data of CO, SO₄²⁻, NO₃⁻, and NH₄⁺ collected by the TRACE-P experiment campaign have been used previously by Wang (2006) for vertical profile evaluation over Pacific regions. Evaluation of vertical profiles of pollutants can help assess the ability of CMAQ in reproducing the transport and chemistry of air pollutants on a hemispheric scale. The aircraft mission with two airplanes, namely DC-8 and P-3B during TRACE-P was conducted in February – April 2001 over the northwestern Pacific region. More details about the design and execution of this aircraft mission can be found from Jacob et al. (2003).

In addition, satellite measurements have been used for model evaluation. These include the tropospheric CO column abundances from the Measurements of Pollution in the Troposphere (MOPITT) (Deeter et al., 2003), the tropospheric NO₂ column abundances from the Global Ozone Monitoring Experiment (GOME) (Burrows, et al., 1999), and the tropospheric O₃ residuals (TORs) derived from the Total Ozone Mapping Spectrometer (TOMS) and the Solar Backscattered Ultraviolet (SBUV) (Fishman et al., 2003), and the aerosol optical depths (AODs) from the Moderate Resolution Imaging Spectroradiometer (MODIS) (Chu et al., 2003; Remer et al., 2005). The MODIS sensor aboard NASA's Terra and Aqua satellite platforms has 36 spectral channels (compared to 4-8 for most sensors) ranged from 0.41 to 15 μm, which bestow MODIS the unique ability to retrieve AOD with much higher accuracy. The MODIS sensor was designed to systematically retrieve aerosol properties over both land and ocean on a daily basis. The MODIS data from the Terra (and

Aqua) satellite provide a daily late-morning view of aerosol and cloud distributions over most of the globe. Terra orbits cross the equator at 10:30 local time. The MODIS data used in this study are monthly averaged level 3 AOD products over both land and ocean at 0.55 μm with a resolution of $1^\circ \times 1^\circ$ retrieved from MOD04-level2 aerosol products from Terra satellite. The MOPITT instrument also aboard the Terra satellite allows retrieval of tropospheric column CO with a horizontal resolution of 22 km by emitting infrared radiation at 4.7 μm in the atmosphere. Global coverage is achieved over cloud-free regions every 3 days. The MOPITT data used here are also monthly averaged column CO with a resolution of $1^\circ \times 1^\circ$. The GOME instrument located on the European Space Agency's (ESA) Second European Remote Sensing Satellite (ERS-2), measures the sunlight scattered from the atmosphere and/or reflected by the surface in nadir viewing geometry ranged from 240 to 790 nm at a spectral resolution of between 0.2 and 0.4 nm. The horizontal resolution of a GOME ground pixel is $40 \times 320 \text{ km}^2$ for the majority of the orbits. The monthly averaged tropospheric column NO_2 used in this study is retrieved from GOME level 2 products with a resolution of $1^\circ \times 1^\circ$. TOMS instrument have been on board a couple of satellites (e.g., Nimbus-7 operated from 1978 through 1993 and Earth Probe operated from 1996 through 2005). The monthly averaged TOR used in this study is retrieved from total ozone column from TOMS and stratospheric ozone profiles from the Solar Backscattered Ultraviolet (SBUV) instruments with a resolution of $1^\circ \times 1.25^\circ$ (Fishman et al., 2003).

The column abundances of CO, NO_2 , and O_3 are calculated using both mass concentrations from CMAQ and meteorological data (i.e., temperature, pressure, and layer thickness) from MM5 outputs and converted into units of $10^{18} \text{ molecules cm}^{-2}$, 10^{14}

molecules cm^{-2} , and Dobson Unit (DU), respectively. CMAQ does not calculate AODs. Following the implementation method of Zhang et al. (2005a, b, 2008, 2009), AODs are estimated based on CMAQ $\text{PM}_{2.5}$ predictions using an empirical equation of Chameides et al. (2002):

$$AOD_{\text{model}} = \sum_{i=1}^N (\sigma_{sp} + \sigma_{ap})_i \times \Delta z_i \quad (1)$$

where σ_{sp} is the scattering coefficient and σ_{ap} is the specific absorption coefficient (both in unit of m^{-1}), Δz_i is the layer thickness (in unit of m), and N is the total number of layers (=16 for the CMAQ simulation in this study).

$$\begin{aligned} \sigma_{sp} &= \sigma_{sp}^{SO_4} + \sigma_{sp}^{NO_3} + \sigma_{sp}^{OC} + \sigma_{sp}^{BC} \\ &= \{ [SO_4] \times \alpha_{sp}^{SO_4} + [NO_3] \times \alpha_{sp}^{NO_3} + [OC] \times \alpha_{sp}^{OC} + [BC] \times \alpha_{sp}^{BC} \} \times f(RH) / 1.0 \times 10^6 \end{aligned} \quad (2)$$

where $\sigma_{sp}^{SO_4}$, $\sigma_{sp}^{NO_3}$, σ_{sp}^{OC} , and σ_{sp}^{BC} are the scattering coefficients for SO_4^{2-} , NO_3^- , OC, and BC (or element carbon (EC)) in the $\text{PM}_{2.5}$ size section, $[SO_4]$, $[NO_3]$, $[OC]$, and $[BC]$ indicate the mass concentrations of SO_4^{2-} , NO_3^- , OC, and BC in $\mu\text{g m}^{-3}$ simulated by CMAQ. The values for specific scattering coefficients (α_{sp}^i) for species i are $\alpha_{sp}^{SO_4} = \alpha_{sp}^{NO_3} = \alpha_{sp}^{OC} = 5.0 \text{ m}^2 \text{ g}^{-1}$, and $\alpha_{sp}^{BC} = 3.0 \text{ m}^2 \text{ g}^{-1}$. $f(RH)$ accounts for the effect of relative humidity on scattering due to deliquescence and is assumed to be 2.3 in this study following Chameides et al. (2002). Also, note that fine NH_4^+ and other organic elements (defined as the non-carbonaceous elements associated with OC such as oxygen and nitrogen) are implicitly included the calculation of σ_{sp} for other species. The absorption from BC-containing aerosols is considered as,

$$\sigma_{ap} = \left\{ [BC]_{hydrophobic} \times \alpha_{ap}^{hydrophobic} + [BC]_{hydrophilic} \times \alpha_{ap}^{hydrophilic} \right\} / 1.0 \times 10^6 \quad (3)$$

where $\alpha_{ap}^{hydrophobic}$ and $\alpha_{ap}^{hydrophilic}$ are the specific absorption coefficients for hydrophobic and hydrophilic BC aerosols, =10.0 and 20.0 m² g⁻¹, respectively. The coefficient of 1×10^6 in Eqs. (2) and (3) converts the concentration from $\mu\text{g m}^{-3}$ to g m^{-3} . The mass concentration of hydrophobic BC is assumed to be 10% of total BC. Fine- and coarse-mode AODs can be derived from MODIS level 3 1°×1° quality assurance products, which correspond to AODs of particles with geometric mean diameter of 0.01- 0.22 μm and 1.0-12.5 μm , respectively, over land and of 0.12- 0.2 μm and 0.8-1.6 μm , respectively, over ocean (Remer et al., 2005; Kaufman et al., 2005). The total MODIS-derived AODs from TERRA satellite are used for model evaluation in this study. Since the MODIS-defined fine-mode AODs can only represent a portion of PM_{2.5} AODs, it is appropriate to compare the total MODIS-derived AODs (i.e., the sum of fine- and coarse-mode AODs) with the PM_{2.5} AODs calculated based on CMAQ PM_{2.5} predictions which are nearly the same as the simulated total AODs because this version of CMAQ does not simulate the emissions, governing processes, and chemical and radiative properties of coarse PM such as sea-salt and dust (except for accounting for the background concentrations of coarse PM).

3.3 Meteorological Predictions

A preliminary performance evaluation of MM5 simulations has been previously conducted by the ICAP project team, in which the National Centers for Environmental Prediction (NCEP) analyses data (e.g., temperature, water vapor mixing ratio, and wind speed and direction at different heights) were used. A brief summary of this performance is

provided below, more details can be found in ICAP (2005). MM5 simulation basically captures the location of synoptic troughs and ridges over Asia and N.A. as well as the Pacific with a few regional differences such as the relatively cooler pool of air over the U.S. at 1000 hPa and 850 hPa compared to the NCEP data. Similarly, the simulated water vapor mixing ratios at 1000 hPa are lower. Seasonal analysis shows a negative bias (colder than observations) in simulated surface temperature, especially during spring and summer, although MM5 basically captures the seasonal trend. Wind speed and direction, which are critical parameters for transport processes, are well predicted by MM5 at four representative altitudes (i.e., 1000 hPa, 850 hPa, 500 hPa, and 250 hPa). In this study, MM5 predictions for the four months are further evaluated over the contiguous U.S. and China using the observed T2, 2-m relative humidity (RH2), WS10, and WD10, and precipitation from all surface monitoring networks as summarized in Table 3.1.

3.3.1 Continental U.S.

Figure 3.2 shows the spatial plots of NMBs between observational data and MM5 simulations for T2, RH2, and weekly precipitation over the U.S. for the four months in 2001. Table 3.2 summarizes the monthly mean performance statistics. The simulated WS at ~20 m (i.e., the midpoint of the first layer of CMAQ) is interpolated to 10-m WS based on Hogstrom's surface similarity theory (Hogstrom et al., 1988) to be compared with the observed 10-m WS. Simulated T2 exhibits a cold bias (with MBs of -0.4°C to -3.8°C) throughout all four months, which is consistent with that of previous NCEP analysis. The model performance varies from season to season with the best in July (NMBs of -0.9% to -10% and NMEs of 10.7% to 12.1%) and the worst in January (NMBs of -38.1% to -54.3%

and NMEs of 43.2% to 75.0%). Such cold biases can be attributed to several reasons including the slow responses of deep soil temperature to synoptic-scale changes in air temperatures and the limitations of the PBL and land-surface schemes currently used in meteorological models in accurately simulating the air-land heat fluxes (Gilliam et al., 2006); the domain-wide underpredictions of skin temperature by MM5 over both the U.S. and China against the NCEP reanalysis results (figures not shown here), the limitations of radiation schemes currently used (Dudhia, 1989, 1993), as well as the incapability of the models at a coarse grid resolution in capturing fine-scale meteorological phenomena. Similar cold biases, although smaller in magnitudes, have also been reported for meteorological simulations at a horizontal grid resolution of 4-36 km (e.g., Gilliam et al., 2006; Wu et al., 2008a; Misenis et al., 2008). Correlation coefficients of 0.80 to 0.87 for T2 for the four months indicate an overall good spatial agreement between observations and predictions, except for January (Figure 3.2), in which the domain-wide NMBs are very high (> 70%), especially over the high latitude regions. The T2 predictions are overall better over the CASTNET sites than over sites from the other two networks in July and October and better over the SEARCH sites in January and April. MM5 gives the worst T2 predictions over the STN sites with an average MB of -3°C for four months. For RH2, the model also performs the best in July and the worst in January, with relatively large biases over the western U.S. The values of R, NMB, and NME range from 0.42 to 0.78, 0 to 27.5%, 19.5% to 36%, respectively, indicating small to moderate overpredictions. For WS10 and WD10, NMBs range from 13.7% to 19.5% and from -6.9% to -4.2%, respectively, indicating a fairly good agreement between observations and predictions, despite relatively poor correlation (with R

values of 0.47 to 0.57 and 0.12 to 0.21, respectively). This contradiction (i.e., a very small bias but a poor correlation) may be due to the compensation of large overpredictions and underpredictions. Since wind direction is a vector, the differences of numeric values in the statistical calculation may not reflect well the actual differences in the wind rose plots, especially when these values are greater than 180° (Zhang et al., 2006a). A careful interpretation is therefore needed in evaluating WD10 using conventional statistics. For weekly precipitation, the spatial distribution shows a relatively good performance over the Midwest U.S. and larger biases over the western U.S. and coastal regions. The domain-wide precipitation is moderately underestimated with NMBs of -30.8% (April) to -41% (July), which will have great impacts on simulated chemical concentrations via scavenging and wet deposition, as illustrated in section 3.1.2.

3.3.2 China

Figure 3.3 shows the spatial plots of NMBs between the NCDC data and MM5 simulations for T2, QV2, and 24-hr precipitation over China for the four months in 2001. Table 3.3 summarizes the performance statistics. In general, MM5 simulations reproduce the spatial distributions of T2 and QV2 very well with R values ranging from 0.84-0.94 and 0.88-0.95, respectively, for all months. MM5, however, gives high cold biases with MBs of $\sim -2.8^\circ\text{C}$ in July and $\sim -3.5^\circ\text{C}$ in January (note that the negative values of NME for January in Table 3.3 is due to the negative observational values of T2). The persistent high cold biases exist over western or southwestern China throughout all four months. This might be due to a poor representation of steep terrains at a coarse grid resolution in this study. For QV2, the model predictions are in very good agreement with the NCDC observations in terms of both

spatial distribution and performance statistics with NMBs of -2.1% (July) to -9.8% (April). For precipitation, one noticeable difference is that the overall NMBs of the simulated precipitation over China are much smaller than those over U.S. (-24.8% vs. -35.9% in January, -14.0% vs. -19.2% in April, -5.5% vs. -41.0% in July, and -15.4% vs. -37.2% in October). The spatial distribution of NMBs, however, displays an even worse pattern over China, with large negative biases (<-70%) occurring mostly over high latitude regions and large positive biases (>70%) occurring mostly over the low latitude regions. The overall small NMBs for precipitation over China are therefore resulted from the compensation of large positive and negative biases.

3.4 Chemical Predictions at Surface

The model predictions of gaseous and PM species are evaluated using available surface observations from the networks in the U.S., China, and Japan shown in Table 3.1 in terms of spatial distribution, temporal variation, and performance statistics.

3.4.1 Continental U.S.

Figure 3.4 compares observed and simulated max 8-hr O₃ for July (i.e., O₃ season) over the U.S. domain in terms of spatial distributions and correlations. CMAQ simulates max 8-hr O₃ mixing ratios quit well with NMBs of -4.2% and 6.2% for CASTNET and AIRS/SEARCH, respectively. CMAQ tends to overpredict max 8-hr O₃ over the eastern U.S. and underpredict over the western U.S. for all sites. The worst performance (with NMBs > 30% or < -30%) occurs over Midwest, Southeastern, and most states along the coasts (e.g., California and Florida). Several factors may contribute to the model bias. First, uncertainties exist in the emissions of O₃ precursors used in this study (Wang, 2006).

Second, a grid resolution of 108 km used in this study may be too coarse to resolve emissions needed for accurate chemical predictions and capture local-scale variations due to mixing and chemistry. Third, the PBL over the complex terrain may not be well represented. Finally, the exclusion of chlorine chemistry (Chang and Allen, 2006) or other possible O₃-related reactions (e.g., the reaction of NO₂ with water vapor reported recently by Li et al. (2008)) in the CB-IV mechanism may also lead to the underprediction of peak O₃ values. Overall, the simulated O₃ mixing ratios are within a factor of 2, as shown in the scatter plots of the correlation. Figure 3.5 shows temporal variations of observed and simulated max 1-hr and 8-hr O₃ mixing ratios at the CASTNET, AIRS, and SEARCH sites. The model performance is fairly consistent at all sites, especially for mean error (ME) for both max 1-hr and 8-hr O₃, with most of daily-average values raging from 10 to 15 ppb. The temporal trend for SEARCH reflects more variability due to smaller number of sites. The MB also reflects more temporal variability compared to the ME, with more days of underpredictions for max 1-hr O₃ than those for max 8-hr O₃ over all sites. Overall the performance for max 1-hr O₃ is better than that for max 8-hr O₃ (see Table 3.4). This might be in part attributed to the fact that the calculation of max 8-hr O₃ some time includes evening hours such as 7 or 8 p.m. and CMAQ has difficulties in simulating the nocturnal O₃ mixing ratios due to a relatively-poor representation of nocturnal PBL (Eder and Yu, 2006). Table 3.4 also summarizes max 1-hr and 8-hr O₃ statistics in the four months. The overall performance is the best in July with NMBs of -12.1% to 4.3% for max 1-hr O₃ and -4.2% to 19.0% for max 8-hr O₃ and the worst in October with NMBs of -37.9% to -15.6% for max 1-hr O₃ and -31.4% to -11.6% for max 8-hr O₃ for all three networks.

As shown in Figure 3.6, CMAQ overpredicts total $PM_{2.5}$ persistently except at a few locations in the western U.S. Large NMBs ($> 50\%$) for $PM_{2.5}$ mostly occur in the western U.S. (e.g., NMBs $> 70\%$ over Arizona, Colorado, Wyoming, Washington, Oregon, and the northern California) and the northeastern U.S. (e.g., NMBs $> 70\%$ over Virginia, Maryland, New Jersey, and New York) in the four months. Small NMBs ($< 20\%$) occur over most sites in the southern California, Missouri, Arkansas, and Louisiana for all months except for January. As shown in Table 3.4, among all four months, CMAQ performs the best in July (with NMBs of 27% and 21.7% for IMPROVE and STN, respectively) and the worst in January (with NMBs of 155.8 % and 22.3 % for IMPROVE and SEARCH, respectively). The spatial patterns of NMBs for BC and OC are comparable to those of $PM_{2.5}$ (figures not shown), indicating their dominance in $PM_{2.5}$ overpredictions. Several factors may contribute to the moderate-to-significant overpredictions of $PM_{2.5}$ in all months. First, the comparison of the emissions over the U.S. in this study with those (NEI 2001) used in the EPA Clean Air Interstate Rule (CAIR, 2005) modeling system shows that the emissions of both SO_2 and NO_x used in this study are higher by $\sim 30\%$ and $\sim 10\%$, respectively, leading to higher SO_4^{2-} and NH_4^+ concentrations (Wang, 2006). Second, the moderate underpredictions of precipitation in all months cause insufficient scavenging of atmospheric aerosols. Third, the biases in other meteorological variables such as T2 and RH2 can propagate into $PM_{2.5}$ predictions. For example, the largest NMBs in $PM_{2.5}$ predictions in January may be partially related to the worst overall meteorology predictions with the largest negative NMB in T2, and the largest positive NMB in RH2. Finally, relatively poor $PM_{2.5}$ performance may also be due to the use of a coarse grid resolution that cannot resolve fine-scale phenomena such as

cloud, precipitation, and subgrid convection.

Figure 3.7 shows consistent overpredictions for PM_{2.5} components in April (i.e., the dust storm season). The values of R are 0.77, 0.69, and 0.89 for IMPROVE, STN, and CASTNET, respectively, for SO₄²⁻ and 0.67 and 0.85 for STN and CASTNET, respectively, for NH₄⁺, indicating strong correlations between observations and predictions. The overall model performance for both SO₄²⁻ and NH₄⁺ is better for CASTNET than IMPROVE and STN. This is likely due to the longer sampling period at CASTNET (i.e., weekly average at CASTNET vs. 24-hour average at IMPROVE and STN). Other possible reasons include a better representation of emissions in the eastern U.S. and difficulties in simulating more complex terrain in the western U.S. and urban areas. Major PM_{2.5} components in the U.S. include SO₄²⁻ (35%), NH₄⁺ (12%), OC (12%), NO₃⁻ (~9%), and BC (3%) and inaccuracies in their predictions contribute to overpredictions in PM_{2.5}. The model performance for NO₃⁻ predictions is much worse than that for SO₄²⁻ and NH₄⁺, with NMBs of 85.6% and 58.1% and NMEs of 150.1% and 107.3% for the IMPROVE and STN sites, respectively. Eder and Yu (2006) indicated that the difficulty in NO₃⁻ predictions is partly due to high uncertainties associated with the gas/particle partitioning of NO₃⁻. CMAQ also systematically overpredicts both BC and OC, with NMBs of 101.7% and 155.4%, respectively. Such biases can be attributed to the uncertainties in primary OC and BC emissions and current model deficiencies in reproducing secondary organic aerosols. As a major PM_{2.5} component (~12% of total PM_{2.5} mass), the considerable overpredictions of OC contribute largely to the overestimation of total PM_{2.5} for all the four months.

3.4.2 China and Japan

Figure 3.8 shows the temporal variations of SO₂, max 1-hr O₃, NO₂, and PM₁₀ over Beijing area (average over 8 sites in the Beijing metropolitan area). CMAQ persistently underpredicts PM₁₀ and NO₂ for all four months (with NMBs of -55.8% to -85.6% and -61.2% to -81.3% as shown in Table 3.5). It overpredicts max 1-hr O₃ in January and underpredicts it in other months. For SO₂, despite overall underpredictions in January and overpredictions in other months (as shown in Table 3.5), CMAQ generally captures the temporal variability of SO₂. Table 3.6 shows that CMAQ significantly underpredicts concentrations of all species except for SO₂ over Japan in all four months, for which slight underpredictions occur for April and October. The model biases for these two observational datasets are highly related to the uncertainties of emission inventories used in this study. Carmichael et al. (2003) indicated that CO emissions of TRACE-P inventory prepared by Streets et al. (2003) from East Asia are probably underestimated by a factor of 3-5. Allen et al. (2004) suggested that Asia fossil fuel and biofuels emissions during TRACE-P should be increased by a factor of 1.6. Tan et al. (2004) also estimated that TRACE-P emission inventory for CO and particulate carbonaceous matter (BC+OC) are underestimated by 50% and 60-90%, respectively. Another possible reason for the poor performance over Beijing and Japan might be due to the coarse grid resolution, which cannot represent the complex local terrain and small-scale atmospheric processes such as mixing and chemistry. The underpredictions of PM₁₀ over Beijing and SPM over Japan are also associated with the poor capability of CMAQ to simulate coarse PM (Noble et al., 2008; Hu et al., 2008), which is a very significant contributor to PM₁₀/SPM over East Asia (Chen et al., 1999; Kim et al., 2003,

2006; Cheng et al., 2005). The concentrations of $PM_{2.5}$ over China account for more than 90% of PM_{10} in CMAQ simulations, with 24% for SO_4^{2-} , 12% for NH_4^+ , 14% for OC, ~11% for NO_3^- , and 4% for BC. The simulated fraction of $PM_{2.5}/PM_{10}$ is much higher than observed annual mean values of 65% and seasonal mean values of 73, 55, 64, and 67% for winter, spring, summer, and fall in Beijing reported by Hao (2006).

3.5 Vertical/Column Predictions

In addition to model evaluations at surface, CMAQ results are evaluated against available observed vertical profiles and column abundances of chemical species to assess its capability in representing transport and chemistry of air pollutants in upper layers. Such an evaluation is critical as most long-range transport (LRT) involves strong atmospheric motions in upper layers. An evaluation of CO, SO_4^{2-} , NO_3^- , and NH_4^+ using aircraft data from TRACE-P (Wang (2006)) indicated that CMAQ performs much better in the PBL (1 km or lower) and the LFT than in the upper free troposphere (UFT). Among all these species, CMAQ captured the best the vertical profile of CO. Both CMAQ and aircraft data reproduced a peak value of SO_4^{2-} at the altitude of 4500 km, indicating the contribution from the volcanic plume of the Miyake-jima Volcano located in the southern Japan (Wang, 2006). In general, CMAQ overpredicted aerosol concentrations at higher altitudes, but underpredicted them at lower altitudes (2 km or lower). More detailed results can be found in Wang (2006).

Figures 3.9-3.12 compare simulated monthly-average spatial distributions of tropospheric CO column, tropospheric NO_2 column, TOR, and AOD with satellite observations for all the months except July during which no MOPITT CO data are available.

Table 3.7 summarizes the corresponding performance statistics. As shown in Figure 3.9, MOPITT and CMAQ show high CO column abundance over continental source and outflow regions in January, April, and October. The high CO columns over Pacific Ocean from MOPITT are likely due to the long-range transport of CO from East Asia (Bian et al., 2007). CMAQ also gives very high CO column over the northern polar region, which may be due to the BCONs used. CO columns are low over high altitude terrains (e.g., the Himalayas and Rocky Mountains). CO column peaks in April, which might be related to the frequent transport events. CMAQ predictions agree well with observations, with NMBs of -8.4%, -11.0%, and 0.9% for January, April, and October, respectively. The MOPITT and CMAQ CO column abundances are also highly correlated with R values of 0.76 and 0.77 for January and October, respectively, although the value of R is lower (0.47) for April.

As shown in Figure 3.10, both GOME and CMAQ NO₂ column abundances show very similar spatial and seasonal patterns, for which the highest NO₂ columns occur over industrialized areas in East Asia, the northeastern U.S., the Great Lake region and California of the U.S. Much lower NO₂ columns (near zero) occur over the remote regions such as the northern Canada and Siberia and oceans. Domain-wide NO₂ columns are the maximum in January for both GOME and CMAQ. The high winter values are likely resulted from a combined effect of decreased loss of NO₂ via its reaction with OH, reduced vertical transport from the PBL to higher altitudes, and slightly increased emissions (Velders et al., 2001). In terms of performance statistics, CMAQ also predicts NO₂ columns very well with a very strong correlation (R ranging from 0.78 to 0.86 for the four months) between observations and predictions. NMBs are 19.4%, -3.9%, -28.3% and 0.9%, respectively, for the four

months. Velders et al. (2001) indicated that the model performance of tropospheric column NO₂ is highly dependent on the simulated NO₂ in the PBL when they used MOZART to study the global tropospheric NO₂ column distribution. CMAQ typically gives more accurate predictions of NO₂ in the PBL as compared with those from most of the global models, because of finer vertical/horizontal grid resolutions, which leads to the very good model column NO₂ performance.

In contrast to other column variables, the seasonal variation for TOMS/SBUV and CMAQ is inconsistent, with maximum TOR occurring in July for TOMS/SBUV but in January for CMAQ, as shown in Figure 3.11. This discrepancy might be resulted from the BCONs for O₃, which are provided by GEOS-CHEM, because simulated TORs are mainly determined by the O₃ mixing ratios in the upper layers where O₃ comes primarily from BCONs. An investigation of BCONs shows that the overall O₃ mixing ratios for upper layers are the highest in January and the lowest in July (the average mixing ratios for O₃ BCONs from layer 10 to 16 are 42.5, 41.7, 37.3, and 37.4 ppb for January, April, July, and October, respectively). However, CMAQ performs well in January with an NMB of 8.9%. The model captures the hot spot of TORs over the Aleutian low in January, which is due to the strong downward cross-tropopause transport of O₃ (Levy et al., 1985).

As shown in Figure 3.12, both MODIS and CMAQ show consistent seasonal variations of AODs with relatively high values near the source regions such as East Asia, northern India, and eastern U.S. Both show maximum AODs in April with the trans-Pacific transport primarily occurring between 30° N to 45° N in all months. The observed maximum AODs in spring are partly attributed to the April 2001 dust event that produces much more

fine particles (in addition to large particles), which is the largest Asian dust event ever observed during the past decade in the U.S. (Jaffe et al., 2003b). Another possibility for this spring maximum is the lifting of Asian anthropogenic pollutants by frequent WCBs to the LFT, where they are rapidly transported across the Pacific Ocean by strong westerlies. CMAQ predictions are lower than those of MODIS domain-wide throughout all four months with a relatively good agreement for January and October ($R = 0.65$ and $NMB = -29.1\%$ for January and $R = 0.59$ and $NMB = -25.5\%$ for October). The most noticeable differences occur in the northern Asia, the western U.S., and Canada (April) and over the Northern Pacific Ocean (April and July), where MODIS AODs are factors of 3-4 higher than CMAQ predictions. The discrepancies may be due to the biases from both MODIS and CMAQ. First, although MODIS can provide more accurate AOD products than those from previous satellite sensors (Remer et al., 2004), it still has large uncertainties, especially over land. Chu et al. (2002) reported MODIS errors of $\Delta AOD = \pm 0.05 \pm 0.2 AOD$ over land and $\Delta AOD = \pm 0.05 \pm 0.05 AOD$ over ocean. Non-sphericity effects associated with dust may also lead to high biases of MODIS AODs over the Pacific (Chu et al., 2005). Second, the CMAQ AODs are calculated by a set of empirical equations with a number of parameters. Different values for these parameters might result in different AOD values. The equations used in this study do not consider other inorganic species, which might also be important to AOD calculations. Third, although the MODIS AOD is mainly determined by the relatively small particles, the coarse particles (e.g, those with diameter more than $2.5 \mu\text{m}$) will also contribute to the total AOD. On the other hand, CMAQ AODs only consider the contributions from $\text{PM}_{2.5}$ particles neglecting those from coarse particles in this study. Fourth, CMAQ v4.4 does

not simulate emissions and physical/chemical processes of sea salt and dusts. Both those particles may also contribute to AODs (Kaufman et al., 2005). Heald et al. (2006) reported that the contribution of dust to the springtime AODs could be as high as that of other pollutants. Finally, the AODs derived from CMAQ PM predictions are associated with the vertical profiles of PM_{2.5} species, which are highly related to the model setup of BCONs. The BCONs for this study are provided from the GEOS-CHEM simulation, so the performance of the GEOS-CHEM simulation will also affect the simulated AODs. Park et al. (2004) indicated that the vertical profiles of SO₄²⁻ simulated by GEOS-CHEM could be lower by a factor of 2 than the observations from DC-8 flights.

3.6. Mechanistic Examination of Trans-Pacific Transport

3.6.1 Horizontal/Vertical Transport

It is well known that the trans-Pacific transport is the strongest in the spring due to the favorable meteorological conditions. The meteorological conditions over the eastern Asia in spring are characterized by three main features: (1) strong cold fronts moving southward across the northern China and Korea; (2) strong mid-latitude cyclones (i.e., low surface pressure system) over desert area of China; (3) and strong westerlies at altitudes above 4 km and latitudes above 20° N (Bey et al., 2001; Jaffe et al., 2003b). The meteorological patterns may lead to two major pathways in spring for trans-Pacific transport of Asia pollution as mentioned previously. By studying the seasonal variability of trans-Pacific transport, Liu et al. (2003) also reported a maximum mid-latitude meteorology-driven transport in spring. A more detailed study for April 2001 is therefore conducted to investigate different transport pathways in spring. Note that spring 2001 was characterized by unusually frequent cold

surge and strong convection events over East Asia, which resulted in unusually strong boundary layer and convective outflows in the troposphere (Liu et al., 2003). CO has been used as a tracer for export study in previous research (Bey et al., 2001; Li et al., 2002; Liu et al., 2003). In addition to CO, other gaseous and aerosol species are examined to provide a complete picture of the transport pathways for various air pollutants from Asia.

Figure 3.13 shows the mean horizontal fluxes of gaseous species (i.e., O₃, SO₂, NO_x, NH₃, CO, HCHO, and PAN), with the wind fields super-imposed, at surface layer and the 12th layer with an altitude of ~5 km. The fluxes (with unit of g m⁻² s⁻¹) are calculated by multiplying wind speeds and gas concentrations in μg m⁻³. Although the mid-latitude transport of CO and O₃ at higher altitudes is much stronger, the transport at lower altitudes cannot be neglected. For PAN, whose lifetime depends highly on temperature (ranging from hours at the surface to months in the upper troposphere (Seinfeld and Pandis, 2006)), the transport mainly occurs at higher altitudes. HCHO has a very similar horizontal transport pattern in different layers. For NO_x, because of its relatively-short tropospheric lifetime (14-21 hours) over East Asia (Kunhikrishnan et al., 2004), the large-scale transport at all altitudes is negligible. Koike et al. (2003) also observed that most of NO_y in Asian outflows is presented as PAN (only 0.5% as NO_x). Since PAN can be transported far downwind, it provides a remote source of NO_x, a very important precursor for O₃ and PM, after descending to lower altitudes and decomposing under a high pressure system. Very small amounts of SO₂ and NH₃ are directly transported at the lower altitudes, likely due to their transformation from gas phase to aerosol phase (i.e., SO₄²⁻ and NH₄⁺) along the transport pathway. Similarly, Figure 3.14 shows the mean horizontal fluxes of aerosol species

(i.e., $\text{PM}_{2.5}$, SO_4^{2-} , NO_3^- , NH_4^+ , BC, OC, and other inorganics) at surface and higher layers. $\text{PM}_{2.5}$, SO_4^{2-} , NH_4^+ , OC, and other inorganics can be transported within the PBL and in the LFT with higher fluxes at higher altitudes. In contrast, the transport of NO_3^- in the PBL is trivial. NO_3^- is mainly transported at higher altitudes. The fluxes for SO_4^{2-} are much higher, (e.g., they account for more than 40% of total $\text{PM}_{2.5}$ fluxes in layer 12) than those for other PM species. The distribution of NH_4^+ displays a very similar pattern to that of SO_4^{2-} . Much small transport for NO_3^- , BC, and OC can be attributed to the strong scavenging effects during the vertical lifting and LRT processes. Insufficient scavenging of SO_2 occurs during the vertical lifting over source regions, which allows its LRT. During the LRT, SO_2 provides the major precursor for SO_4^{2-} formation, which makes the trans-Pacific transport of SO_4^{2-} more efficient than other $\text{PM}_{2.5}$ species (Koike et al., 2003).

Figure 3.15 shows the vertical structure of the average horizontal fluxes for gaseous and aerosol species between 25-50° N. The transport mechanisms differ from species by species. The horizontal transports for O_3 , CO, $\text{PM}_{2.5}$, and SO_4^{2-} are noticeable at all altitudes, with the strongest fluxes found between 3-7 km (corresponding to the depth of LFT). NH_4^+ , BC, OC, and other inorganic species have much higher fluxes in the PBL near the source regions, but they are mainly transported at higher altitudes. For other species such as SO_2 , PAN, HCHO, and NO_3^- , the LRT occurs primarily in the free troposphere. The transports of NH_3 and NO_x are much smaller at all altitudes. Liu et al. (2003) indicated that the eastward export of Asian CO is the strongest at 30-45° N in the PBL and at 20-35° N in the LFT. The CMAQ simulation shows a very similar pattern, i.e., the strongest export at 35-50° N in the PBL and at 20-35° N in the LFT (Wang, 2006).

3.6.2 Process Analysis

In this study, IPR is applied and analyzed to illustrate the roles of various physical/chemical processes in affecting the trans-Pacific transport and quantifying the impacts of Asian pollution export on the U.S. air quality. PA is conducted for the four-month baseline simulations and one-month (April) sensitivity simulation without AAE. The IPRs for 30 species (i.e., 11 individual gas-phase species, 7 lumped gas-phase species, and 12 lumped PM species) have been calculated throughout three sub-domains (East Asia, the Pacific, and the U.S.). IPRs include the contributions of major processes such as horizontal transport (HORZ), vertical transport (VERT), mass adjustment term (ADJC), dry deposition (DDEP), gas-phase chemistry (CHEM), aerosol chemistry (AERO), cloud physics (CLDS; including both cloud convection, chemistry, and wet deposition), and emissions (EMIS). Note that ADJC is used to compensate for the mass inconsistency of trace species in chemical transport models, which might be caused by highly-parameterized physical and cloud algorithms, an inappropriate set of governing equations, or the misapplication of FDDA schemes (Byun and Ching, 1999). The original outputs of IPRs are in the units of ppb hr^{-1} for gases and $\mu\text{g m}^{-3} \text{hr}^{-1}$ for aerosols in each grid cell. They are post-processed to generate the daily mass changes for each species due to different processes and then generate the monthly-mean daily mass changes for one sub-domain by averaging all grid cells in a sub-domain during the one-month period. In order to investigate the integrated process contributions at different altitudes, the vertical domain is divided into three sub-layers: PBL (from surface to ~ 2.7 km (layers 1-10)), LFT (from ~ 2.7 km to ~ 8 km (layers 11-14)), and UFT (from ~ 8 km to ~ 16 km (layers 15-16)). The process contribution can be either positive

or negative, indicating build-up or consumption, respectively, of a species concentration due to a specific process.

Figure 3.16 shows the simulated accumulative IPRs for O_3 in the three sub-layers for the three sub-domains in the four months. The contribution of gas-phase chemistry to O_3 has very similar seasonal variations for all three sub-layers over the three sub-domains, except for the extremely-low values for January over the U.S. Interestingly, the major production process of the PBL O_3 over the U.S. in January is the vertical transport from higher altitudes (e.g., the UFT). The contributions of cloud processes to the O_3 mixing ratio are very small over the entire domain throughout the year. Dry deposition is the major sink for O_3 in PBL over East Asia and the U.S. The horizontal and vertical transport exhibits noticeable seasonal variations. For example, in the PBL over East Asia, the signs of horizontal and vertical transports are always opposite, with vertical transport as the source of O_3 in January and October and horizontal transport as the source of O_3 in April and July. It should be noted that the positive values of vertical transport in the PBL represent the possible subsidence of air pollutants into the PBL and the negative values represent the lifting of air pollutants from PBL to free troposphere. Over the U.S., the horizontal transport provides a persistent sink of O_3 in the PBL, indicating the export of O_3 out of the U.S. The positive vertical transport in January, April, and October in the PBL over U.S. indicates the possible influence from trans-Pacific transport. Over the Pacific, horizontal transport in the LFT is always positive, indicating the year-round effects of Asian outflow of O_3 by the prevailing westerlies, which peaks in April. It should also be noticed that the values of mass adjustment term are sometimes very large in the LFT and UFT, which is most likely due to the very

large wind speed and divergence of wind fields aloft that require large adjustment in the advection scheme.

Figure 3.17 shows simulated accumulative IPRs for $PM_{2.5}$. Emissions and aerosol chemistry are dominant processes to contribute to $PM_{2.5}$ concentrations in the PBL over East Asia and the U.S. The domain-wide contributions of emissions from East Asia are greater than those from the U.S. by a factor of 2-3. Different from O_3 , the cloud processes play a much more important role in determining the concentrations of $PM_{2.5}$, but dry deposition contributes relatively small to $PM_{2.5}$ concentrations. MM5 may not sufficiently represent clouds very well (Colle and Mass, 2000; Grubisic et al., 2005), particularly at the coarse grid resolution used in this study, which may partially explain the biases in $PM_{2.5}$ predictions. Similar to O_3 , the horizontal and vertical transports are the most important processes over the entire domain throughout the four months. The positive contributions of vertical transport in the LFT over both East Asia and the U.S. indicate the lifting of $PM_{2.5}$ from PBL to the free troposphere. The positive contributions of horizontal transport in both the PBL and LFT over the Pacific indicate the dominance of the Asian outflows in those layers, particularly in the LFT, which is consistent with the mean horizontal fluxes shown in Figure 3.14.

Figure 3.18 shows the IPR differences (baseline-sensitivity) between baseline and sensitivity simulations in April, 2001 to illustrate the contributions of AAEs to O_3 and $PM_{2.5}$ over the three sub-domains. For O_3 , horizontal/vertical transport is influenced the most by AAEs throughout the entire domain and at all altitudes. The influence of AAEs on chemical process is also significant in the PBL, especially over East Asia (due to the contributions of AAEs to O_3 precursors). The negative value for chemical process over the U.S. indicates a

slightly lower O_3 production from the gas-phase chemistry when AAEs are presented, which is consistent with the small decrease of NO_x in the U.S. due to the AAEs (see Figure 3.19). The presence of AAEs results in higher concentrations of radicals (e.g., hydroxyl radical (OH) and peroxyacetyl radical (CH_3COO_2)) which in turn lead to a higher conversion of NO_x by those radicals to form HNO_3 and PAN and thus a slightly lower O_3 production over the U.S., as compared with the sensitivity without AAEs. The positive contribution (by ~58% among all the processes) from vertical transport over the PBL of U.S. indicates the dominant AAE-associated influence on the PBL O_3 due to the large-scale subsidence. For $PM_{2.5}$, the impacts of Asia outflows on the cloud and aerosol processes are also important, with the highest impact on the source region, in addition to horizontal/vertical transport. The influences on the aerosol processes in the PBL of three sub-domains are always positive (note that the values for aerosol processes for both baseline and sensitivity simulations are always positive), which means more aerosol particles are produced due to the AAEs. On the contrary, the influences on cloud processes are always negative except for a small positive value in the UFT over East Asia (note that the values for cloud processes for both baseline and sensitivity simulations are always negative), indicating more aerosols formed from AAEs are removed from cloud processes. The difference of emission process over the Pacific shows a small positive value instead of zero, which is mainly due to the inclusion of a small portion of the northeastern Asian continent in the Pacific sub-domain. The influence of AAEs on the process contributions of the horizontal/vertical transport for $PM_{2.5}$ over all sub-domains and sub-layers is similar to that for O_3 .

As shown in the fluxes analyses in section 4.1 and PA in this section, the mechanisms

for the trans-Pacific transport differ from species by species. The upward fluxes by cold fronts, which provide the major transport pathway for the Asian outflow, can lift the air pollutants (e.g., O₃ and PM_{2.5}) in the PBL into the LFT over East Asia, where they are further transported horizontally by strong westerlies. The uplifted Asian air pollutants finally enter the PBL of the U.S. through large-scale subsidence. CMAQ also captures the relatively-strong fluxes for several species such as CO, O₃, and PM_{2.5} in the PBL over the Pacific (see Figure 3.15), which provides the evidence for another potential pathway in the PBL.

3.7 Impact of Asian Pollution Export on the U.S.

The contribution of Asian anthropogenic emissions to regional air pollution in the U.S. is examined through the sensitivity simulation without these emissions. The enhancements of both gaseous and aerosol species over the U.S. are quantified by calculating the differences between the baseline and sensitivity simulations. Figure 3.19 shows both the absolute and relative contributions of Asian anthropogenic emissions to the concentrations of gaseous species and PM_{2.5} components for both the eastern and western U.S. in April 2001. As expected, the western U.S. receives much higher influx of air pollutants from the trans-Pacific transport than the eastern U.S. The background surface concentrations of O₃ and CO increase by ~1 and ~2 ppb, respectively (or by 2.4% and 1.7%, respectively) over the western U.S. The enhancement for SO₂ is much higher over the western U.S. than the eastern U.S., indicating the relatively-fast conversion of SO₂ to SO₄²⁻ along the transport pathway. Compared with other gases, NO_x shows a different pattern over the entire U.S. with a negative contribution of Asian anthropogenic emissions to the NO_x mixing ratios in the U.S., which may be associated with the negligible import of NO_x from Asia and more conversion

of NO_x to its sink (e.g., HNO_3 , PAN, or N_2O_5) in the U.S. The concentration enhancement of SO_4^{2-} (~20% for the western U.S.) dominates among the gas and PM species, indicating that SO_4^{2-} is the major component of trans-Pacific anthropogenic aerosols. The simulated average SO_4^{2-} concentration enhancement of $\sim 0.37 \mu\text{g m}^{-3}$ over the western U.S. in this study is close to that from Heald et al. (2006). Their study suggested a seasonal average of $0.16 \mu\text{g m}^{-3}$ with 50% uncertainty and 24-hour maximum average of $0.6 \mu\text{g m}^{-3}$ of SO_4^{2-} enhancements in the northwestern U.S., especially in the state of Washington, during the springtime due to the Asian pollutant transport. The relative enhancement for PM species is much higher than that for gas species, indicating that the trans-Pacific transport for aerosols is more efficient. NH_4^+ associated with the formation of SO_4^{2-} , is the second major component (with an enhancement of ~18% for the western U.S.). The contributions of Asian anthropogenic emissions, to background NO_3^- , BC, OC, and others are relatively small (~5% for the western U.S.), which is due to their insignificant transport.

Table 3.8 summarizes the monthly and annual mean daily total pollutant export out of the PBL over both East Asia and the U.S. in 2001. The total export is calculated by summing up the integrated daily total contributions of dry deposition, gas-phase chemistry, aerosol process, cloud/aqueous process, and emissions from IPRs over the PBL (layers 1-10) of East Asia (20-50° N and 70-130° E) and the U.S. (20-50° N and 70-125° W). The positive values in Table 3.8 represent the net exports out of the PBL to the free troposphere and the negative values represent the net imports into the PBL from the free troposphere. The monthly mean exports of different pollutants show a strong seasonality. For NO_y and $\text{PM}_{2.5}$, the maximum export out of the Asian PBL occurs in April and the minimum export occurs in October,

while that out of the U.S. PBL is the maximum in July and the minimum in January. The net export amounts of O₃ out of the PBL over both subdomains are the maximum in July due to its highest photochemical production during the O₃ season. The direct O₃ export amounts are much lower over East Asia than those over the U.S., especially for April and July, due to relatively lower photochemical production of O₃ but relatively higher dry deposition loss over East Asia than over the U.S. (see Figure 3.16). The annual mean export amounts of O₃, NO_x, NO_y, and PM_{2.5} over the U.S. are estimated to be 2.04, 0.14, 0.62 Gmoles day⁻¹ and 27.51 Ggrams day⁻¹, respectively, for 2001. For comparison, the export amounts estimated by Liang et al. (1998) are 3.8, 0.17, and 0.40 Gmoles day⁻¹ for O₃, NO_x, and NO_y, respectively, based on the 1990 national emission inventory which provides higher emissions than the NEI 1999 version 1 used in this study. The 2001 annual mean export amounts of NO_x, NO_y, and PM_{2.5} from the Asian PBL are estimated to be 0.05 Gmoles day⁻¹, 0.44 Gmoles day⁻¹, and 48.18 Ggrams day⁻¹, respectively. Despite no net export for O₃ (-0.11 Gmoles day⁻¹) and lower export amount for NO_x, the amount of PM_{2.5} exported from the Asian PBL is much higher than that from the U.S. PBL on an annual basis.

Table 3.9 shows the monthly mean import of different pollutants into the U.S. PBL due to the Asian anthropogenic emissions in April 2001 estimated using two methods: the IPR method and the combined IPR and flux method. In the IPR method, the imports are obtained by subtracting total exports over the U.S. calculated from the IPRs of the sensitivity simulation from those of the baseline simulation in April 2001 (see Table 3.8), accounting for all the potential import and export from the top of the PBL and four sides of the U.S. subdomain. In the combined IPR and flux method, two steps are taken to obtain the net

imports. The vertical exports out of the PBL are first calculated by integrating vertical transport terms from IPRs over the U.S. and the horizontal exports are calculated by integrating the horizontal fluxes (where fluxes in the units of mole $\text{m}^{-2} \text{s}^{-1}$ for gases or gram $\text{m}^{-2} \text{s}^{-1}$ for $\text{PM}_{2.5}$ = wind speed parallel to the latitude line in the unit of m s^{-1} \times the concentration of pollutants in the units of mole m^{-3} for gases or gram m^{-3} for $\text{PM}_{2.5}$ in each grid cell) in the PBL along the most western boundary side (20-50° N and 125° W) for the U.S. in April. The imports are then obtained by calculating the differences in the sum of the calculated vertical export and the horizontal fluxes between baseline and sensitivity simulations. In the second method, westerly is assumed to be the prevailing wind for flux calculation, namely, the imports are assumed to take place only from the top of the PBL and along the western side of the U.S. subdomain and no export from the top and side boundaries is accounted for. This assumption results in higher import amounts for most pollutants than those estimated by the IPR method, as shown in Table 3.9. The net import amounts of O_3 , NO_y , and $\text{PM}_{2.5}$ into the U.S. PBL from Asia anthropogenic emissions are 0.11 Gmoles day^{-1} , 0.014 Gmoles day^{-1} , and 0.49 Ggrams day^{-1} , respectively, based on the IPR method and 0.31 Gmoles day^{-1} , 0.027 Gmoles day^{-1} , and 4.1 Ggrams day^{-1} , respectively, based on the combined IPR and flux method. For NO_x , while the combined IPR and flux method gives a small amount of import (0.0006 Gmoles day^{-1}), the IPR method estimates a net export of 0.002 Gmoles day^{-1} from the U.S. PBL (i.e., no import from Asia). Nevertheless, both methods provide an estimate of the relative amounts of pollutant imports from Asia anthropogenic emissions into the U.S. PBL, with an upper limit estimated by the combined IPR and flux method due to its import only assumption.

REFERENCES

- Akimoto, H. (2003), Global air quality and pollution, *Science*, *302*, 1716-1719.
- Allen, D., K. Pickering, and M. Fox-Rabinovitz (2004), Evaluation of pollutant outflow and CO sources during TRACE-P using model-calculated, aircraft-based, and measurements of Pollution in the Troposphere (MOPITT)-derived CO concentrations, *J. Geophys. Res.*, *109*, D15S03, doi:10.1029/2003JD004250.
- Anderson, T. L., Y. Wu, D. A. Chu, B. Schmid, J. Redemann, and O. Dubovik (2005), Testing the MODIS satellite retrieval of aerosol fine-mode fraction, *J. Geophys. Res.*, *110*, D18204, doi:10.1029/2005JD005978.
- Andreae, M., O., H. Berresheim, and T. W. Andreae (1988), Vertical distribution of dimethyl sulfide, sulfur dioxide, aerosol ions and radon over the northeast pacific ocean, *J. Atmos. Chem.*, *6*, 149– 173.
- Aulinger, A., V. Matthias, and M. Quante (2007), Introducing a partitioning mechanism for PAHs into the community multiscale air quality modeling system and its application to simulating the transport of benzo(a)pyrene over Europe, *J. Appl. Meteor. Climatol.*, *46*, 1718-1730.
- Berntsen, T. K., S. Karlsdottir, and D. A. Jaffe (1999), Influence of Asian emissions on the composition of air reaching the North Western United States, *Geophys. Res. Lett.*, *26*(14), 2171-2174.
- Bertschi, I. T., D. A. Jaffe, L. Jaeglé, H. U. Price, and J. B. Dennison (2004), PHOBEA/ITCT 2002 airborne observations of transpacific transport of ozone, CO, volatile organic compounds, and aerosols to the northeast Pacific: Impacts of Asian

anthropogenic and Siberian boreal fire emissions, *J. Geophys. Res.*, *109*, D23S12, doi:10.1029/2003JD004328.

Bey, I., D. J. Jacob, J. A. Logan, and R. M. Yantosca (2001), Asian chemical outflow to the Pacific in spring: origins, pathways, and budgets, *J. Geophys. Res.*, *106*, 23097–23113.

Bian, H., M. Chin, S. R. Kawa, B. Duncan, A. Arellano, and P. Kasibhatla (2007), Sensitivity of global CO simulations to uncertainties in biomass burning sources, *J. Geophys. Res.*, *112*, D23308, doi:10.1029/2006JD008376.

Binkowski, F. S., and S. J. Roselle (2003), Models-3 community multiscale air quality (CMAQ) model aerosol component, 1. Model description, *J. Geophys. Res.*, *108*, 4183, doi:10.1029/2001JD001409.

Burrows, J. P., et al. (1999), The Global Ozone Monitoring Experiment (GOME): Mission concept and first scientific results, *J. Atmos. Sci.*, *56*, 151-175.

Byun, D. W., and J. S. Ching (1999), Science algorithms of the EPA models-3 community multiscale air quality (CMAQ) modeling system, U.S. Environmental Protection Agency, Washington, D.C., EPA/600/R-99/030 (NTIS PB2000-100561).

Byun, D. W., and K. L. Schere (2006), Review of the governing equations, computational algorithms, and other components of the models-3 Community Multi-scale Air Quality (CMAQ) modeling system, *Appl. Mech. Rev.*, *59*, 51-77.

Carmichael, G. R., et al. (2003), Evaluating regional emission estimates using the TRACE-P observations, *J. Geophys. Res.*, *108*(D21), 8810, doi:10.1029/2002JD003116.

Chameides, W. L., C. Luo, R. Salor, D. Streets, Y. Huang, M. Bergin, and F. Giorgi (2002), Correlation between model-calculated anthropogenic aerosols and satellite-derived

cloud optical depths: Indication of indirect effect? *J. Geophys. Res.*, *107*(D10), 4085, doi:10.1029/2000JD00208.

Chang, S., and D. T. Allen (2006), Atmospheric chlorine chemistry in southeast Texas: Impacts on ozone formation and control, *Environ. Sci. Technol.*, *40*, 251-262.

Chen, M.-L., I.-F. Mao, and I.-K. Lin (1999), The PM_{2.5} and PM₁₀ particles in urban areas of Taiwan, *Sci. Total. Environ.*, *226*, 227-235.

Cheng, T., D. Lu, G. Wang, and Y. Xu (2005), Chemical characteristics of Asian dust aerosol from Hunshan Dake Sandland in Northern China, *Atmos. Environ.*, *39*, 2903-2911.

Chin, M., P. Ginoux, R. Lucchesi, B. Huebert, R. Weber, T. Anderson, S. Masonis, B. Blomquist, A. Bandy, and D. Thornton (2003), A global aerosol model forecast for the ACE-Asia field experiment, *J. Geophys. Res.*, *108* (D23), 8654, doi:10.1029/2003JD003642.

Chin, M., T. Diehl, P. Ginoux, and W. Malm (2007), Intercontinental transport of pollution and dust aerosols: Implications for regional air quality, *Atmos. Chem. Phys.*, *7*, 5501-5517.

Chu, D. A., Y. J. Kaufman, C. Ichoku, L. A. Remer, D. Tanre, and B. N. Holben (2002), Validation of MODIS aerosol optical depth retrieval over land, *Geophys. Res. Lett.*, *29*(12), 1671, doi:10.1029/2001GL013205.

Chu, D. A., Y. J. Kaufman, G. Zibordi, J. D. Chern, J. Mao, C. Li, and B. N. Holben (2003), Global monitoring of air pollution over land from the Earth Observing System-Terra Moderate Resolution Imaging Spectroradiometer (MODIS), *J. Geophys. Res.*, *108*(D21), 4661, doi:10.1029/2002JD003179.

- Chu, D. A., et al. (2005), Evaluation of aerosol properties over ocean from Moderate Resolution Imaging Spectroradiometer (MODIS) during ACE-Asia, *J. Geophys. Res.*, *110*, D07308, doi:10.1029/2004JD005208.
- Colle, B. A., and C. F. Mass (2000), The 5–9 February 1996 flooding event over the Pacific Northwest: Sensitivity studies and evaluation of the MM5 precipitation forecasts, *Mon. Wea. Rev.* *128*, 593–617.
- Deeter, M. N., et al. (2003), Operational carbon monoxide retrieval algorithm and selected results for the MOPITT instrument, *J. Geophys. Res.*, *108*(D14), 4399, doi:10.1029/2002JD003186.
- Dudhia, J. (1989), Numerical study of convection observed during the winter monsoon experiment using a mesoscale two-dimensional model. *J. Atmos. Sci.*, *46*, 3077–3107.
- Dudhia, J. (1993), Radiation studies with a high-resolution mesoscale model, proceedings of the 3rd Atmospheric Radiation Measurement (ARM) Science Team Meeting, Norman, Oklahoma, 1-4 March.
- Eder, B., and S. Yu (2006), A performance evaluation of the 2004 release of Models-3 CMAQ, *Atmos. Environ.*, *40*, 4811-4824.
- EPA (2001), Draft guidance for demonstrating attainment of air quality for PM_{2.5} and regional haze, the U.S. Environmental Protection Agency, Research Triangle Park, NC.
- EPA (2005), Technical support document for the Clean Air Interstate Rule: Air quality modeling, Office of Air Quality Planning and Standards, Research Triangle Park, NC, Docket No. OAR-2005-0053-2151.

- EPA (2007), Guidance on the use of models and other analyses for demonstrating attainment of air quality goals for ozone, PM_{2.5}, and regional haze, the U.S. Environmental Protection Agency, Research Triangle Park, NC, EPA-454/B-07-002.
- Fairlie, T. D., D. J. Jacob, and R. J. Park (2007), The impact of transpacific transport of mineral dust in the United States, *Atmos. Environ.*, *41*, 1251-1266.
- Fiore, A., D. J. Jacob, H. Liu, R. M. Yantosca, T. D. Fairlie, and Q. Li (2003a), Variability in surface ozone background over the United States: Implications for air quality policy, *J. Geophys. Res.*, *108*(D24), 4787, doi:10.1029/2003JD003855.
- Fiore, A., D. J. Jacob, R. Mathur, and R. V. Martin (2003b), Application of empirical orthogonal functions to evaluate ozone simulations with regional and global models, *J. Geophys. Res.*, *108* (D14), 4431, 10.1029/2002JD003151.
- Fiore, A. M., J. J. West, L. W. Horowitz, V. Naik, and M. D. Schwarzkopf (2008), Characterizing the tropospheric ozone response to methane emission controls and the benefits to climate and air quality, *J. Geophys. Res.*, *113*, D08307, doi:10.1029/2007JD009162.
- Fishman, J., A. E. Wozniak, and J. K. Creilson (2003), Global distribution of tropospheric ozone from satellite measurements using the empirically corrected tropospheric ozone residual technique: Identification of the regional aspects of air pollution, *Atmos. Chem. Phys.*, *3*, 893-907.
- Gilliam, R., C. Hogrefe, and S. T. Rao (2006), New methods for evaluating meteorological models used in air quality applications, *Atmos. Environ.*, *40*, 5073-5086.

- Goldstein, A. H., D. B. Millet, M. McKay, L. Jaeglé, L. Horowitz, O. Cooper, R. Hudman, D. J. Jacob, S. Oltmans, and A. Clarke (2004), Impact of Asian emissions on observations at Trinidad Head, California, during ITCT 2K2, *J. Geophys. Res.*, *109*, D23S17, doi:10.1029/2003JD004406.
- Grell, G., J. Dudhia, and D. Stauffer (1994), A description of the fifth-generation Penn State/NCAR Mesoscale model (MM5) NCAR Tech. Note NCAR/TN-398+STR, National Center for Atmospheric Research, Boulder, Colorado.
- Grubisic, V., R. K. Vellore, and A. W. Huggins (2005), Quantitative precipitation forecasting of wintertime storms in the Sierra Nevada: sensitivity to the microphysical parameterization and horizontal resolution, *Mon. Wea. Rev.* *133*, 2834–2859.
- Hao, Ji-Ming (2006), Regional Air Pollution and Air Quality Modeling in Beijing, Invited seminar at the Department of Marine, Earth, and Atmospheric Sciences, North Carolina State University, Raleigh, NC 27695, April 17.
- Heald, C. L., D. J. Jacob, R. J. Park, B. Alexander, T. D. Fairlie, and R. M. Yantosca (2005), Transpacific transport of Asian anthropogenic aerosols and its impact on surface air quality in the United States, *J. Geophys. Res.*, *111*, D14310, doi:10.1029/2005JD006847.
- Hogstrom, U. (1988), Non-dimensional wind and temperature profiles in the atmospheric surface layer: A re-evaluation. *Boundary-Layer Meteorol.*, *42*, 55-78.

- Horowitz, L. W., et al. (2003), A global simulation of tropospheric ozone and related tracers: Description and evaluation of MOZART, version 2, *J. Geophys. Res.*, *108*(D24), 4784, doi:10.1029/2002JD002853.
- Hu, X.-M., Y. Zhang, M. Z. Jacobson, and C. K. Chan (2008), Coupling and evaluating gas/particle mass transfer treatments for aerosol simulation and forecast, *J. Geophys. Res.*, *113*, D11208, doi:10.1029/2007JD009588.
- Husar, R. B., et al. (2001), Asian dust events of April 1998, *J. Geophys. Res.*, *106*, 18,317–18,330.
- ICAP (2005), Intercontinental transport and climatic effects of air pollutants (ICAP): Final report, Carolina Environmental Program, University of North Carolina at Chapel Hill, Chapel Hill, NC, http://www.meas.ncsu.edu/aqforecasting/ICAP/PDF/ICAP_PhaseII_final_JRE.pdf.
- IPCC (2007), Climate Change 2007: The Physical Science Basis, Contribution of Working Group I to the Fourth Assessment Report of the Intergovernmental Panel on Climate Change [Solomon, S., et al. (eds.)], Cambridge University Press, Cambridge, United Kingdom and New York, NY, USA.
- Jacob, D. J., J. A. Logan, and P. P. Murti (1999), Effect of rising Asian emission on surface ozone in the United States. *Geophys. Res. Lett.*, *26*, 2175–2178.
- Jacob, D., J. Crawford, M. Kleb, V. Connors, R. Bendura, J. Raper, G. Sachse, J. Gille, and L. Emmons (2003), The transport and chemical evolution over the Pacific (TRACE-P) mission: Design, execution, and overview of first results, *J. Geophys. Res.*, *108*(D20), 8781, doi:10.1029/2002JD003276.

- Jaeglé, L., D. A. Jaffe, H. U. Price, P. Weiss-Penzias, P. I. Palmer, M. J. Evans, D. J. Jacob, and I. Bey (2003), Sources and budgets for CO and O₃ in the northeastern Pacific during the spring of 2001: Results from the PHOBEA-II Experiment, *J. Geophys. Res.*, *108*, D20, 8802, doi:10.1029/2002JD003121.
- Jaffe, D. A., and S. Strode (2008), Sources, fate and transport of atmospheric mercury from Asia, *Environ. Chem.*, *5*, 121, doi:10.1071/EN08010.
- Jaffe, D. A., et al. (1999), Transport of Asian air pollution to North America, *Geophys. Res. Lett.*, *26*, 711–714.
- Jaffe, D. A., I. McKendry, T. Anderson, and H. Price (2003a), Six ‘new’ episodes of trans-Pacific transport of air pollutants. *Atmos. Environ.*, *37*, 391–404.
- Jaffe, D. A., J. Snow, and O. Cooper (2003b), The 2001 Asian dust events: Transport and impact on surface aerosol concentrations in the U.S., *Eos*, *84*(46), 501–516.
- Jang, J.-C. C., H. E. Jeffries, D. Byun, and J. E. Pleim (1995a), Sensitivity of ozone to model grid resolution—I. Application of high-resolution regional acid deposition model, *Atmos. Environ.*, *29*(21), 3085-3100.
- Jang, J.-C. C., H. E. Jeffries, D. Byun, and J. E. Pleim (1995b), Sensitivity of ozone to model grid resolution—II. Detailed process analysis for ozone chemistry, *Atmos. Environ.*, *29*(21), 3101-3114.
- Jeffries, H. E., and S. Tonnesen (1994), A comparison of two photochemical reaction mechanisms using mass balance and process analysis. *Atmos. Environ.*, *28*, 2991-3003.

- Kim, K.-H., G.-H. Choi, C.-H. Kang, J.-H. Lee, J. Y. Kim, Y. H. Youn, and S. R. Lee (2003), The chemical composition of fine and coarse particles in relation with Asian Dust events, *Atmos. Environ.*, *37*, 753-765.
- Kim, K.-H., C.-H., Kang, J.-H. Lee, K.-C. Choi, Y.-H. Youn, and S. M. Hong (2006), Investigation of airborne lead concentrations in relation to Asian Dust events and air mass transport pathways, *J. Aer. Sci.*, *37*, 1809-1825.
- Koike, M. et al. (2003), Export of anthropogenic reactive nitrogen and sulfur compounds from the East Asia region in spring, *J. Geophys. Res.*, *108*(D20), 8789, doi:10.1029/2002JD003284.
- Kunhikrishnan, T., M. G. Lawrence, R. von Kuhlmann, A. Richter, A. Ladstätter-Weißenmayer, and J. P. Burrows (2004), Analysis of tropospheric NO_x over Asia using the Model of Atmospheric Transport and Chemistry (MATCH-MPIC) and GOME-satellite observations, *Atmos. Environ.*, *38*, 581–596.
- Kuo, H. L., and W. H. Raymond (1980), A quasi-one-dimensional cumulus cloud model and parameterization of cumulus heating and mixing effects, *Mon. Wea. Rev.*, *108*, 991-1009.
- Levy, H., II., J. D. Mahlman, W. J. Moxim, and S. C. Liu (1985), Tropospheric ozone: The role of transport, *J. Geophys. Res.*, *90*, 3753-3772.
- Li, Q., D. J. Jacob, I. Bey, P. I. Palmer, B. N. Duncan, B. D. Field, R. V. Martin, A. M. Fiore, R. M. Yantosca, D. D. Parrish, P. G. Simmonds, and S. J. Oltmans (2002), Transatlantic transport of pollution and its effects on surface ozone in Europe and North America, *J. Geophys. Res.*, *107*, 4166-4189

- Li, S., J. Matthews, and A. Sinha (2008), Atmospheric Hydroxyl Radical Production from Electronically Excited NO₂ and H₂O, *Science*, *319*, 1657-1660.
- Liao, H., P. J. Adams, S. H. Chung, J. H. Seinfeld, L. J. Mickley, and D. J. Jacob (2003), Interactions between tropospheric chemistry and aerosols in a unified general circulation model, *J. Geophys. Res.*, *108*, 4001, doi:10.1029/2001JD001260.
- Liu, H., D. J. Jacob, I. Bey, R. M. Yantosca, B. N. Duncan, and G. W. Sachse (2003), Transport pathways for Asian pollution outflow over the Pacific: Interannual and seasonal variations. *J. Geophys. Res.*, *108*(D20), 8786, doi:10.1029/2002JD003102.
- Liu, J, D. L. Mauzerall, and L. W. Horowitz (2008), Source-receptor relationship between East Asian sulfur dioxide emissions and Northern Hemisphere sulfate concentrations, *Atmos. Chem. Phys.*, *8*, 3721-3733.
- Matthias, V., A. Aulinger, and M. Quante (2008), Adapting CMAQ to investigate air quality pollution in North Sea coastal regions, *Env. Mod. and Sof.*, *23*, 356-368.
- McKendry, I. G., J. P. Hacker, R. Stull, S. Sakiyam, D. Mignacca, and K. Reid (2001), Long-range transport of Asian dust to the Lower Fraser Valley, British Columbia, Canada, *J. Geophys. Res.*, *106*, 18,361-18,370.
- Misenis, C., Y. Zhang, X.-M. Hu, G. Grell, J. Fast, and S. Peckham (2008), An examination of WRF/Chem: Physical parameterizations, nesting options, and grid Resolutions, *Atmos. Environ.* (manuscript in preparation).
- Nolte, C. G., P. V. Bhave, J. R. Arnold, R. L. Dennis, K. M. Zhang, and A. S. Wexler (2008), Modeling urban and regional aerosols—Application of the CMAQ-UCD Aerosol Model to Tampa, a coastal urban site, *Atmos. Environ.*, *42*, 3179-3191.

- Park, R. J., D. J. Jacob, B. D. Field, R. M. Yantosca, and M. Chin (2004), Natural and trans-boundary pollution influences on sulfate-nitrate-ammonium aerosols in the United States: implications for policy, *J. Geophys. Res.*, *109*, D15204, 10.1029/2003JD004473.
- Parrish, D. D., C. J. Hahn, E. J. Williams, R. B. Norton, F. C. Fehsenfeld, H. B. Singh, J. D. Shetter, B. W. Gandrud, and B. A. Ridley (1992), Indications of photochemical histories of Pacific air masses from measurements of atmospheric trace species at Point Arena, California, *J. Geophys. Res.*, *97*(D14), 15,883-15901.
- Parrish, D. D., Y. Kondo, O. R. Cooper, C. A. Brock, D. A. Jaffe, M. Trainer, T. Ogawa, G. Hübler, and F. C. Fehsenfeld (2004), Intercontinental Transport and Chemical Transformation 2002 (ITCT 2K2) and Pacific Exploration of Asian Continental Emission (PEACE) experiments: An overview of the 2002 winter and spring intensives. *J. Geophys. Res.*, *109*, D23S01, doi:10.1029/2004JD004980.
- Pleim, J. E., and A. Xiu (2003), Development of a land surface model. Part II: Data assimilation, *J. Appl. Meteor.*, *42*(12), 1811–1822.
- Reisner, J., R. M. Rasmussen, and R. T. Bruintjes (1998), Explicit forecasting of supercooled liquid water in winter storms using the MM5 mesoscale model. *Q. J. R. Meteorol. Soc.* *124B*, 1071–1107.
- Remer, L. A, et al. (2005), The MODIS aerosol algorithm, products, and validation, *J. Atmos. Sci.*, *62*(4), 947-973.
- Seigneur, C., et al. (2000), Guidance for the performance evaluation of three-dimensional air quality modeling systems for particulate matter and visibility. *J. Air Waste Manage. Assoc.*, *50*, 588-599.

- Seinfeld, J. H., and S. N. Pandis (2006), *Atmospheric Chemistry and Physics: From Air Pollution to Climate Change*, 2nd ed., Wiley, New York.
- Seinfeld, J. H., et al. (2004), ACE-ASIA: Regional climatic and atmospheric chemical effects of Asian dust and pollution, *Bull. Amer. Meteor. Soc.*, 85(3), 367-380.
- Stohl, A., S. Eckhardt, C. Forster, P. James, and N. Spichtinger (2002), On the pathways and timescales on intercontinental air pollution transport, *J. Geophys. Res.*, 107(D23), 4684, doi:10.1029/2001JD001396.
- Streets, D. G., T. C. Bond, and G. R. Carmichael (2003), An inventory of gaseous and primary aerosol emissions in Asia in the year 2000, *J. Geophys. Res.*, 108(D21), 8809, doi:10.1029/2002JD003093.
- Tan, Q., W. L. Chameides, D. Streets, T. Wang, J. Xu, M. Bergin, and J. Woo (2004), An evaluation of TRACE-P emission inventories from China using a regional model and chemical measurements, *J. Geophys. Res.*, 109, D22305, doi:10.1029/2004JD005071.
- VanCuren, R. A. (2003), DELTA Group, Asian aerosols in North America: Extracting the chemical composition and mass concentration of the Asian continental aerosol plume from long-term aerosol records in the western United States, *J. Geophys. Res.*, 108(D20), 4623, doi:1029/2003JD003459.
- Velders, G. J. M., C. Granier, R. W. Portmann, K. Pfeilsticker, M. Wenig, T. Wagner, U. Platt, A. Richter, and J. P. Burrows (2001), Global tropospheric NO₂ column distributions: Comparing the three-dimensional model calculations with GOME measurements, *J. Geophys. Res.*, 106(D12), 12,643-12,666.

- Wang, B. (2006), Intercontinental and regional modeling of air pollutants transport over the pacific regions, Ph.D. thesis, 183 pp., North Carolina State University, Raleigh.
- Wu, S.-Y., S. Krishnan, Y. Zhang, and V. Aneja (2008a), Modeling atmospheric transport and fate of ammonia in North Carolina, Part I. Evaluation of meteorological and chemical predictions, *Atmos. Environ.*, *42*, 3419–3436.
- Wu, S.-Y., J.-L., Hu, Y. Zhang, and V. P. Aneja (2008b), Modeling atmospheric transport and fate of ammonia in North Carolina, Part II. Effect of ammonia emissions on fine particulate matter formation, *Atmos. Environ.*, *42*, 3437–3451.
- Xiu, A., and J. E. Pleim (2001), Development of a land surface model. Part I: Application in a mesoscale meteorological model, *J. Appl. Meteor.*, *40*, 192–209.
- Yienger, J. J., M. Galanter, T. A. Holloway, M. J. Phadnis, S. K. Guttikunda, G. R. Carmichael, W. J. Moxim, and H. Levy II (2000), The episodic nature of air pollution transport from Asia to North America, *J. Geophys. Res.*, *105*, 26,931– 26,946.
- Yu, S., B. Eder, R. Dennis, S. Chu, and S. Schwartz (2006), New unbiased symmetric metrics for the evaluation of air quality models. *Atmos. Sci. Lett.*, *7*, 26-34.
- Zhang, M., et al. (2003), Large-scale structure of trace gas and aerosol distributions over the western Pacific Ocean during the Transport and Chemical Evolution Over the Pacific (TRACE-P) experiment, *J. Geophys. Res.*, *108*(D21), 8820, doi:10.1029/2002JD002946.

- Zhang, M., I. Uno, R. Zhang, Z. Han, Z. Wang, and Y. Pu (2006), Evaluation of the Models-3 Community Multi-scale Air Quality (CMAQ) modeling system with observations obtained during the TRACE-P experiment: Comparison of ozone and its related species, *Atmos. Environ.*, *40*, 4874-4882.
- Zhang, Y., B. Pun, S.-Y. Wu, K. Vijayaraghavan, and C. Seigneur (2004), Application and evaluation of two air quality models for particulate matter for a Southeastern U.S. episode, *J. Air & Waste Manage. Assoc.*, *54*, 1478-1493.
- Zhang, Y., H. E. Snell, K. Vijayaraghavan, and M. Z. Jacobson (2005a), Evaluation of regional PM predictions with satellite and surface measurements, presentation at the 24th Annual Meeting of American Association for Aerosol Research, Austin, Texas, 17-21 October.
- Zhang, Y., H. E. Snell, and K. Vijayaraghavan (2005b), A preliminary evaluation of a regional air quality model with measurements from MODIS and surface monitoring networks. presentation at the MODIS Science Team Meeting, Baltimore, Maryland, 22-24 March.
- Zhang, Y., K. Vijayaraghavan, and C. Seigneur (2005c), Evaluation of three probing techniques in a three-dimensional air quality model, *J. Geophys. Res.*, *110*, D02305, doi:10.1029/2004JD005248.
- Zhang, Y., P. Liu, B. Pun, and C. Seigneur (2006a), A comprehensive performance evaluation of MM5-CMAQ for the Summer 1999 Southern Oxidants Study episode- Part I: Evaluation protocols, databases, and meteorological predictions, *Atmos. Environ.*, *40*, 4825-4838.

- Zhang, Y., P. Liu, A. Queen, C. Misener, B. Pun, and C. Seigneur (2006b), A comprehensive performance evaluation of MM5-CMAQ for the Summer 1999 Southern Oxidants Study episode-Part II: Gas and aerosol predictions, *Atmos. Environ.*, *40*, 4839-4855.
- Zhang, Y., P. Liu, B. Pun, and C. Seigneur (2006c), A comprehensive performance evaluation of MM5-CMAQ for the Summer 1999 Southern Oxidants Study episode-Part III: Diagnostic and mechanistic evaluations, *Atmos. Environ.*, *40*, 4856-4873.
- Zhang, Y., J.-P. Huang, D. K. Henze, and J. H. Seinfeld (2007), The role of isoprene in secondary organic aerosol formation on a regional scale, *J. Geophys. Res.*, *112*, D20207, doi:10.1029/2007JD008675.
- Zhang, Y., K. Vijayaraghavan, and H. E. Snell (2009), Probing into regional O₃ and PM pollution in the U.S., Part I. A 1-year CMAQ simulation and evaluation using satellite and surface data, *J. Geophys. Res.* *114*, D22304, doi:10.1029/2009JD011898.

Table 3.1. Summary of observational databases used in the model evaluation.

| Database | | | Variables/Species | Data Frequency | Number of Sites | |
|-----------|-----------|---------|---|---|---|-------------------------|
| Surface | U.S. | Met. | CASTNET | T2, RH2, WS10, WD10 | Hourly | ~80 |
| | | | SEARCH | T2, RH2, WS10, WD10 | Hourly | 8 |
| | | | STN | T2 | 1 in 3 days; 24-h average | ~100 |
| | | | NADP | Precipitation | Weekly total | ~220 |
| | | GAS | AIRS-AQS | O ₃ | Hourly | ~1000 |
| | | | CASTNET | O ₃ | Hourly | ~80 |
| | | | SEARCH | O ₃ | Hourly | 8 |
| | | | PM | CASTNET | SO ₄ ²⁻ , NO ₃ ⁻ , NH ₄ ⁺ | Weekly average |
| | | IMPROVE | | PM _{2.5} , SO ₄ ²⁻ , NO ₃ ⁻ , EC, OC | 1 in 3 days; 24-h average | ~100 |
| | | STN | | PM _{2.5} , SO ₄ ²⁻ , NO ₃ ⁻ , NH ₄ ⁺ | 1 in 3 days; 24-h average | ~60 |
| | | SEARCH | | PM _{2.5} | Daily average | 8 |
| | | China | Met. | NCDC | T2, QV2, WS10, WD10 | Hourly or every 3 hours |
| | GAS | | NEMCC | O ₃ , SO ₂ , NO ₂ | O ₃ : max 1-hr; others: daily average | 8 |
| PM | NEMCC | | PM ₁₀ | Daily average | | |
| Japan | GAS | NIES | CO, SO ₂ , NO, NO ₂ | Monthly average | Over 1000 | |
| | PM | NIES | SPM | Monthly average | | |
| Satellite | GOME | | Column NO ₂ | Monthly average | N/A | |
| | MODIS | | AOD | Monthly average | | |
| | MOPITT | | Column CO | Monthly average | | |
| | TOMS/SBUV | | TOR | Monthly average | | |

* AIRS-AQS: the Aerometric Information Retrieval System-Air Quality Subsystem; CASTNET: the Clean Air Status and Trends Network; GOME: the Global Ozone Monitoring Experiment; IMPROVE: the Interagency Monitoring of Protected Visual Environments; MODIS: the Moderate Resolution Imaging Spectroradiometer; MOPITT: the Measurements of Pollution in the Troposphere; NADP: the National Acid Deposition Program; NCDC: the National Climate Data Center; NEMCC: the National Environmental Monitoring Centre of China; NIES: the National Institute for Environmental Studies; SEARCH: the Southeastern Aerosol Research and Characterization; STN: the Speciated Trends Network; TOMS/SBUV: the Total Ozone Mapping Spectrometer and the Solar Backscattered Ultraviolet.

T2: temperature at 2-m; RH2: relative humidity at 2-m; WS10: wind speed at 10-m; WD10: wind direction at 10-m; QV2: water vapor mixing ratio; SPM: suspended particulate matter (with aerodynamic diameter less than and equal to 7.0 μm).

Table 3.2. Performance statistics for meteorological predictions over the U.S. in January, April, July, and October in 2001.

| Month | Variables | CASTNET | | | | SEARCH | | | | STN | NADP |
|-------|-------------|---------|---------|--------------------------|----------|---------|---------|--------------------------|----------|---------|--------------|
| | | T2 (°C) | RH2 (%) | WS10 (ms ⁻¹) | WD10 (°) | T2 (°C) | RH2 (%) | WS10 (ms ⁻¹) | WD10 (°) | T2 (°C) | Precip. (mm) |
| Jan. | Data Number | 24413 | 55865 | 53597 | 53685 | 4751 | 5739 | 5747 | 5747 | 212 | 741 |
| | Mean Obs. | 6.2 | 72.3 | 2.4 | 200.3 | 9.0 | 63.0 | 2.17 | 206.4 | 7.1 | 13.3 |
| | Mean Pred. | 2.8 | 92.2 | 2.7 | 186.5 | 5.6 | 74.4 | 2.77 | 218.8 | 3.3 | 8.5 |
| | Mean Bias | -3.4 | 19.9 | 0.3 | -13.8 | -3.4 | 11.4 | 0.60 | 12.4 | -3.8 | -4.8 |
| | Correlation | 0.80 | 0.42 | 0.52 | 0.21 | 0.81 | 0.07 | 0.44 | 0.16 | 0.81 | 0.70 |
| | NMB (%) | -54.1 | 27.5 | 13.7 | -6.9 | -38.1 | 18.0 | 27.4 | 6.0 | -54.3 | -35.9 |
| | NME (%) | 75.0 | 36.0 | 54.2 | 46.9 | 43.2 | 42.1 | 60.1 | 51.6 | 61.8 | 56.8 |
| Apr. | Data Number | 50030 | 53975 | 53909 | 53936 | 5405 | 5406 | 5368 | 5377 | 511 | 617 |
| | Mean Obs. | 12.2 | 61.7 | 2.7 | 190.0 | 20.1 | 66.1 | 2.60 | 187.3 | 15.0 | 12.2 |
| | Mean Pred. | 9.9 | 71.5 | 3.1 | 182.0 | 17.0 | 74.3 | 2.96 | 160.1 | 11.5 | 9.9 |
| | Mean Bias | -2.3 | 9.8 | 0.4 | -8.0 | -3.1 | 8.2 | 0.36 | -27.2 | -3.5 | -2.3 |
| | Correlation | 0.85 | 0.60 | 0.57 | 0.14 | 0.85 | 0.40 | 0.59 | 0.26 | 0.88 | 0.85 |
| | NMB (%) | -19.2 | 15.9 | 15.4 | -4.2 | -15.6 | 12.5 | 14.1 | -14.5 | -23.1 | -19.2 |
| | NME (%) | 30.8 | 33.2 | 52.1 | 51.1 | 17.8 | 32.9 | 41.8 | 47.2 | 25.2 | 30.8 |
| Jul. | Data Number | 57407 | 57285 | 57157 | 57887 | 5491 | 5486 | 5433 | 5623 | 993 | 775 |
| | Mean Obs. | 20.8 | 67.5 | 2.0 | 185.2 | 27.7 | 74.2 | 1.81 | 189.8 | 25.2 | 20.6 |
| | Mean Pred. | 20.6 | 67.5 | 2.4 | 176.4 | 24.9 | 79.5 | 1.81 | 164.8 | 22.7 | 12.1 |
| | Mean Bias | -0.2 | 0.0 | 0.4 | -8.8 | -2.8 | 5.3 | 0.0 | -25.0 | -2.5 | -8.5 |
| | Correlation | 0.83 | 0.78 | 0.47 | 0.12 | 0.70 | 0.25 | 0.36 | 0.144 | 0.86 | 0.53 |
| | NMB (%) | -0.9 | 0.0 | 19.5 | -4.7 | -9.9 | 7.2 | -0.2 | -13.2 | -10.0 | -41.0 |
| | NME (%) | 11.8 | 19.4 | 60.7 | 52.5 | 12.1 | 22.8 | 52.4 | 53.9 | 10.7 | 74.3 |
| Oct. | Data Number | 54802 | 56477 | 57032 | 57797 | 5440 | 5447 | 5160 | 5454 | 775 | 709 |
| | Mean Obs. | 12.8 | 63.1 | 2.5 | 191.0 | 19.2 | 67.5 | 2.26 | 163.2 | 15.4 | 19.4 |
| | Mean Pred. | 11.7 | 64.6 | 3.0 | 176.5 | 16.0 | 62.6 | 2.91 | 186.5 | 13.2 | 12.2 |
| | Mean Bias | -1.1 | 1.5 | 0.5 | -14.5 | -3.2 | -4.9 | 0.65 | 23.3 | -2.2 | -7.2 |
| | Correlation | 0.87 | 0.72 | 0.51 | 0.16 | 0.85 | 0.48 | 0.57 | 0.11 | 0.89 | 0.75 |
| | NMB (%) | -8.3 | 2.5 | 19.4 | -7.6 | -16.3 | -7.3 | 28.6 | 14.3 | -14.4 | -37.2 |
| | NME (%) | 21.9 | 24.0 | 60.2 | 49.0 | 19.3 | 27.2 | 57.1 | 73.9 | 17.5 | 57.7 |

*T2-temperature at 2-m; RH2-relative humidity at 2-m; WS10-wind speed at 10-m; WD10-wind direction at 10-m; NMB-normalized mean bias; NME-normalized mean error.

Table 3.3. Performance statistics for meteorological predictions over China in January, April, July, and October in 2001.

| Month | Variables | NCDC | | | | |
|-------|-------------|---------|-------------|--------------------------|---------------|--------------|
| | | T2 (°C) | QV2 (kg/kg) | WS10 (ms ⁻¹) | WD10 (degree) | Precip. (mm) |
| Jan. | Data Number | 89613 | 35182 | 65211 | 65213 | 1525 |
| | Mean Obs. | -1.86 | 0.0028 | 3.01 | 192.4 | 1.44 |
| | Mean Pred. | -5.32 | 0.0026 | 3.64 | 169.6 | 1.09 |
| | Mean Bias | -3.46 | -0.0002 | 0.63 | -22.8 | -0.35 |
| | Correlation | 0.94 | 0.95 | 0.55 | 0.11 | 0.66 |
| | NMB (%) | 186.3 | -7.0 | 20.8 | -11.9 | -24.8 |
| | NME (%) | -241.8 | 22.0 | 52.1 | 60.1 | 79.5 |
| Apr. | Data Number | 89437 | 35008 | 72815 | 72822 | 2022 |
| | Mean Obs. | 13.1 | 0.0054 | 3.51 | 192.8 | 2.30 |
| | Mean Pred. | 9.34 | 0.0049 | 4.09 | 178.4 | 1.98 |
| | Mean Bias | -3.76 | -0.0005 | 0.58 | -14.4 | -0.32 |
| | Correlation | 0.88 | 0.94 | 0.55 | 0.08 | 0.44 |
| | NMB (%) | -28.8 | -9.8 | 16.3 | -7.5 | -14.0 |
| | NME (%) | 34.3 | 21.8 | 48.9 | 55.5 | 102.4 |
| Jul. | Data Number | 81668 | 34587 | 64388 | 64399 | 2808 |
| | Mean Obs. | 24.2 | 0.0123 | 2.91 | 182.7 | 4.82 |
| | Mean Pred. | 21.4 | 0.0120 | 3.26 | 185.2 | 4.55 |
| | Mean Bias | -2.8 | -0.0003 | 0.35 | 2.5 | -0.27 |
| | Correlation | 0.84 | 0.88 | 0.44 | 0.06 | 0.27 |
| | NMB (%) | -11.8 | -2.1 | 12.0 | 1.3 | -5.5 |
| | NME (%) | 15.2 | 17.5 | 51.4 | 52.7 | 121.5 |
| Oct. | Data Number | 92242 | 36328 | 68323 | 68327 | 1849 |
| | Mean Obs. | 13.9 | 0.0069 | 2.77 | 193.3 | 2.56 |
| | Mean Pred. | 11.4 | 0.0065 | 3.35 | 157.3 | 2.16 |
| | Mean Bias | -2.5 | -0.0004 | 0.58 | -36.0 | -0.40 |
| | Correlation | 0.91 | 0.93 | 0.52 | 0.01 | 0.15 |
| | NMB (%) | -18.0 | -5.6 | 20.9 | -18.6 | -15.4 |
| | NME (%) | 24.1 | 17.7 | 52.9 | 61.6 | 108.5 |

* T2-temperature at 2-m; QV2-water vapor mixing ratio; WS10-wind speed at 10-m; WD10-wind direction at 10-m; NMB-normalized mean bias; NME-normalized mean error.

Table 3.4. Performance statistics for chemical predictions over the U.S. in January, April, July, and October in 2001.

| Month | | Max 1-hr O ₃ (ppb) | | | Max 8-hr O ₃ (ppb) | | | PM _{2.5} (µg m ⁻³) | | | SO ₄ ²⁻ (µg m ⁻³) | | |
|-------|-------------|-------------------------------|-------|-------|-------------------------------|-------|-------|---|------|------|---|-------|-------|
| | | AIRS | CAST | SEAR | AIRS | CAST | SEAR | IMP | STN | SEAR | CAST | IMP | STN |
| Jan. | Data Number | 15333 | 2201 | 237 | 15048 | 2189 | 237 | 1879 | 146 | 92 | 606 | 1936 | 140 |
| | Mean Obs. | 32.9 | 34.9 | 35.7 | 27.9 | 31.3 | 30.7 | 3.96 | 18.2 | 15.7 | 2.44 | 1.09 | 2.92 |
| | Mean Pred. | 33.9 | 27.1 | 31.3 | 31.0 | 26.3 | 28.9 | 10.12 | 22.2 | 19.4 | 1.26 | 1.05 | 1.75 |
| | Mean Bias | 1.0 | -7.8 | -4.4 | 3.1 | -5.0 | -1.8 | 6.16 | 4.0 | 3.7 | -1.18 | -0.04 | -1.17 |
| | Correlation | 0.52 | 0.39 | 0.48 | 0.50 | 0.54 | 0.61 | 0.44 | 0.29 | 0.56 | 0.63 | 0.55 | 0.30 |
| | NMB (%) | 3.2 | -22.6 | -12.2 | 11.3 | -16.1 | -5.7 | 155.8 | 22.3 | 23.5 | -48.4 | -2.9 | -40.0 |
| | NME (%) | 26.5 | 31.4 | 24.9 | 32.1 | 29.8 | 23.3 | 170.2 | 62.5 | 43.0 | 57.5 | 61.5 | 56.6 |
| Apr. | Data Number | 29993 | 2267 | 197 | 29276 | 2232 | 197 | 2125 | 365 | 87 | 551 | 2246 | 359 |
| | Mean Obs. | 52.5 | 54.3 | 56.3 | 47.7 | 50.4 | 51.2 | 6.03 | 11.1 | 15.2 | 3.05 | 1.54 | 3.16 |
| | Mean Pred. | 48.7 | 44.2 | 47.5 | 45.4 | 43.4 | 47.3 | 9.39 | 16.8 | 17.5 | 3.45 | 2.32 | 3.74 |
| | Mean Bias | -3.8 | -10.1 | -8.8 | -2.3 | -7.0 | -3.9 | 3.36 | 5.7 | 2.3 | 0.40 | 0.78 | 0.58 |
| | Correlation | 0.54 | 0.51 | 0.71 | 0.53 | 0.62 | 0.75 | 0.29 | 0.41 | 0.67 | 0.89 | 0.77 | 0.69 |
| | NMB (%) | -7.3 | -18.5 | -15.7 | -4.7 | -13.8 | -7.7 | 55.7 | 51.5 | 15.4 | 13.0 | 50.7 | 18.4 |
| | NME (%) | 18.5 | 22.3 | 18.6 | 18.8 | 19.5 | 14.8 | 82.3 | 70.6 | 33.4 | 25.4 | 66.5 | 42.4 |
| Jul. | Data Number | 33369 | 2356 | 237 | 32604 | 2318 | 234 | 2298 | 719 | 211 | 603 | 2306 | 703 |
| | Mean Obs. | 58.5 | 55.4 | 59.5 | 51.1 | 49.7 | 51.1 | 7.25 | 13.3 | 16.9 | 4.22 | 2.38 | 4.47 |
| | Mean Pred. | 58.2 | 48.7 | 62.0 | 54.2 | 47.7 | 60.8 | 9.20 | 16.2 | 22.5 | 5.98 | 3.39 | 6.83 |
| | Mean Bias | -0.3 | -6.7 | 2.5 | 3.1 | -2.0 | 9.7 | 1.95 | 2.9 | 5.6 | 1.76 | 1.01 | 2.36 |
| | Correlation | 0.55 | 0.50 | 0.74 | 0.55 | 0.50 | 0.75 | 0.64 | 0.64 | 0.66 | 0.88 | 0.78 | 0.78 |
| | NMB (%) | -0.7 | -12.1 | 4.3 | 6.2 | -4.2 | 19.0 | 27.0 | 21.7 | 32.9 | 41.9 | 42.0 | 52.7 |
| | NME (%) | 24.4 | 24.3 | 18.2 | 26.3 | 23.2 | 24.4 | 54.7 | 45.8 | 45.2 | 52.1 | 67.6 | 71.9 |
| Oct. | Data Number | 28649 | 2388 | 230 | 28058 | 2349 | 228 | 2672 | 607 | 102 | 643 | 2658 | 588 |
| | Mean Obs. | 45.9 | 45.3 | 47.9 | 39.7 | 40.8 | 40.8 | 5.24 | 11.4 | 12.2 | 2.00 | 1.33 | 2.52 |
| | Mean Pred. | 38.6 | 33.3 | 38.4 | 35.1 | 32.0 | 36.1 | 7.94 | 12.7 | 14.2 | 2.23 | 1.67 | 2.98 |
| | Mean Bias | -7.3 | -12.0 | -9.5 | -4.6 | -8.8 | -4.7 | 2.7 | 1.3 | 2.0 | 0.23 | 0.34 | 0.46 |
| | Correlation | 0.58 | 0.53 | 0.64 | 0.57 | 0.64 | 0.61 | 0.44 | 0.46 | 0.79 | 0.88 | 0.85 | 0.78 |
| | NMB (%) | -15.6 | -26.4 | -19.8 | -11.6 | -21.6 | -11.4 | 51.5 | 11.7 | 16.0 | 11.7 | 25.6 | 17.9 |
| | NME (%) | 24.0 | 28.8 | 23.0 | 23.9 | 26.1 | 20.2 | 74.2 | 46.8 | 32.5 | 26.4 | 49.5 | 46.5 |

* IMP- IMPROVE; CAST-CASTNET; SEAR-SEARCH; NMB-normalized mean bias; NME-normalized mean error.

Table 3.4 (Continued)

| Month | | NO ₃ ⁻ (µg m ⁻³) | | NH ₄ ⁺ (µg m ⁻³) | | BC (µg m ⁻³) | OC (µg m ⁻³) | TC (µg m ⁻³) |
|-------|-------------|--|-------|--|-------|--------------------------|--------------------------|--------------------------|
| | | IMP | STN | CAST | STN | IMP | IMP | STN |
| Jan. | Data Number | 1929 | 140 | 606 | 140 | 1923 | 1924 | 138 |
| | Mean Obs. | 0.98 | 3.88 | 1.35 | 1.97 | 0.22 | 0.81 | 5.83 |
| | Mean Pred. | 1.67 | 4.11 | 1.59 | 1.79 | 0.40 | 2.26 | 4.37 |
| | Mean Bias | 0.69 | 0.23 | 0.24 | -0.18 | 0.18 | 1.45 | -1.46 |
| | Correlation | 0.46 | 0.40 | 0.83 | 0.38 | 0.32 | 0.16 | 0.13 |
| | NMB (%) | 70.7 | 6.0 | 17.8 | -8.9 | 81.6 | 180.3 | -25.1 |
| | NME (%) | 134.0 | 76.2 | 38.1 | 56.9 | 115.8 | 207.4 | 62.5 |
| Apr. | Data Number | 2240 | 359 | 551 | 359 | 2229 | 2234 | 355 |
| | Mean Obs. | 0.46 | 1.42 | 0.99 | 1.12 | 0.17 | 0.79 | 3.08 |
| | Mean Pred. | 0.86 | 2.25 | 1.46 | 1.84 | 0.35 | 2.03 | 2.92 |
| | Mean Bias | 0.40 | 0.83 | 0.47 | 0.72 | 0.18 | 1.24 | -0.16 |
| | Correlation | 0.43 | 0.49 | 0.85 | 0.67 | 0.21 | 0.04 | 0.22 |
| | NMB (%) | 85.6 | 58.1 | 48.0 | 65.3 | 101.7 | 155.4 | -5.4 |
| | NME (%) | 150.1 | 107.3 | 53.1 | 78.5 | 126.4 | 181.5 | 55.6 |
| Jul. | Data Number | 2303 | 466 | 603 | 702 | 2306 | 2324 | 697 |
| | Mean Obs. | 0.27 | 0.94 | 1.23 | 1.36 | 0.22 | 1.17 | 3.27 |
| | Mean Pred. | 0.10 | 0.43 | 1.50 | 1.77 | 0.31 | 2.07 | 2.25 |
| | Mean Bias | -0.17 | -0.51 | 0.27 | 0.41 | 0.09 | 0.90 | -1.02 |
| | Correlation | 0.26 | 0.11 | 0.86 | 0.60 | 0.35 | 0.20 | 0.38 |
| | NMB (%) | -63.6 | -54.4 | 22.0 | 30.1 | 37.2 | 76.3 | -31.1 |
| | NME (%) | 87.5 | 84.2 | 36.9 | 61.2 | 69.8 | 107.1 | 46.1 |
| Oct. | Data Number | 2652 | 501 | 643 | 588 | 2683 | 2676 | 573 |
| | Mean Obs. | 0.33 | 1.55 | 0.69 | 0.84 | 0.25 | 1.16 | 3.82 |
| | Mean Pred. | 0.18 | 0.49 | 0.66 | 0.87 | 0.36 | 2.24 | 2.72 |
| | Mean Bias | -0.15 | -1.06 | -0.03 | 0.03 | 0.11 | 1.08 | -1.10 |
| | Correlation | 0.24 | 0.00 | 0.85 | 0.36 | 0.33 | 0.11 | 0.44 |
| | NMB (%) | -44.7 | -68.3 | -4.7 | 4.2 | 43.8 | 93.6 | -28.7 |
| | NME (%) | 90.1 | 84.3 | 25.2 | 71.9 | 81.2 | 131.2 | 49.6 |

Table 3.5. Performance statistics for O₃, SO₂, NO₂, and PM₁₀ in Beijing, China in January, April, July, and October in 2001.

| Month | Variables ¹ | Max 1-hr O ₃ (mg m ⁻³) | SO ₂ (mg m ⁻³) | NO ₂ (mg m ⁻³) | PM ₁₀ (mg m ⁻³) |
|-------|------------------------|--|--|--|--|
| Jan. | Data Number | 31 | 31 | 31 | 31 |
| | Mean Obs. | 40.6 | 185.0 | 81.7 | 158.0 |
| | Mean Pred. | 57.6 | 68.0 | 31.7 | 70.0 |
| | Mean Bias | 17.0 | -117.0 | -50.0 | -88.0 |
| | Correlation | 0.56 | 0.54 | 0.43 | 0.48 |
| | NMB (%) | -41.7 | -63.3 | -61.2 | -55.8 |
| | NME (%) | 44.2 | 63.4 | 61.2 | 57.9 |
| Apr. | Data Number | 30 | 30 | 30 | 30 |
| | Mean Obs. | 95.8 | 34.0 | 65.9 | 210.0 |
| | Mean Pred. | 86.8 | 37.3 | 15.3 | 34.0 |
| | Mean Bias | -9.0 | 3.3 | -50.6 | -176.0 |
| | Correlation | -0.03 | 0.28 | 0.38 | 0.14 |
| | NMB (%) | -9.36 | 9.80 | -76.8 | -83.6 |
| | NME (%) | 25.5 | 49.4 | 76.8 | 83.6 |
| Jul. | Data Number | 31 | 31 | 31 | 31 |
| | Mean Obs. | 138.0 | 11.7 | 60.1 | 118.0 |
| | Mean Pred. | 106.0 | 30.9 | 11.2 | 48.0 |
| | Mean Bias | -32.0 | 19.2 | -48.9 | -70.0 |
| | Correlation | -0.09 | 0.38 | 0.10 | 0.35 |
| | NMB (%) | -23.3 | 163.9 | -81.3 | -59.0 |
| | NME (%) | 26.7 | 167.9 | 81.3 | 59.5 |
| Oct. | Data Number | 31 | 31 | 31 | 31 |
| | Mean Obs. | 75.4 | 23.1 | 93.3 | 179.0 |
| | Mean Pred. | 59.7 | 4.5 | 18.8 | 26.0 |
| | Mean Bias | -15.7 | -18.6 | -74.5 | -153.0 |
| | Correlation | 0.10 | 0.39 | 0.12 | 0.42 |
| | NMB (%) | -20.7 | 93.7 | -79.9 | -85.6 |
| | NME (%) | 43.2 | 110.5 | 79.9 | 85.6 |

¹NMB-normalized mean bias; NME-normalized mean error.

Table 3.6. Performance statistics for chemical predictions over Japan in January, April, July, and October in 2001.

| Month | Variables ¹ | CO (ppb) | SO ₂ (ppb) | NO (ppb) | NO ₂ (ppb) | SPM ² (μg m ⁻³) |
|-------|------------------------|----------|-----------------------|----------|-----------------------|--|
| Jan. | Data Number | 132 | 1478 | 1456 | 1467 | 1542 |
| | Mean Obs. | 564.0 | 3.9 | 15.4 | 17.8 | 22.2 |
| | Mean Pred. | 203.0 | 2.2 | 1.6 | 8.1 | 7.3 |
| | Mean Bias | -361.0 | -1.7 | -13.8 | -9.7 | -14.9 |
| | Correlation | 0.48 | 0.21 | 0.51 | 0.60 | 0.36 |
| | NMB (%) | -64.0 | -43.5 | -89.5 | -54.5 | -67.3 |
| | NME (%) | 64.0 | 53.4 | 89.6 | 56.7 | 67.4 |
| Apr. | Data Number | 131 | 1490 | 1448 | 1465 | 1537 |
| | Mean Obs. | 444.0 | 6.0 | 6.6 | 16.9 | 33.9 |
| | Mean Pred. | 192.0 | 4.5 | 0.6 | 6.6 | 17.0 |
| | Mean Bias | -252.0 | -1.5 | -6.0 | -10.3 | -16.9 |
| | Correlation | 0.27 | 0.35 | 0.21 | 0.44 | 0.16 |
| | NMB (%) | -56.7 | -25.5 | -91.1 | -60.7 | -49.7 |
| | NME (%) | 56.8 | 40.5 | 91.1 | 62.8 | 49.9 |
| Jul. | Data Number | 131 | 1475 | 1446 | 1465 | 1537 |
| | Mean Obs. | 336.0 | 5.3 | 5.5 | 12.6 | 35.1 |
| | Mean Pred. | 150.0 | 2.8 | 0.4 | 5.3 | 15.3 |
| | Mean Bias | -186.0 | -2.5 | -5.1 | -7.3 | -19.8 |
| | Correlation | 0.42 | 0.30 | 0.13 | 0.47 | 0.40 |
| | NMB (%) | -55.5 | -47.5 | -93.4 | -57.9 | -56.3 |
| | NME (%) | 55.7 | 56.4 | 93.4 | 60.9 | 56.6 |
| Oct. | Data Number | 130 | 1467 | 1452 | 1468 | 1541 |
| | Mean Obs. | 482.0 | 4.2 | 9.9 | 16.9 | 27.6 |
| | Mean Pred. | 165.0 | 4.0 | 0.5 | 7.0 | 8.0 |
| | Mean Bias | -317.0 | -0.2 | -9.4 | -9.9 | -19.6 |
| | Correlation | 0.43 | 0.41 | 0.35 | 0.58 | 0.37 |
| | NMB (%) | -65.7 | -6.3 | -94.6 | -58.6 | -71.0 |
| | NME (%) | 65.7 | 48.0 | 94.7 | 60.4 | 71.0 |

¹NMB-normalized mean bias; NME-normalized mean error.

²SPM-suspended particulate matter, corresponding PM with aerodiameter less than or equal to 7 μm.

Table 3.7. Performance statistics for column predictions over the ICAP domain in January, April, July, and October in 2001¹.

| Month | Variables ² | AOD | NO ₂ Column | CO Column ³ | TOR |
|-------|------------------------|-------|------------------------|------------------------|-------|
| Jan. | Data Number | 9816 | 25569 | 10312 | 7725 |
| | Mean Obs. | 0.17 | 12.8 | 2.14 | 28.3 |
| | Mean Pred. | 0.11 | 15.3 | 1.96 | 30.9 |
| | Mean Bias | -0.06 | 2.5 | -0.18 | 2.6 |
| | Correlation | 0.55 | 0.79 | 0.76 | 0.21 |
| | NMB (%) | -37.9 | 19.4 | -8.4 | 8.9 |
| | NME (%) | 46.0 | 62.4 | 11.6 | 27.4 |
| Apr. | Data Number | 12387 | 36760 | 16048 | 7900 |
| | Mean Obs. | 0.36 | 8.7 | 2.41 | 36.0 |
| | Mean Pred. | 0.17 | 8.4 | 2.14 | 26.6 |
| | Mean Bias | -0.19 | -0.3 | -0.27 | -9.4 |
| | Correlation | 0.49 | 0.86 | 0.47 | 0.56 |
| | NMB (%) | -51.2 | -3.9 | -11.0 | -26.1 |
| | NME (%) | 52.5 | 43.5 | 15.1 | 26.6 |
| Jul. | Data Number | 15334 | 48230 | -- | 8075 |
| | Mean Obs. | 0.25 | 6.7 | -- | 37.9 |
| | Mean Pred. | 0.13 | 4.8 | -- | 18.2 |
| | Mean Bias | -0.12 | -1.9 | -- | -19.7 |
| | Correlation | 0.23 | 0.78 | -- | 0.46 |
| | NMB (%) | -47.5 | -28.3 | -- | -51.9 |
| | NME (%) | 57.6 | 55.9 | -- | 52.1 |
| Oct. | Data Number | 13455 | 40325 | 13936 | 8075 |
| | Mean Obs. | 0.16 | 9.23 | 1.79 | 30.6 |
| | Mean Pred. | 0.10 | 9.31 | 1.80 | 21.2 |
| | Mean Bias | -0.06 | 0.08 | 0.01 | -9.4 |
| | Correlation | 0.62 | 0.85 | 0.77 | 0.21 |
| | NMB (%) | -38.4 | 0.9 | 0.9 | -30.9 |
| | NME (%) | 44.6 | 48.6 | 10.0 | 32.1 |

¹The units for column NO₂, CO and TOR are 10¹⁴ molecules cm⁻², 10¹⁸ molecules cm⁻², and DU, respectively.

²NMB-normalized mean bias; NME-normalized mean error.

³--, no CO observations.

Table 3.8. The monthly average 24-hr total export of O₃, NO_x, NO_y, and PM_{2.5} out of the PBL over different sub-domains in January, April, July, and October 2001.

| Species ¹ | Total Export | Jan. | Apr. | | Jul. | Oct. | Annual |
|----------------------|--------------|----------|----------|-------------|----------|----------|----------|
| | | Baseline | Baseline | Sensitivity | Baseline | Baseline | Baseline |
| O ₃ | Asia | -0.59 | 0.12 | -3.44 | 0.83 | -0.76 | -0.11 |
| | US | -0.86 | 2.80 | 2.91 | 4.48 | 1.74 | 2.04 |
| NO _x | Asia | 0.08 | 0.06 | -0.01 | 0.04 | 0.03 | 0.05 |
| | US | 0.24 | 0.09 | 0.088 | 0.06 | 0.18 | 0.14 |
| NO _y | Asia | 0.47 | 0.54 | -0.13 | 0.48 | 0.29 | 0.44 |
| | US | 0.58 | 0.595 | 0.609 | 0.68 | 0.61 | 0.62 |
| PM _{2.5} | Asia | 57.99 | 60.13 | -11.80 | 47.06 | 27.59 | 48.18 |
| | US | 18.00 | 30.12 | 30.61 | 37.31 | 24.63 | 27.51 |

¹The units for O₃, NO_x, NO_y, and PM_{2.5} are Gmole day⁻¹, Gmole day⁻¹, Gmole day⁻¹, and Gg day⁻¹, respectively.

Table 3.9. The monthly average 24-hr total import of O₃, NO_x, NO_y, and PM_{2.5} from Asia into the PBL over the U.S. in April 2001 using two different methods.

| Species* | IPR method | Combining IPR and Flux method |
|-------------------|------------|-------------------------------|
| O ₃ | 0.11 | 0.31 |
| NO _x | 0.002 | 0.0006 |
| NO _y | 0.014 | 0.027 |
| PM _{2.5} | 0.49 | 4.1 |

*The units for O₃, NO_x, NO_y, and PM_{2.5} are Gmole day⁻¹, Gmole day⁻¹, Gmole day⁻¹, and Gg day⁻¹, respectively.

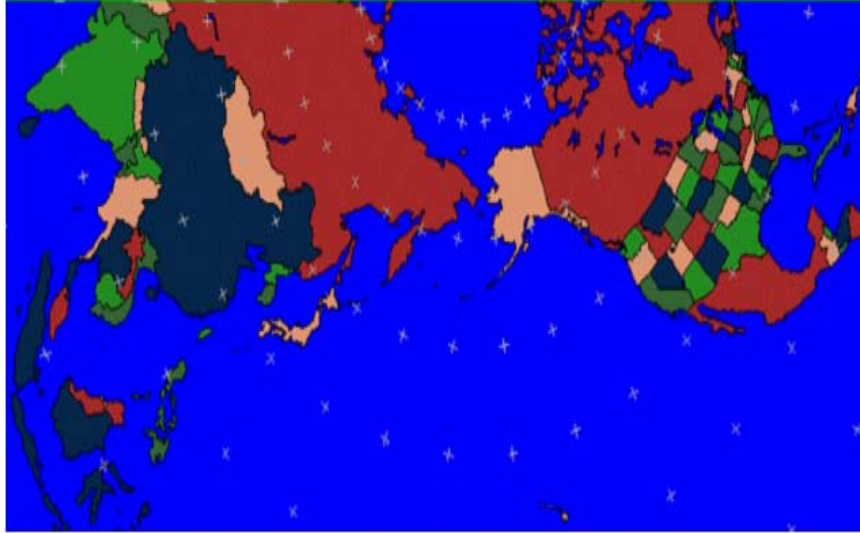
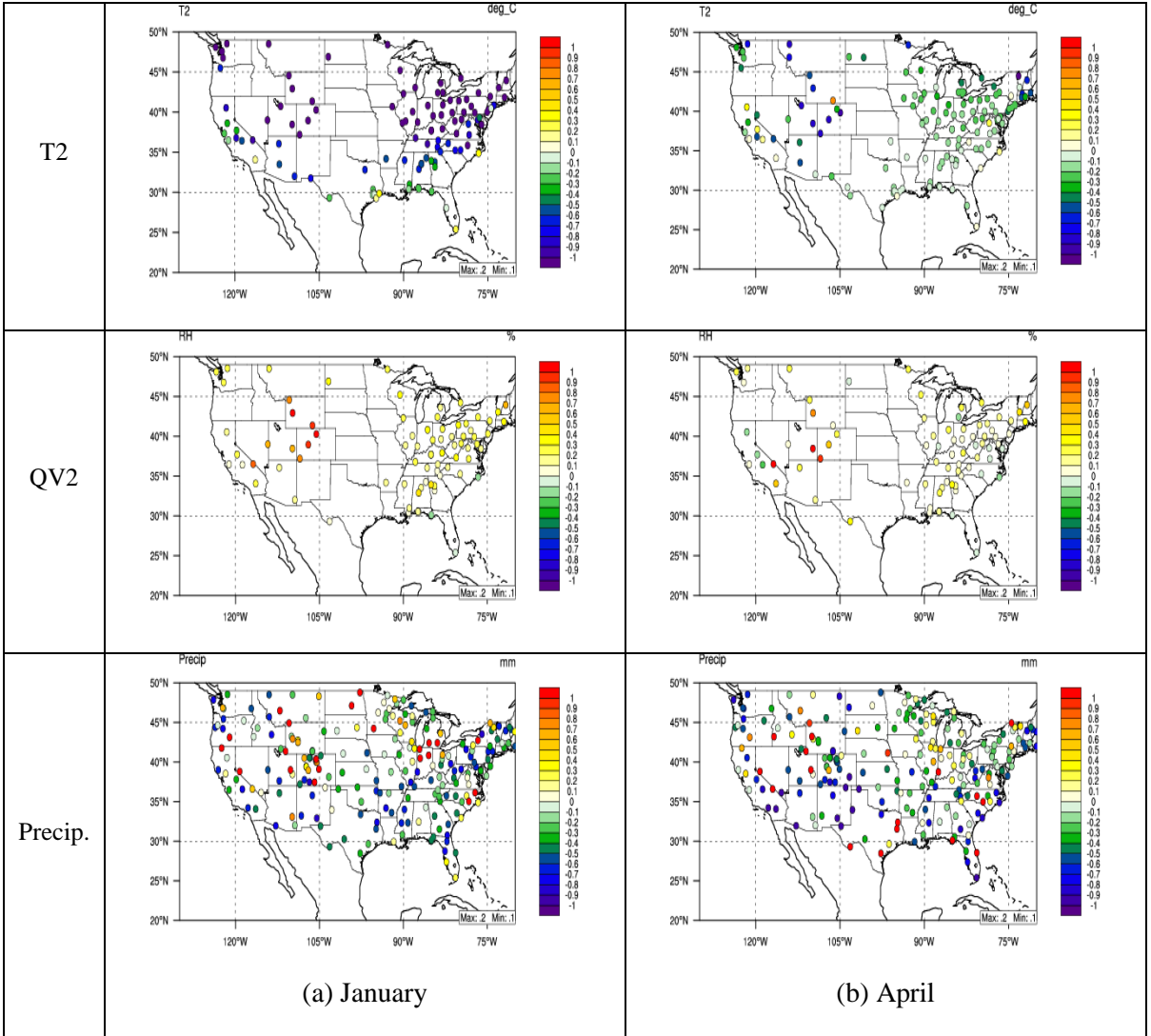


Figure 3.1. Modeling domain for the ICAP trans-Pacific transport study.

Figure 3.2. Spatial distributions of NMBs between observations and MM5 simulations for temperature at 2-m (T2), RH at 2-m (RH2), and weekly total precipitation (Precip.) over the U.S. for January, April, July, and October 2001.



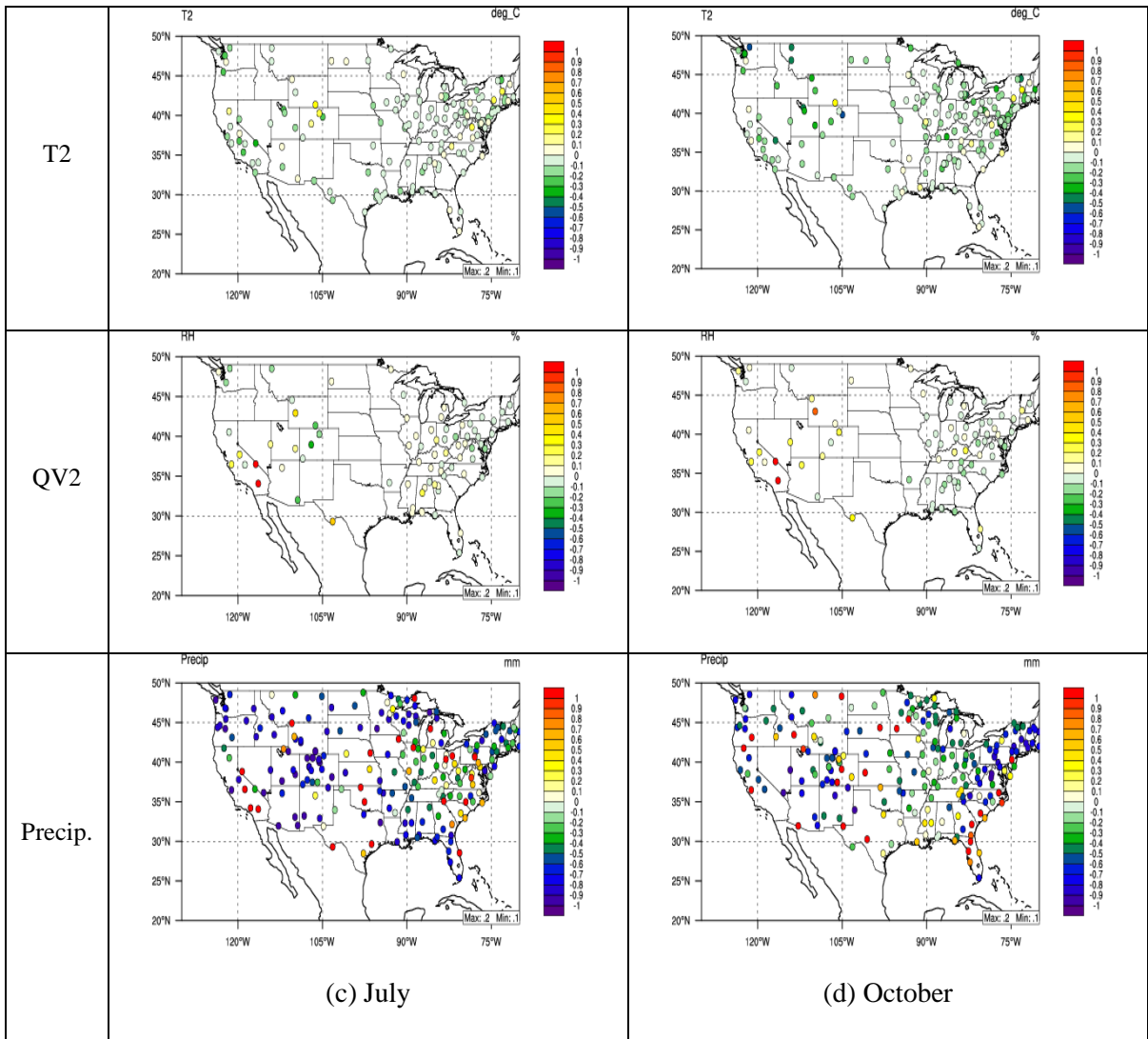
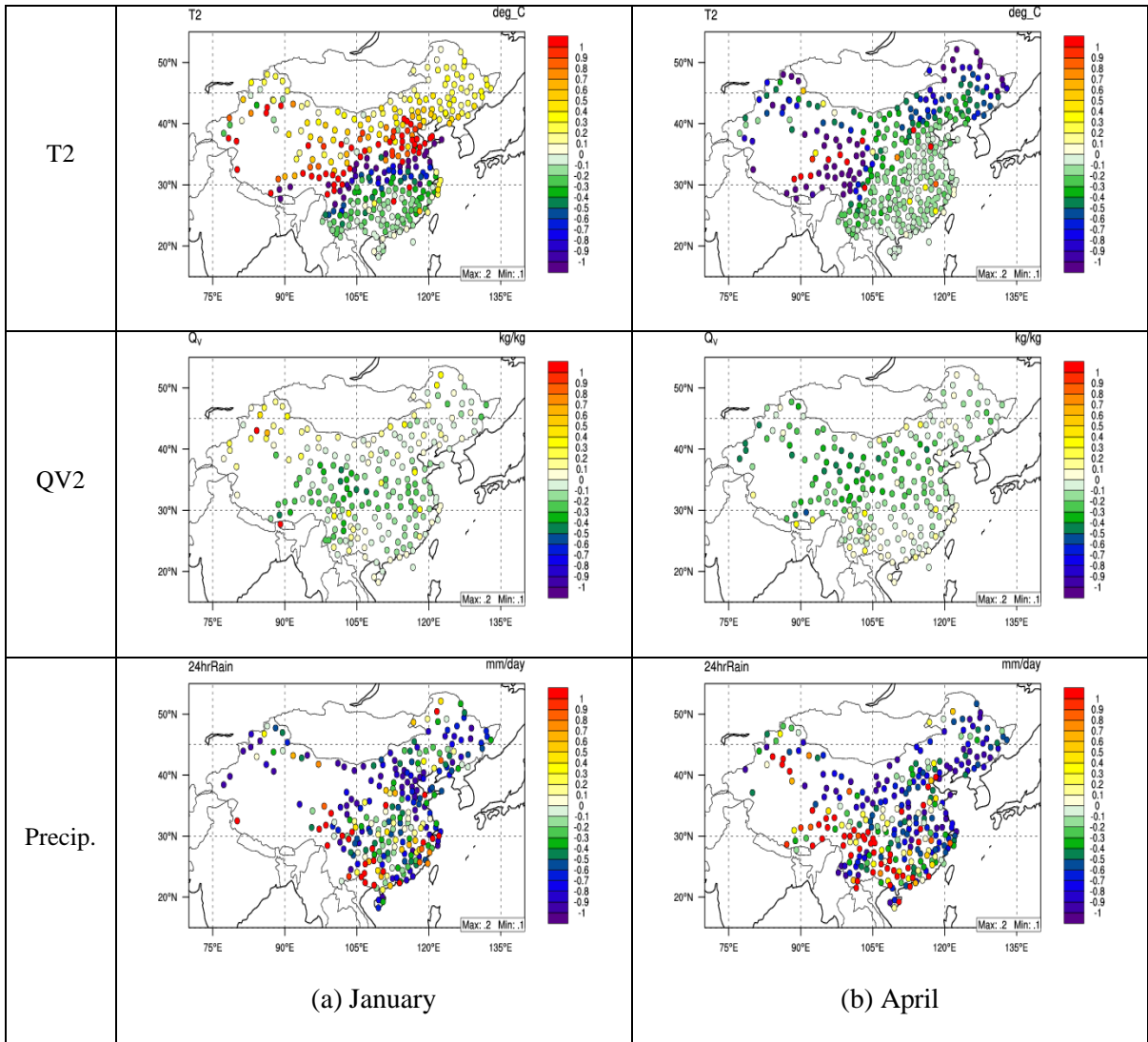
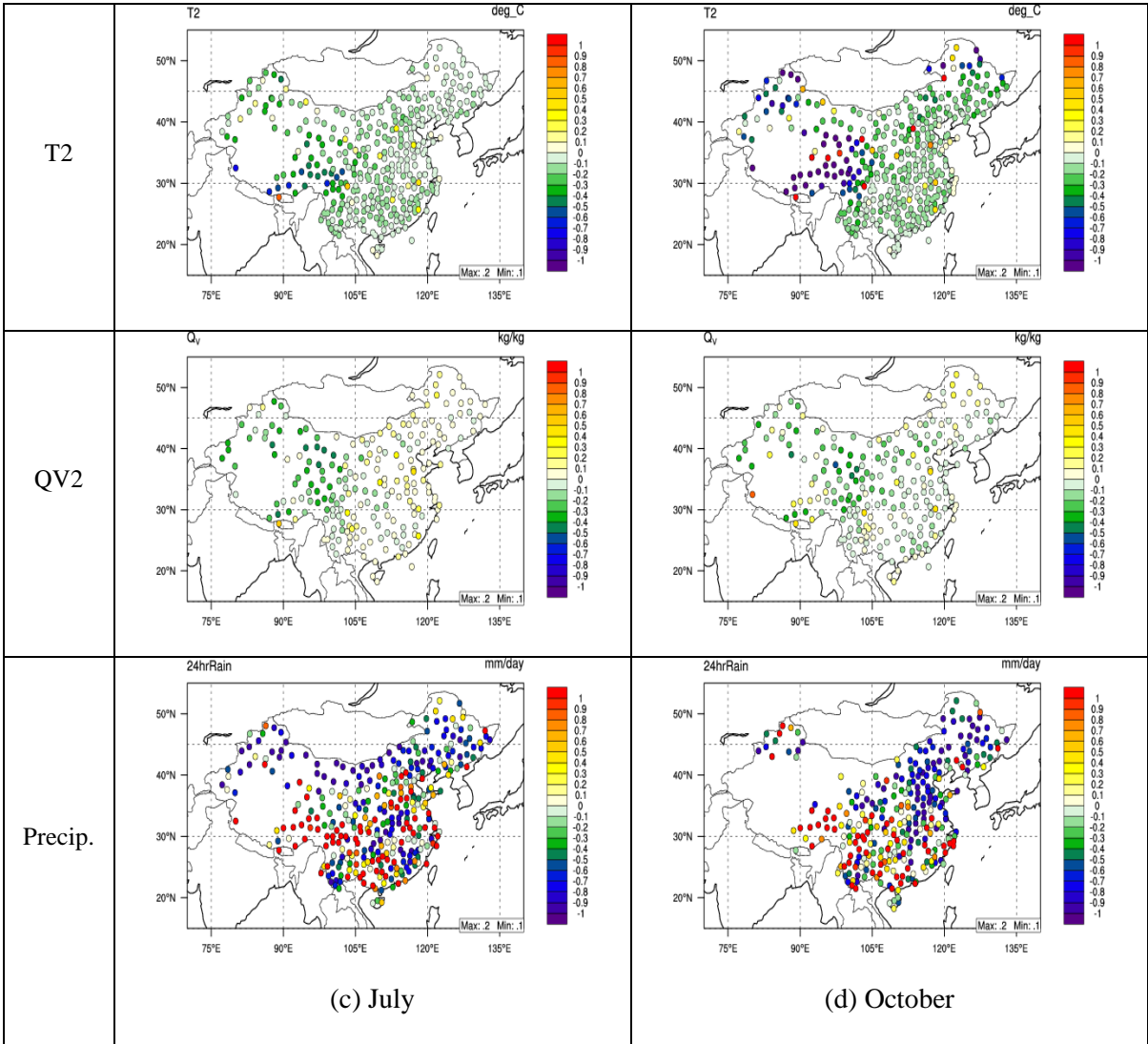


Figure 3.3. Spatial distributions of NMBs between NCDC observational data and MM5 simulations for temperature at 2-m (T2), water vapor mixing ratio at 2-m (QV2), and 24-hr precipitation (Precip.) over China for January, April, July, and October 2001.





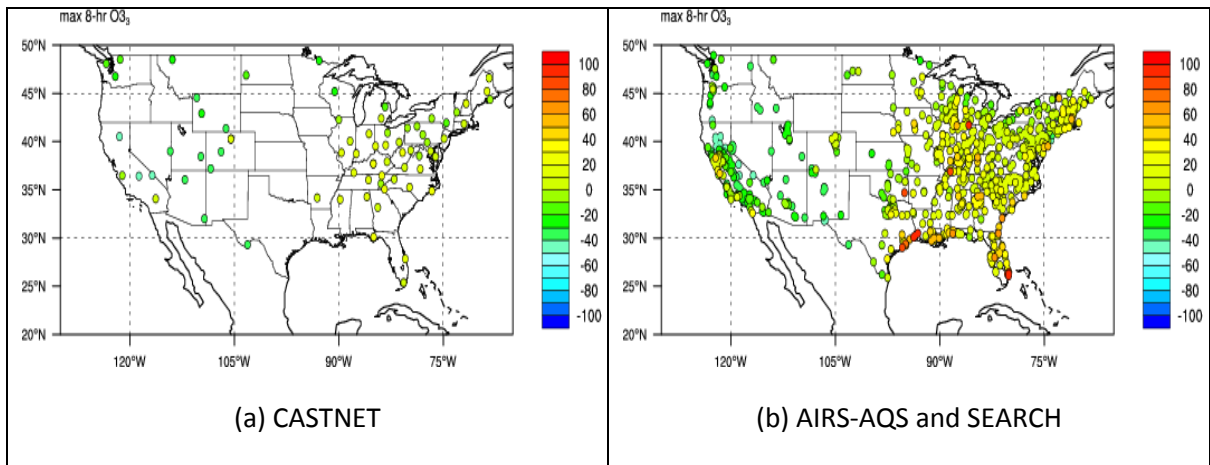


Figure 3.4. Spatial distribution of NMBs for simulated max 8-hr O₃ concentration at the (a) CASTNET and (b) AIRS-AQS and SEARCH sites in July 2001.

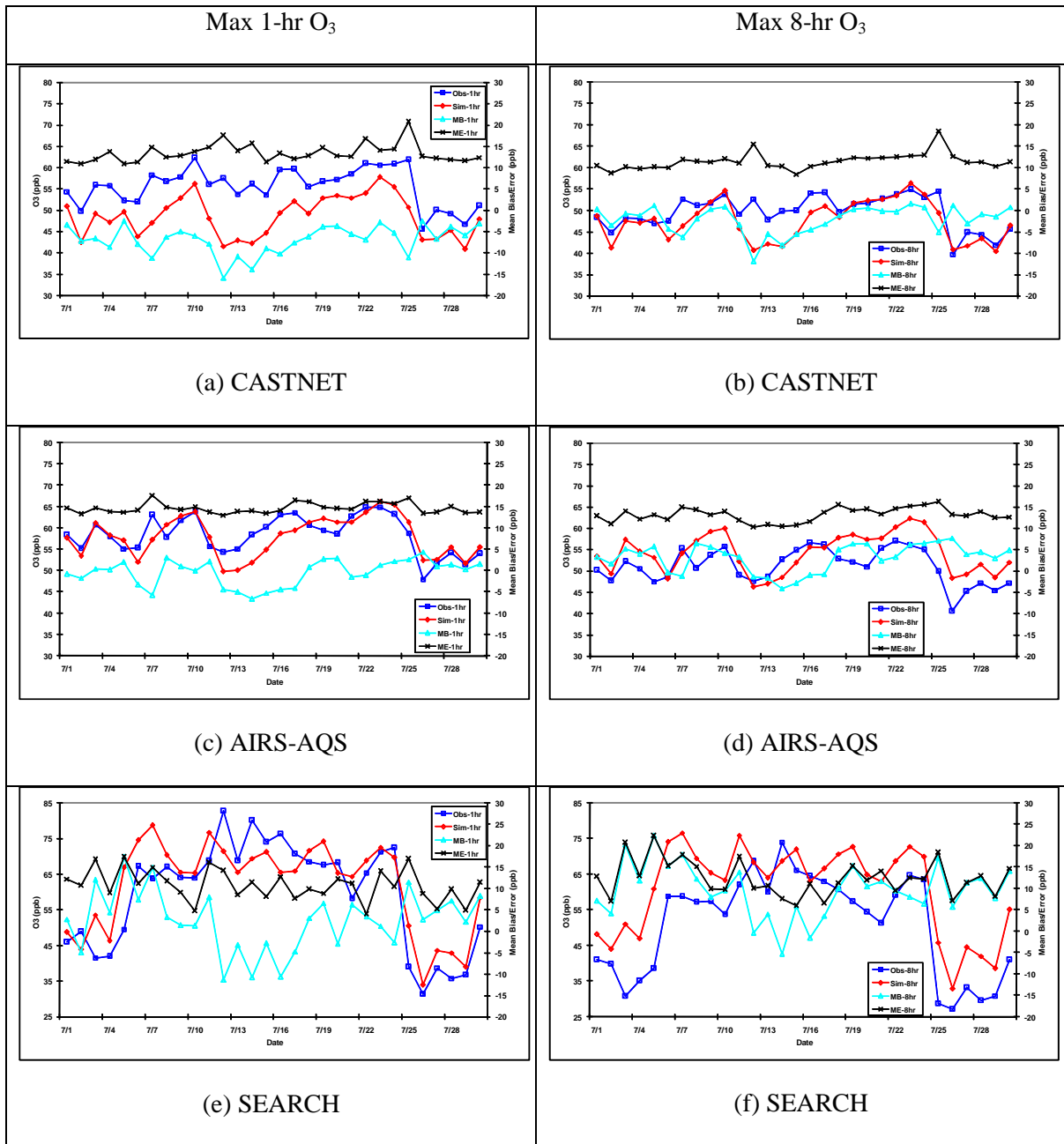


Figure 3.5. The daily variation of domain mean concentration, ME, and MB for max 1-hr and 8-hr O₃ over the CASTNET, AIRS-AQS, and SEARCH sites in July 2001.

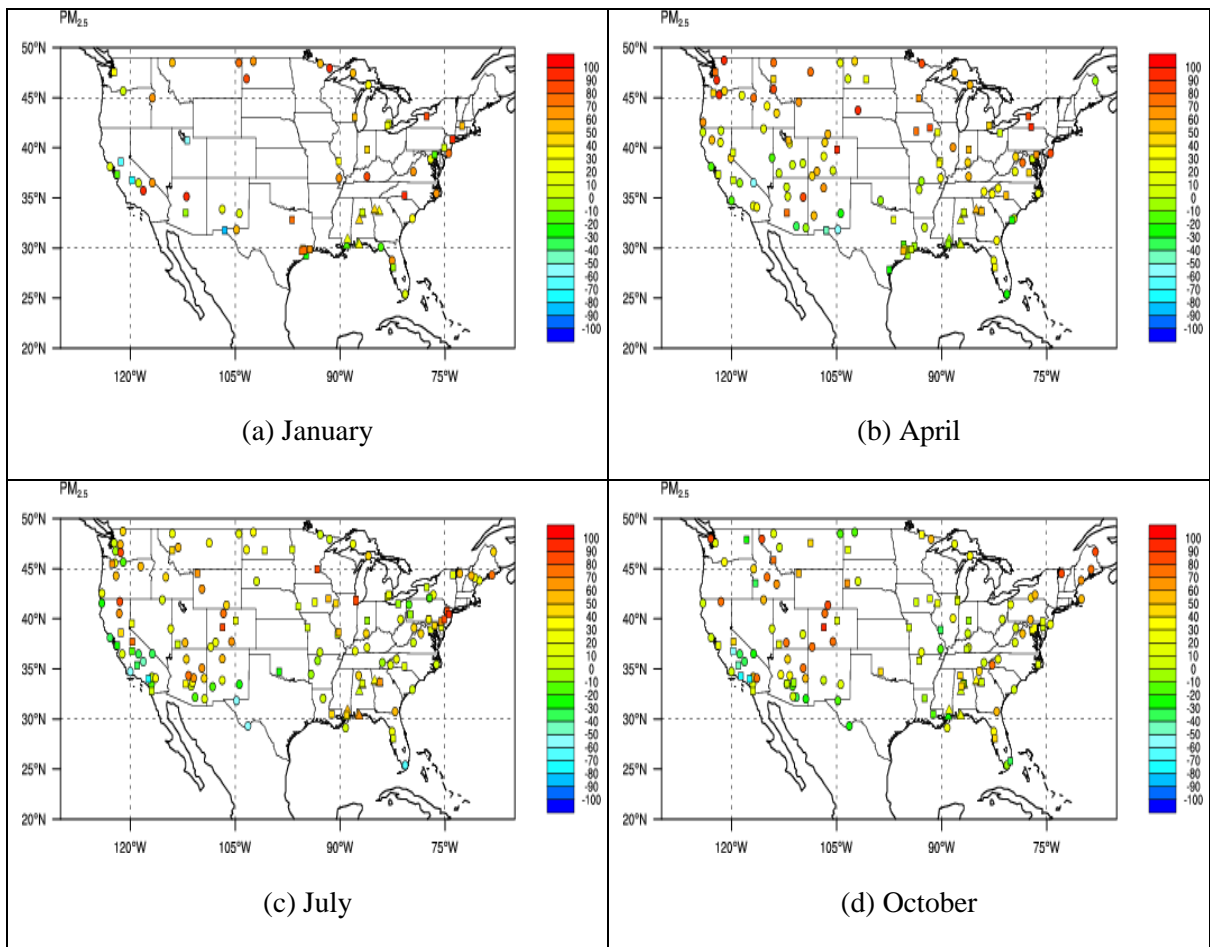


Figure 3.6. The normalized mean biases of simulated daily PM_{2.5} concentrations at the IMPROVE (circle), STN (square), and SEARCH (triangle) monitoring sites for January, April, July, and October 2001.

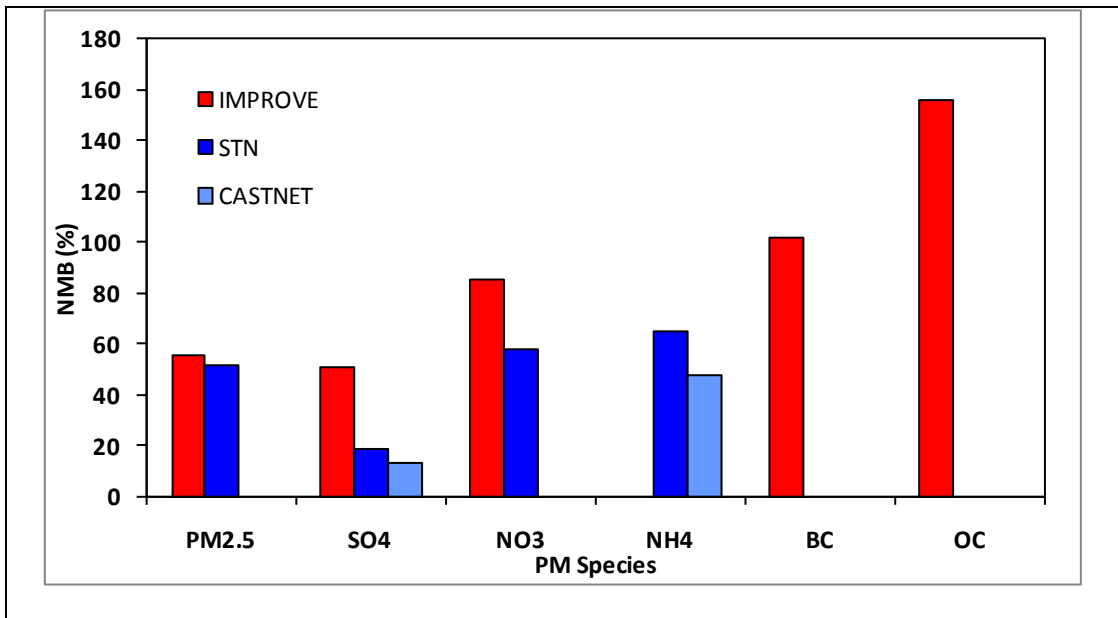


Figure 3.7. The normalized mean bias of simulated monthly $PM_{2.5}$ and its components at the IMPROVE, STN, and CASTNET monitoring sites for April 2001.

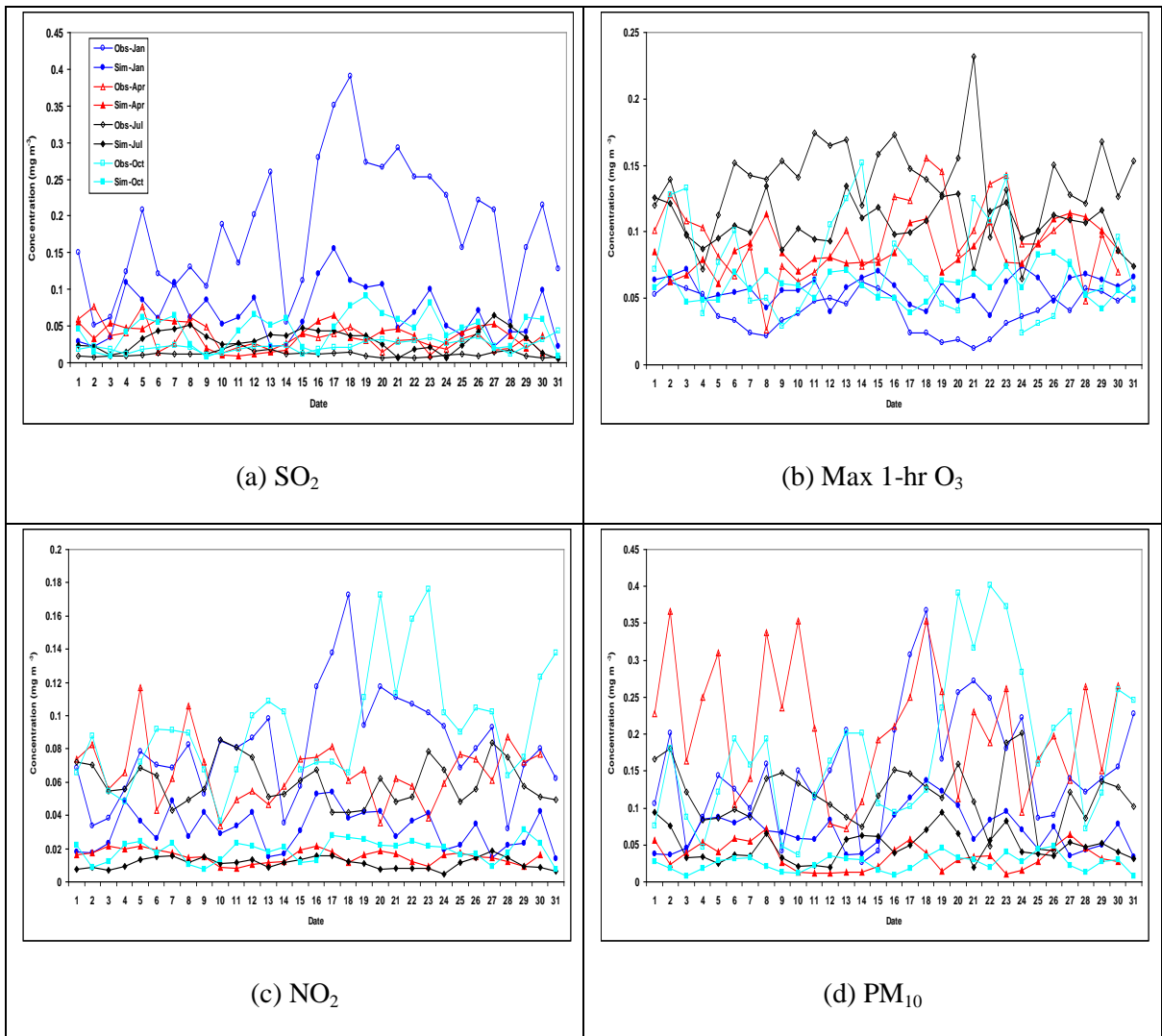


Figure 3.8. Daily variation of concentrations of (a) SO_2 , (b) max 1-hr O_3 , (c) NO_2 , and (d) PM_{10} at Beijing for January, April, July, and October 2001.

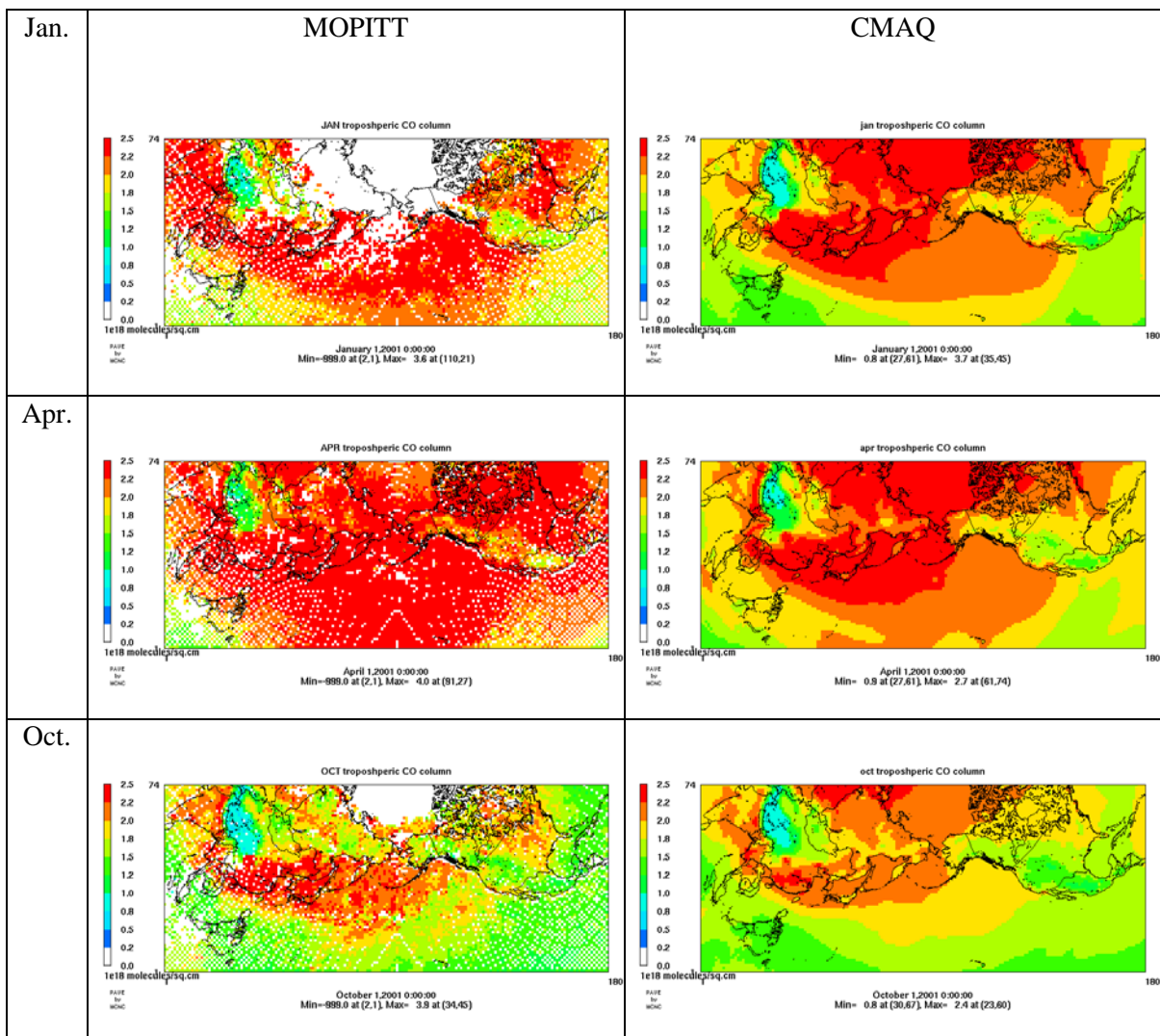


Figure 3.9. Spatial distribution of CO column from MOPITT satellite observations and CMAQ simulation for January, April, and October, 2001. No MOPITT data are available for July, 2001.

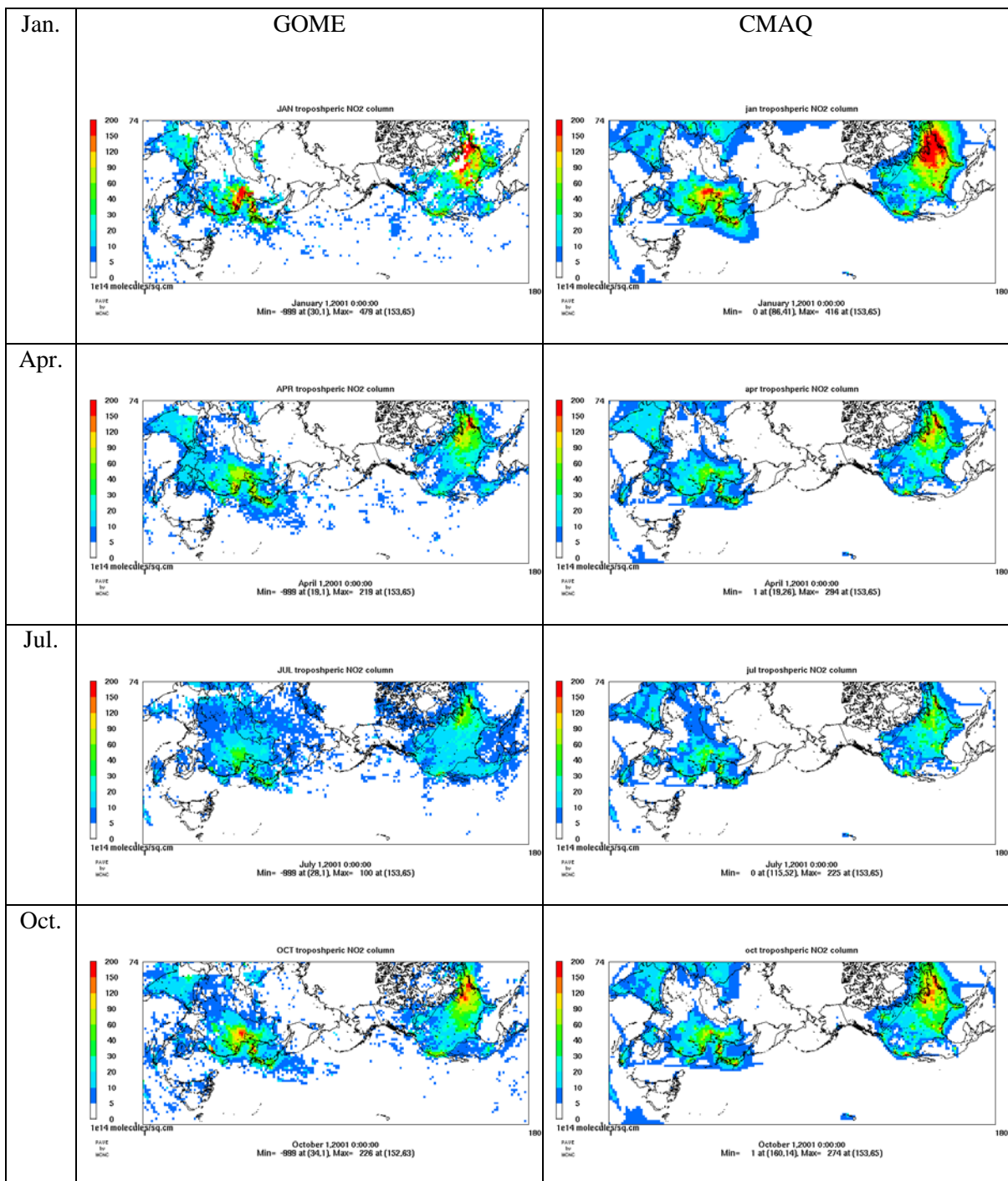


Figure 3.10. Spatial distribution of NO₂ column from GOME satellite observations and CMAQ simulation for January, April, July, and October, 2001.

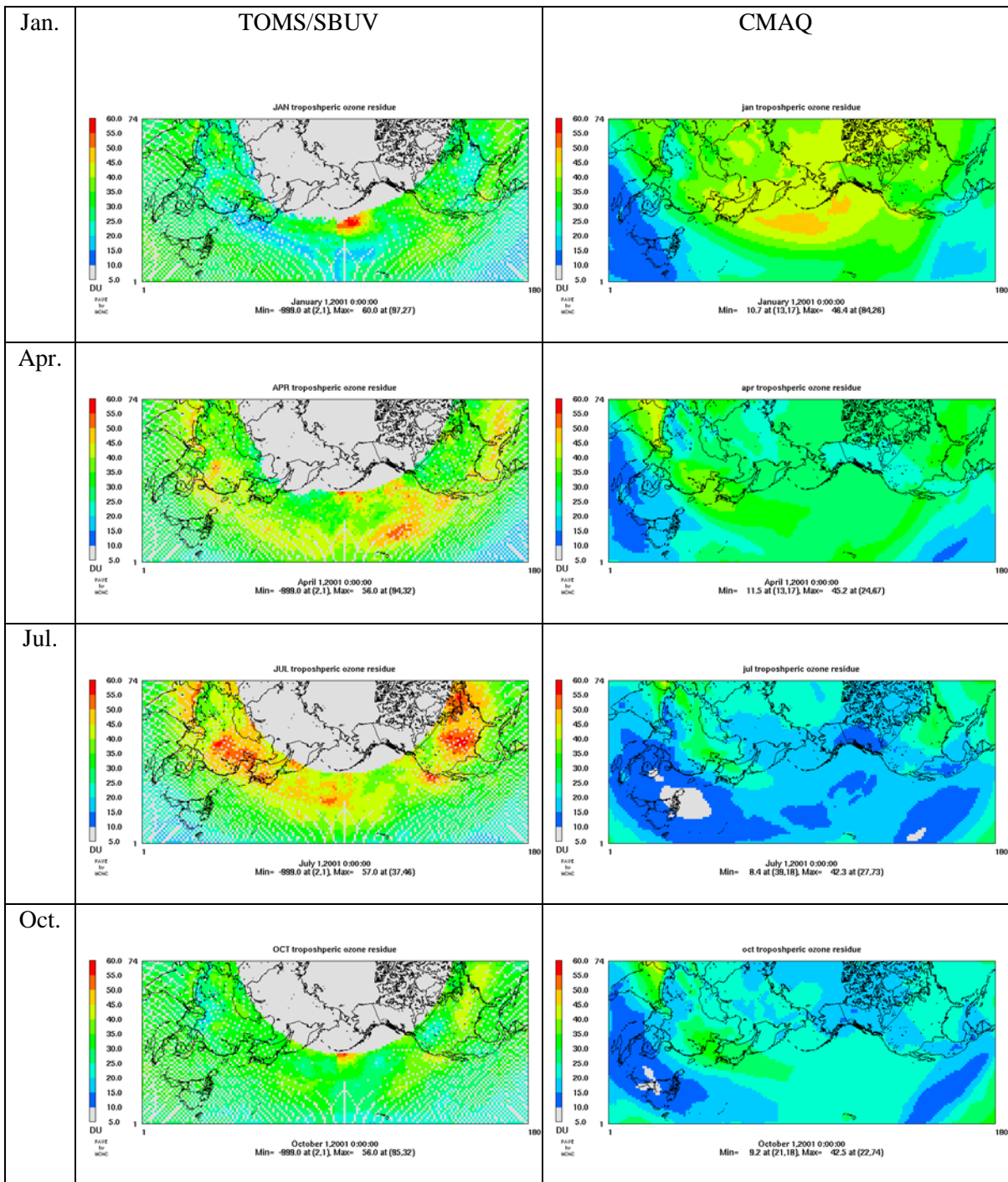


Figure 3.11. Spatial distribution of TORs from TOMS/SBUV satellite observations and CMAQ simulation for January, April, July, and October, 2001.

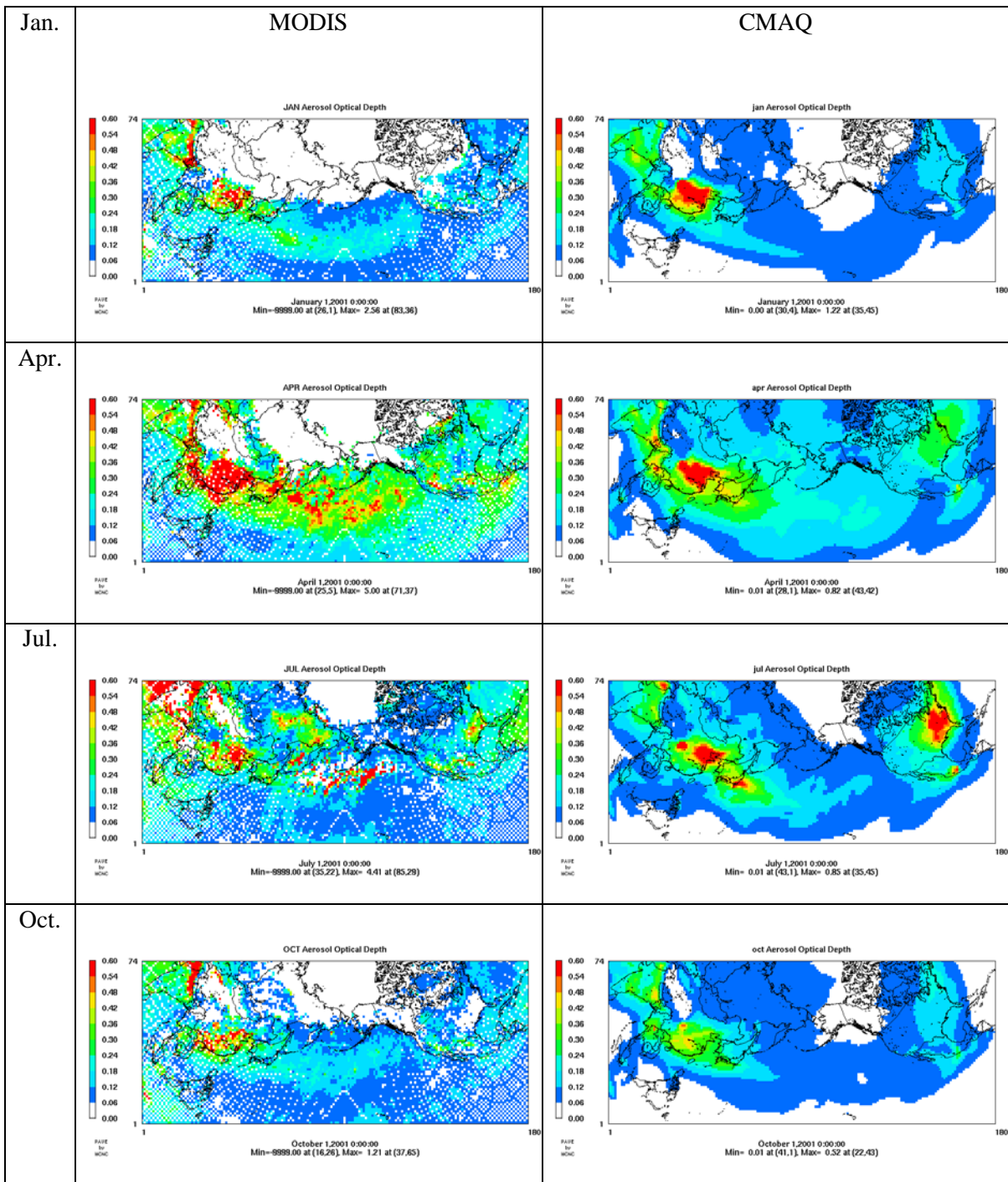


Figure 3.12. Spatial distribution of AODs from MODIS satellite observations and CMAQ simulation for January, April, July, and October, 2001.

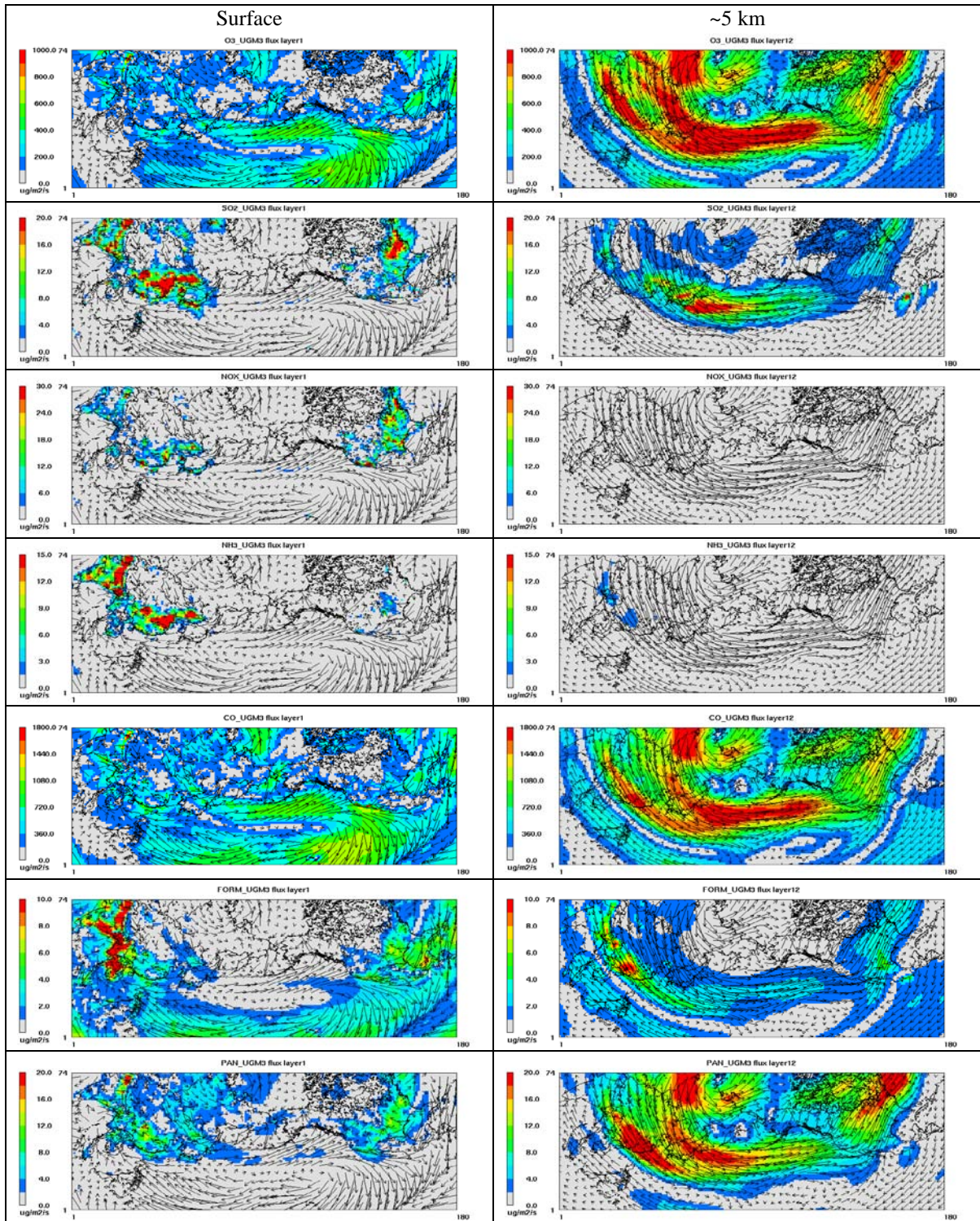


Figure 3.13. Horizontal fluxes of O₃, SO₂, NO_x, NH₃, CO, HCHO, and PAN (from top to bottom), super-imposed with the wind fields, at surface layer and the layer with altitude of ~5 km for April 2001.

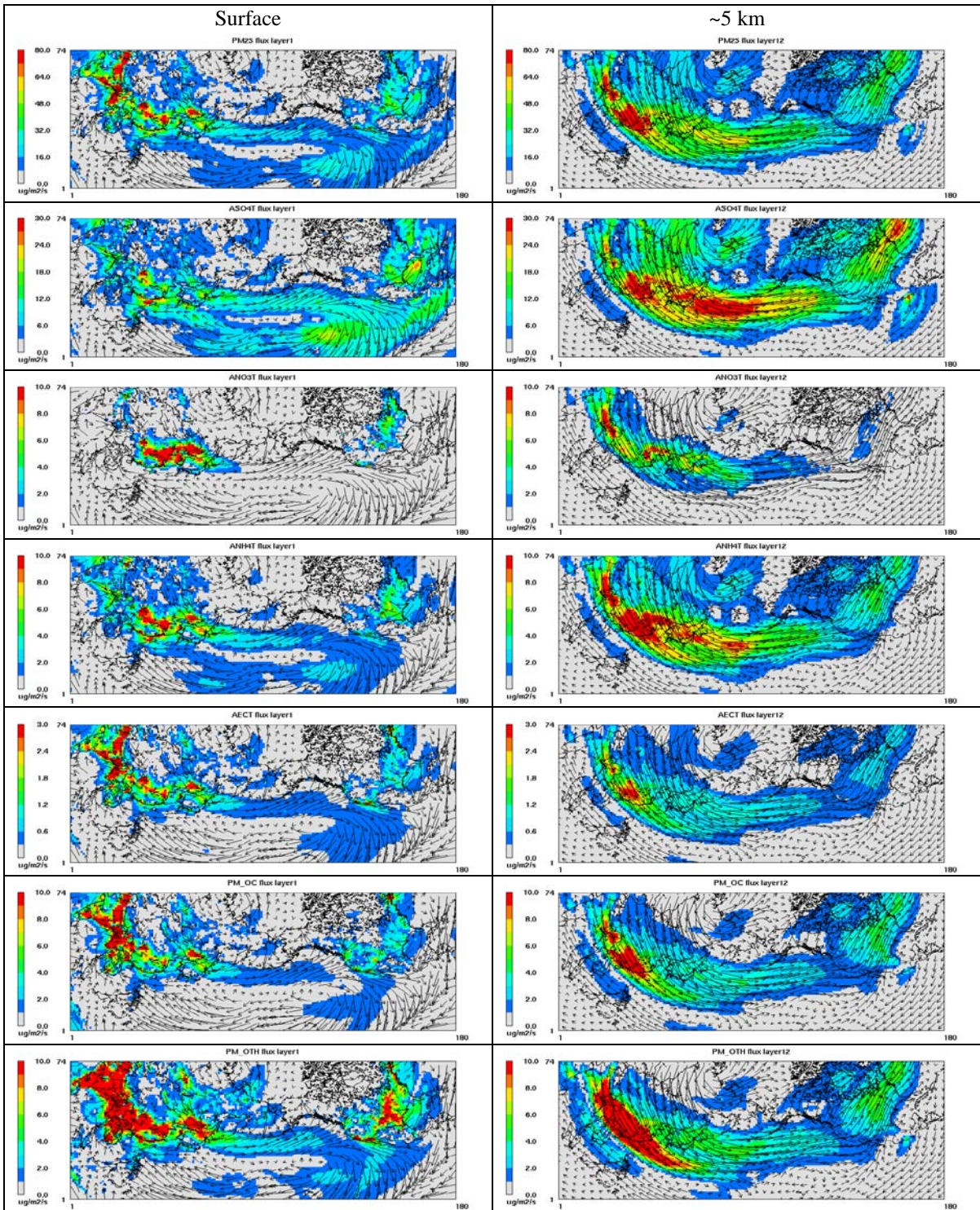
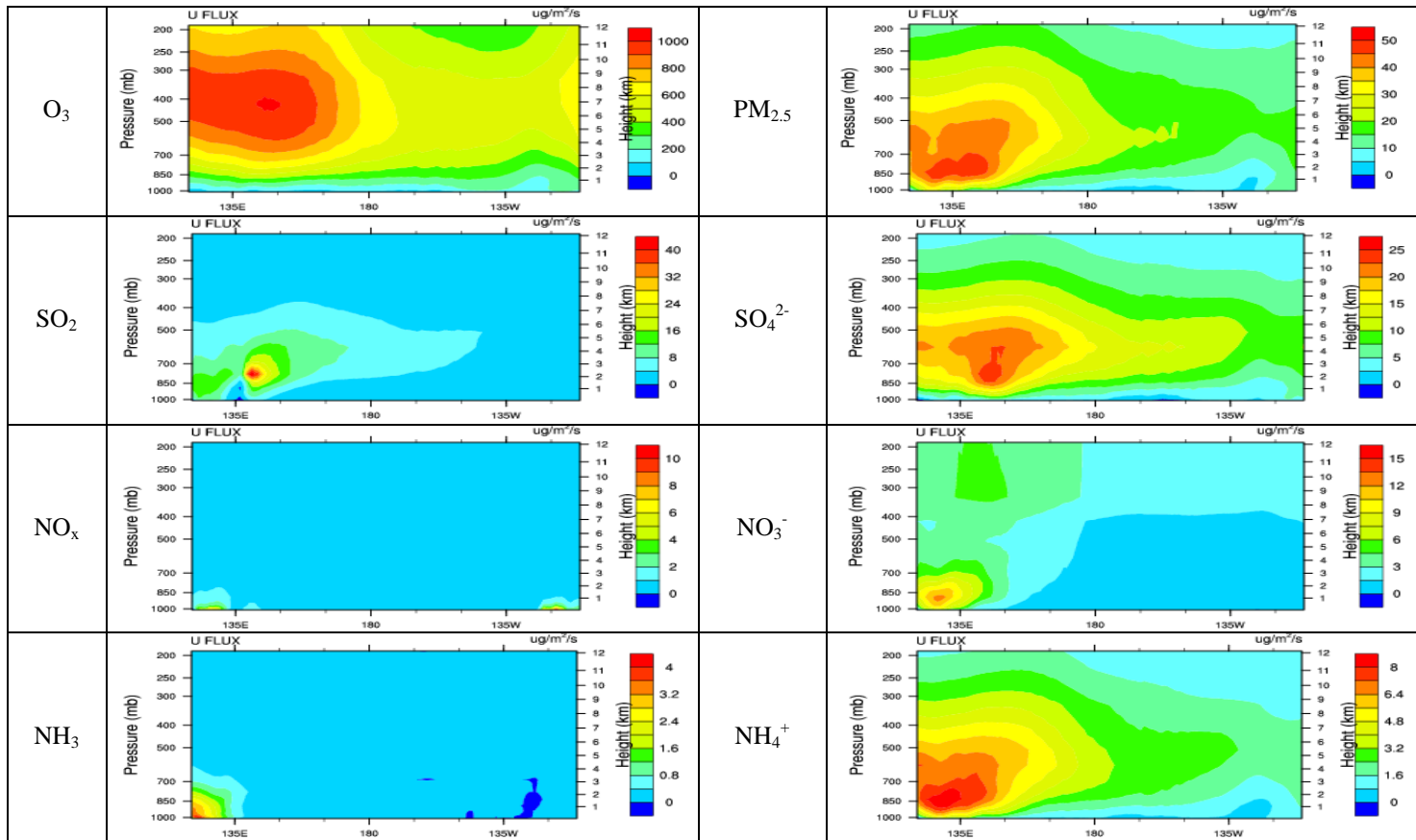


Figure 3.14. Horizontal fluxes of PM_{2.5}, SO₄²⁻, NO₃⁻, NH₄⁺, BC, OC, and other inorganic aerosols (from top to bottom), super-imposed with the wind fields, at surface layer and the layer with an altitude of ~5 km for April 2001.

Figure 3.15. X-Z cross-sections of average horizontal fluxes of O₃, SO₂, NO_x, NH₃, CO, HCHO, PAN, PM_{2.5}, SO₄²⁻, NO₃⁻, NH₄⁺, BC, OC, and other inorganic aerosols between 25-50° N for April 2001.



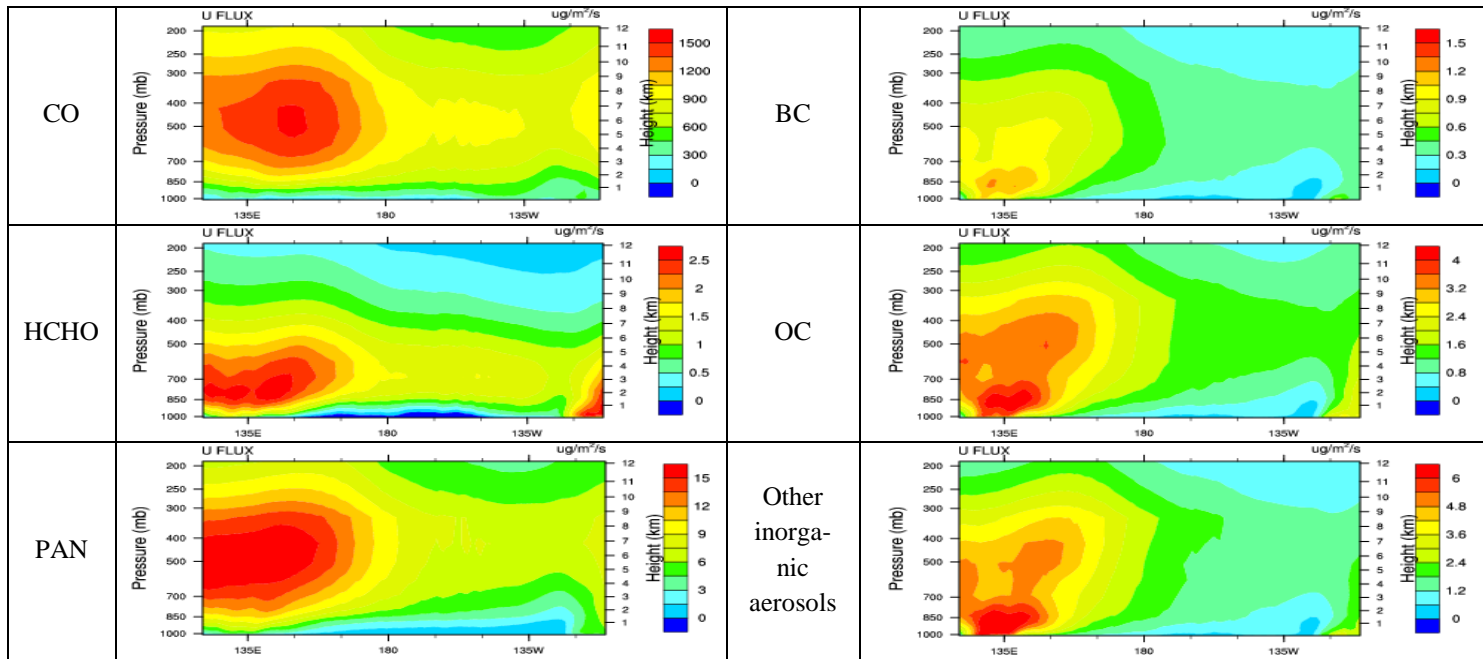
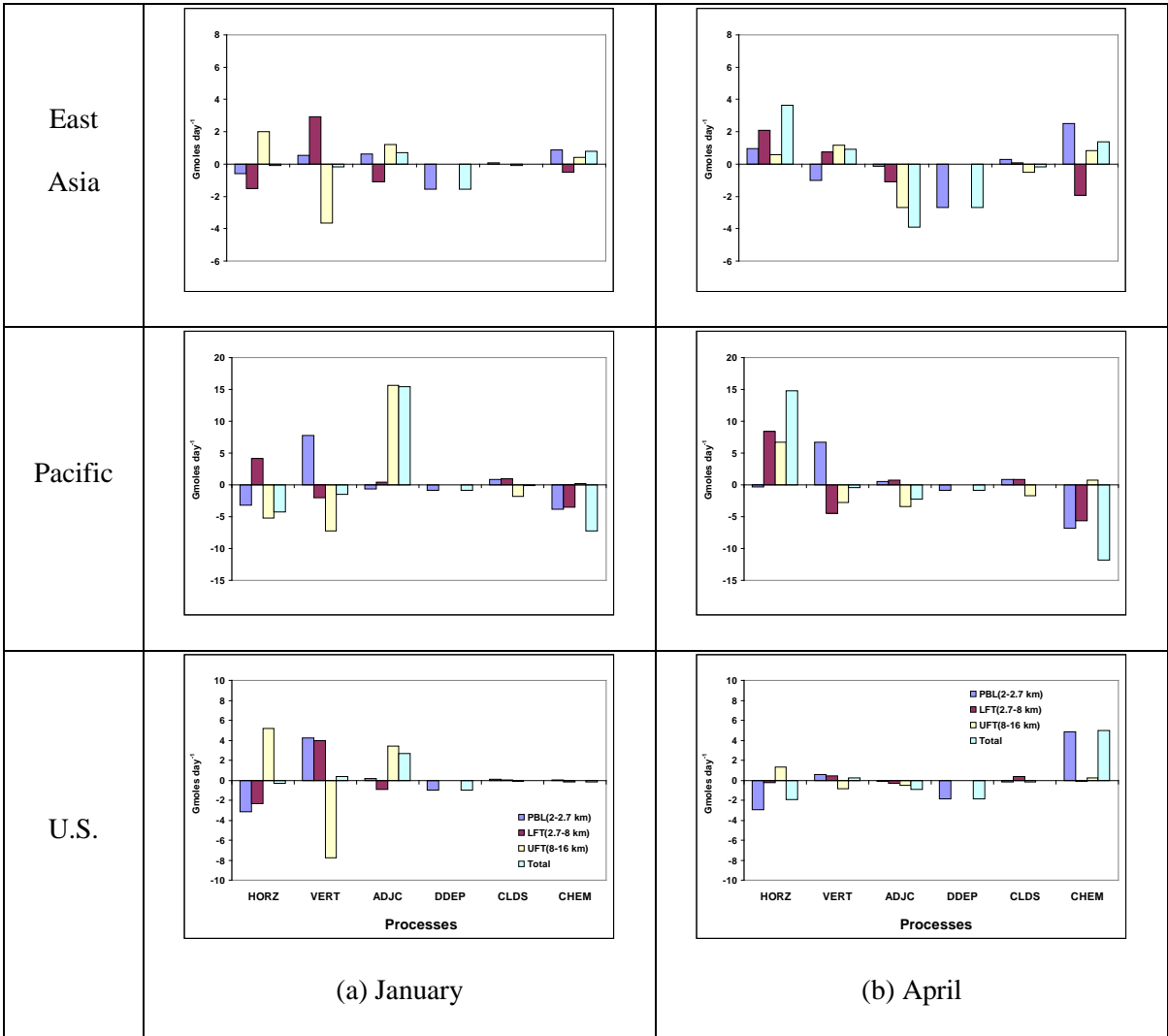


Figure 3.16. Accumulative IPRs for O₃ for different sub-domains for January, April, July, and October 2001.



(a) January

(b) April

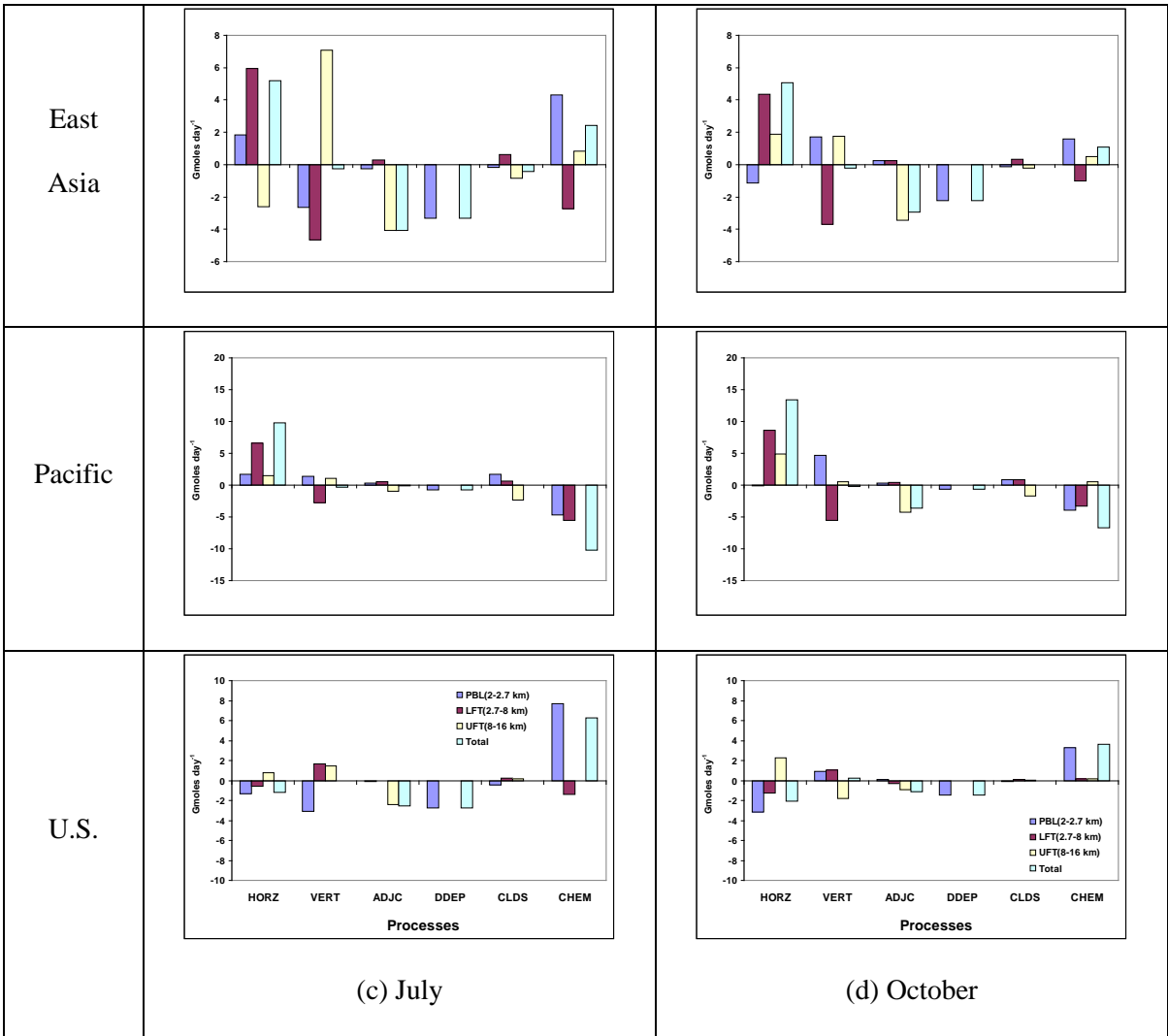
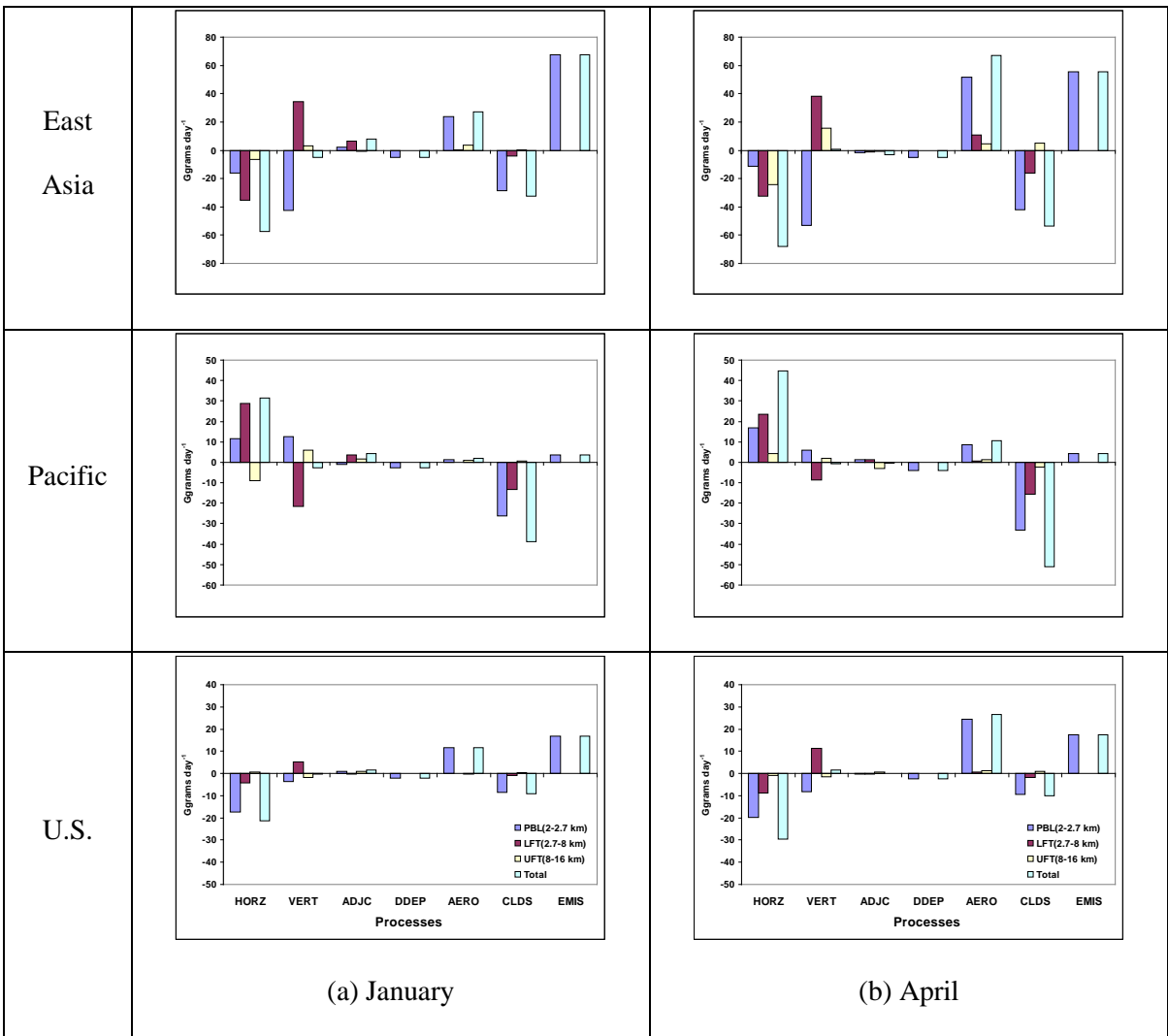
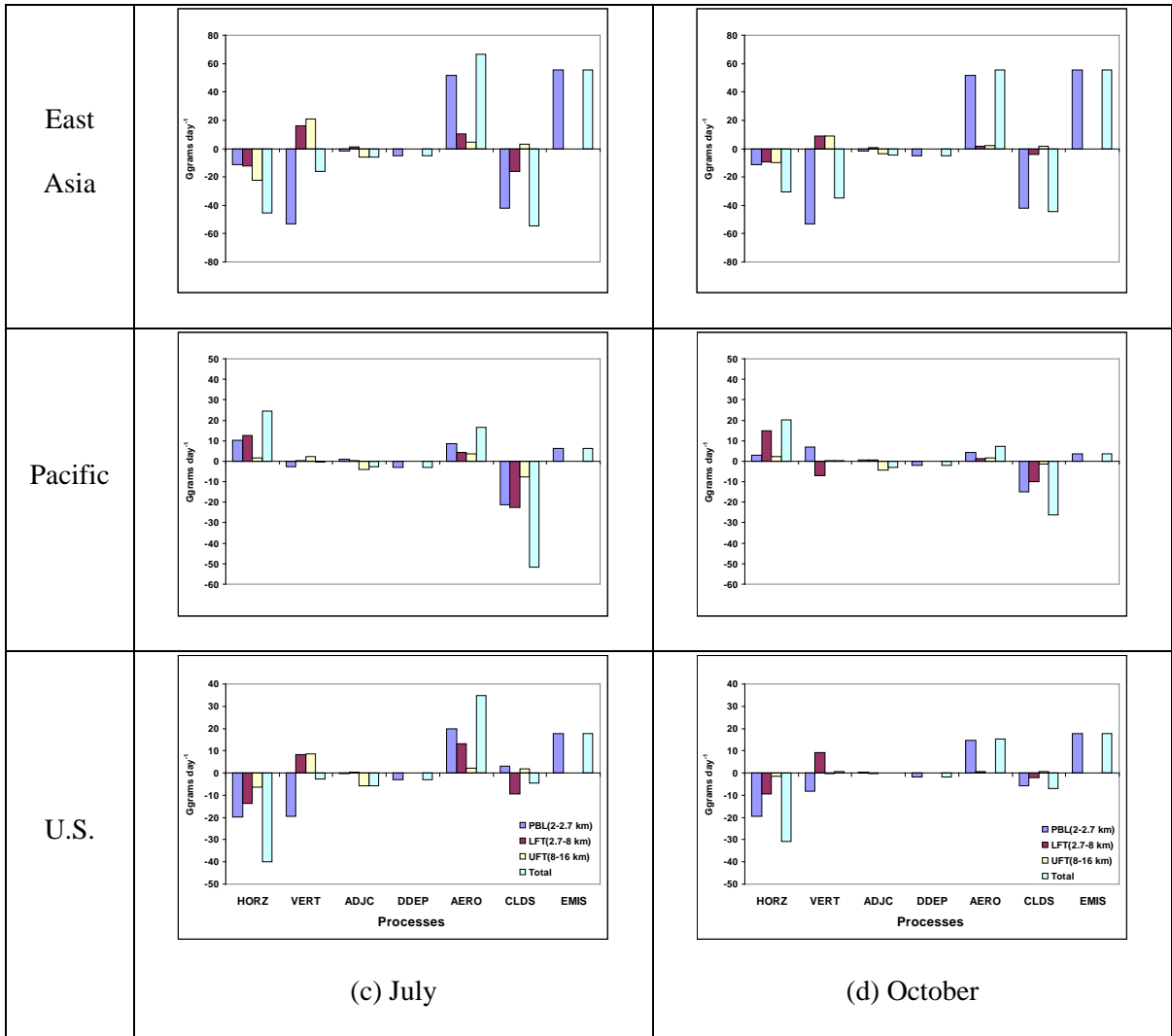


Figure 3.17. Accumulative IPRs for $PM_{2.5}$ for different sub-domains for January, April, July, and October 2001.





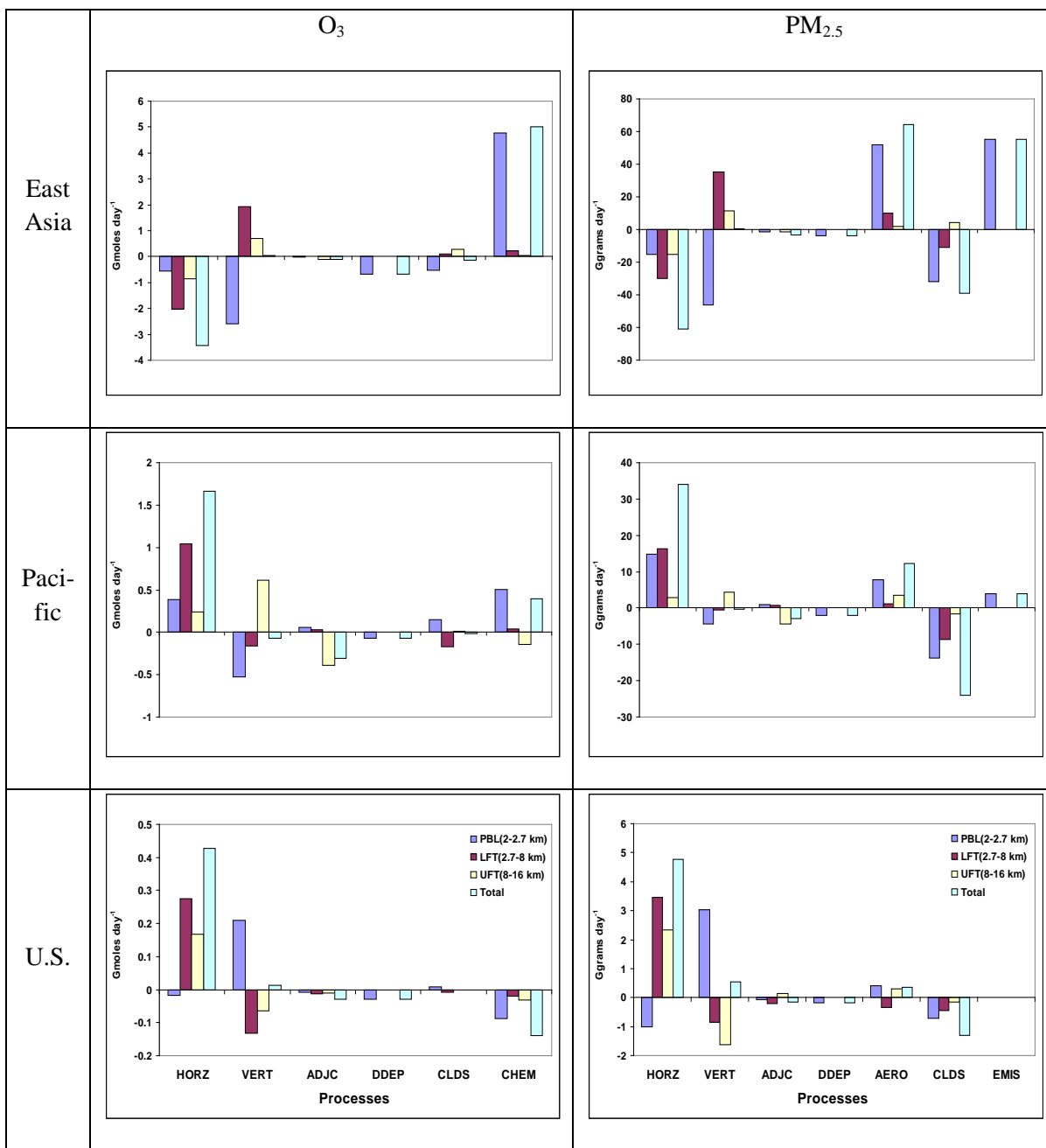


Figure 3.18. IPR differences between baseline and sensitivity simulations for O_3 and $PM_{2.5}$ for different sub-domains for April 2001.

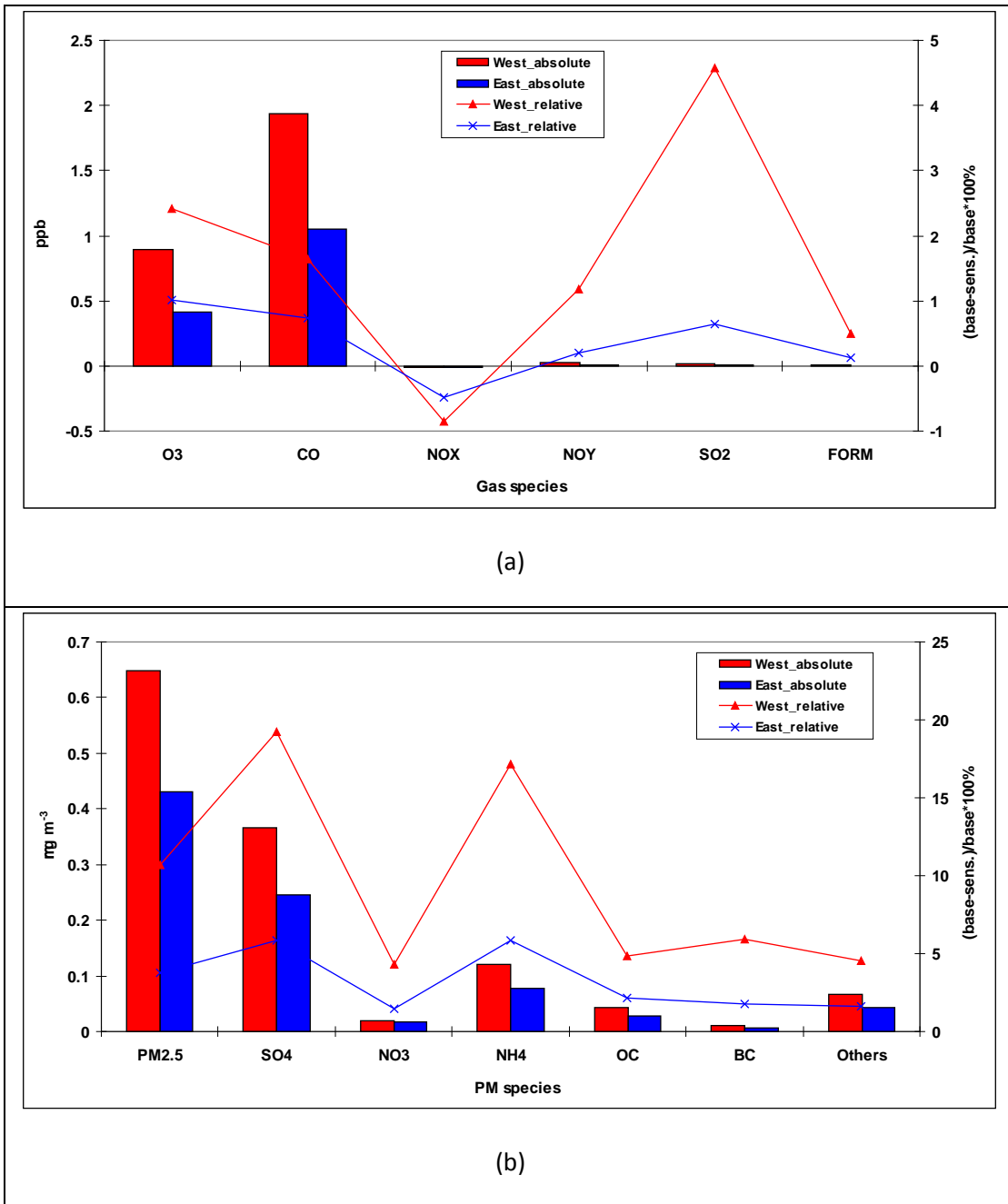


Figure 3.19. Absolute and relative contributions of different (a) gaseous species and (b) PM_{2.5} components over the western U.S. and eastern U.S. due to Asian anthropogenic emissions (AAEs) for April 2001.

CHAPTER 4. IMPLEMENTATION OF ONLINE DUST EMISSIONS

AND DUST-RELATED CHEMISTRY INTO CMAQ

AND INITIAL APPLICATION TO THE 2001 APRIL DUST EPISODE

As shown in Chapter 3, the U.S. EPA's CMAQ modeling system version 4.4 has been applied over the trans-Pacific domain to study the long range transport of Asian air pollutants and its impact on regional air quality over North America. CMAQ reasonably reproduces observed mass concentrations of most air pollutants and capture their transport mechanisms. CMAQ, however, is incapable of reproducing observed mass concentrations of PM₁₀ and AOD, due to the lack of mineral dust treatments in CMAQ. In this chapter, this limitation is overcome by implementing an online dust emission and heterogeneous chemistry module into CMAQ v4.7 in order to investigate the role of dust in affecting chemical predictions of air pollutants. In addition, the default inorganic thermodynamic equilibrium module ISORROPIA 1.7 (Nenes et al., 1998, 1999) in CMAQ v4.7 is updated to ISORROPIA II (Fountoukis and Nenes, 2007). The resulting CMAQ with the above new treatments is referred to as CMAQ-Dust hereafter. CMAQ-Dust is then applied to April 2001 ICAP episode to investigate dust transport, the role of dust in affecting chemical predictions of air pollutants, and the impact of the crustal species (e.g., calcium (Ca²⁺), potassium (K⁺), and magnesium (Mg²⁺)) associated with dust particles on the inorganic gas/particle partitioning through their partitioning of thermodynamic equilibrium. The objective of study is to enhance CMAQ's capability in simulating PM and their interactions with photochemical cycles, as well as long range transport of air pollutants associated with dust storms.

4.1 Incorporation of Mineral Dust Treatments into CMAQ

4.1.1 Online Dust Emission Module

In this work, two established and commonly-used schemes are selected, adapted, and incorporated into CMAQ. These two schemes are the one introduced by Westphal et al. (1987) (refer to as the Westphal scheme hereafter) and the one introduced by Zender et al. (2003) (refer to as the Zender scheme hereafter). A major difference between the two schemes is that the Zender scheme splits the dust flux into two components, horizontally saltating mass flux of large particles (Q_s) and vertical mass flux of dust (F_d), whereas the Westphal scheme calculates vertical fluxes directly. The Zender scheme can thus better mimic the actual physical mechanism of dust emissions than the Westphal scheme. Comparison of the two dust emission schemes in CMAQ permits an assessment of the sensitivity of dust emissions and spatial distributions to different dust flux calculations and the resulting impacts on PM concentrations and photochemical cycles for urban/regional applications. A detailed description about these two schemes is given below.

A parameterization scheme developed by Westphal et al. (1987) and recently revised by Choi and Fernando (2008) has been implemented into CMAQ. Westphal et al. (1987) proposed that the vertical mass fluxes of dust particles with diameter less than 10 μm can be expressed as a function of surface friction velocity (u_*) based on measurements in the Saharan desert, deserts of the southwestern U.S., and Israeli deserts in Asia. The associated formulas for the dust vertical flux, F_d ($\text{g m}^{-2} \text{s}^{-1}$), are expressed as follows:

$$F_d = EF \times (1 - RF) \times 10^{-14} u_*^4 \quad (3.1)$$

when $u_* \geq u_{*t}$ for predominantly silt and clay soil

$$F_d = EF \times (1 - RF) \times 10^{-13} u_*^3 \quad (3.2)$$

when $u_* \geq u_{*t}$ for predominantly sandy soil

where u_* is the surface friction velocity, u_{*t} is the threshold surface friction velocity, RF is a reduction factor over different land types based on the 24 U.S. Geophysical Survey (USGS) land use categories (in this study, we assume only three types of land use categories can produce the dust and they are shrubland, mixed shrub/grassland, and barren or sparsely vegetated land). The values for RF are 0.7, 0.75, and 0.1, respectively for them and more details can be found in Choi and Fernando (2008). EF is a constant and is originally set to 0.13. In the original scheme of Westphal et al. (1987), they assumed a constant u_{*t} which might be valid for regional scale studies but is subject to high uncertainties for larger scale simulation. Recently, Choi and Fernando (2008) improved the scheme by considering the effects of soil texture (i.e., soil percentage of sand, silt, and clay) and soil moisture on u_{*t} , which makes the scheme more suitable for larger scale study. In addition to the soil texture and moisture, there are several other factors that may affect the values of u_{*t} , such as the particle size distribution of soils and the drag partitioning between the traditional aerodynamic roughness length and “smooth” roughness length (Marticorena and Bergametti, 1995). The aerodynamic roughness length of the bare ground includes the nonerodible elements such as pebbles, rocks, and vegetation and the “smooth” roughness length only represents potentially erodible particles without any nonerodible elements. The latter is typically less than the former and the resulting drag partitioning will increase the values of u_{*t} . In the current version of module, only the soil moisture and texture are considered due to the lack of other information. An initial value of u_{*t} , u_{*tI} , is first decided using a

semiempirical expression developed by Marticorena et al. (1997) for different land use types. They are 0.43, 0.43, and 0.304 m s⁻¹ for shrubland, mixed shrub/grassland, and barren or sparsely vegetated land, respectively. An updated value of u_{*t} is then calculated using the following empirical formula (Fecan et al., 1999):

$$u_{*t} = u_{*t1} \left[1 + 121(w - w')^{0.68} \right]^{0.5} \quad \text{when } w > w' \quad (3.3)$$

and

$$u_{*t} = u_{*t1} \quad \text{when } w \leq w' \quad (3.4)$$

where w is the gravimetric soil moisture (kg kg⁻¹) and w' is the threshold gravimetric soil moisture. They are determined by the following empirical formulas (Fecan et al., 1999; Zender et al., 2003):

$$w = \theta \rho_w / \rho_{p,d} \quad (3.5)$$

$$\rho_{p,d} = \rho_p (1.0 - \theta_s) \quad (3.6)$$

$$\theta_s = 0.489 - 0.126 M_{sand} \quad (3.7)$$

$$w' = 14 M_{clay}^2 + 17 M_{clay} \quad (3.8)$$

where θ is the volumetric soil moisture (m³ m⁻³) from the NCEP/NCAR reanalysis data, $\rho_w = 1000 \text{ kg m}^{-3}$ is the density of water, $\rho_p = 2600 \text{ kg m}^{-3}$ is the mean soil particle density, $\rho_{p,d}$ is the bulk density of dry soil, θ_s is volumetric saturation soil moisture (m³ m⁻³), and M_{sand} and M_{clay} are the mass fractions of sand and clay, respectively, in the soil.

The dust emission parameterization of Zender et al. (2003) that has been extensively used in several global models (e.g., Liao and Seinfeld, 2005; Fairlie et al., 2007, 2010;

Nowotnick et al., 2010) has also been implemented into CMAQ in this work. In the Zender scheme, Q_s ($\text{g m}^{-1} \text{s}^{-1}$) is expressed explicitly as a function of u_* and u_{*t} according to the theory of White (1979). The formulas are as follows:

$$Q_s = EF \frac{c_s \rho u_*^3}{g} \times \left(1 - \frac{u_{*t}^2}{u_*^2}\right) \times \left(1 + \frac{u_{*t}}{u_*}\right) \quad \text{when } u_* > u_{*t} \quad (3.9)$$

$$Q_s = 0 \quad \text{when } u_* \leq u_{*t} \quad (3.10)$$

when $u_* \leq u_{*t}$

where $c_s = 2.61$, ρ is the atmospheric density and g is acceleration of gravity. Different from the Westphal scheme, u_{*t} , is determined by a more complicated semi-empirical relationship (Iversen and White, 1982):

$$u_{*t}(D) = \left[\frac{0.1666681 \rho_p g D}{-1 + 1.928 \text{Re}_{*t}^{0.0922}} \left(1 + \frac{6 \times 10^{-7}}{\rho_p g D^{2.5}}\right) \right]^{1/2} \rho^{-1/2} \quad \text{when } 0.03 \leq \text{Re}_{*t} \leq 10 \quad (3.11)$$

$$u_{*t}(D) = \left[0.0144 \rho_p g D \left(1 - 0.0858 e^{-0.0617(\text{Re}_{*t} - 10)}\right) \left(1 + \frac{6 \times 10^{-7}}{\rho_p g D^{2.5}}\right) \right]^{1/2} \rho^{-1/2} \quad \text{when } \text{Re}_{*t} > 10 \quad (3.12)$$

where ρ_p is the mean soil particle density, D is the average diameter of saltation particles and is assumed to be the optimal particle size, $D_0 \approx 75 \mu\text{m}$ under typical conditions on Earth (Zender et al., 2003), Re_{*t} is the threshold friction Reynolds number and is estimated using an empirical expression introduced by Marticorena and Bergametti (1995):

$$\text{Re}_{*t} = 1331D^{1.56} + 0.38 \quad (3.13)$$

An updated value of u_{*t} is calculated based on u_{*tI} and equations (3.3) – (3.8). The horizontal saltation mass flux Q_s is then converted to a vertical dust mass flux F_d (the final

dust flux in Zender scheme and in unit of $\text{g m}^{-2} \text{s}^{-1}$) by:

$$F_d = T \times S \times \alpha \times Q_s \quad (3.14)$$

where T is a global tuning factor and is set to be $T = 7.0 \times 10^{-4}$, following Zender et al. (2003), S is the source erodibility factor with values from 0 to 1 and confines dust emissions to topographic depressions in desert and semi-desert areas of the world (Ginoux et al., 2001) and α (m^{-1}) is empirically parameterized based on Marticorena and Bergametti (1995):

$$\alpha = 100e^{[(13.4M_{\text{clay}} - 6.0)\ln 10]} \quad (3.15)$$

where M_{clay} is the mass fraction of clay particles in parent soil and restricted to $M_{\text{clay}} < 0.2$.

The soil texture data used for both schemes are generated by the Weather Research & Forecasting Model (WRF) Preprocessing System (WPS) and are essentially taken from the U.S. State Soil Geographic (STATSGO) soil database with a 1-km grid resolution. u_* comes directly from a meteorological model (e.g., WRF). The land use data as mentioned previously are from the USGS dataset also with 1-km grid resolution. The simulated snow cover and precipitation data are used for determining whether the dust emissions will be generated over each grid cell of the simulation domain. In summary, the data to be used to generate the dust emission come from various sources including the observation reanalysis data (e.g., NCEP data), other model simulations (e.g., WRF outputs), statistical survey data (e.g., STATSGO and USGS data), and empirical expression (e.g., u_{*ll}). In the dust emission module, only 3 types of land use categories as mentioned previously are assumed to generate mineral dust (Choi and Fernando, 2008). They are shrub land, mixed shrub/grass land, and barren or sparsely vegetated land. Nickovic et al. (2001) have classified the particle sizes of

mineral dust into four categories based on the contents of clay, small silt, large silt, and sand. Only the first two types, clay and small silt, are considered as PM₁₀. In this way, the dust flux generated from equations (3.1), (3.2), and (3.14) are further multiplied by a fraction, which is based on the STATSGO soil texture data to approximate the fluxes of dust PM₁₀ in a given grid cell (Choi and Fernando, 2008). According to MRI (2005), the PM_{2.5}/PM₁₀ ratio for typical fugitive dust sources is 0.1, so the fluxes of dust PM_{2.5} can be obtained by multiplying the fluxes of dust PM₁₀ by 0.1.

4.1.2 Heterogeneous Chemistry on the Surface of Dust

Nine heterogeneous reactions (see Table 4.1) on the surfaces of dust are implemented into CMAQ to explore potential impacts of mineral dust on chemical predictions.

Absorption and heterogeneous reactions of gases on the surfaces of dust are assumed to be irreversible (Zhang and Carmichael, 1999). Following the method of Schwartz (1986), the uptake of gases onto mineral dust particles is defined by a pseudo first-order heterogeneous rate constant K_i (m³ s⁻¹) for species i as follows:

$$K_i = \left(\frac{d_p}{2D_i} + \frac{4}{v_i \gamma_i} \right)^{-1} S_p \quad (10)$$

where, d_p is the dust particle diameter (m), D_i is the gas-phase molecular diffusion coefficient for species i (m² s⁻¹), v_i is the mean molecular velocity of species i (m s⁻¹), S_p is the surface area density of dust particles (m² m⁻³) and is determined from the CMAQ simulation, and γ_i is the uptake coefficient for species i . The concentrations of selected gas species and the corresponding aerosol products will be simulated by incorporating those pseudo first-order

reactions (see Table 4.1). The uptake coefficients γ of nine species considered in this study are largely based on the work of Bian and Zender (2003) and summarized in Table 4.1 (The original references for the reactions and γ are also listed). Note that uncertainties in γ are very large and may be up to three orders of magnitude for certain species (Zhang and Carmichael, 1999; Bian and Zender, 2003). For example, some studies have reported the values of γ ranging from 2.0×10^{-6} to 2.5×10^{-3} for O_3 and from 2.0×10^{-6} to 1.6×10^{-2} for HNO_3 (Goodman et al., 2000; Underwood et al., 2001; Michel et al., 2002). The γ values used in this study represent the best estimate or lower limit values from the literatures (Zhang and Carmichael, 1999; Bian and Zender 2003) and a set of upper limit values for several reactions are also tested through the sensitivity simulation. Most of the aforementioned models consider the uptake of HNO_3 onto the surfaces of dust particle to be an irreversible process. However, experimental evidences (Knipping and Dabdub, 2002; Rivera-Figueroa et al., 2003; Ndor et al., 2009) suggested that the reaction of gaseous nitric oxide with HNO_3 on surfaces may convert HNO_3 to photochemically-active NO_x back into the atmosphere. This so-called “renoxification” process is also considered in this study.

4.1.3 Incorporation of ISORROPIA II and Crustal Species Treatments into CMAQ

4.1.3.1 Incorporation of ISORROPIA II into CMAQ

It has been shown that the consideration of crustal materials in predicting the partitioning of NO_3^- and NH_4^+ , especially in areas where mineral dust comprises a significant portion of aerosols, is very important and can potentially improve model predictions (Jacobson, 1999; Moya et al., 2002; Fountoukis and Nenes, 2007). The newly-developed

thermodynamic equilibrium module ISORROPIA II includes the thermodynamics of crustal materials of Ca^+ , K^+ , and Mg^{2+} based on the preexisting suite of components of ISORROPIA model. The model determines the subsystem set of equilibrium equations and solves for the equilibrium state using the chemical potential method. ISORROPIA uses pre-calculated tables of binary activity coefficients and water activities of pure salt solutions, which speed up calculations significantly. ISORROPIA also offers the ability to solve for the “reverse problem” and makes a metastable assumption when incorporated in CMAQ, which assumes that only aqueous-phase particles are formed. More details about ISORROPIA II can be found in Fountoukis and Nenes (2007). Following the incorporation of the online dust emission module and dust related heterogeneous chemistry, three new crustal species (i.e., Ca^+ , K^+ , and Mg^{2+}) are added into CMAQ and the default thermodynamic module (e.g., ISORROPIA v1.7) in CMAQ is replaced by ISORROPIA II, to study the impact of those crustal species on the inorganic gas/particle partitioning through aerosol thermodynamic equilibrium. This implementation of crustal species treatment is expected to provide a more complete picture of the physical and chemical processes associated with mineral dust.

The emissions of crustal species are based on online-calculated dust emissions. Since the newest version of CMAQ (i.e., CMAQ v4.7) simulates the gas/particle partitioning in all three PM size modes (i.e., Aiken, accumulation, and coarse modes), the emissions of crustal species are speciated for both fine- and coarse-mode dust. 10% of the emitted crustal species are assumed to be in the accumulation mode and 90% are in the coarse mode (Midwest Research Institute, 2005). In the model, crustal species are also treated spatially-uniformed, which means all emissions of the crustal species are proportional to those of dust, because of

the lack of information on the chemical composition and mineralogy of dust particles. The ratio between crustal species and dust is assumed to be 1.022×10^{-2} , 1.701×10^{-2} , 7.08×10^{-3} for K^+ , Ca^+ , and Mg^{2+} , respectively, based on Van Pelt and Zobeck (2007).

4.1.3.2 Study of Effects of Crustal Materials on the Gas/Particle Partitioning Using Box Models of ISORROPIAv1.7, ISORROPIA II, and EQUISOLV II

In this section, three aerosol equilibrium modules: ISORROPIA v1.7, ISORROPIA II, and EQUISOLV II (the major characteristics of ISORROPIA II and EQUISOLV II are summarized in Table 4.2) are applied to study the gas/particle partitioning of inorganic species using observational data from the sampling experiment conducted at Hong Kong University of Science and Technology (HKUST) in 1997-1998 and the 1999-2001 California Regional $PM_{10}/PM_{2.5}$ Air Quality Studies (CRPAQS). The performance of these box thermodynamic modules in predicting PM concentrations and gas/particle partitioning with and without crustal materials is examined.

The observational data for the box model study are respectively from the sampling experiments at Hong Kong (HK), China, and CRPAQS study at Angiola and Fresno, CA, USA, which include the concentrations of SO_4^{2-} , NO_3^- , NH_4^+ , chloride (Cl^-), sodium (Na^+), Ca^{2+} , K^+ , and Mg^{2+} and gaseous ammonia (NH_3) and nitric acid (HNO_3). The Hong Kong site is far from industrial and commercial areas and represents the typical coastal area. The samplings was performed on July 23-24, 28-29, in 1997 and January 8, May 7-9, 11 in 1998, for a total 14 sets of samples. Each sample was collected continuously for 4 or 24 hours. More details about the data can be found in Zhuang et al. (1999). CRPAQS is a multi-year observational and modeling study that involves multiple organizations and has been

conducted in northern California with a focus on the Central Valley, where the concentrations of PM frequently exceed the NAAQSs, owing to the combination of mobile, industrial, agricultural, and residential sources (McDade, 2002). A comprehensive data analysis has been conducted using data from two experimental sites (Angiola and Fresno) of the CRPAQS for the period of December 14, 2000 to January 18, 2001 during which PM concentrations (especially nitrate and ammonium) were the highest throughout the year (McDade, 2002). 12 sets of samples out of those experimental data are used here. In this study, the above 26 sets of observational data (14 from HK and 12 from CRPAQS) are used to set up two sets of inputs. In the first set of inputs, temperature, relative humidity (RH), total amount of species in both the gas and aerosol phases such as total sulfate ($\text{TSO}_4 = \text{SO}_4^{2-}$), total nitrate ($\text{TNO}_3 = \text{HNO}_3 + \text{NO}_3^-$), total ammonium ($\text{TNH}_4 = \text{NH}_3 + \text{NH}_4^+$), total chloride ($\text{TCl} = \text{HCl} + \text{Cl}^-$), and sodium (Na^+) are included. In the second set of inputs, crustal species such as calcium (Ca^+), potassium (K^+), and magnesium (Mg^{2+}) are also included for both ISORROPIA II and EQUISOLV II.

Figures 4.1 and 4.2 show the simulations results of the calculated aerosol NO_3^- , NH_4^+ , and Cl^- , gaseous HNO_3 and NH_3 , particulate hydrogen ion (in form of pH values), and particle water content from ISORROPIA v1.7, ISORROPIA II (with and without crustal species) and EQUISOLV II (with and without crustal species) for all 26 cases of HK and CRPAQS data. Generally the partitioning of TNO_3 , TNH_4 , and TCl between gas and aerosol phases and water content and pH values are quite similar for all the cases between ISORROPIA v1.7 and ISORROPIA II without crustal species. The partitioning of TNO_3 ,

TNH₄, and TCl without crustal species by ISORROPIA II and EQUISOLVII is also very close for most cases, except for several cases (e.g., 1/8/98-2, 5/7/98, 5/9/98, and 5/11/98 at Hong Kong), in which, EQUISOLV II predicts higher concentrations of aerosol NO₃⁻ and NH₄⁺ for the first two cases and lower concentrations of aerosol NO₃⁻ and NH₄⁺ for the third case. As most of all the 26 cases are in high RH (> 70%) conditions and also all these cases are ammonia-rich ([TNH₄]/[TSO₄] > 2.0) cases, three simulations give very similar results, which is consistent with the conclusions of Ansari and Pandis (1999b) and Zhang et al. (2000). In most cases, the aqueous particle predicted by EQUISOLV II is more acidic than that predicted by ISORROPIA, which may be attributed to the different numerical methods used to calculate H⁺ ions, different methods used for binary activity coefficient calculation, and the assumption of a constant pH in ISORROPIA II when crustal species are in excess as compared to the anions (e.g., for the case 12/15/00 at Angiola). From the chemical regime analysis, the average [TNH₄]/[TSO₄] at Angiola and Fresno is extremely high (> 20) compared to that at HK (from 2 to 6), which means all thermodynamics modules perform in the extremely ammonia-rich conditions and will result in a very high percentage of TNO₃ partitioning into the aerosol NO₃⁻ (Figure 4.2). When aerosol phase is dominant, small relative errors in predictions of aerosol NO₃⁻ lead to large relative errors for gaseous NH₃, since the total concentrations of the prediction and the observation are the same.

Jacobson (1999) and Moya et al. (2002) indicated that the crustal materials such as Ca²⁺, K⁺, and Mg²⁺ can significantly influence the thermodynamics equilibrium of the volatile species such as NH₄⁺ and NO₃⁻, but the effects can be complex and counterintuitive. In our study, the inclusion of crustal species for both ISORROPIA II and EQUISOLVII give

similar effects on the partitioning of TNO_3 , TNH_4 , and TCl for most of cases (especially at Angiola and Fresno), in which both modules predict lower concentrations of aerosol NH_4^+ , but higher concentrations of NO_3^- and Cl^- , due to the competition of crustal species and NH_4^+ with the available anions (referred as the charge balance effect, since NO_3^- is expected to increase to maintain the charge balance). Exceptional cases include 1/8/98-3 and 1/8/98-6 at HK, in which ISORROPIA II predicts lower concentration of NO_3^- and EUQISOLV II predicts higher concentrations of NO_3^- as compared to the results without consideration of crustal species, although both modules consistently predict lower concentration of NH_4^+ . The reason might be associated with different sets of equilibrium reactions for ammonium treated in two modules and needs to be verified in the future test.

4.2 Model Framework, Configurations, Simulation Setup, and Evaluation Protocols

The dust treatments including two online dust emission modules, dust related heterogeneous chemistry, and crustal species and associated inorganic thermodynamics module ISORROPIA II have been initially incorporated in CMAQ v4.4 (refer to as MM5/CMAQ-Dust) and applied to the April 2001 ICAP dust episode (Wang et al., 2010). Figure 4.3 demonstrates the flow chart of all physical and chemical processes treated in CMAQ. The subroutines with major modifications are highlighted with red color, which include VDIFF for vertical diffusion, AERO_EMIS for aerosol emission calculation, MDEMIS/OPMDEMIS for mineral dust emissions, AERO for aerosol chemistry driver, AEROPROC for aerosol mass transfer/dynamics, AERO_DEP for aerosol dry deposition, and EQL3 for thermodynamic equilibrium. It should be noted that this version of CMAQ generated some unrealistic dust emissions over the Tibet Plateau and southwestern China (as

shown in Figure 4.4), which are fixed by using source erodibility factor S as introduced in Section 4.1. Figure 4.4 also shows that both Westphal and Zender schemes from MM5/CMAQ-Dust yield comparable monthly total dust emissions over the whole domain (65.5 Tg/mo for Westphal scheme vs. 65.9 Tg/mo for Zender scheme), but with noticeable difference of spatial distribution. The daily emission results (figures not shown) of both schemes capture two major dust storm events reported in April 2001. Because of the similarity of dust emissions by two schemes and the more complex dust flux calculation by the Zender scheme, we select the Zender scheme for all other CMAQ v4.7-Dust simulations as introduced later in this section.

Overall, the results from CMAQ v4.4 are promising and give us confidence in applying all those dust treatments in the newest version of CMAQ v4.7. The rationale to transfer all the dust treatments into CMAQ v4.7 is obvious since there are several major updates to advance the underlying science in CMAQ v4.7 since CMAQ v4.4. One of the most important features in CMAQ v4.7 is the inclusion of coarse-mode aerosol chemistry (Pilinis et al., 2000; Capaldo et al., 2000), which is very important for dust studies since dust particles are normally dominated by the coarse particles. Other enhancements in CMAQ v4.7 include: addition of the new gas-chemistry mechanism (i.e., the CB05 and associated Euler Backward Iterative (EBI) solver; incorporation of online sea salt emission module; update on aerosol dry deposition algorithm; enhancement of SOA module by considering SOA products from isoprene, sesquiterpene, etc.; modification of the calculation of heterogeneous N_2O_5 reaction probability to be a function of temperature, relative humidity, and aerosol compositions.

The new dust version of CMAQ v4.7 (refer to as CMAQ-Dust hereafter) is applied to the ICAP 2001 April dust episode. The domain includes the eastern Asia, North Pacific, and North America with several dust source regions such as the western India, northwest/central China, and western U.S. covered. The horizontal grid resolution is 108 km and vertical resolution includes 16 layers from the surface to approximately 100 hPa (at ~16 km). In order to set up the ICAP simulation using CMAQ-Dust, we regenerated the meteorological fields using Weather Research & Forecasting Model (WRF) version 3.2 with the analysis Four Dimensional Data Assimilation (FDDA) due to the fact that several new variables (e.g., the dry deposition velocities for several new species in CB05 mechanism) are needed by CMAQ v4.7 but not available from the old ICAP MM5 meteorological files. The physical/chemical options used for the WRF/CMAQ-Dust simulation are summarized in Table 4.3 and they include Yonsei University (YSU) PBL scheme (Hong et al., 2006), thermal diffusion land surface parameterization scheme (Dubia, 1996), Grell 3D ensemble cumulus cloud scheme (Grell and Devenyi, 2002), WRF Single Moment (WSM) 6-class graupel microphysics parameterization scheme (Hong and Lim, 2006), Goddard short wave radiation scheme (Chou and Suarez, 1994), and Rapid Radiative Transfer Model (RRTM) long wave radiation scheme (Mlawer et al., 1997), CB05 gas-phase chemistry mechanism (Yarwood et al., 2005), and AERO5 aerosol chemistry (Roselle et al., 2008). The initial/boundary conditions (ICONS/BCONs) for WRF simulation are from the NCEP/NCAR FNL dataset. We have also conducted some sensitivity WRF simulations with other physical options or ICONS/BCONs (e.g., CCSM data set). The above options and the FNL dataset give the best overall model performance and thus are used in the final simulations. The

emissions for anthropogenic sources are the same with those described in Chapter 3. The emission data for U.S. is based on the National Emissions Inventory (NEI) 1999 version 1. The emission inventory for Mexico is prepared from the Big Bend Regional Aerosol and Visibility Observational Study (BRAVO) 1999 database. For Canada, the 1995 area and mobile (on-road and non-road) source inventory is used. The emission inventory in Asia is generated from the Transport and Chemical Evolution over the Pacific (TRACE-P) and the Aerosol Characterization Experiment-Asia (ACE-Asia) data (Streets et al., 2003). The sea salt and dust emissions are generated online using the method from Zhang et al. (2005) and the one developed by this study, respectively. The ICONs and BCONs for chemical species are taken from GEOS-Chem (Park et al., 2004).

To investigate the dust influences, a total of eight full month (April 2001) simulations are conducted. They include the baseline simulation with default CMAQ v4.7 and without any dust treatments (BASELINE), the simulation with ISORROPIA II and without any dust treatment (NO_DUST), the simulation with dust emissions only (DUST_EMIS_ONLY), the simulation with dust emission and crustal species treatment (CRUST_ONLY), and the simulation with all dust treatments including dust related heterogeneous chemistry (DUST), the simulation as DUST but with a subset of high γ values for N_2O_5 , NO_2 , and NO_3 in Table 4.1 (DUST_HIGHY), the simulation as DUST but with ISORROPIA v1.7 (DUST_ISO1.7), and the simulation as DUST but by removing Asian anthropogenic emissions (DUST_CUT). Model performance evaluation for WRF v3.2 simulations is conducted and will be compared with the old ICAP MM5 simulation in Section 4.3. The model performance for chemical species and their implication for model improvement will be investigated in Section 4.4. The

impacts of various dust treatments on the spatial distribution of different chemical species and Asian anthropogenic emissions on U.S. air quality will be discussed in Section 4.5.

The model evaluation for meteorological and chemical variables is conducted using the same protocols as introduced in Chapter 3. The statistical measures used here include the correlation coefficient (R), the normalized mean bias (NMB), and the normalized mean error (NME) (Seigneur et al., 2000; Zhang et al., 2006). The WRF v3.2 simulation results are evaluated against the observational data from the Clean Air Status and Trends Network (CASTNET), the Speciation Trends Network (STN), and the National Acid Deposition Program (NADP) over U.S. and the National Climate Data Center (NCDC) of NOAA over China. Chemical predictions of CMAQ-Dust are evaluated against the available ground and satellite-based measurements and also compared with the results from CMAQ 4.4 (Chapter 3) in order to show the potential model performance improvement. Surface observational data include those from the Clean Air Status and Trends Network (CASTNET), the Interagency Monitoring of Protected Visual Environments (IMPROVE), the Speciation Trends Network (STN), the Aerometric Information Retrieval System (AIRS)-Air Quality System (AQS), the Southeastern Aerosol Research and Characterization study (SEARCH) over the U.S.; those from the National Environmental Monitoring Centre of China (NEMCC) over China, and chemical data from the National Institute for Environmental Studies (NIES) over Japan. Satellite column data include tropospheric CO columns from the Measurements of Pollution in the Troposphere (MOPITT) (Deeter et al., 2003), tropospheric NO₂ column from the Global Ozone Monitoring Experiment (GOME) (Burrows et al., 1999), tropospheric O₃ residuals (TORs) from the Total Ozone Mapping Spectrometer (TOMS) and the Solar

Backscattered Ultraviolet (SBUV) (Fishman et al., 2003), and AOD from the Moderate Resolution Imaging Spectroradiometer (MODIS) (Chu et al., 2003; Remer et al., 2005).

The AOD calculations follow the method introduced in Chapter 3 and are improved by considering the contributions from sea salts, dust, and other coarse-mode particles. The scattering coefficient σ_{sp} is calculated as follows:

$$\begin{aligned}\sigma_{sp} &= \sigma_{sp}^{SO_4} + \sigma_{sp}^{NO_3} + \sigma_{sp}^{OC} + \sigma_{sp}^{BC} + \sigma_{sp}^{NH_4} + \sigma_{sp}^{Na} + \sigma_{sp}^{Cl} + \sigma_{sp}^{FS} + \sigma_{sp}^{CM} \\ &= \{ [SO_4] \times \alpha_{sp}^{SO_4} + [NO_3] \times \alpha_{sp}^{NO_3} + [OC] \times \alpha_{sp}^{OC} + [BC] \times \alpha_{sp}^{BC} + [NH_4] \times \alpha_{sp}^{NH_4} + [Na] \times \alpha_{sp}^{Na} + [Cl] \times \alpha_{sp}^{Cl} \} \\ &\quad \times f(RH) / 1.0 \times 10^6 + \{ [FS] \times \alpha_{sp}^{FS} + [CM] \times \alpha_{sp}^{CM} \} / 1.0 \times 10^6\end{aligned}$$

where $\sigma_{sp}^{SO_4}$, $\sigma_{sp}^{NO_3}$, σ_{sp}^{OC} , σ_{sp}^{BC} , $\sigma_{sp}^{NH_4}$, σ_{sp}^{Na} , σ_{sp}^{Cl} , σ_{sp}^{FS} , and σ_{sp}^{CM} are the scattering coefficients for SO_4^{2-} , NO_3^- , OC, BC, NH_4^+ , Na^+ , and Cl^- in the $PM_{2.5}$ size section, fine-mode soil including dust and other inorganic aerosols, and coarse masses including coarse-mode dust, sea-salt, and other aerosols. The values for specific scattering coefficients (α_{sp}^i) for species i are $\alpha_{sp}^{SO_4} = \alpha_{sp}^{NO_3} = \alpha_{sp}^{OC} = \alpha_{sp}^{NH_4} = \alpha_{sp}^{Na} = \alpha_{sp}^{Cl} = 5.0 \text{ m}^2 \text{ g}^{-1}$, $\alpha_{sp}^{BC} = 3.0 \text{ m}^2 \text{ g}^{-1}$, $\alpha_{sp}^{FS} = 1.0 \text{ m}^2 \text{ g}^{-1}$, and $\alpha_{sp}^{CM} = 0.6 \text{ m}^2 \text{ g}^{-1}$ (Malm et al., 1994). $f(RH)$ accounts for the effect of relative humidity on scattering due to deliquescence and is assumed to be 2.3 in this study following Chameides et al. (2002).

4.3 Evaluation of Meteorological Variables

Figures 4.5 and 4.6 show the spatial plots of NMBs between observational data and WRF simulation with FNL data as inputs and UV PBL nudging for 2-m temperature (T2), 2-m water vapor mixing ratio (Q2) or relative humidity (RH2), and precipitation over China and U.S. in April 2001. Table 4.4 summarizes the statistical performance for the above

variables plus wind speed and direction over different networks. WRF generally underpredicts T2 over China with domain-wide NMB of -20.6%, especially over the northern and western China where larger NMBs of -40% up to -100% occur. Some overpredictions occur in the southwestern China. The poor T2 predictions over the western China are likely due to the poor representation of steep terrains at a coarse grid resolution (Wang et al., 2009). The predictions of T2 over the U.S. have low domain-wide biases with NMBs of 4.9% (CASTNET) and -4.2% (STN) with small overpredictions over the northeastern U.S. and moderate to large underpredictions over the western U.S. The reasons for this discrepancy are likely due to several reasons including the slow responses of deep soil temperatures to synoptic-scale changes in air temperatures and the limitations of the PBL and land-surface schemes currently used in meteorological models in accurately simulating the air-land heat fluxes (Gilliam et al., 2006), the limitations of radiation schemes currently used (Dudhia, 1989), as well as the incapability of the models at a coarse grid resolution in capturing fine-scale meteorological phenomena (Wang et al., 2009). The correlation coefficients for T2 are very high over all networks with R values of 0.88 for CASTNET, 0.87 for STN, and 0.87 for NCDC, respectively. For Q2 or RH2, the model also performs well in terms of both spatial distribution and statistical performance. The domain-wide average NMBs are 8.1% for Q2 against NCDC and 14.2% for RH2 against CASTNET and R values are 0.91 and 0.68, respectively. Their NMBs over majority of NCDC and CASTNET sites are within $\pm 20\%$. Relatively high NMBs are found in the northern and western China and western U.S., indicating a poor performance of WRF over complex terrains. WRF predicts precipitation relatively poor compared to T2 and RH2 (or Q2) likely due to that WRF cannot capture

small-scale dynamical processes, topography, and rapid diurnal evolution of PBL with relatively large grid resolution (Kursinski et al., 2008), with lower domain-wide mean underpredictions in China than in the U.S (NMBs of -31.5% vs. -54.1%). The spatial distribution of NMBs in China, however, displays a worse pattern, with large negative biases ($< -70\%$) occurring mostly over high latitude regions and large positive biases ($> 70\%$) occurring mostly over the low latitude regions. The overall small domain-wide mean NMB for precipitation over China is therefore resulted from the compensation of large positive and negative biases. WRF also overpredicts 10 m wind speed (WS10) with an overall NMB of 45.6% against CASTNET and slightly overpredicts 10m wind direction (WD10) with an NMB of 6.3%. The performance statistics for other WRF simulations (e.g., CCSM data and other nudging options) are also included in Table 4.4. The WRF simulation using FNL data and UV PBL nudging gives overall the best performance and thus is used for all the CMAQ-Dust simulations.

When comparing the simulation results of WRF (FNL with UV PBL nudging) with MM5, we find the WRF predicts higher WS10 (i.e., domain-wide average 4.0 ms^{-1} versus 3.1 ms^{-1}), indicating that WRF meteorology in CMAQ v4.7 favors the dust emissions. Much higher correlation for WD10 (i.e., R values of 0.5 versus 0.14) indicates the wind field generated by WRF may be more close to the actual one. Generally, WRF predicts much better T2 and slightly better RH2 than MM5 especially over U.S. (as shown in Figures 4.5 and 4.6 and Table 4.4). However, the prediction of precipitation is worse by WRF. Overall, the meteorological predictions by WRF v3.2 are consistent with other meteorological models

such as MM5 that were used to provide meteorological inputs for air quality studies (e.g., Wang et al., 2009; Zhang et al., 2011).

4.4 Evaluation of Chemical Variables

4.4.1 Dust Emission Fluxes and Dust Concentrations

As discussed in Sections 4.1 and 4.2, a source erodibility factor S is used in CMAQ-Dust to exclude the unrealistic dust emissions generated by MM5/CMAQ-Dust. A factor, EF , has also been increased to 0.5. EF is originally set to be 0.13 in both dust schemes to represent that only 13% of erodible lands are capable of emitting dust (Liu and Westphal, 2001), however the value was based on the land surface conditions in 1950s (Clements et al., 1957) and we believe a higher value should be used for current conditions over arid areas and thus set it as 0.5 in CMAQ-Dust. The monthly total dust emission generated by CMAQ-Dust using Zender and Westphal schemes are 111.4 and 110.9 Tg/month, respectively, almost double the amount generated by MM5/CMAQ-Dust. Despite the increase of dust emissions, our estimation is still smaller than that reported by Laurent et al. (2006), who estimated that dust emissions over China could reach 300 Tg in April 2001. However, there exist large uncertainties in dust emission estimations from different models. Uno et al. (2006) reported that dust emissions during a 10-day period in a dust season over China could range from 27 Tg to 336 Tg, with a mean of 120 Tg from eight different dust models. Zender et al. (2003) also estimated the annual dust emission can reach 415 Tg over Asia although they did not provide the monthly dust emission estimations. Overall, the amount of dust emissions produced in this work is consistent with previous studies (e.g., Zender et al., 2003; Laurent et al., 2006; Uno et al., 2006) and may represent a lower limit for the April 2001 dust event.

Figure 4.7 shows the predicted monthly-mean dust emission rate generated by the Zender and Westphal schemes and dust concentrations in fine (Aitken and accumulation) and coarse modes (refer to as $Dust_{\text{fine}}$ and $Dust_{\text{coarse}}$, respectively) at surface and ~5 km from the Zender scheme only. The layer with ~5 km altitude is chosen to represent the layer with the maximum dust transport in the lower free troposphere. In general, from both schemes, dust emissions occur over regions where high wind speeds, low vegetation, and no snow cover occur. The areas with the strongest sources are located in the Taklimakan desert and Gobi desert over China and Mongolia. Areas with less pronounced dust sources include the western India, the southwestern and Great Plains regions over the U.S., and Sonoran desert of Mexico. The spatial pattern of dust emissions is consistent with previous studies (Ginoux et al., 2001; Prospero et al., 2002, Zender et al., 2003; Tang et al., 2004). CMAQ-Dust also captures the dust outbreak event during April 4-14 (figures not shown). As shown in Figure 4.7, the maximum surface concentrations of $dust_{\text{fine}} (\geq 80 \mu\text{g m}^{-3})$ and $dust_{\text{coarse}} (\geq 200 \mu\text{g m}^{-3})$ are apparent over source regions, where large particles have not deposited yet. Due to the much faster deposition rates of $dust_{\text{coarse}}$, the spatial distributions and abundance of $dust_{\text{fine}}$ and $dust_{\text{coarse}}$ are similar over down-wind areas and remote regions. The surface concentration of dust particles can reach 5-30 $\mu\text{g m}^{-3}$ for both $dust_{\text{fine}}$ and $dust_{\text{coarse}}$ over the down-wind areas such as the eastern China, Japan, the northeastern India, and Midwest U.S. The long-range transport can build up the surface concentrations of dust up to 5 $\mu\text{g m}^{-3}$ over the remote regions such as the eastern Pacific and eastern U.S. The concentrations of both $dust_{\text{fine}}$ and $dust_{\text{coarse}}$ over the down-wind and remote areas at ~5 km are higher than the

surface indicating the long-range transport of dust particles are more efficient at higher altitude.

4.4.2 Evaluation of Chemical Variables and Implication of Model Improvement

Tables 4.5 and 4.6 summarize performance statistics of several major chemical species over U.S., Beijing (China), and Japan among three simulations (i.e., simulations BASELINE, DUST, and MM5/CMAQ v4.4 without dusts). Over U.S., the model performance for O₃ in simulation DUST is fairly good with NMBs of -12.9% to 2.0% and NMEs of 16.7% to 18.1% for max 1-h O₃ and with NMBs of -5.4% to 5.9% and NMEs of 15.1% to 17.9% for max 8-h O₃. Simulation DUST tends to predict more O₃ than CMAQ v4.4 mainly due to the use of CB05 mechanism and a little bit less O₃ than simulation BASELINE due to the heterogeneous uptake of O₃ on dust particles. The NMBs and NMEs are slightly better in simulation DUST indicating an improvement in predicting O₃ chemistry. Compared with the CMAQ v4.4, simulation DUST predict PM_{2.5} better at the STN and SEARCH sites (with NMBs of -10.1% vs. 15.4% for SEARCH and 26.5% vs. 51.5% for STN), however, gives higher overpredictions at the IMPROVE sites (NMBs increase from 55.7% to 66.3%). The better performance should be due to the better representation of aerosol chemistry in the new version of CMAQ and the worse performance may indicate some potential overestimation of dust emissions since most of IMPROVE sites are in the western U.S. Over Beijing and Japan, model performance of simulation DUST is more comparable with both BASELINE and CMAQ v4.4 for most of gaseous species. The NMBs for NO₂ over Beijing and CO, SO₂, NO, and NO₂ over Japan are -71.9%, -58.7%, -35.5%, -91.1% and -64.3%, respectively for simulation DUST, indicating a significant

underestimation of emissions for those species over Asia. For PM₁₀ and suspended particulate matter (SPM), the model performance of simulation DUST is much better compared with BASELINE and CMAQ v4.4 (NMBs of -45.8% vs. -80.9% and -83.6% for PM₁₀ and -34.7% vs. -50.9% and -49.7% for SPM, respectively) due to the contribution of dust particles. However the model still underpredicts those species, indicating that the dust emissions might be underestimated over the deserts in China. This finding is consistent with the analysis in Section 4.4.1.

Figures 4.8 and 4.9 show the spatial distribution of column variables from satellite observations, CMAQ v4.4, BASELINE simulation and DUST simulation in April 2001. Table 4.7 summarizes the corresponding performance statistics. Simulation DUST predicts the columns CO, TOR, and NO₂ quite well with NMBs of -9.0%, -17.2%, and 10.0%, respectively and shows very similar pattern compared with simulation BASELINE. The correlation coefficients are also high for all three column variables. Compared with CMAQ v4.4, both simulations BASELINE and DUST give the comparable performance for NO₂, slightly better performance for column CO, and considerable performance improvement for TOR due to the use of CB05 mechanism. More importantly, the dust treatments in simulation DUST greatly improve AOD predictions especially over the Pacific Ocean with the domain-wide NMB reduced from -35.4% (CMAQ v4.4) and -20.2% (BASELINE) to -7.8%. In summary, the model evaluation results for chemical species discussed here show very promising model improvements over the old version model and give us confidence in applying this dust version of CMAQ for further research studies.

4.5 Impact of Dust Treatments in CMAQ

4.5.1 Impact of Crustal Species Treatments

Crustal species can affect gas/particle partitioning into both fine and coarse modes of PM. Figures 4.10 and 4.11 show the spatial distribution of differences between simulations CRUST_ONLY and DUST_EMIS_ONLY for surface layer concentrations of gases including SO₂, NH₃, HNO₃ and aerosols including PM_{2.5}, PM_{coarse}, and their compositions such as SO₄²⁻, NO₃⁻, NH₄⁺, and Cl⁻ in April 2001. For non-volatile species (e.g., SO₄²⁻) and EC, OC, and other inorganic aerosols (OIN) that are not simulated by aerosol thermodynamic and dynamic model (figures for them not shown here), two simulations show very small discrepancies (generally < ±0.01 μg m⁻³). Compared with DUST_EMIS_ONLY, CRUST_ONLY predicts relatively lower SO₄²⁻ (about 0.1 μg m⁻³) over East Asia, due to less oxidation of SO₂ to form sulfuric acid (H₂SO₄). Less oxidation of SO₂ is due to lower concentrations of oxidants (e.g., H₂O₂) from CRUST_ONLY, which are resulted from different partitioning of HNO₃/NO₃⁻ between two simulations. For volatile species such as NO₃⁻ and NH₄⁺, the effects of crustal species are much more significant. The addition of crustal species decreases the predicted concentrations of fine-mode NH₄⁺ throughout the domain, which is indicates a charge balance effect (i.e., NH₄⁺ is replaced by crustal species such as Ca²⁺) and is consistent with the box model results in Section 4.1.3. On the other hand, the impact of crustal species on NO₃⁻ is more complicated with the enhancement of fine-mode NO₃⁻ concentrations over dust source regions and reduction over down-wind heavily polluted areas such as the eastern China and northern India. The increase of NO₃⁻ can be explained by the charge balance effect. Two factors may help explain the decrease of

NO_3^- . The first factor is the activity effect introduced by Jacobson (1999). The basic equilibrium-coefficient equation for reaction $\text{NH}_3(\text{g}) + \text{HNO}_3(\text{g}) \rightleftharpoons \text{NH}_4^+ + \text{NO}_3^-$ can be expressed as:

$$\frac{\{NH_4^+\}\{NO_3^-\}}{\{NH_3(\text{g})\}\{HNO_3(\text{g})\}} = \frac{m_{NH_4^+}m_{NO_3^-}\gamma_{NH_4^+,NO_3^-}^2}{p_{NH_3}(\text{g})p_{HNO_3}(\text{g})} = K_{eq}(T) \quad (3.16)$$

where the m 's are molalities, the p 's are gas-phase partial pressures, and $\gamma_{NH_4^+,NO_3^-}$ is the mean mixed activity coefficient of NH_4NO_3 , and $K_{eq}(T)$ is the temperature-dependent equilibrium coefficient. $K_{eq}(T)$ is a constant at a given T. As reported by Jacobson (1999), the inclusion of crustal species may increase $\gamma_{NH_4^+,NO_3^-}^2$ dramatically over heavily polluted areas. In order to sustain equation (3.16), both $m_{NH_4^+}$ and $m_{NO_3^-}$ need to decrease significantly. The above effect is called activity effect and can partly explain the reduction in NO_3^- over those regions.

Another factor could be due to the aerosol growth of fine-mode NO_3^- into coarse-mode NO_3^- as shown in Figures 4.11 and 4.14e-f, since most of crustal species are assumed in the coarse mode. Figure 4.14e-f shows clearly that the inclusion of crustal species tends to shift NO_3^- from fine-mode into coarse-mode over more polluted areas. Fine-mode Cl^- shows a similar pattern as NO_3^- over the East Asia except over dust source regions in China (due to the lack of Cl^- sources), indicating the similar activity effect. The mixing ratios of gas phase NH_3 and HNO_3 are increased and decreased, respectively as expected according to the mass balance effect. Overall, inclusion of crustal species tends to reduce the concentration of $\text{PM}_{2.5}$ over the East Asia, due to a combine effect of decreases of both NO_3^- and NH_4^+ . Coarse-mode NO_3^- increases significantly due to the growth from fine-mode NO_3^- and inclusion of coarse-

mode crustal species. On the other hand, coarse-mode NH_4^+ increases can be attributed to the growth of fine-mode particles and also the large increase of NO_3^- that requires more cations for neutralization.

4.5.2 Impact of Heterogeneous Chemistry

Heterogeneous chemistry on the surface of dust affects the concentrations of gases and PM. Figure 4.12 shows the spatial distribution of differences between simulations DUST and CRUST_ONLY for surface layer O_3 , NO_x , SO_2 , HNO_3 , N_2O_5 , and HO_x in April 2001. The mixing ratios of O_3 , SO_2 , N_2O_5 , and HO_x are reduced in the presence of dust due to irreversible uptakes. However the patterns for NO_x and HNO_3 are a little bit different. The spatial distribution of O_3 reduction corresponds well with the dust distribution shown in Figure 4.7. The decrease of monthly-average surface O_3 mixing ratios can be up to 3.8 ppb (~9%) over the dust source region, which is comparable to those reported by previous studies (Dentener et al., 1996; Tang et al., 2004; Pozzoli et al., 2008a). The decrease of SO_2 mixing ratios can be up to ~0.3 ppb (~5% over the polluted areas and 30% over the dust source regions). The distribution of SO_2 reduction is somehow different with that of O_3 with the highest reduction occurring in the down-wind polluted areas where SO_2 emissions are the highest. Different from other gases, the mixing ratios of NO_x increase due to renoxification that converting HNO_3 back to NO_x at the surface of dust, with the largest increase over the eastern China where NO_x emissions are the highest. The small decrease in the mixing ratios of HNO_3 is an interesting phenomenon, since the increase of NO_x indicates the heterogeneous uptake of HNO_3 should be significant and we expect to see more decrease of HNO_3 . Therefore there must be some other mechanisms that also generate HNO_3 to

compensate the decrease of HNO_3 via heterogeneous chemistry. The small decrease of both fine- and coarse-mode NO_3^- in figure 4.13 suggests there might be evaporation of NO_3^- occurring in aerosol chemistry. The addition of large amount of SO_4^{2-} generated by heterogeneous uptake alternates the chemical regime of aerosols and then tends to replace NO_3^- as ions. The decrease of both NO_3 and N_2O_5 mixing ratio is relatively small compared with other species mainly due to its less abundance in the atmosphere. HO_x mixing ratio is reduced by up to 80% (up to 8 ppt) over the dust source regions and by 20-30% (up to 2 ppt) over the down-wind polluted areas because of the heterogeneous loss. The results are consistent to those of OH reported by Bian and Zender (2003). H_2O_2 mixing ratio is increased mainly due to the heterogeneous uptake on the dust particles that converts HO_2 to H_2O_2 .

Figure 4.13 shows the spatial distribution of differences between simulations DUST and CRUST_ONLY for surface layer concentrations of $\text{PM}_{2.5}$, $\text{PM}_{\text{coarse}}$, and their composition including SO_4^{2-} , NO_3^- , and NH_4^+ . Fine-mode and coarse-mode SO_4^{2-} concentrations are enhanced by up to 1.1 and 0.12 $\mu\text{g m}^{-3}$ (15% and more than 100%), respectively, due to the SO_2 heterogeneous reaction with fine-mode dust over the heavily-polluted areas such as the eastern China and northern India. The larger percentage increase in the concentrations of coarse-mode SO_4^{2-} is because they are very small in the absence of dust. Fine-mode NH_4^+ concentrations also increase due to the charge balance effect (i.e., more cations are needed to neutralize increased SO_4^{2-} anions). The overall effects of heterogeneous reactions on NO_3^- are small and much lower than those reported by Tang et al. (2004) and Bauer et al. (2004), partly due to the competition effect of SO_4^{2-} discussed above.

Another reason may be due to the lower γ values used in this study (e.g., 0.001 versus 0.1 or 0.01 for HNO_3 , 4.4×10^{-5} versus 1.0×10^{-4} for NO_2 , and 0.001 versus 0.02 for N_2O_5), as compared with Tang et al. (2004) and Bauer et al. (2004). Figures 4.14a-d show the results for several major species associated with those heterogeneous reactions when we use higher limit γ , we can see much higher enhancement of NO_3^- concentrations. Overall, inclusion of dust related heterogeneous chemistry tends to increase the concentration of $\text{PM}_{2.5}$ over the domain.

4.5.3 The Overall Impact of Dust Treatments

Figures 4.15 and 4.16 show the spatial distribution of differences between simulations DUST and NO_DUST for various gaseous and aerosol species at the surface layer and an upper layer with ~5km altitude in April 2001. The plots demonstrate the combination effect of both crustal species and heterogeneous chemistry on the chemical predictions in CMAQ-Dust. As shown, the surface monthly mixing ratios of O_3 , SO_2 , and HO_x are reduced with the dust treatment and the distributions correspond well with those shown in Figure 4.12, indicating dominant influences from heterogeneous chemistry. The increase of NO_x over most of the domain is due to the renoxification process as discussed previously. The impact of dust treatment on the spatial pattern of HNO_3 correlates well with that shown in Figure 4.10, indicating the dominant effects from $\text{HNO}_3/\text{NO}_3^-$ partitioning. As shown in Figure 4.11, the increase of surface concentrations for SO_4^{2-} (both fine- and coarse-mode) over Asia with the dust treatment is mainly due to heterogeneous chemistry and the decrease over Pacific and Atlantic Ocean and the northeastern U.S. is probably due to the less production of H_2SO_4 from the gas-phase oxidation as a result of reduced HO_x that dominates over the effect of

heterogeneous chemistry. For those volatile species (i.e., NO_3^- and NH_4^+), the differences between simulations DUST and NO_DUST are determined mainly by the effects of crustal species. The overall impact of dust treatments on $\text{PM}_{2.5}$ and coarse PM are large with the concentration enhancements of up to $\sim 330 \mu\text{g m}^{-3}$ for $\text{PM}_{2.5}$ and $\sim 1440 \mu\text{g m}^{-3}$ for coarse PM, respectively, over the dust source regions and $\sim 2 \mu\text{g m}^{-3}$ for both $\text{PM}_{2.5}$ and coarse PM over Pacific and Atlantic Ocean.

Contrast to the distribution in the surface layer, the decrease of O_3 at 5 km is more pronounced in the down-wind/remote areas instead of dust source regions. This finding reflects that sufficient amounts of dust particles have been transported efficiently to the remote areas and become aged to provide surface sites for heterogeneous uptake of O_3 at higher altitudes; and the aged dust particles over the remote areas can uptake O_3 more efficiently than fresh-emitted dust particles. The similar patterns are also found for SO_2 and HNO_3 . By contrast, the impacts of dust treatments on NO_x and HO_x are much smaller at higher altitudes, indicating less abundance of those species than at surface. For the PM species, the impacts of dust treatments are also more pronounced at 5 km over many areas far from dust source regions, indicating more efficient uptake of precursors on aged dust particles (Fairlie et al., 2010). The concentration enhancement of $\text{PM}_{2.5}$ and coarse PM due to dust treatments at higher altitudes are much larger over the down-wind and remote areas (up to $\sim 5 \mu\text{g m}^{-3}$ for $\text{PM}_{2.5}$ and $\sim 10 \mu\text{g m}^{-3}$ for $\text{PM}_{\text{coarse}}$ over the Pacific Ocean), indicating more efficient transport at higher altitudes.

4.5.4 Impact of Asian Pollution on the U.S. Air Quality with Dust Treatments

In this section, we will reexamine the contribution of Asian anthropogenic emissions to regional air pollution in the U.S. when considering the dust treatments. The enhancements of both gaseous and aerosol species over the U.S. are quantified by calculating the differences between simulations DUST and DUST_CUT as shown in Figure 4.17. As expected, the western U.S. receives much higher influx of air pollutants from the trans-Pacific transport than the eastern U.S. The background surface concentrations of O_3 and CO increase by ~ 1.5 and ~ 2.5 ppb, respectively (or by 3.6% and 2.1%, respectively) over the western U.S. The enhancement for SO_2 and NO_y is much higher over the western U.S. than the eastern U.S. Compared with other gases, NO_x shows a different pattern over the entire U.S. with a negative contribution of Asian anthropogenic emissions to the NO_x mixing ratios in the U.S., which may be associated with the negligible import of NO_x from Asia and more conversion of NO_x to its sink (e.g., HNO_3 , PAN, or N_2O_5) in the U.S. The concentration enhancements of SO_4^{2-} and NH_4^+ (both by $\sim 20\%$ for the western U.S.) dominate among the PM species, indicating that $(NH_4)_2SO_4$ is the major aerosol component of trans-Pacific anthropogenic aerosols. The relative enhancement for $PM_{2.5}$ in the western U.S. is lower than that shown in Figure 3.19 (i.e., $\sim 5\%$ vs. $\sim 10\%$) is mainly due to the inclusion of dust particles in $PM_{2.5}$ that increase the base $PM_{2.5}$ concentration significantly. In contrast with other PM species and also with results shown in Figure 3.19, the enhancement of NO_3^- is negative in both eastern and western U.S. This is due to the inclusion of the crustal species in CMAQ-Dust. The long-range transport of NO_3^- is much weaker when compared with SO_4^{2-} , so when removing Asian anthropogenic emissions, the concentrations of SO_4^{2-} are

reduced significantly, which requires more anion aerosols to neutralize the crustal species.
Therefore concentrations of NO_3^- are increased instead.

REFERENCES

- Ansari, A. S., and S. N. Pandis (1999a), Prediction of multicomponent inorganic atmospheric aerosol behavior, *Atmos. Environ.*, *33*, 745-757.
- Ansari, A. S., and S. N. Pandis (1999b), An analysis of four models predicting the partitioning of semi-volatile inorganic aerosol components, *Aero. Sci. Tech.*, *31*, 129-153.
- Bassett, M. E., and J. H. Seinfeld (1983), Atmospheric equilibrium model of sulfate and nitrate aerosol, *Atmos. Environ.*, *17*, 2237 – 2252.
- Bauer, S. E., Y. Balkanski, M. Schulz, D. A. Hauglustaine, and F. Dentener (2004), Global modeling of heterogeneous chemistry on mineral aerosol surfaces: Influence on tropospheric ozone chemistry and comparison to observations, *J. Geophys. Res.*, *109*, D02304, doi:10.1029/2003JD003868.
- Bian, H., and C. S. Zender (2003), Mineral dust and global tropospheric chemistry: Relative roles of photolysis and heterogeneous uptake, *J. Geophys. Res.*, *108*, 4672, doi:10.1029/2002JD003143.
- Burrows, J. P., et al. (1999), The Global Ozone Monitoring Experiment (GOME): Mission concept and first scientific results, *J. Atmos. Sci.*, *56*, 151-175.
- Campbell, S. W., M. C. Evans, and N. D. Poor (2002), Predictions of size-resolved aerosol concentrations of ammonium, chloride and nitrate at a bayside site using EQUISOLV II, *Atmos. Environ.*, *36*, 4299-4307.

- Capaldo, K. P., C. Pilinis, and S. N. Pandis (2000), A computationally efficient hybrid approach for dynamic gas/aerosol transfer in air quality models, *Atmos. Environ.*, *34*, 3617-3627.
- Carmichael, G. R., L. K. Peters, and K. Saylor (1991), The Stem-II regional scale acid deposition and photochemical oxidation model-I. An overview of model development and applications, *Atmos. Environ.*, *25A*, 2077-2090.
- Choi, Y.-J., and H. J. S. Fernando (2008), Implementation of a windblown dust parameterization into MODELS-3/CMAQ: Application to episodic PM events in the US/Mexico border, *Atmos. Environ.*, *42*, 6039-6046.
- Chou M.-D., and M. J. Suarez (1994), An efficient thermal infrared radiation parameterization for use in general circulation models. NASA Tech. Memo. 104606, 3, 85pp.
- Chu, D. A., Y. J. Kaufman, G. Zibordi, J. D. Chern, J. Mao, C. Li, and B. N. Holben (2003), Global monitoring of air pollution over land from the Earth Observing System-Terra Moderate Resolution Imaging Spectroradiometer (MODIS), *J. Geophys. Res.*, *108(D21)*, 4661, doi:10.1029/2002JD003179.
- Clegg, S. L., K. S. Pitzer, and P. Brimblecombe (1992), Thermodynamics of multicomponent, miscible, ionic solutions. II. Mixture including unsymmetrical electrolytes, *J. of Phys. Chem.*, *96*, 9470-9479.
- Clegg, S. L., P. Brimblecombe, and A. S. Wexler (1998), A thermodynamic model of the system $H^+ - NH_4^+ - Na^+ - SO_4^{2-} - NO_3^- - Cl^- - H_2O$ at 298.15 K, *J. of Phys. Chem.*, *102*, 2155-2171.

- Clements, T., T. H. Merriam, R. O. Stone, J. L. Eimann, and H. L. Reade (1957), A study of desert surface conditions, Tech. Rep. EP-53, 130 pp., U.S. Army, Natick Lab., Natick, Mass.
- Deeter, M. N., et al. (2003), Operational carbon monoxide retrieval algorithm and selected results for the MOPITT instrument, *J. Geophys. Res.*, *108*(D14), 4399, doi:10.1029/2002JD003186.
- Dentener, F. J., G. R. Carmichael, Y. Zhang, J. Lelieveld, and P. J. Crutzen (1996), Role of mineral aerosol as a reactive surface in the global troposphere, *J. Geophys. Res.*, *101*, 22,869– 22,889.
- Dudhia, J., 1996: A multi-layer soil temperature model for MM5. Preprints, 6th Annual MM5 Users Workshop, Boulder, CO.
- Fairlie, T. D., D. J. Jacob, and R. J. Park (2007), The impact of transpacific transport of mineral dust in the United States, *Atmos. Environ.*, *41*, 1251-1266.
- Fairlie, T. D., D. J. Jacob, J. E. Dibb, B. Alexander, M. A. Avery, A. van Donkelaar, and L. Zhang (2010), Impact of mineral dust on nitrate, sulfate, and ozone in transpacific Asian pollution plumes, *Atmos. Chem. Phys.*, *10*, 3999-4012.
- Fecan F., B. Marticorena, and G. Bergametti (1999), Parameterization of the increase of the aeolian erosion threshold wind friction velocity due to soil moisture for arid and semi-arid areas. *Ann. Geophys.* *17*, 149–157.
- Fishman, J., A. E. Wozniak, and J. K. Creilson (2003), Global distribution of tropospheric ozone from satellite measurements using the empirically corrected tropospheric ozone residual technique: Identification of the regional aspects of air pollution, *Atmos. Chem.*

Phys., 3, 893-907.

- Fountoukis, C. and A. Nenes (2007), ISORROPIA II: a computationally efficient thermodynamic equilibrium model for K^+ - Ca^{2+} - Mg^{2+} - NH_4^+ - SO_4^{2-} - NO_3^- - Cl^- - H_2O aerosols, *Atmos. Chem. Phys.*, 7, 4639-4659.
- Fridlind, A. M., and M. Z. Jacobson (2000), A study of gas-aerosol equilibrium and aerosol pH in the remote marine boundary layer during the First Aerosol Characterization Experiment (ACE 1), *J. Geophys. Res.*, 105, 17325-17340.
- Ginoux, P., M. Chin, I. Tegen, J. M. Prospero, B. Holben, O. Dubovik, and S. Lin (2001), Sources and distributions of dust aerosols simulated with the GOCART model, *J. Geophys. Res.*, 106(D17), 22055-22074.
- Goodman, A. L., G. M. Underwood, and V. H. Grassian (2000), A laboratory study of the heterogeneous reaction of nitric acid on calcium carbonate particles, *J. Geophys. Res.*, 105, 29,053–29,064.
- Grell, G. A. and D. Dévényi (2002), A generalized approach to parameterizing convection combining ensemble and data assimilation techniques, *Geophys. Res. Lett.*, 29, doi:10.1029/2002GL015311.
- Hodzic, A, B. Bessagnet, and R. Vautard (2006), A model evaluation of coarse-mode nitrate heterogeneous formation on dust particles, *Atmos. Environ.*, 40, 4158-4171.
- Hong, S. Y., Y. Noh, and J. Dudhia (2006), A new vertical diffusion package with explicit treatment of entrainment processes, *Mon. Wea. Rev.*, 134(9), 2318–2341.
- Hong, S. Y., and J. Lim (2006), The WRF Single Moment 6-class microphysics scheme (WSM6), *Journal of the Korean Meteorological Society*, 42, 129-151.

IPCC (2007), *Climate Change 2007: The Physical Science Basis*, Contribution of Working Group I to the Fourth Assessment Report of the Intergovernmental Panel on Climate Change [Solomon, S., et al. (eds.)], Cambridge University Press, Cambridge, United Kingdom and New York, NY, USA.

Jacobson, M. Z., A. Tabazadeh, and R. P. Turco (1996), Simulating equilibrium within aerosols and nonequilibrium between gases and aerosols, *J. Geophys. Res.*, *101*, 9079-9091.

Jacobson, M. Z. (1999), Studying the effects of calcium and magnesium on size-distributed nitrate and ammonium with EQUISOLV II, *Atmos. Environ.*, *33*, 3635-3649.

Kim, Y. P., J. H. Seinfeld, and P. Saxena (1993a), Atmospheric gas-aerosol equilibrium I. Thermodynamic model, *Aero. Sci. Tech.*, *19*, 157-181.

Kim, Y. P., J. H. Seinfeld, and P. Saxena (1993b), Atmospheric gas-aerosol equilibrium II. Analysis of common approximations and activity coefficients calculation methods, *Aero. Sci. Tech.*, *19*, 181-198.

Knipping, E. M., and D. Dabdub (2002), Modeling surface-mediated renoxification of the atmosphere via reaction of gaseous nitric oxide with deposited nitric acid, *Atmos. Environ.*, *36*, 5741-5748.

Kumar, N., F. W. Lurmann, S. N. Pandis, and A. S. Ansari (1998), Final Report: analysis of atmospheric chemistry during 1995 integrated monitoring study. Final Report Prepared for the California Air Resources Board, Sacramento, CA, by Sonoma Technology Inc., Santa Rosa, CA.

- Kursinski, E. R., R. A. Bennett, D. Gochis, S. I. Gutman, K. L. Holub, R. Mastaler, C. Minjarez Sosa, I. Minjarez Sosa, and T. van Hove (2008), Water vapor and surface observations in northwestern Mexico during the 2004 NAME Enhanced Observing Period, *Geophys. Res. Lett.*, *35*, L03815, doi:10.1029/2007GL031404.
- Laurent, B., B. Marticorena, G. Bergametti, and F. Mei (2006), Modeling mineral dust emissions from Chinese and Mongolian deserts, *Global and Planetary Change*, *52*, 121-141.
- Li, L., Z. M. Chen, Y. H. Zhang, T. Zhu, J. L. Li, and J. Ding (2006), Kinetics and mechanism of heterogeneous oxidation of sulfur dioxide by ozone on surface of calcium carbonate, *Atmos. Chem. Phys.*, *6*, 2453-2464.
- Li, H. J., T. Zhu, D. F. Zhao, Z. F. Zhang, and Z. M. Chen (2010), Kinetics and mechanisms of heterogeneous reaction of NO₂ on CaCO₃ surfaces under dry and wet conditions, *Atmos. Chem. Phys.*, *10*, 463-474
- Liao, H., and J. H. Seinfeld (2005), Global impacts of gas-phase chemistry-aerosol interactions on direct radiative forcing by anthropogenic aerosols and ozone, *J. Geophys. Res.*, *110*, D18208, doi:10.1029/2005JD005907.
- Liu, M., and D. L. Westphal (2001), A study of the sensitivity of simulated mineral dust production to model resolution, *J. Geophys. Res.*, *106*, 18099-18112.
- Mahowald, N., K. Kohfeld, M. Hansson, Y. Balkanski, S. P. Harrison, I. C. Printice, M. Schulz, and H. Rodhe (1999), Dust sources and deposition during the last glacial maximum and current climate: A comparison of model results with paleodata from ice cores and marine sediments, *J. Geophys. Res.*, *104*, 15,895-15,916.

- Malm, W. C., J. F. Sisler, D. Huffman, R. A. Eldred, and T. A. Cahill (1994), Spatial and seasonal trends in particle concentration and optical extinction in the United States, *J. Geophys. Res.*, *99*, 1347– 1370.
- Manktelow, P. T., K. S. Carslaw, G. W. Mann, and D. V. Spracklen (2010), The impact of dust on sulfate aerosol, CN and CCN during an East Asian dust storm, *Atmos. Chem. Phys.*, *10*, 365–382.
- Martcorena, B., and G. Bergametti (1995), Modeling the atmospheric dust cycle: 1. Design of a soil-derived dust emission scheme, *J. Geophys. Res.*, *100*(D8), 16,415-16,430.
- Martcorena, B., G. Bergametti, B. Aumont, Y. Callot, C. N'Doume, and M. Legrand (1997), Modeling the atmospheric dust cycle: 2. Simulation of Saharan dust sources, *J. Geophys. Res.*, *102*, 4387-4404.
- McDade, C. E (2002), California Regional PM₁₀/PM_{2.5} Air Quality Study (CRPAQS) Introduction to Site Documentation Reports. California Regional PM₁₀/PM_{2.5} Air Quality Study Technical Committee c/o California Air Resources Board Sacramento, CA. by ENSR International Camarillo, CA.
- McNaughton et al. (2009), Observations of heterogeneous reactions between Asian pollution and mineral dust over the Eastern North Pacific during INTEX-B, *Atmos. Chem. Phys.*, *9*, 8283–8308.
- Meng, Z., D., Dabdub, and J. H. Seinfeld (1998), Size-resolved and chemically resolved model of atmospheric aerosol dynamics, *J. Geophys. Res.*, *103*, 3419-3435.

- Michel, A. E., C. R. Usher, and V. H. Grassian (2002), Heterogeneous and catalytic uptake of ozone on mineral oxides and dusts: A Knudsen cell investigation, *Geophys. Res. Lett.*, *29(14)*, 1665, doi:10.1029/2002GL014896.
- Mlawer, E. J., S. J. Taubman, P. D. Brown, M. J. Iacono, and S. A. Clough (1997), Radiative transfer for inhomogeneous atmospheres: RRTM, a validated correlated-k model for the longwave. *J. Geophys. Res.*, *102*, 16,663-16,682.
- Moya, M., S. N. Pandis, and M. Z. Jacobson (2002), Is the size distribution of urban aerosols determined by thermodynamic equilibrium?: An application to Southern California, *Atmos. Environ.*, *36*, 2349-2365.
- Midwest Research Institute (2005), Analysis of fine fraction of particulate matter in fugitive dust, prepared for the WRAP by Midwest Research Institute. Project No.110397, 12 October.
- Ndour, M., B. D'Anna, C. George, O. Ka, Y. Balkanski, J. Kleffmann, K. Stemmler, and M. Ammann (2008), Photoenhanced uptake of NO₂ on mineral dust: Laboratory experiments and model simulations, *Geophys. Res. Lett.*, *35*, L05812, doi:10.1029/2007GL032006.
- Ndour, M., P. Conchon, B. D'Anna, O. Ka, and C. George (2009), Photochemistry of mineral dust surface as a potential atmospheric renoxification process, *Geophys. Res. Lett.*, *36*, L05816, doi:10.1029/2008GL036662.
- Nenes, A., C. Pilinis, and S. N. Pandis (1998), ISORROPIA: a new thermodynamic equilibrium model for multiphase multicomponent marine aerosols, *Aquatic Geochemistry* *4*, 123-152.

- Nenes, A., C. Pilinis, and S. N. Pandis (1999), Continued development and testing of a new thermodynamic aerosol module for urban and regional air quality models. *Atmos. Environ.*, *33*, 1553-1560.
- Nickovic, S., G. Kallos, A. Papadopoulos, and O. Kakaliagou (2001), A model for prediction of desert dust cycle in the atmosphere. *J. Geophys. Res.*, *106*, 18113–18129.
- Nowottnick, E., P. Colarco, R. Ferrare, G. Chen, S. Ismail, B. Anderson, and E. Browell (2010), Online simulations of mineral dust aerosol distributions: Comparisons to NAMMA observations and sensitivity to dust emission parameterization, *J. Geophys. Res.*, *115*, D03202, doi:10.1029/2009JD012692.
- Park, R. J., D. J. Jacob, B. D. Field, R. M. Yantosca, and M. Chin (2004), Natural and trans-boundary pollution influences on sulfate-nitrate-ammonium aerosols in the United States: implications for policy, *J. Geophys. Res.*, *109*, D15204, 10.1029/2003JD004473.
- Pilinis, C., and J. H. Seinfeld (1987), Continued development of a general equilibrium model for inorganic multicomponent atmospheric aerosols, *Atmos. Environ.*, *21*, 2453-2466.
- Pilinis, C., K. P. Capaldo, A. Nenes, and S. N. Pandis (2000), MADM-A new multicomponent aerosol dynamic model, *Aero. Sci. Tech.*, *32*, 482-502.
- Pozzoli, L., I. Bey, S. Rast, M. G. Schultz, P. Stier, and J. Feichter (2008a), Trace gas and aerosol interactions in the fully coupled model of aerosol-chemistry-climate ECHAM5-HAMMOZ: 1. Model description and insights from the spring 2001 TRACE-P experiment, *J. Geophys. Res.*, *113*, D07308, doi:10.1029/2007JD009007.
- Pozzoli, L., I. Bey, S. Rast, M. G. Schultz, P. Stier, and J. Feichter (2008b), Trace gas and aerosol interactions in the fully coupled model of aerosol-chemistry-climate ECHAM5-

HAMMOZ: 2. Impact of heterogeneous chemistry on the global aerosol distributions, *J. Geophys. Res.*, *113*, D07309, doi:10.1029/2007JD009008.

Prospero J. M., P. Ginoux, O. Torres, S. E. Nicholson, and T. E. Gill (2002), Environmental characterization of global sources of atmospheric soil dust identified with the nimbus 7 total ozone mapping spectrometer (TOMS) absorbing aerosol product, *Rev. Geophys.*, *40*(1), 1002, doi:10.1029/2000RG000095.

Remer, L. A, et al. (2005), The MODIS aerosol algorithm, products, and validation, *J. Atmos. Sci.*, *62*(4), 947-973.

Rivera-Figueroa, A. M., A. L. Sumner, and B. J. Finlayson-Pitts (2003), Laboratory studies of potential mechanisms of renoxification of tropospheric nitric acid, *Environ. Sci. Technol.*, *37*, 548-554.

Rodriguez, M. A., and D. Dabdub (2004), IMAGES-SCAPE2: A modeling study of size- and chemically resolved aerosol thermodynamics in a global chemical transport model, *J. Geophys. Res.*, *109*, D02203.

Roselle et al. (2008), Incremental testing of updates to the Community Multiscale Air Quality (CMAQ) modeling system version 4.7, presentation at the 7th annual CMAS conference, Chapel Hill, NC, October 6-8.

Satheesh, S. K., and K. K. Moorthy (2005), Radiative effects of natural aerosols: A review, *Atmos. Environ.*, *39*, 2089-2110.

Saxena, P., A. B. Hudischewskyj, C. Seigneur, and J. H. Seinfeld (1986) A comparative study of equilibrium approaches to the chemical characterization of secondary aerosols, *Atmos. Environ.*, *20*, 1471-1483.

- Schwartz, S. E. (1986), Mass-transport considerations pertinent to aqueous phase reactions of gases in liquid-water clouds, in *Chemistry of Multiphase Atmospheric System*, NATO ASI Ser., Ser. G: Ecol. Sci., vol. 6, edited by W. Jaeschke, Springer-Verlag, New York, pp. 415-471.
- Seigneur, C., et al. (2000), Guidance for the performance evaluation of three-dimensional air quality modeling systems for particulate matter and visibility. *J. Air Waste Manage. Assoc.*, 50, 588-599.
- Seinfeld, J. H., and S. N. Pandis (2006), *Atmospheric Chemistry and Physics: From Air Pollution to Climate Change*, 2nd ed., Wiley, New York.
- Shao, Y. (2001), A model for mineral dust emission, *J. Geophys. Res.*, 106, 20,239-20,254.
- Song, C. H., C. M. Kim, Y. J. Lee, G. R. Carmichael, B. K. Lee, and D. S. Lee (2007), An evaluation of reaction probabilities of sulfate and nitrate precursors onto East Asian dust particles, *J. Geophys. Res.*, 112, D18206, doi:10.1029/2006JD008092.
- Streets, D. G., T. C. Bond, and G. R. Carmichael (2003), An inventory of gaseous and primary aerosol emissions in Asia in the year 2000, *J. Geophys. Res.*, 108(D21), 8809, doi:10.1029/2002JD003093.
- Tanaka, T. (2007), Global dust budget, in *Encyclopedia of Earth*, edited by H. Hanson.
- Tang, Y., et al. (2004), Impacts of dust on regional tropospheric chemistry during the ACE-Asia experiment: A model study with observations, *J. Geophys. Res.*, 109, D19S21, doi:10.1029/2003JD003806.

- Tang, M. J., J. Thieser, G. Schuster, and J. N. Crowley (2010), Uptake of NO₃ and N₂O₅ to Saharan dust, ambient urban aerosol and soot: a relative rate study, *Atmos. Chem. Phys.*, *10*, 2965–2974.
- Tegen, I., and I. Fung (1994), Modeling of mineral dust in the atmosphere: Source, transport, and optical thickness, *J. Geophys. Res.*, *99*(D11), 22,897–22,914
- Tie, X., S. Madronich, S. Walters, D. P. Edwards, P. Ginoux, N. Mahowald, R. Zhang, C. Lou, and G. Brasseur (2005), Assessment of the global impact of aerosols on tropospheric oxidants, *J. Geophys. Res.*, *110*, D03204, doi:10.1029/2004JD005359.
- Underwood, G. M., C. H. Song, M. Phadnis, G. R. Carmichael, and V. H. Grassian (2001), Heterogeneous reactions of NO₂ and HNO₃ on oxides and mineral dust: A combined laboratory and modeling study, *J. Geophys. Res.*, *106*, 18,055– 18,066.
- Uno I., et al. (2003), Regional chemical weather forecasting system CFORS: Model descriptions and analysis of surface observations at Japanese island stations during the ACE-Asia experiment, *J. Geophys. Res.*, *108*(D23), 8668, doi:10.1029/2002JD002845.
- Uno I., et al. (2006), Dust model intercomparison (DMIP) study over Asia: Overview, *J. Geophys. Res.*, *111*, D12213, doi: 10.1029/2005JD006575.
- Van Pelt, R. S, and T. M. Zobeck (2007), Chemical constituents of fugitive dust, *Environ. Monit. Assess.*, *130*, 3–16, doi:10.1007/s10661-006-9446-8.
- Wagner, C., F. Hanisch, N. Holmes, H. de Coninck, G. Schuster, and J. N. Crowley (2008), The interaction of N₂O₅ with mineral dust: aerosol flow tube and Knudsen reactor studies, *Atmos. Chem. Phys.*, *8*, 91–109.

- Wang, K., Y. Zhang, C. Jang, S. Phillips, and B. Wang (2009), Modeling intercontinental air pollution transport over the trans-Pacific Region in 2001 using community multiscale air quality (CMAQ) model, *J. Geophys. Res.*, *114*, doi:10.1029/2008JD010807.
- Wang, K., Y. Zhang, C. Jang, S. Phillips, A. Nenes, and C. Fountoukis (2010), Implementation of dust treatments into CMAQ and initial application to the April 2001 Asian dust episode, presentation at the 12th Conference on Atmospheric Chemistry/the 90th AMS Annual Meeting, Atlanta, GA, January 17-21.
- Westphal, D. L., O. B. Toon, and T. N. Carlson (1987), A two-dimensional numerical investigation of the dynamics and microphysics of Saharan dust storms, *J. Geophys. Res.*, *92*(D3), 3027-3049.
- Wexler, A. S., and J. H. Seinfeld (1991), Second-generation inorganic aerosol model, *Atmos. Environ.*, *25A*, 2731-2748.
- White, B. R. (1979), Soil transport by winds on Mars, *J. Geophys. Res.*, *84*, 4643-4651.
- Yarwood, G., S. Rao, M. Yocke, and G. Z. Whitten (2005), Updates to the carbon bond mechanism: CB05, Report to the U. S. Environmental Protection Agency, RT-04-00675.
- Yue, X., H. Wang, Z. Wang, and K. Fan (2009), Simulation of dust aerosol radiative feedback using the Global Transport Model of Dust: 1. Dust cycle and validation, *J. Geophys. Res.*, *114*, D10202, doi:10.1029/2008JD010995.
- Zaveri, R. A., R. C. Easter, and A. S. Wexler (2005a), A computationally efficient multicomponent equilibrium solver for aerosols (MESA), *J. Geophys. Res.*, *110*, D24203, doi:10.1029/2004JD005618.

- Zaveri, R. A., R. C. Easter, and A. S. Wexler (2005b), A new method for multicomponent activity coefficients of electrolytes in aqueous atmospheric aerosols, *J. Geophys. Res.*, *110*, D02201, doi:10.1029/2004JD004681.
- Zender, C. S., H. Bian, and D. Newman (2003), Mineral Dust Entrainment and Deposition (DEAD) model: Description and 1990s dust climatology, *J. Geophys. Res.*, *108(D14)*, 4416, doi:10.1029/2002JD002775.
- Zhang, Y., Y. Sunwoo, V. Kotamarthi, and G. R. Carmichael (1994), Photochemical oxidant processes in the presence of dust: An evaluation of the impact of dust on particulate nitrate and ozone formation, *J. Appl. Meteorol.*, *33*, 813– 824.
- Zhang, Y., and G.R. Carmichael (1999), The Role of mineral aerosol in tropospheric chemistry in East Asia - a model study, *Jrn. Appl. Meteor.*, *38(3)*, 353-366.
- Zhang, Y., C. Seigneur, J. H. Seinfeld, M. Jacobson, S. L. Clegg, and F. S. Binkowski (2000), A comparative review of inorganic aerosol thermodynamic equilibrium modules: similarities, differences, and their likely causes, *Atmos. Environ.*, *34*, 117-137.
- Zhang, K. M., E. M. Knipping, A. S. Wexler, P. V. Bhave, and G. S. Tonnesen (2005), Size distribution of sea-salt emissions as a function of relative humidity, *Atmos. Environ.*, *39*, 3373-3379.
- Zhang, Y., P. Liu, B. Pun, and C. Seigneur (2006a), A comprehensive performance evaluation of MM5-CMAQ for the Summer 1999 Southern Oxidants Study episode- Part I: Evaluation protocols, databases, and meteorological predictions, *Atmos. Environ.*, *40*, 4825-4838.

- Zhang, Y., Cheng, S.-H., Y.-S. Chen, and W.-X. Wang (2011), Application of MM5 in China: Model evaluation, seasonal variations, and sensitivity to horizontal grid resolutions, *Atmos. Environ.*, in press.
- Zhu, S., T. Butler, R. Sander, J. Ma, and M. G. Lawrence (2010), Impact of dust on tropospheric chemistry over polluted regions: a case study of the Beijing megacity, *Atmos. Chem. Phys.*, *10*, 3855-3873.
- Zhuang, H., C. K. Chan, M. Fang, and A. S. Wexler (1999), Size distributions of particulate sulfate, nitrate, and ammonium at a coastal site in Hong Kong, *Atmos. Environ.*, *33*, 843-853.
- Zimmermann, P. H. (1988), Moguntia: A handy global tracer model in *Air Pollution Modeling and its Applications*, vol. VI, edited by H. van Dop, Plenum, New York.

Table 4.1. Reactions and uptake coefficients considered in this study (modified from Bian and Zender, 2003).

| Species | Reactions | Uptake coefficients, γ (lower limit) | Uptake coefficients, γ (upper limit) | References* |
|-------------------------------|--|---|---|---|
| H ₂ O ₂ | H ₂ O ₂ + Dust → Products | 1.0×10^{-4} | 0.18 | Dentener et al. (1996) |
| HNO ₃ | HNO ₃ + Dust → 0.5NO ₃ ⁻ + 0.5NO _x | 1.1×10^{-3} | 0.2 | Dentener et al. (1996); DeMore et al. (1997); Underwood et al. (2001) |
| HO ₂ | HO ₂ + Fe(II) → Fe(III) + H ₂ O ₂ | 0.1 | 1 | Dentener et al. (1996); Zhang and Carmichael (1999) |
| N ₂ O ₅ | N ₂ O ₅ + Dust → 2NO ₃ ⁻ | 1.0×10^{-3} | 0.1 | Dentener et al. (1996); DeMore et al. (1997) |
| NO ₂ | NO ₂ + Dust → NO ₃ ⁻ | 4.4×10^{-5} | 2×10^{-4} | Underwood et al. (2001) |
| NO ₃ | NO ₃ + Dust → NO ₃ ⁻ | 0.1 | 0.23 | Seinfeld and Pandis (2006); Zhang and Carmichael (1999) |
| O ₃ | O ₃ + Dust → Products | 5.0×10^{-5} | 1×10^{-4} | Dentener et al. (1996); Zhang and Carmichael (1999) |
| OH | OH + Dust → Products | 0.1 | 1 | Zhang and Carmichael (1999) |
| SO ₂ | SO ₂ + Dust → SO ₄ ²⁻ | 1.0×10^{-4} | 2.6×10^{-4} | Zhang and Carmichael (1999) |

Table 4.2. Major characteristics of ISORROPIA II and EQUISOLV II.

| | ISORROPIA II* | EQUISOLV II |
|------------------------|--|---|
| Chemical species | $\text{NH}_3(\text{g})$, $\text{HNO}_3(\text{g})$, $\text{HCl}(\text{g})$, $\text{H}_2\text{O}(\text{g})$, $\text{NH}_4^+(\text{aq})$, $\text{Na}^+(\text{aq})$, $\text{H}^+(\text{aq})$, $\text{Cl}^-(\text{aq})$, $\text{NO}_3^-(\text{aq})$, $\text{SO}_4^{2-}(\text{aq})$, $\text{OH}^-(\text{aq})$, $\text{H}_2\text{O}(\text{aq})$, $\text{Ca}^{2+}(\text{aq})$, $\text{K}^+(\text{aq})$, $\text{Mg}^{2+}(\text{aq})$, $\text{NH}_3(\text{aq})$, $\text{HNO}_3(\text{aq})$, $\text{HCl}(\text{aq})$, $\text{HSO}_4^-(\text{aq})$, $(\text{NH}_4)_2\text{SO}_4(\text{s})$, $\text{NH}_4\text{HSO}_4(\text{s})$, $(\text{NH}_4)_3\text{H}(\text{SO}_4)_2(\text{s})$, $\text{NH}_4\text{NO}_3(\text{s})$, $\text{NH}_4\text{Cl}(\text{s})$, $\text{NaCl}(\text{s})$, $\text{NaNO}_3(\text{s})$, $\text{NaHSO}_4(\text{s})$, $\text{Na}_2\text{SO}_4(\text{s})$, $\text{CaSO}_4(\text{s})$, $\text{Ca}(\text{NO}_3)_2(\text{s})$, $\text{CaCl}_2(\text{s})$, $\text{K}_2\text{SO}_4(\text{s})$, $\text{KHSO}_4(\text{s})$, $\text{KNO}_3(\text{s})$, $\text{KCl}(\text{s})$, $\text{MgSO}_4(\text{s})$, $\text{Mg}(\text{NO}_3)_2(\text{s})$, $\text{MgCl}_2(\text{s})$ | ISORROPIA II + $\text{HCO}_3^-(\text{aq})$, $\text{CO}_3^{2-}(\text{aq})$, $\text{NH}_4\text{HCO}_3(\text{s})$, $\text{NaHCO}_3(\text{s})$, $\text{Na}_2\text{CO}_3(\text{s})$, $\text{CaCO}_3(\text{s})$, $\text{Ca}(\text{HCO}_3)_2(\text{s})$, $\text{K}_2\text{CO}_3(\text{s})$, $\text{KHCO}_3(\text{s})$, $\text{MgCO}_3(\text{s})$, $\text{Mg}(\text{HCO}_3)_2(\text{s})$ |
| Activity coefficients | Kusik-Meissner method (Kusik and Meissner, 1978) for binary activity coefficients and Bromley method (Bromley, 1973) for multi-component activity coefficient | A number of sources such as Hamer and Wu (1972), Goldberg (1981), Bassett and Seinfeld (1983), and Pitzer methods (1991) for binary activity coefficients and Bromley method (Bromley, 1973) for multi-component activity coefficient |
| Water activity | Zdanovskii, Robinson and Stokes (ZSR) method (Robinson and Stokes, 1965) | ZSR method (Robinson and Stokes, 1965) |
| Temperature dependence | Equilibrium constants, deliquescence relative humidity (DRH), mutual deliquescence relative humidity (MDRH), and activity coefficients | Equilibrium constants, DRHs, and activity coefficients |
| Composition dependence | MDRHs | MDRHs |
| Metastable treatment | Only aqueous phase can be formed | Both aqueous and solid phases can be formed |
| Solution method | Bisectional | Mass flux iteration (MFI) and analytical equilibrium iteration (AEI) |

*Subscripts (g), (aq), and (s) denote gas, aqueous and solid, respectively.

Table 4.3. The configurations of WRF/CMAQ v4.7-Dust used in the model simulation.

| | |
|--------------------------|---------------------|
| Shortwave Radiation | Goddard |
| Longwave Radiation | RRTM |
| Planetary Boundary Layer | YSU |
| Land Surface | Thermal diffusion |
| Microphysics | WSM 6-class graupel |
| Cumulus | Grell 3D ensemble |
| Gas-phase Mechanism | CB05 |
| Aerosol Module | AERO5 |

Table 4.4. Performance statistics for meteorological predictions over U.S. and China from MM5 and WRF simulations in April 2001.

| | Variables | CASTNET (U.S.) | | | | STN (U.S.) | NADP (U.S.) | NCDC (China) | | |
|-------------------------------|-------------|----------------|---------|--------------------------|---------------|------------|--------------|--------------|------------|--------------|
| | | T2 (°C) | RH2 (%) | WS10 (ms ⁻¹) | WD10 (degree) | T2 (°C) | Precip. (mm) | T2 (°C) | Q2 (kg/kg) | Precip. (mm) |
| WRF (CCSM) with PBL nudging | Data Number | 12.2 | 61.7 | 2.7 | 190.0 | 15.0 | 17.8 | 13.1 | 0.00545 | 2.3 |
| | Mean Obs. | 13.6 | 67.4 | 5.4 | 207.7 | 15.4 | 6.4 | 9.7 | 0.00528 | 0.65 |
| | Mean Pred. | 0.61 | 0.40 | 0.21 | 0.13 | 0.56 | 0.12 | 0.72 | 0.73 | 0.03 |
| | Correlation | 1.4 | 5.8 | 2.7 | 17.6 | 0.4 | -11.4 | -3.4 | -0.00017 | -1.65 |
| | MB | 7.0 | 23.7 | 4.0 | 122.7 | 6.4 | 26.2 | 7.5 | 0.00272 | 6.12 |
| | RMSE | 11.8 | 9.4 | 97.7 | 9.3 | 2.8 | -64.1 | -3.4 | -3.1 | -71.6 |
| | NMB (%) | 45.7 | 31.1 | 118.1 | 49.8 | 34.1 | 95.5 | 44.6 | 37.8 | 108.9 |
| NME (%) | 12.8 | 70.3 | 4.6 | 204.9 | 14.3 | 8.3 | 10.7 | 0.00596 | 1.7 | |
| WRF (FNL) without PBL nudging | Mean Pred. | 0.89 | 0.70 | 0.55 | 0.48 | 0.87 | 0.57 | 0.88 | 0.92 | 0.31 |
| | Correlation | 0.6 | 8.6 | 1.9 | 14.9 | -0.7 | -9.5 | -2.5 | 0.00051 | -0.63 |
| | MB | 3.6 | 19.3 | 2.8 | 100.9 | 3.6 | 19.8 | 5.1 | 0.00168 | 5.63 |
| | RMSE | 5.2 | 14.0 | 69.2 | 7.8 | -4.4 | -53.4 | -18.8 | 9.3 | -27.5 |
| | NMB (%) | 22.4 | 24.6 | 82.5 | 32.7 | 17.7 | 69.8 | 29.3 | 23.5 | 102.5 |
| | NME (%) | 12.2 | 61.7 | 2.7 | 190.0 | 15.0 | 17.8 | 13.1 | 0.00545 | 2.3 |

Table 4.4. (continued)

| | Variables | CASTNET (U.S.) | | | | STN (U.S.) | NADP (U.S.) | NCDC (China) | | |
|-------------------------------|-------------|----------------|---------|--------------------------|---------------|------------|--------------|--------------|------------|--------------|
| | | T2 (°C) | RH2 (%) | WS10 (ms ⁻¹) | WD10 (degree) | T2 (°C) | Precip. (mm) | T2 (°C) | Q2 (kg/kg) | Precip. (mm) |
| WRF (FNL) with UV PBL nudging | Mean Pred. | 12.8 | 70.4 | 4.0 | 202.1 | 14.3 | 8.2 | 10.4 | 0.00589 | 1.6 |
| | Correlation | 0.88 | 0.68 | 0.54 | 0.50 | 0.87 | 0.56 | 0.87 | 0.91 | 0.35 |
| | MB | 0.6 | 8.8 | 1.2 | 12.0 | -0.6 | -9.6 | -2.7 | 0.00044 | -0.72 |
| | RMSE | 3.7 | 19.7 | 2.3 | 96.1 | 3.6 | 19.9 | 5.4 | 0.00169 | 5.42 |
| | NMB (%) | 4.9 | 14.2 | 45.6 | 6.3 | -4.2 | -54.1 | -20.6 | 8.1 | -31.5 |
| | NME (%) | 23.2 | 25.0 | 67.4 | 30.8 | 17.9 | 70.0 | 31.1 | 23.6 | 97.6 |
| MM5 | Mean Pred. | 9.9 | 71.5 | 3.1 | 182.0 | 11.5 | 13.3 | 9.34 | 0.0049 | 1.98 |
| | Correlation | 0.85 | 0.60 | 0.57 | 0.14 | 0.88 | 0.57 | 0.88 | 0.94 | 0.44 |
| | MB | -2.3 | 9.8 | 0.4 | -8.1 | -3.5 | -5.9 | -3.8 | -0.00053 | -0.32 |
| | RMSE | 5.0 | 28.2 | 1.8 | 124.7 | 5.0 | 18.3 | 5.9 | 0.00154 | 5.31 |
| | NMB (%) | -19.2 | 15.9 | 15.4 | -4.2 | -23.1 | -30.8 | -28.8 | -9.8 | -14.0 |
| | NME (%) | 30.8 | 33.2 | 52.1 | 51.1 | 25.2 | 60.3 | 34.3 | 21.8 | 102.4 |

Table 4.5. Performance statistics for chemical predictions over the U.S. from simulations BASELINE, DUST, and CMAQv4.4 in April 2001.

| | Variables | AIRS | CASTNET | SEARCH | AIRS | CASTNET | SEARCH | IMPROVE | STN | SEARCH |
|----------|-------------|------------------------------|---------|--------|------------------------------|---------|--------|---|------|--------|
| | | Max 1 h O ₃ (ppb) | | | Max 8 h O ₃ (ppb) | | | PM _{2.5} (µg m ⁻³) | | |
| BASELINE | Data Number | 29993 | 2267 | 197 | 29276 | 2232 | 197 | 2125 | 365 | 87 |
| | Mean Obs. | 52.7 | 54.3 | 56.4 | 47.8 | 50.4 | 51.4 | 5.7 | 11.1 | 14.3 |
| | Mean Pred. | 54.1 | 48.9 | 49.9 | 51.1 | 48.1 | 49.6 | 7.0 | 11.9 | 11.2 |
| | Correlation | 0.50 | 0.49 | 0.63 | 0.47 | 0.58 | 0.71 | 0.43 | 0.48 | 0.34 |
| | NMB (%) | 2.8 | -9.8 | -11.5 | 6.8 | -4.7 | -3.6 | 21.8 | 6.8 | -21.5 |
| | NME (%) | 16.6 | 17.0 | 17.6 | 17.9 | 15.5 | 14.8 | 55.1 | 42.2 | 52.2 |
| DUST | Data Number | 29993 | 2267 | 197 | 29276 | 2232 | 197 | 2125 | 365 | 87 |
| | Mean Obs. | 52.7 | 54.3 | 56.4 | 47.8 | 50.4 | 51.4 | 5.7 | 11.1 | 14.3 |
| | Mean Pred. | 53.7 | 48.6 | 49.1 | 50.7 | 47.7 | 48.3 | 9.5 | 14.1 | 12.8 |
| | Correlation | 0.49 | 0.48 | 0.63 | 0.47 | 0.57 | 0.71 | 0.32 | 0.40 | 0.37 |
| | NMB (%) | 2.0 | -10.5 | -12.9 | 5.9 | -5.4 | -4.2 | 66.3 | 26.5 | -10.1 |
| | NME (%) | 16.7 | 17.4 | 18.1 | 17.9 | 15.8 | 15.1 | 86.4 | 53.1 | 52.9 |
| CMAQv4.4 | Data Number | 29993 | 2267 | 197 | 29276 | 2232 | 197 | 2125 | 365 | 87 |
| | Mean Obs. | 52.5 | 54.3 | 56.3 | 47.7 | 50.4 | 51.2 | 6.03 | 11.1 | 15.2 |
| | Mean Pred. | 48.7 | 44.2 | 47.5 | 45.4 | 43.4 | 47.3 | 9.39 | 16.8 | 17.5 |
| | Correlation | 0.54 | 0.51 | 0.71 | 0.53 | 0.62 | 0.75 | 0.29 | 0.41 | 0.67 |
| | NMB (%) | -7.3 | -18.5 | -15.7 | -4.7 | -13.8 | -7.7 | 55.7 | 51.5 | 15.4 |
| | NME (%) | 18.5 | 22.3 | 18.6 | 18.8 | 19.5 | 14.8 | 82.3 | 70.6 | 33.4 |

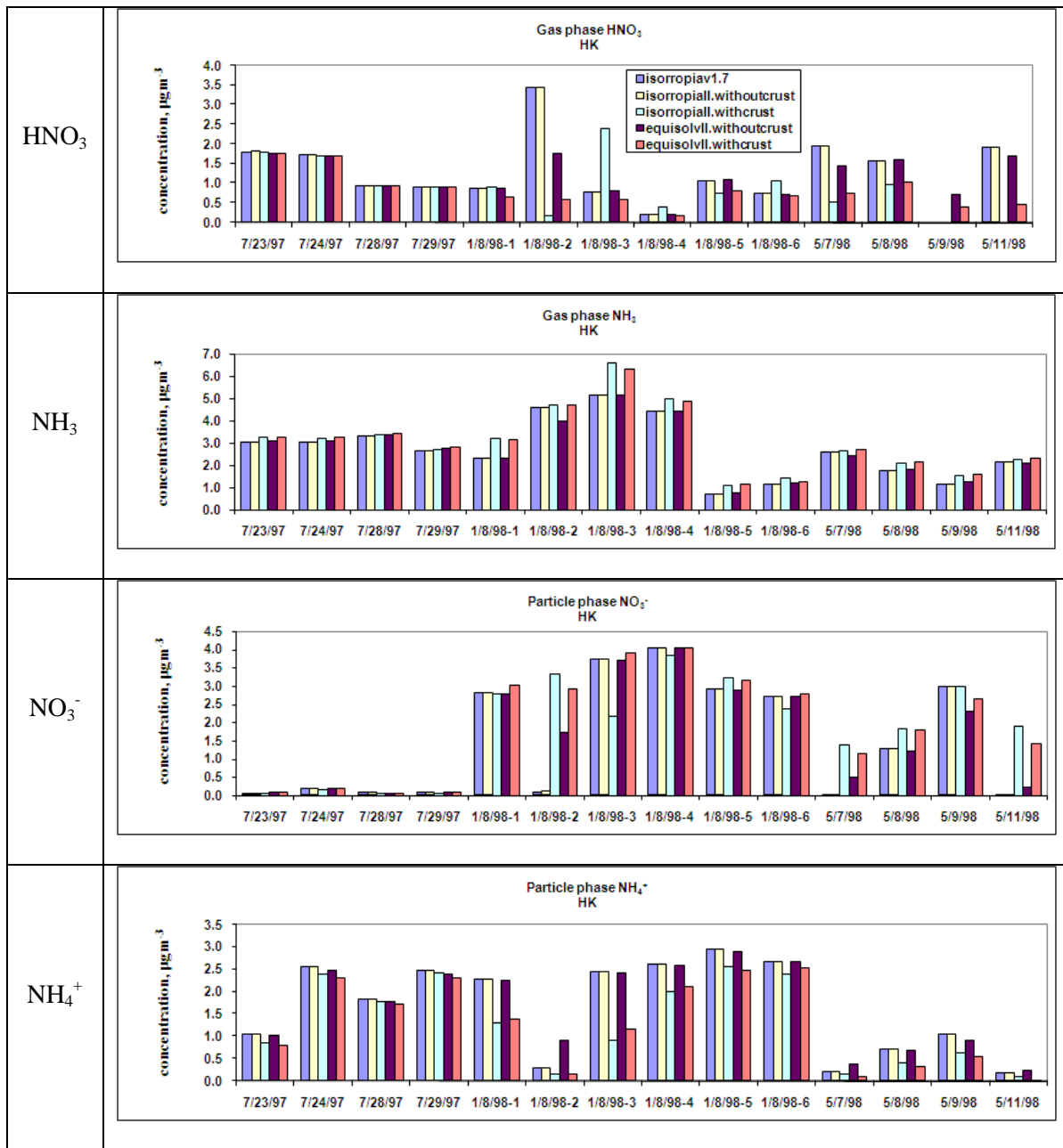
Table 4.6. Performance statistics for chemical predictions over Asia from simulations BASELINE, DUST, and CMAQv4.4 in April 2001.

| | Variables | Beijing | | | | Japan | | | | |
|----------|-------------|--|--|--|---|-------------|--------------------------|-------------|--------------------------|------------------------------|
| | | Max 1h O ₃ (µg m ⁻³) | SO ₂ (µg m ⁻³) | NO ₂ (µg m ⁻³) | PM ₁₀ (µg m ⁻³) | CO (ppb) | SO ₂ (ppb) | NO (ppb) | NO ₂ (ppb) | SPM (µg m ⁻³) |
| BASELINE | Data Number | 30 | 30 | 30 | 30 | 131 | 1490 | 1448 | 1465 | 1537 |
| | Mean Obs. | 95.8 | 34.0 | 65.9 | 209.6 | 443.5 | 6.0 | 6.6 | 16.9 | 33.9 |
| | Mean Pred. | 112.4 | 39.5 | 18.6 | 39.9 | 183.0 | 3.9 | 0.6 | 6.0 | 16.6 |
| | Correlation | 0.01 | 0.17 | 0.25 | 0.13 | 0.30 | 0.39 | 0.19 | 0.48 | 0.15 |
| | NMB (%) | 17.3 | 16.2 | -71.8 | -80.9 | -58.7 | -35.2 | -91.1 | -64.2 | -50.9 |
| | NME (%) | 30.6 | 56.0 | 71.8 | 80.9 | 58.7 | 43.8 | 91.2 | 65.4 | 51.1 |
| DUST | Data Number | 30 | 30 | 30 | 30 | 131 | 1490 | 1448 | 1465 | 1537 |
| | Mean Obs. | 95.8 | 34.0 | 65.9 | 210.0 | 443.5 | 6.0 | 6.6 | 16.9 | 33.9 |
| | Mean Pred. | 108.9 | 38.8 | 18.5 | 113.6 | 183.0 | 3.9 | 0.6 | 6.0 | 22.1 |
| | Correlation | 0.01 | 0.17 | 0.25 | 0.11 | 0.30 | 0.39 | 0.19 | 0.48 | 0.19 |
| | NMB (%) | 13.7 | 14.2 | -71.9 | -45.8 | -58.7 | -35.5 | -91.1 | -64.3 | -34.7 |
| | NME (%) | 27.7 | 55.1 | 71.9 | 79.9 | 58.7 | 44.0 | 91.1 | 65.4 | 35.8 |
| CMAQv4.4 | Data Number | 30 | 30 | 30 | 30 | 131 | 1490 | 1448 | 1465 | 1537 |
| | Mean Obs. | 95.8 | 34.0 | 65.9 | 210.0 | 443.5 | 6.0 | 6.6 | 16.9 | 33.9 |
| | Mean Pred. | 86.8 | 37.3 | 15.3 | 34.0 | 192.0 | 4.5 | 0.6 | 6.6 | 17.0 |
| | Correlation | -0.03 | 0.28 | 0.38 | 0.14 | 0.27 | 0.35 | 0.21 | 0.44 | 0.16 |
| | NMB (%) | -9.36 | 9.80 | -76.8 | -83.6 | -56.7 | -25.5 | -91.1 | -60.7 | -49.7 |
| | NME (%) | 25.5 | 49.4 | 76.8 | 83.6 | 56.8 | 40.5 | 91.1 | 62.8 | 49.9 |

Table 4.7. Performance statistics for column predictions over the ICAP domain from simulations BASELINE, DUST, and CMAQv4.4 in April 2001.

| | Variables | CO | TOR | NO ₂ | AOD |
|----------|-------------|-------|-------|-----------------|-------|
| BASELINE | Data Number | 16048 | 7900 | 36760 | 12387 |
| | Mean Obs. | 2.41 | 36.0 | 8.7 | 0.274 |
| | Mean Pred. | 2.19 | 29.9 | 9.4 | 0.219 |
| | Correlation | 0.55 | 0.65 | 0.85 | 0.63 |
| | NMB (%) | -9.0 | -16.9 | 8.6 | -20.2 |
| | NME (%) | 12.9 | 18.5 | 48.2 | 34.8 |
| DUST | Data Number | 16048 | 7900 | 36760 | 12387 |
| | Mean Obs. | 2.41 | 36.0 | 8.7 | 0.27 |
| | Mean Pred. | 2.19 | 29.8 | 9.6 | 0.25 |
| | Correlation | 0.55 | 0.65 | 0.85 | 0.63 |
| | NMB (%) | -9.0 | -17.2 | 10.0 | -7.8 |
| | NME (%) | 12.9 | 18.6 | 48.6 | 34.6 |
| CMAQv4.4 | Data Number | 16048 | 7900 | 36760 | 12387 |
| | Mean Obs. | 2.41 | 36.0 | 8.7 | 0.27 |
| | Mean Pred. | 2.14 | 26.6 | 8.4 | 0.18 |
| | Correlation | 0.47 | 0.56 | 0.86 | 0.61 |
| | NMB (%) | -11.0 | -26.1 | -3.9 | -35.4 |
| | NME (%) | 15.1 | 26.6 | 43.5 | 41.2 |

Figure 4.1. Comparisons of different volatile species and variables between simulations of ISORROPIA v1.7, ISORROPIA II (with and without crust), EQUISOLV II (with and without crust) at the Hong Kong site.



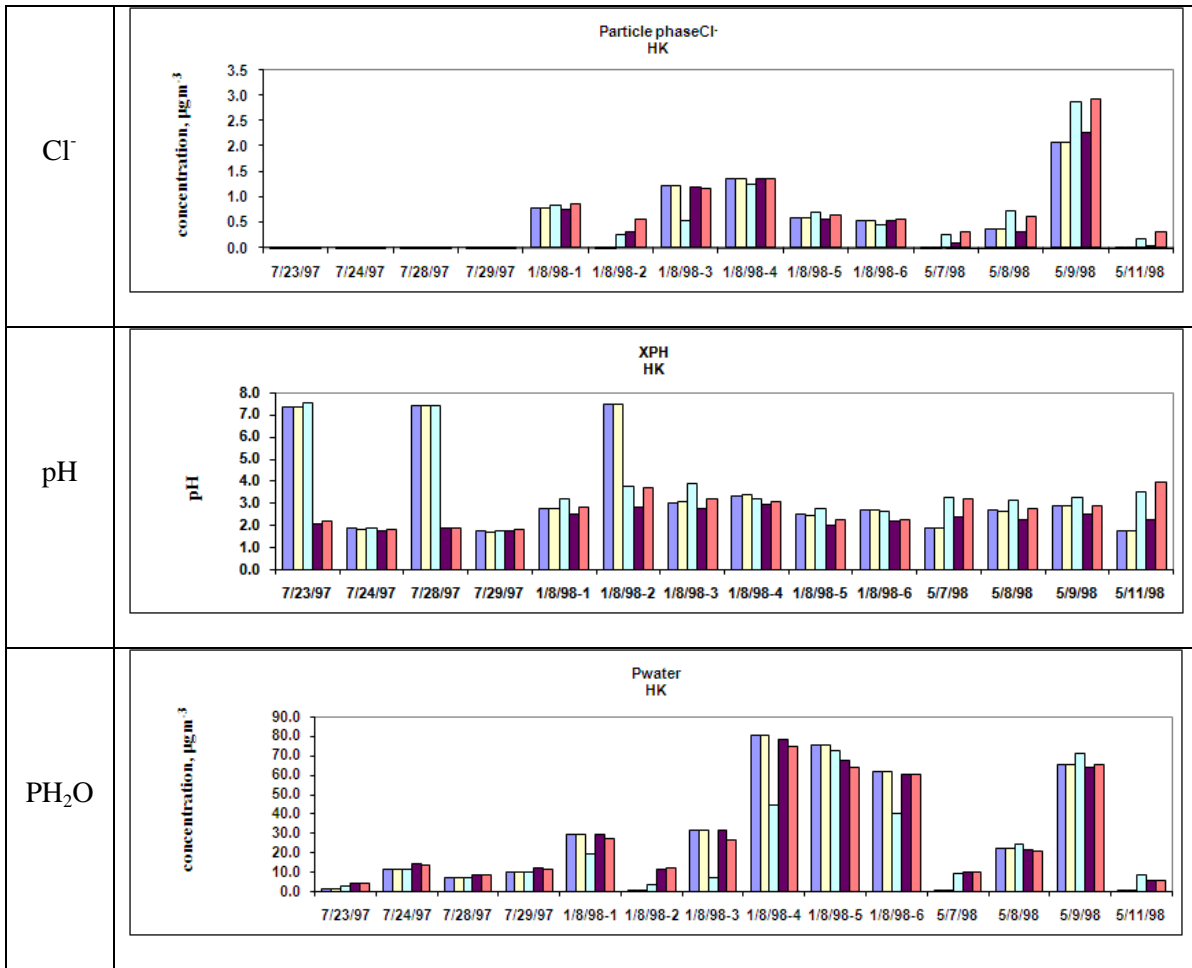
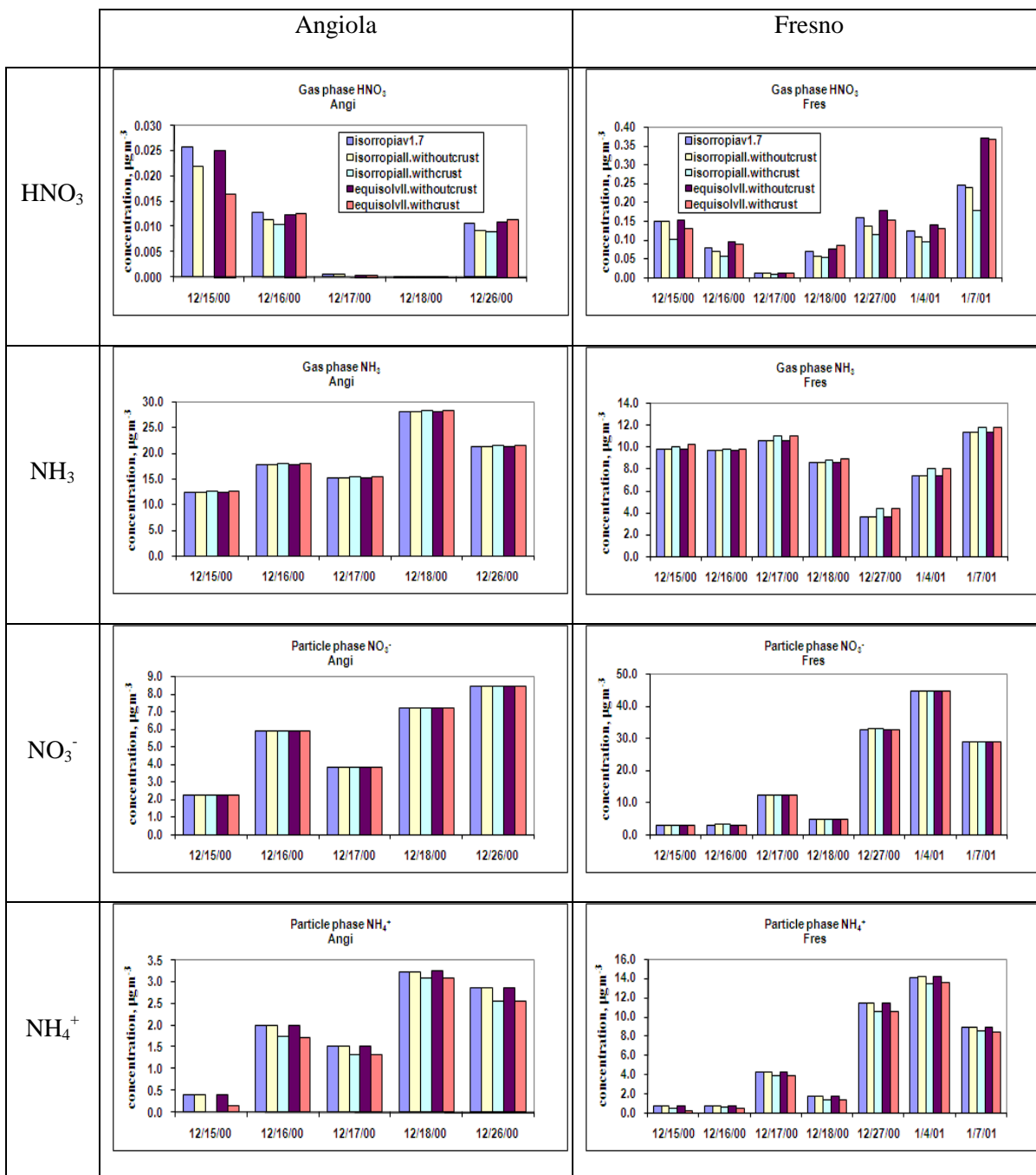
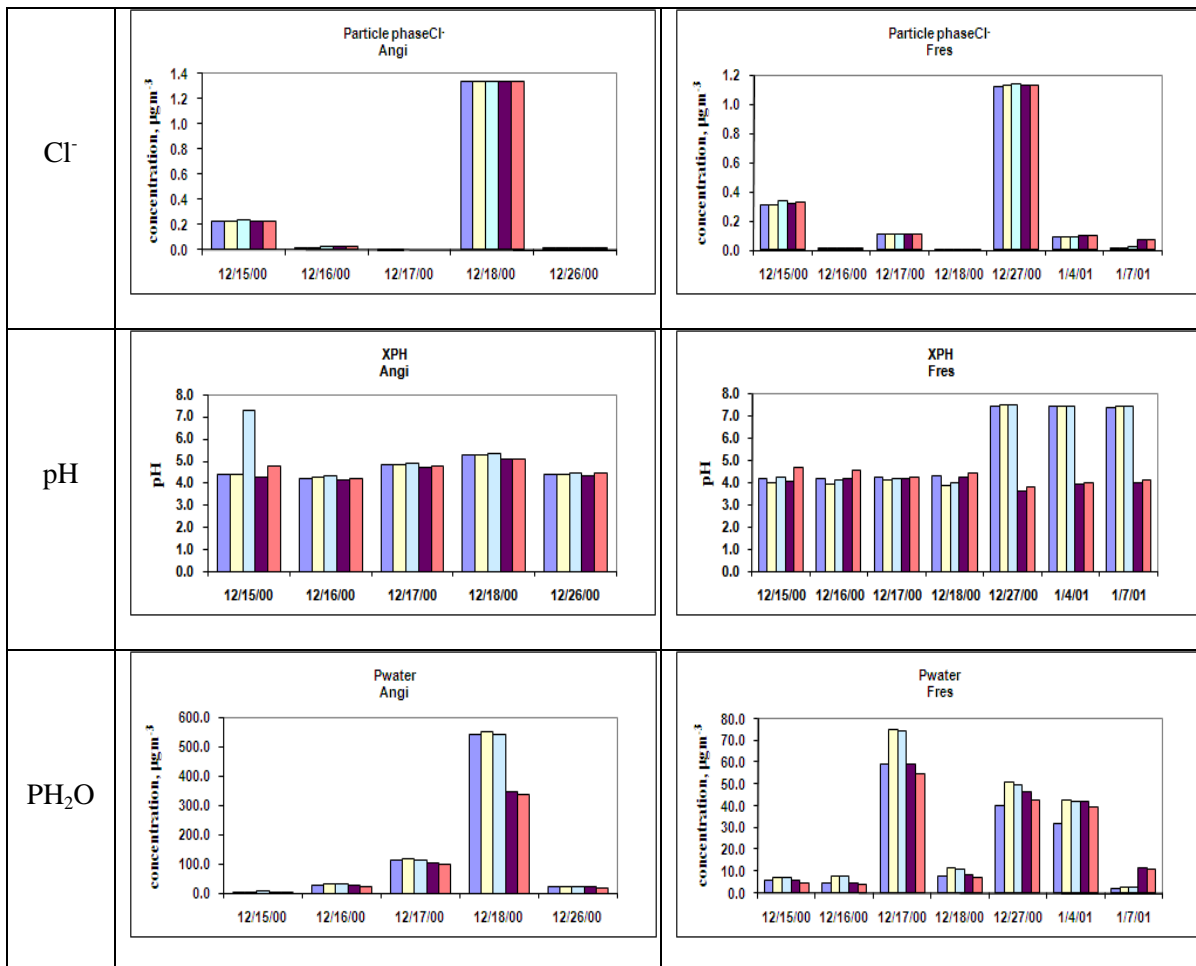


Figure 4.2. Comparisons of different volatile species and variables between simulations of ISORROPIA v1.7, ISORROPIA II (with and without crust), EQUISOLV II (with and without crust) at Angiola and Fresno.





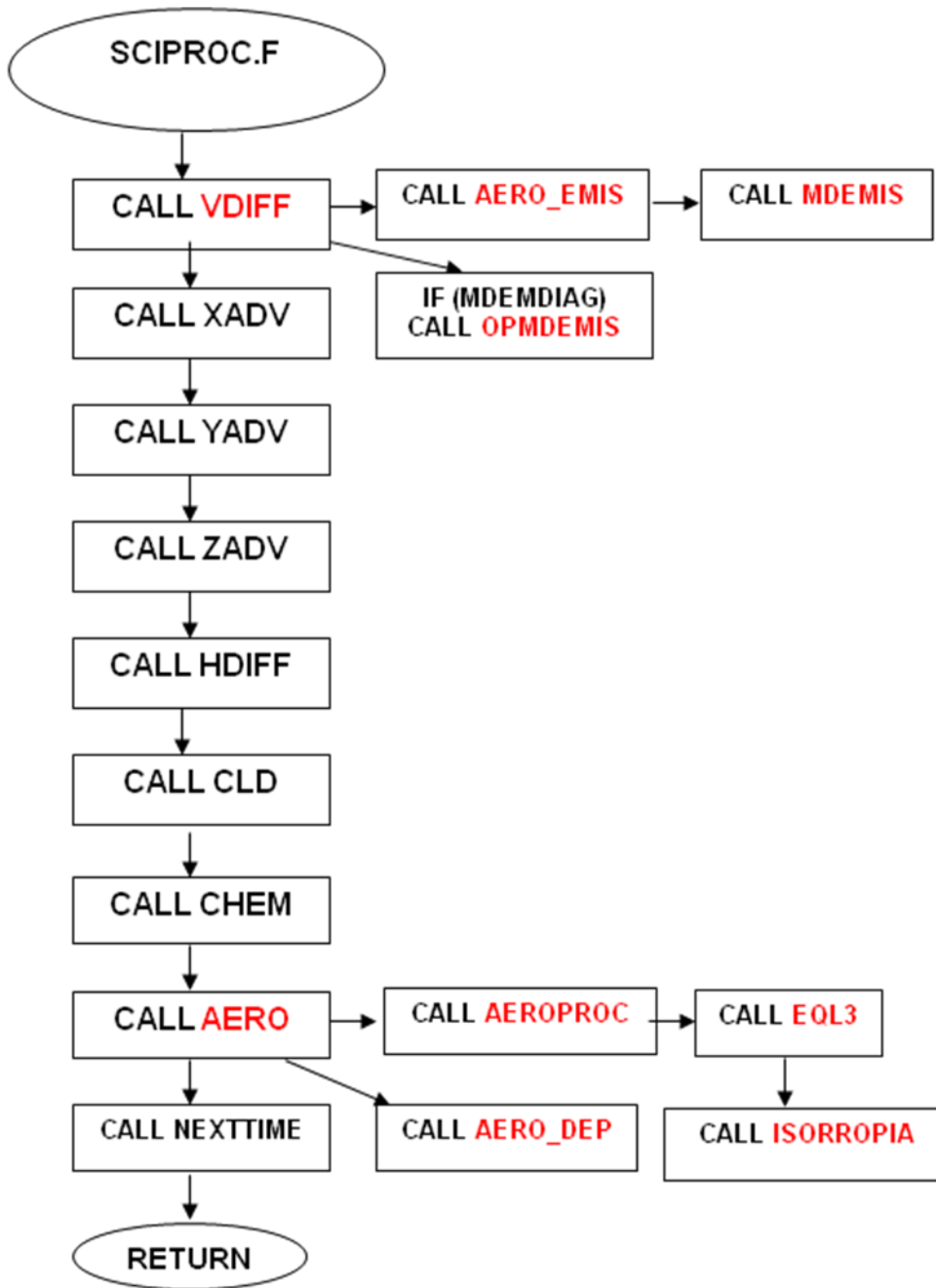


Figure 4.3. Flow chart of the physical and chemical drivers in CMAQ

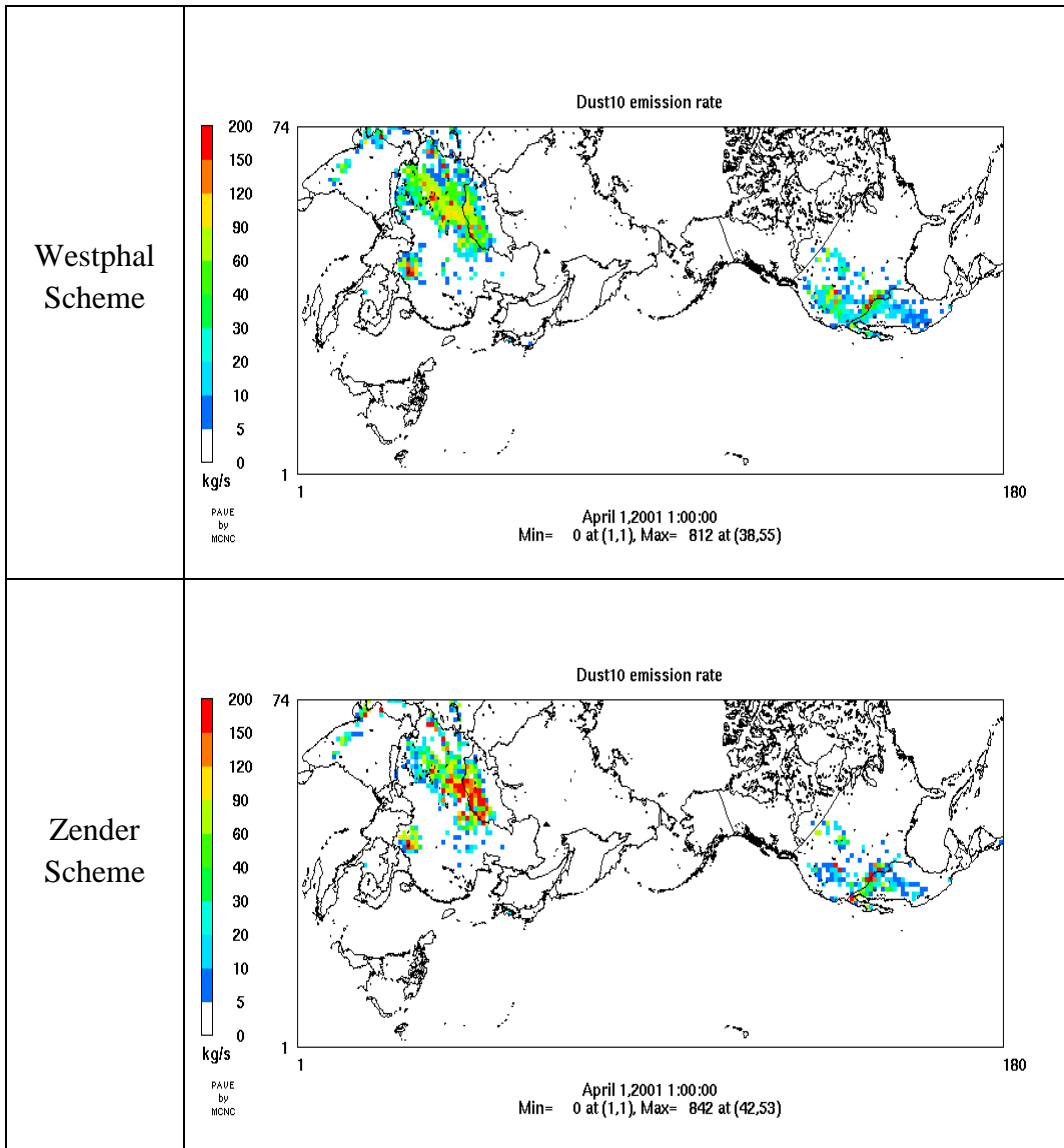


Figure 4.4. The monthly-mean dust emission rates generated by the Westphal and Zender schemes used in MM5/CMAQ v4.4.

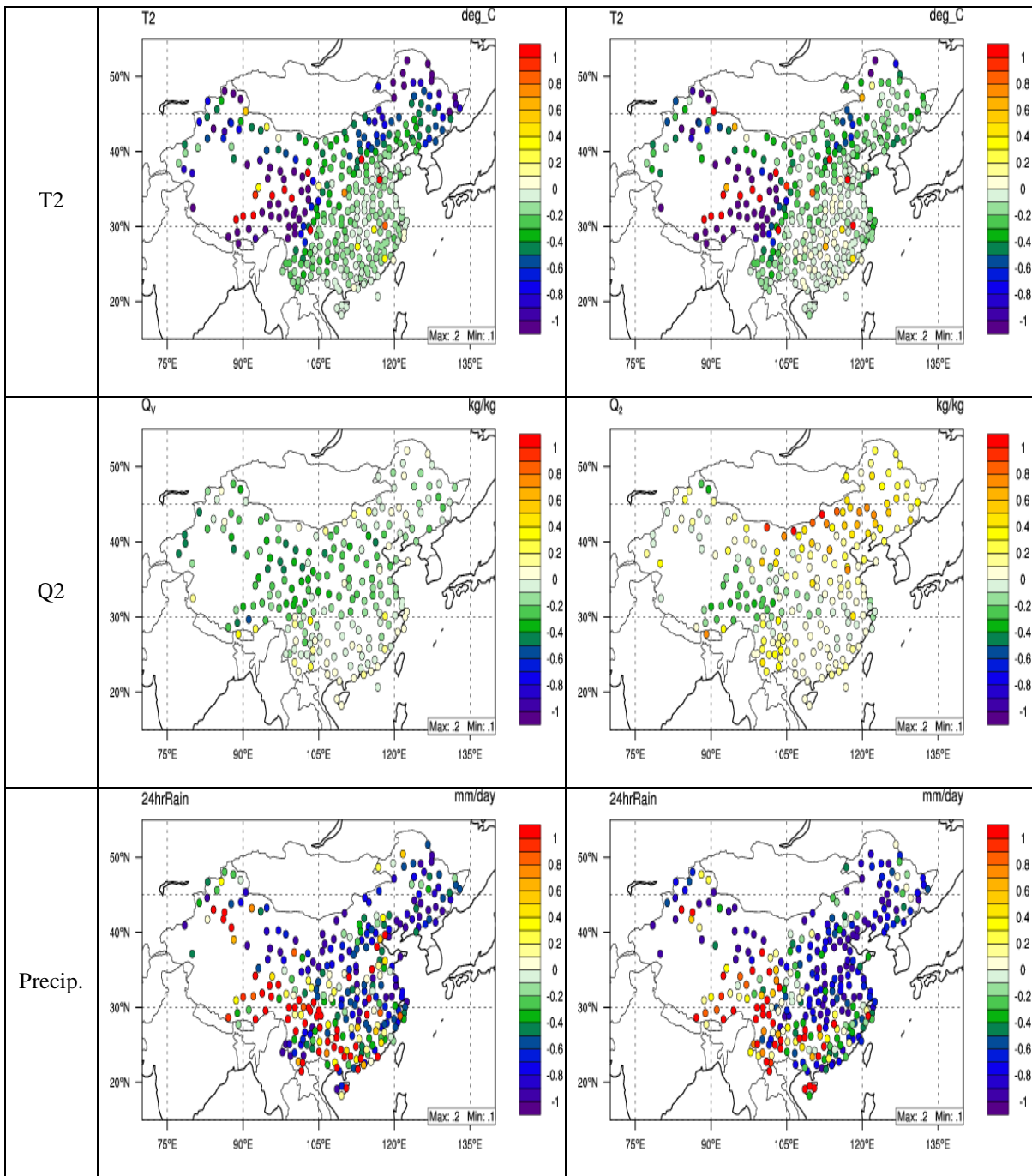


Figure 4.5. Spatial distribution of NMBs between observations and MM5 simulation (left panel) and WRF simulation (right panel) for temperature at 2 m (T2), water vapor mixing ratio at 2 m (Q2), and 24-h total precipitation (Precip.) over China for April 2001.

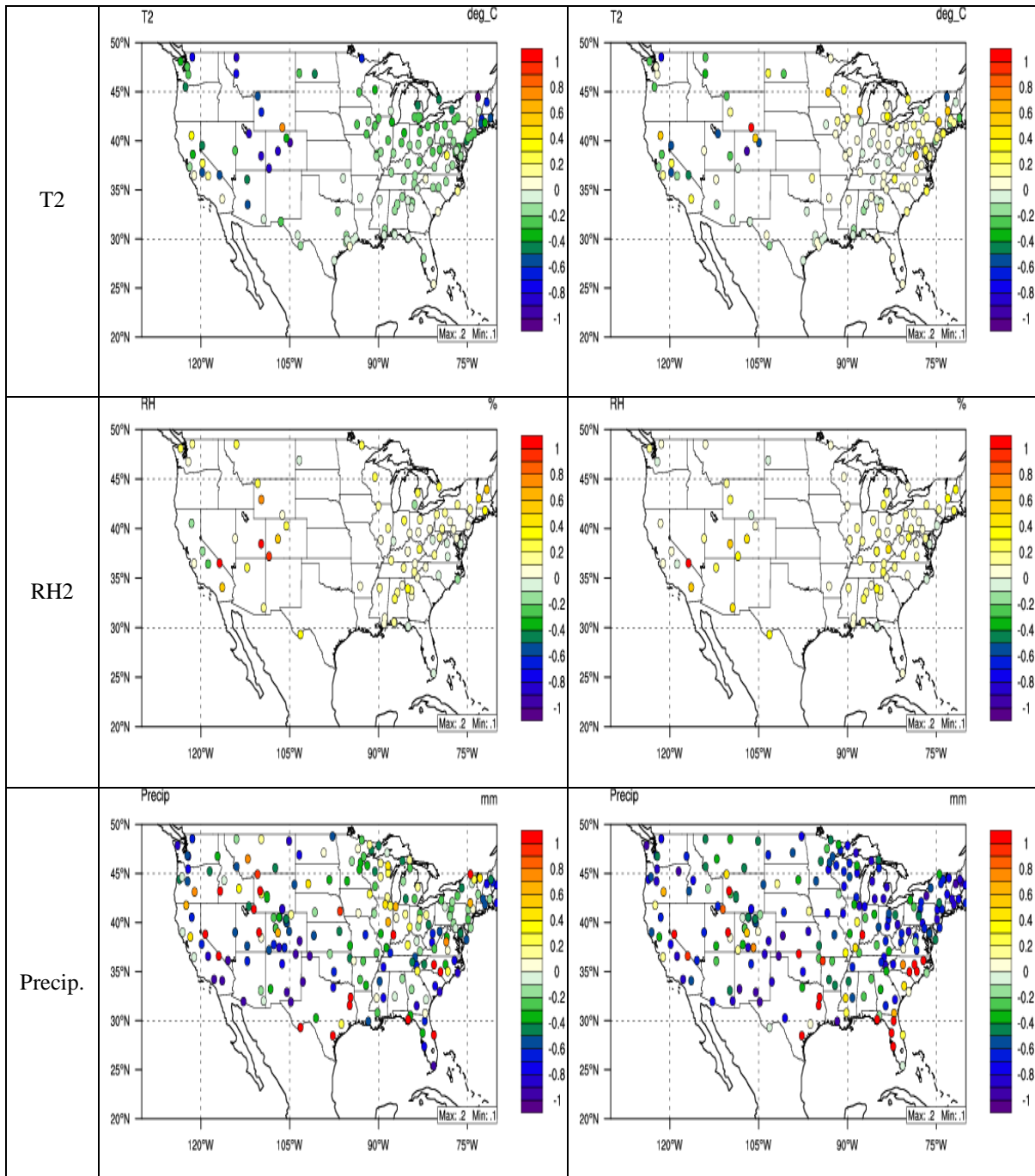


Figure 4.6. Spatial distribution of NMBs between observations and MM5 simulation (left panel) and WRF simulation (right panel) for temperature at 2 m (T2), relative humidity at 2 m (RH2), and weekly total precipitation (Precip.) over U.S. for April 2001.

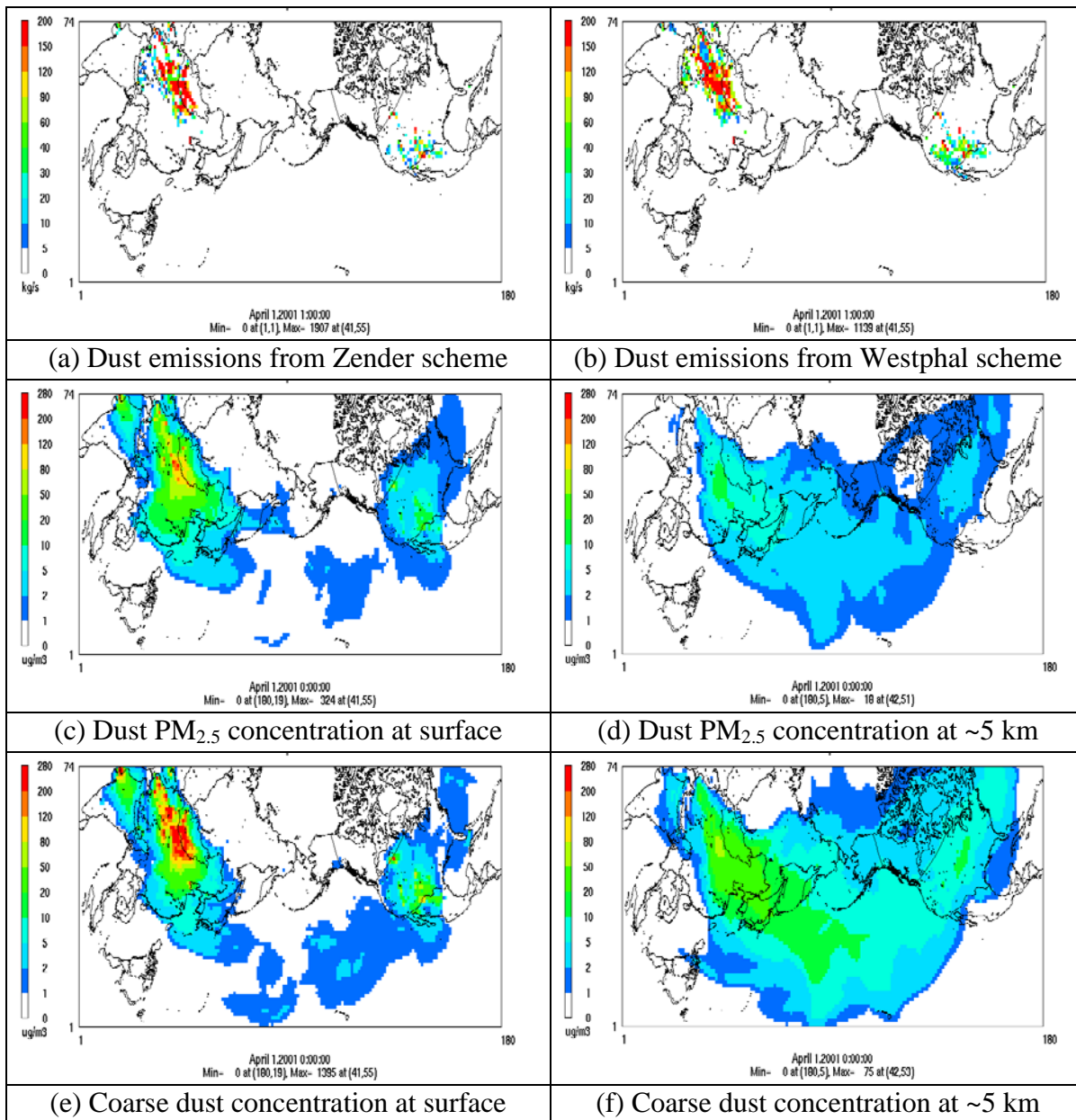


Figure 4.7. The predicted monthly-mean dust emission rates generated by (a) Zender and (b) Westphal schemes, (c) and (d) for fine and (e) and (f) for coarse dust concentrations at surface and ~5 km from the Zender scheme in CMAQ-Dust.

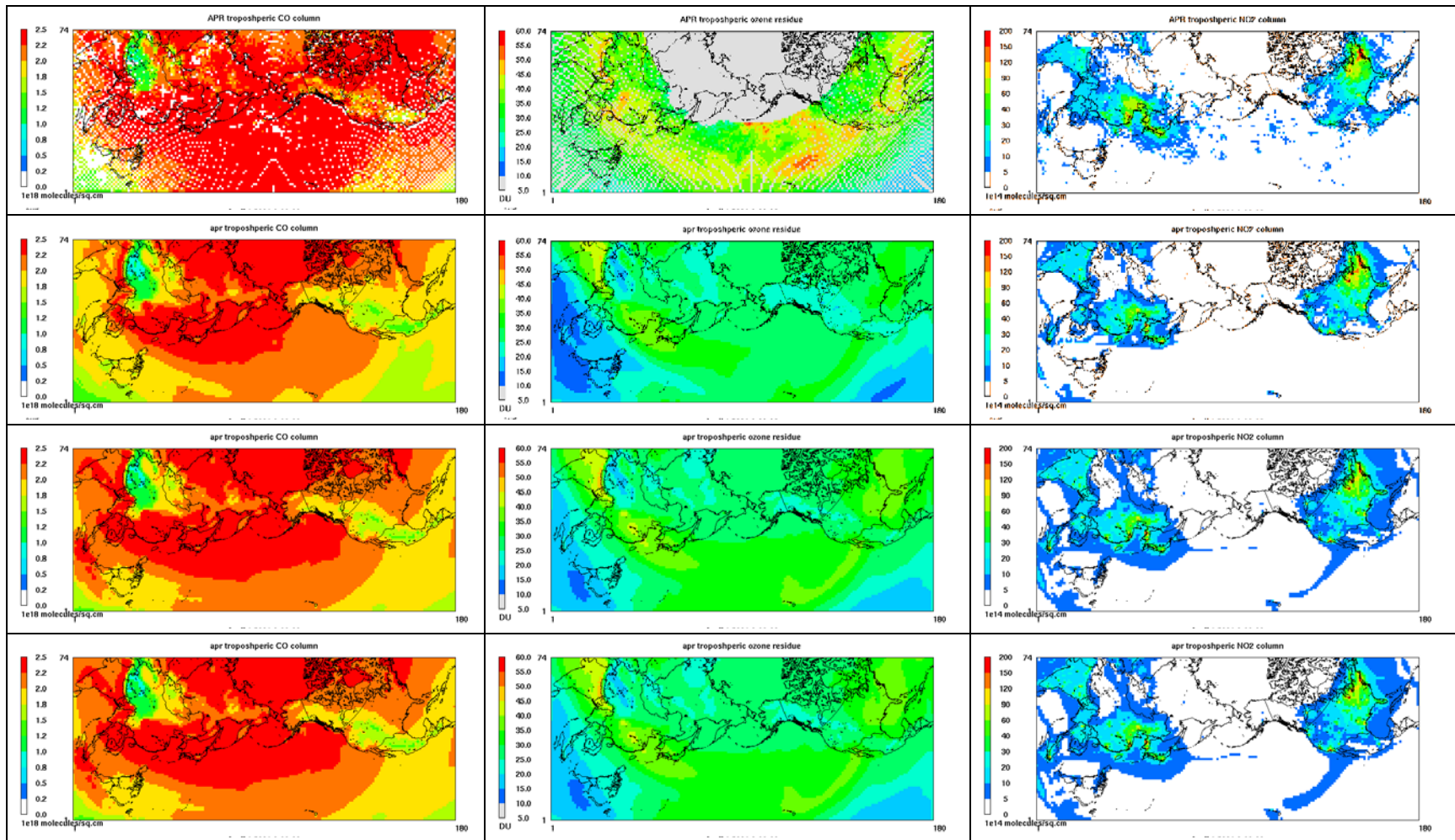


Figure 4.8. Spatial distribution of column variables (from left to right: CO, TOR, NO₂) from satellite observations (1st row), CMAQ v4.4 (2nd row), BASELINE simulation (3rd row) and DUST simulation (4th row) in April 2001.

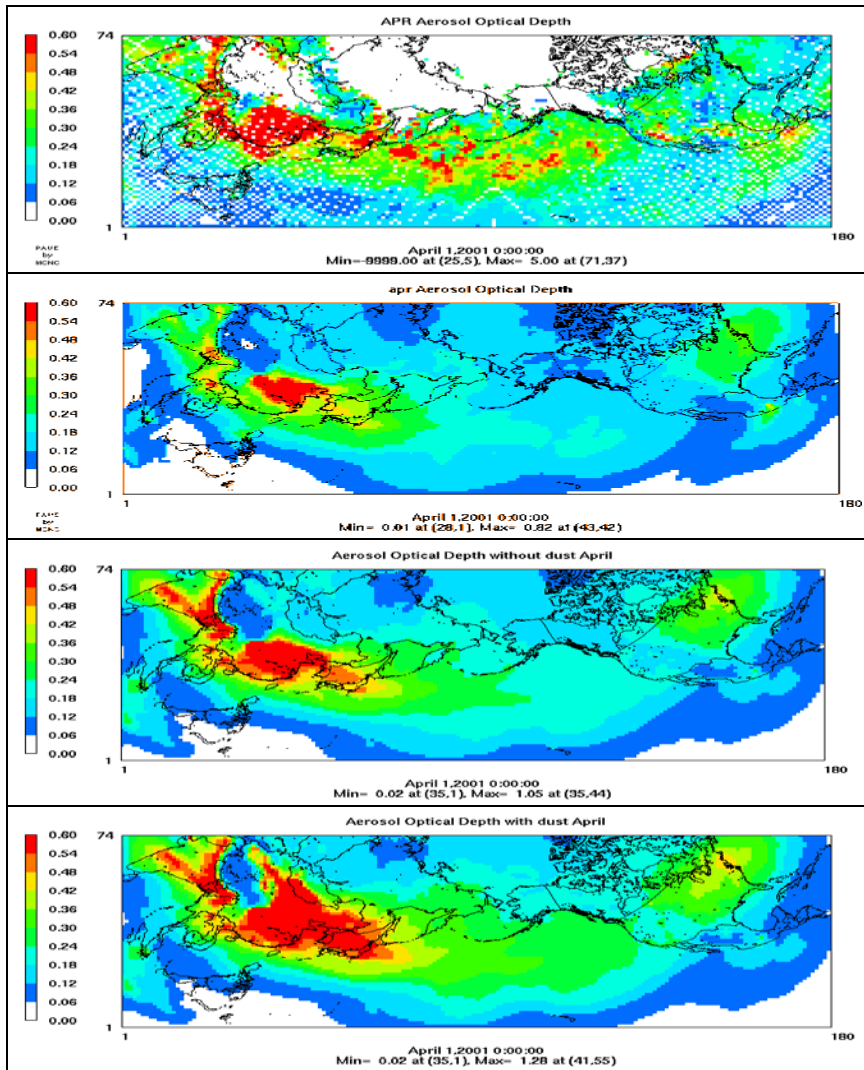


Figure 4.9. Spatial distribution of AOD from satellite observations (1st row), CMAQ v4.4 (2nd row), BASELINE simulation (3rd row) and DUST simulation (4th row) in April 2001.

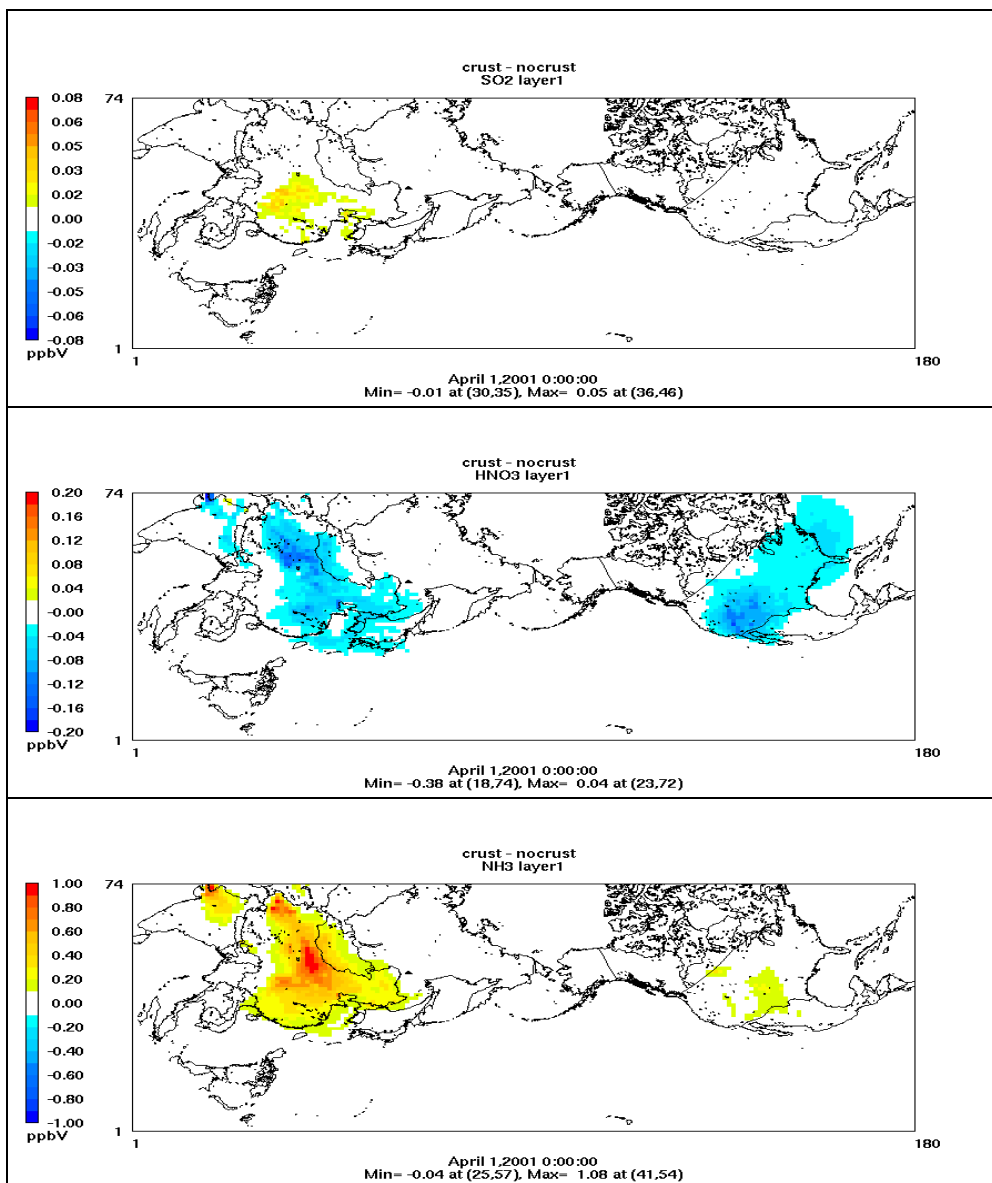


Figure 4.10. Spatial distribution of differences between simulations with crustal species (CRUST_ONLY) and without crustal species (DUST_EMIS_ONLY) for surface layer SO_2 , HNO_3 , and NH_3 in April 2001.

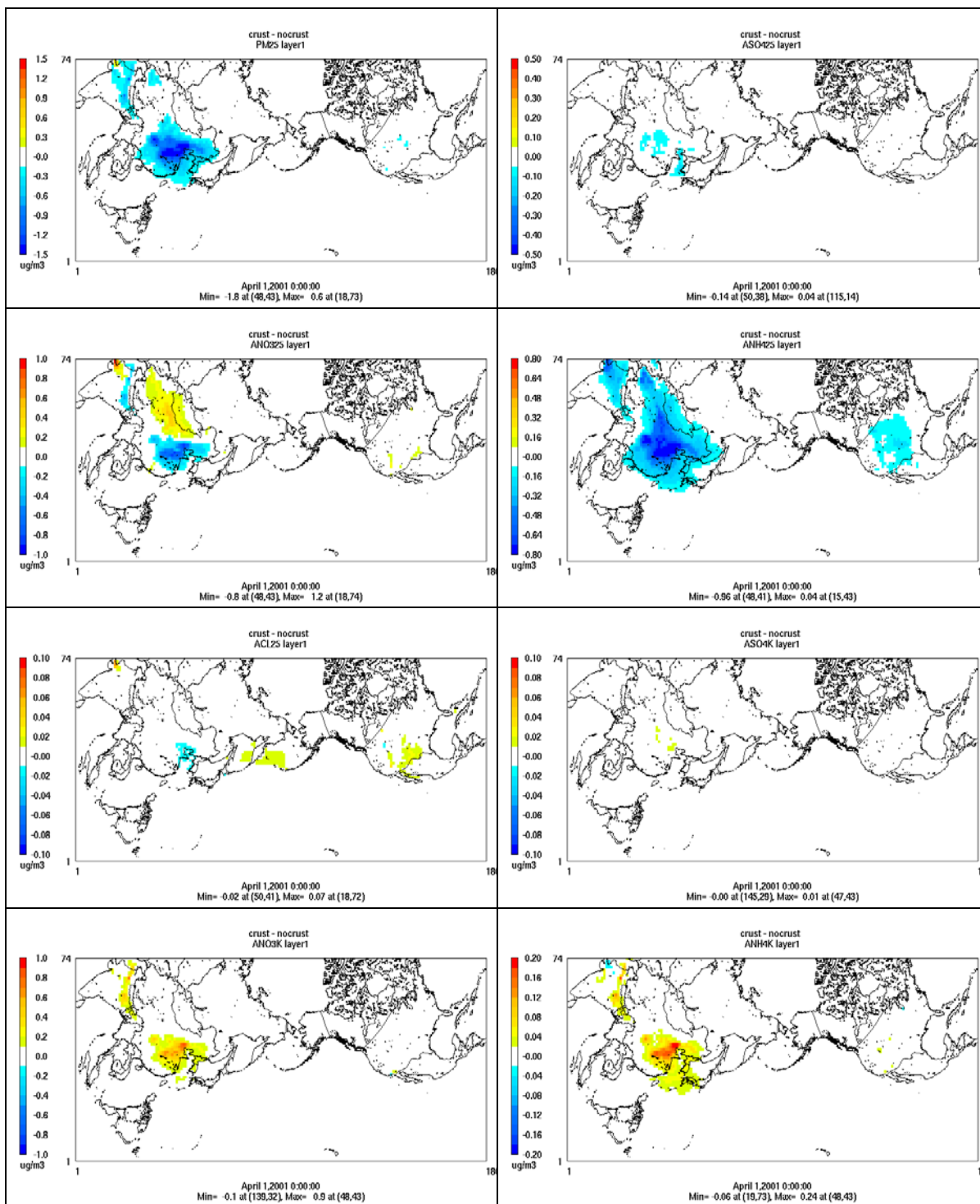


Figure 4.11. Spatial distribution of differences between simulations with crustal species (CRUST_ONLY) and without crustal species (DUST_EMIT_ONLY) for surface layer PM_{2.5}, fine-mode SO₄²⁻, fine-mode NO₃⁻, fine-mode NH₄⁺, fine-mode Cl⁻, coarse-mode SO₄²⁻, coarse-mode NO₃⁻, and coarse-mode NH₄⁺ in April 2001.

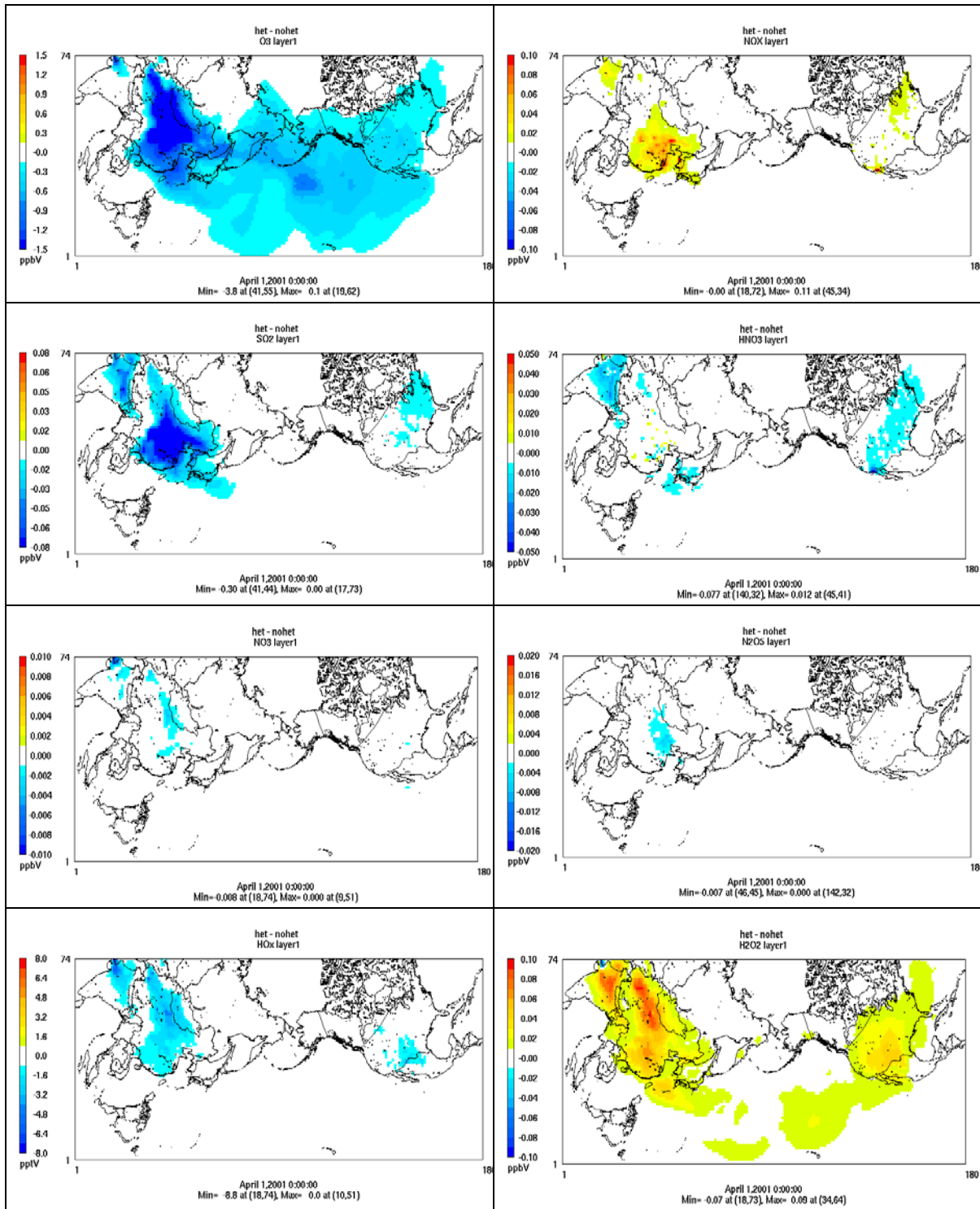


Figure 4.12. Spatial distribution of differences between simulations with heterogeneous chemistry (DUST) and without heterogeneous chemistry (CRUST_ONLY) for surface layer O₃, NO_x, SO₂, HNO₃, NO₃, N₂O₅, HO_x, and H₂O₂ in April 2001.

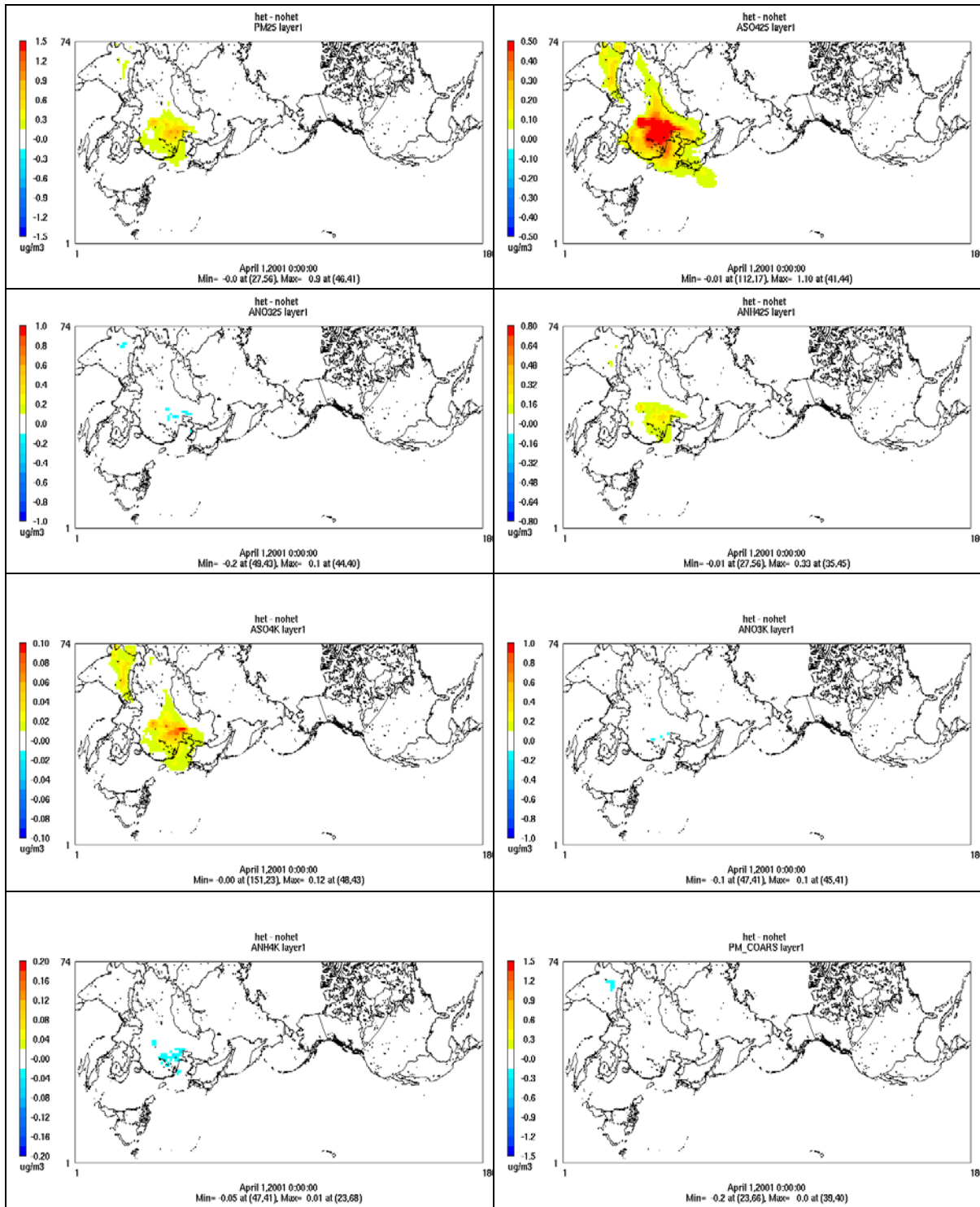


Figure 4.13. Spatial distribution of differences between simulations with heterogeneous chemistry (CRUST_ONLY) and without heterogeneous chemistry (het-nohet) for surface layer PM_{2.5}, fine-mode SO₄²⁻, NO₃⁻, and NH₄⁺, and coarse-mode SO₄²⁻, NO₃⁻, NH₄⁺, and PM.

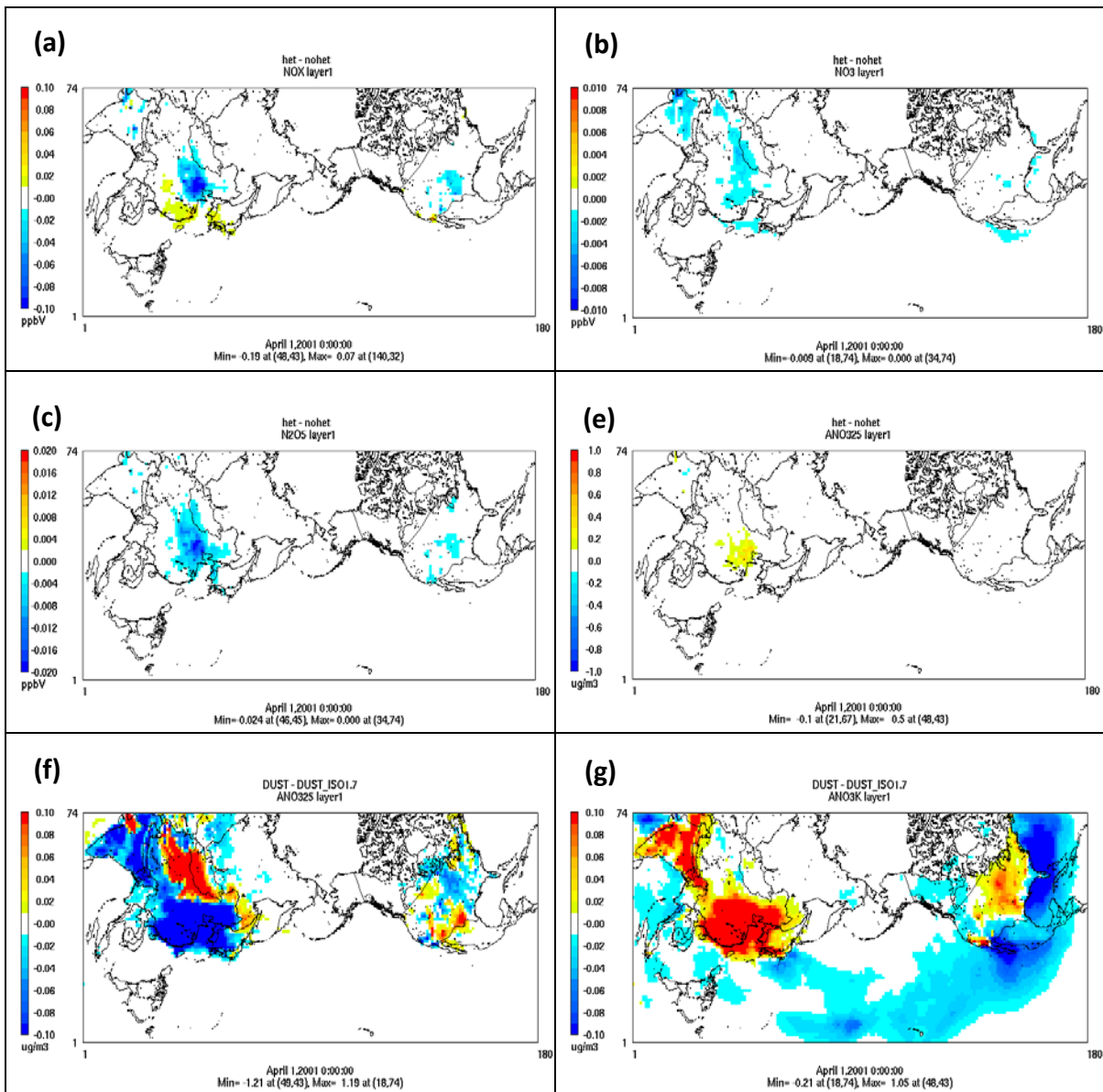
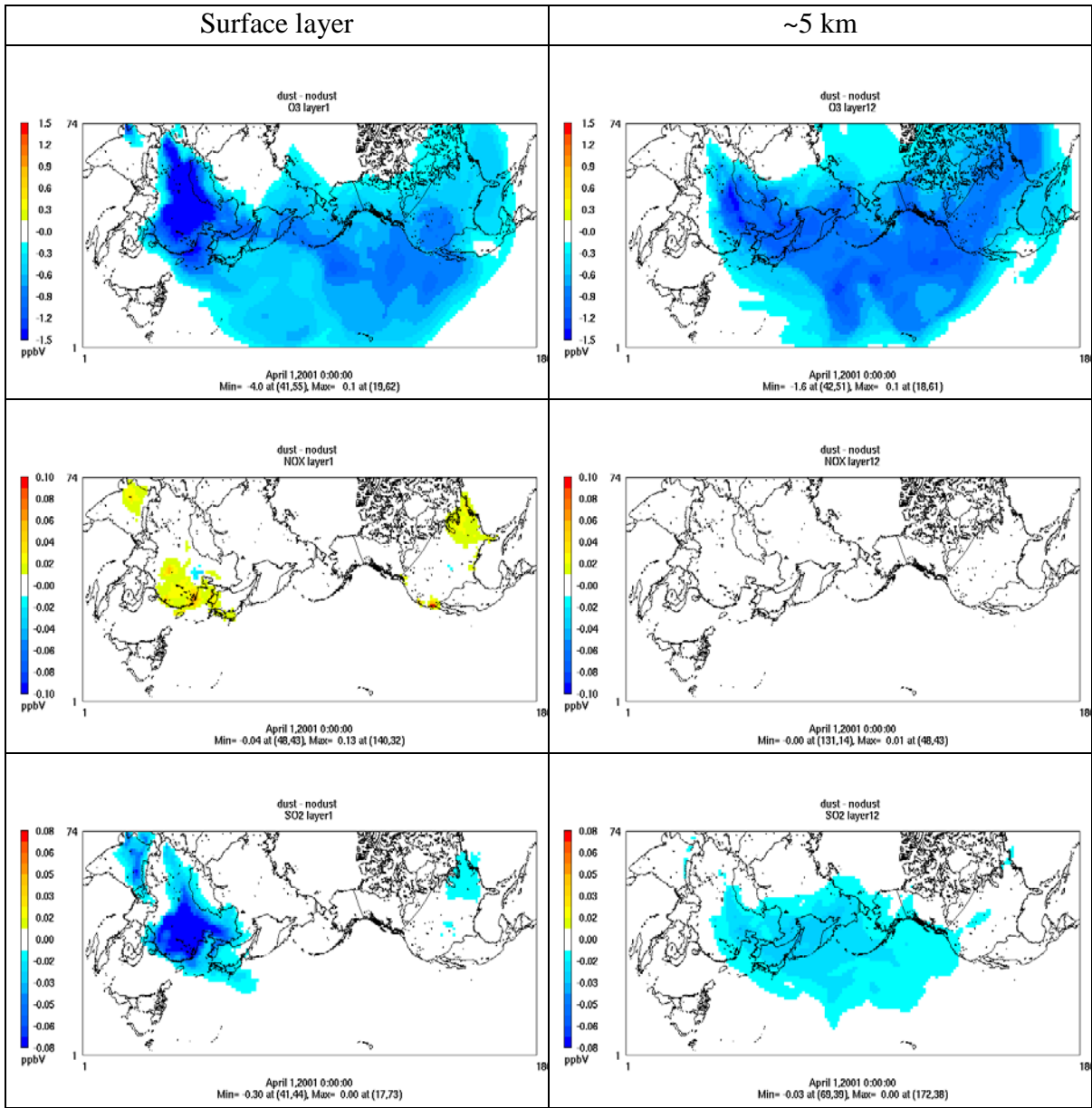


Figure 4.14. Spatial distribution of differences between simulations DUST_HIGHY and CRUST_ONLY for surface layer NO_x , NO_3 , N_2O_5 , and NO_3^- (a-d) and differences between simulations DUST and DUST_ISO1.7 for fine-mode NO_3^- and coarse-mode NO_3^- (e-f) in April 2001.

Figure 4.15. Spatial distribution of differences between simulations with dust treatment (DUST) and without dust treatment (NO_DUST) for surface layer (left panel) and the layer with ~5 km altitude (right panel) O_3 , NO_x , SO_2 , HNO_3 , HO_x , and H_2O_2 in April 2001.



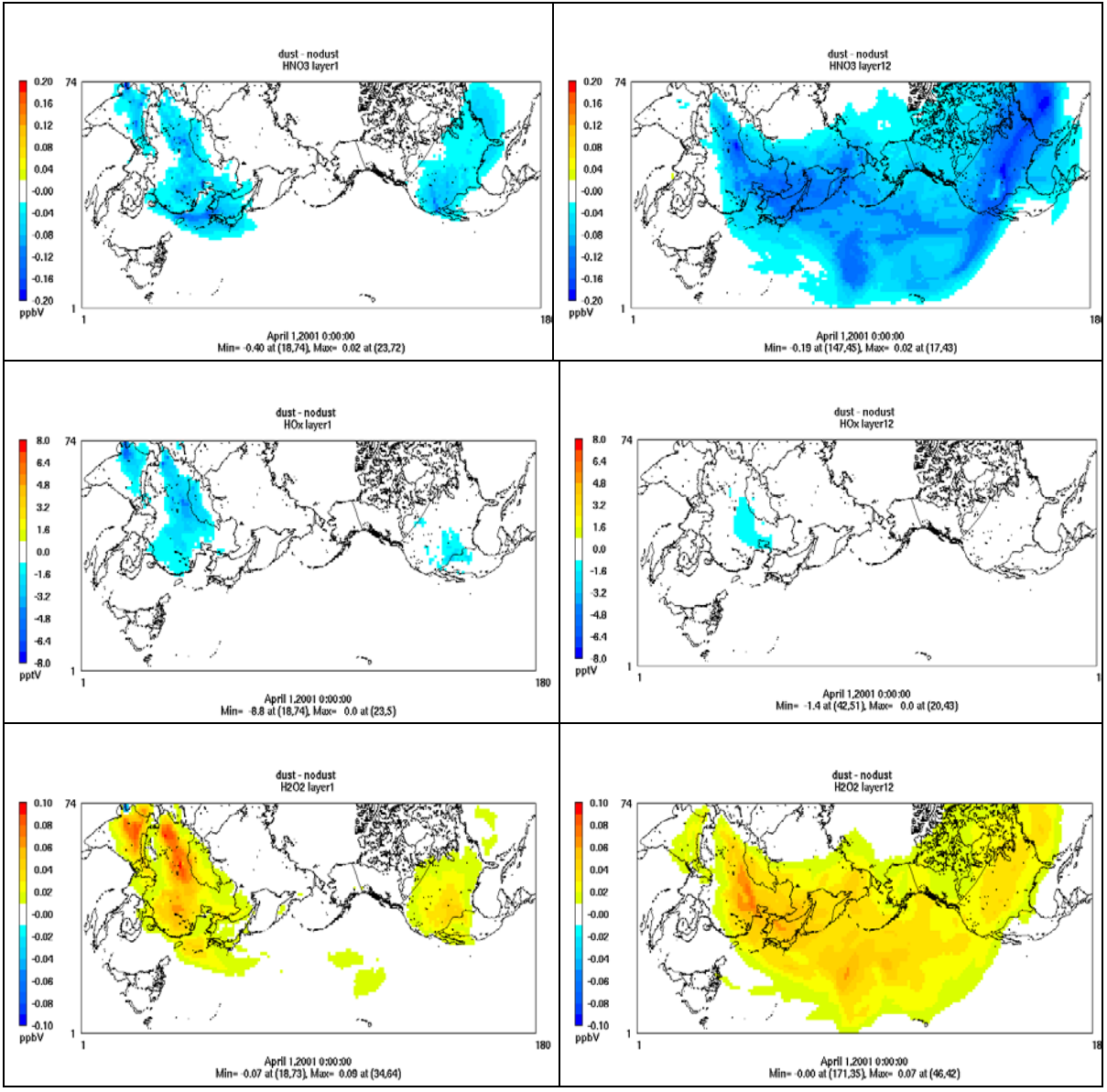
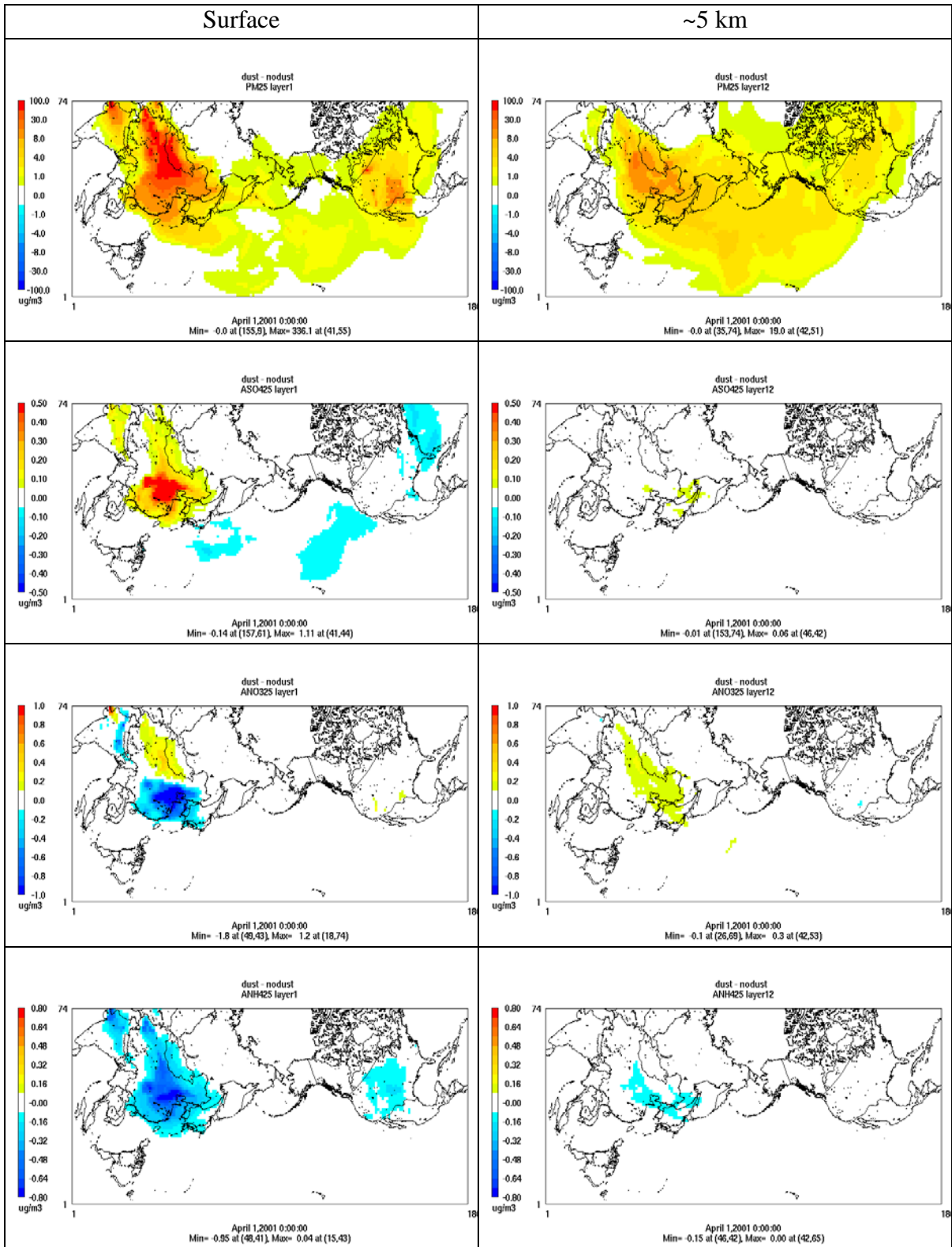
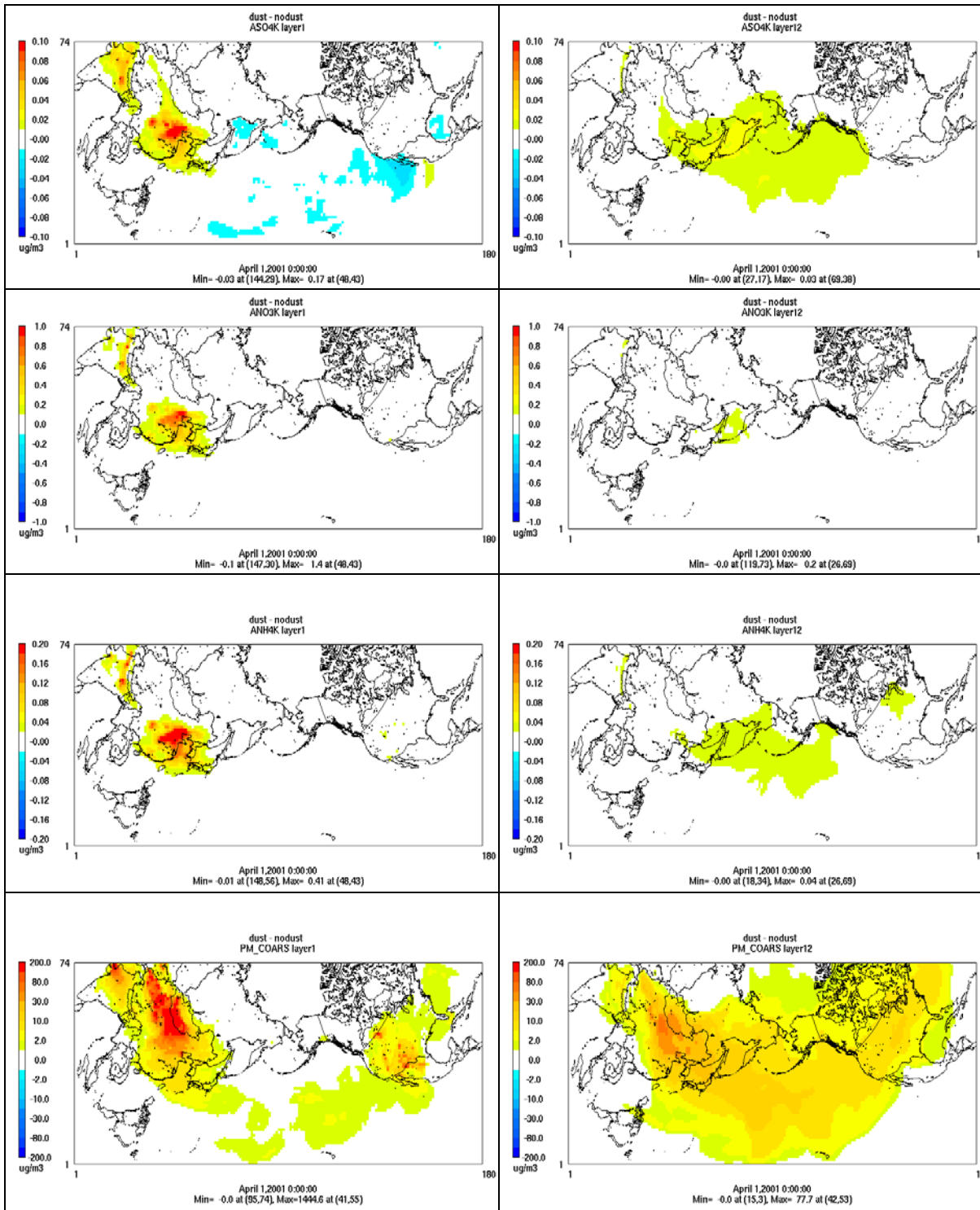


Figure 4.16. Spatial distribution of differences between simulations with dust treatment (DUST) and without dust treatment (NO_DUST) for surface layer (left panel) and the layer with ~5 km altitude (right panel) $\text{PM}_{2.5}$, fine-mode SO_4^{2-} , NO_3^- , and NH_4^+ , and coarse-mode SO_4^{2-} , NO_3^- , NH_4^+ , and PM in April 2001.





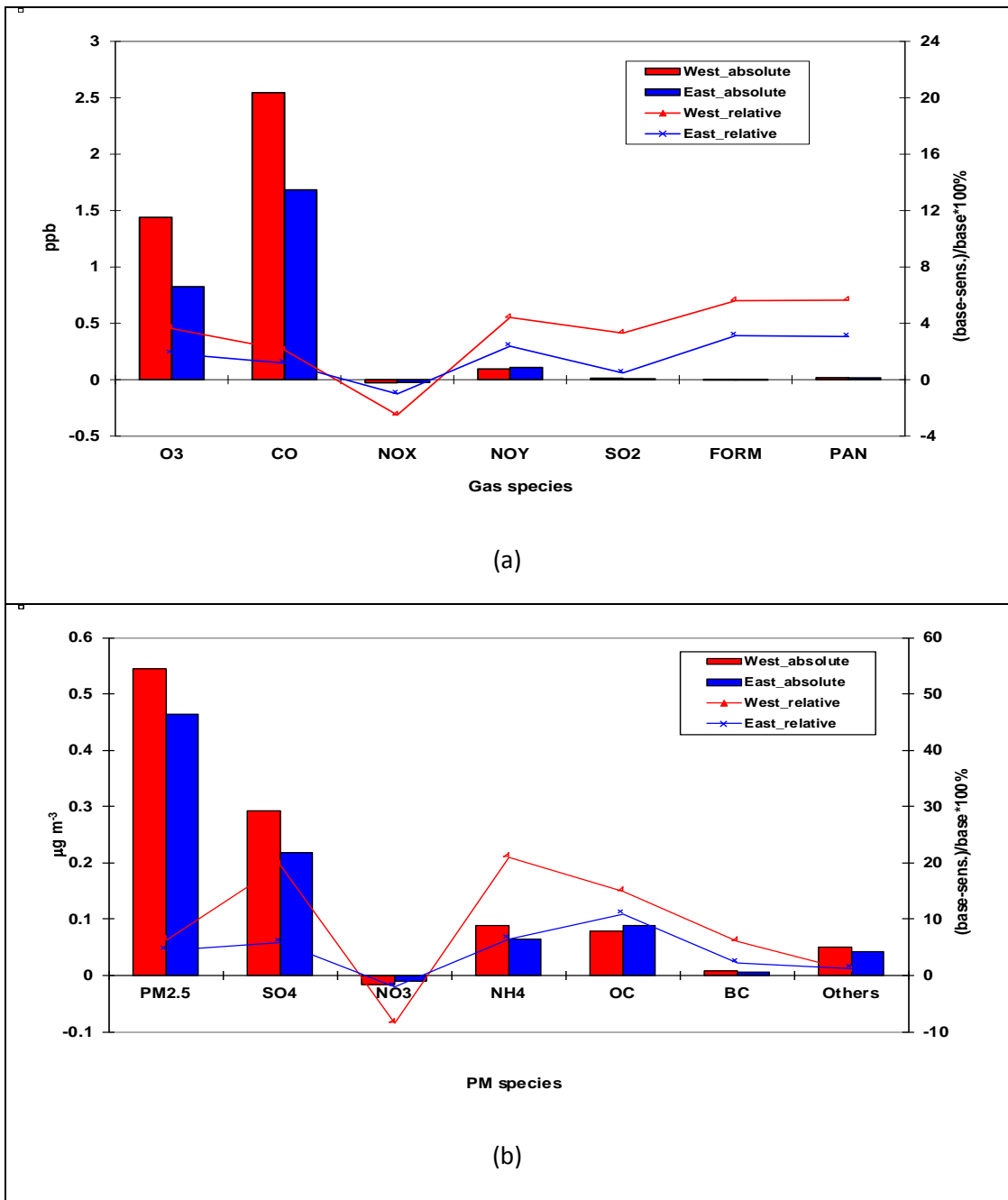


Figure 4.17. Absolute and relative contributions of different (a) gaseous species and (b) PM_{2.5} components over the western U.S. and eastern U.S. due to AAEs between simulations DUST and DUST_CUT for April 2001.

CHAPTER 5. EVALUATION AND PROCESS ANALYSIS
OF THE U.S. EPA'S 2002 MULTIPLE-POLLUTANT
AIR QUALITY MODELING PLATFORM

Multiple full year simulations with the multiple-pollutant (MP) version of CMAQv4.6 (referred to as CMAQ-MP hereafter) have been conducted over the nested 36/12 km domains that cover the entire or a portion of continental U.S. for 2002 by the U.S. EPA (Phillips et al., 2008; U.S. EPA, 2008). In this chapter, a comprehensive model evaluation is performed by comparing simulated concentrations of O₃, PM_{2.5} and its components, precursors of O₃ and PM_{2.5}, major air toxics, as well as Hg deposition with measurements collected from ground-based monitoring networks and satellites. The possible reasons that influence prediction biases of major pollutants are identified. The seasonal photochemical characteristics are examined and the relative contributions of controlling processes to the formation and destruction of key pollutants are quantified through PA tool imbedded in CMAQ. The objectives of this study are to examine the capability and performance of CMAQ-MP in reproducing temporal and spatial patterns of air pollutants, guide diagnostic evaluations for model improvements and further model development, and build confidence in the utilization of CMAQ-MP to air quality regulatory and research communities.

5.1 Model Configurations, Observational Data, and Evaluation Protocols

5.1.1 Model System and Configurations

In the EPA's 2002 MP modeling platform, CMAQ-MP has been developed and applied to predict the concentrations of O₃ and its precursors, PM_{2.5} and its components, Hg, and 38 other HAPs as well as the interactions among them in one model simulation. The

default version of CMAQ v4.6, released in October 2006, included a number of major updates to improve the underlying science from older versions. These enhancements include: inclusion of the new gas-chemistry mechanism (i.e., the CB05 and associated Euler Backward Iterative (EBI) solver; update of the aerosol thermodynamics module ISORROPIA from version 1.5 to 1.7; accounting for the dependence of heterogeneous N_2O_5 reaction probability on temperature, relative humidity, and aerosol compositions; and incorporation of the updated version of the Asymmetric Convective Model (ACM2) for cloud treatment. Additional details regarding the new features of CMAQ v4.6 can be found at the official CMAQ website (<http://www.cmascenter.org/help/documentation.cfm>). The corresponding MP version model was developed by modifying algorithms for gas chemistry, aerosols, clouds, and emissions used in the previous Hg and HAPs versions of the CMAQ (i.e., CMAQ-Hg and CMAQ-HAPs; Bullock and Brehme, 2002, 2006; Hutzell et al., 2006; Luecken et al., 2006; Roselle et al., 2007) and merging them into the default CMAQ v4.6. The CMAQ-MP includes elemental Hg (Hg^0), divalent gaseous Hg (Hg(II) or Hg^2), particulate Hg (PHg), 31 additional gas-phase HAPs, 6 toxic metals, and diesel PM as well as CAPs in the base version of CMAQ. The chemical reactions for chlorine, mercury, and HAPs, have been combined with the CB05 chemical mechanism (Yarwood et al., 2005; Sarwar et al., 2008) and implemented together into the CMAQ modeling system. The gas chemical mechanism of CMAQ-MP consists of 219 reactions, which include 156 reactions from base CB05 mechanism, 21 reactions for chlorine chemistry, 38 reactions for gas-phase HAPs, and 4 reactions for gas-phase Hg (Roselle et al., 2007). Those reactions for HAPs and Hg mainly involve the oxidations by radicals such as hydroxyl radical (OH) and nitrate radical (NO_3). A

modified version of aerosol module version 4 (AERO4) also contains the treatment of sea salt emissions. The vertical diffusion module associated with aerosol emissions is updated for the CMAQ-MP aerosol simulations. The CMAQ-MP uses the dry deposition module adopted from CMAQ-Hg. The aqueous chemistry of Hg in the cloud module is largely based on CMAQ-Hg, which includes 7 aqueous-phase Hg kinetic and 6 equilibrium chemical reactions. The aqueous-phase chemistry for other species such as SO₂ is based on the Regional Acid Deposition Model (RADM, Chang et al., 1987; Stockwell et al., 1990).

In this study, CMAQ-MP is applied to three annual (2002) simulations conducted by the U.S. EPA (Phillips et al., 2008; U.S. EPA, 2008) over different domains, which include a parent domain (continental U.S. (CONUS)) with a horizontal grid resolution of 36-km and two sub-domains (EUS and WUS) with a finer grid resolution of 12-km over portions of the eastern and western U.S., as shown in Figure 5.1. The vertical resolution for each domain includes 14 layers from the surface to approximately 100 hPa (at ~15 km) using a sigma-pressure coordinate system. The height of first model layer is ~38 m. The meteorological inputs for each CMAQ domain are simulated separately by the U.S. EPA using the 5th generation PSU/NCAR mesoscale model (MM5, Grell et al., 1994) v3.6.3 for the 36-km continental U.S. domain and MM5 v3.7.2 for 12-km eastern U.S. domain and by the Western Regional Air Partnership (WRAP) using MM5 v3.6.2 for 12-km western U.S. domain (Kemball-Cook et al., 2004; Kemball-Cook et al., 2005). All the three MM5 simulations are conducted with the four dimensional data assimilation (FDDA) and use the Pleim-Xiu land surface model (Xiu and Pleim, 2001; Pleim and Xiu, 2003), ACM planetary boundary layer (PBL) parameterization schemes (Pleim and Chang, 1992), and the RRTM longwave and

Dudhia shortwave radiation schemes (Dudhia, 1989; Mlawer et al., 1997). While the EPA simulations use the Reisner I scheme (Reisner et al., 1993) for microphysics and the Kain-Fritsch II scheme (Kain, 2003) for the subgrid or cumulus convection, WRAP simulation uses the Reisner II scheme (Reisner et al., 1998) and the Betts-Miller scheme (Betts and Miller, 1993), correspondingly. The MM5 hourly meteorological outputs are converted to CMAQ compatible inputs with the Meteorology-Chemistry Interface Processor (MCIP) version 3.1. The emissions are generated with the Sparse Matrix Operator Kernel Emission system (SMOKE) version 2.3 based on the EPA's 2002 National Emissions Inventory (NEI) version 3.0 for all domains. The boundary conditions (BCONs) and initial conditions (ICONS) of the 36-km domain are provided by a global chemistry transport model, GEOS-Chem (Yantosca, 2004), for key CAPs and Hg species and the ones of 12-km domains are taken from the 36-km simulation. For HAPs species, BCONs of 36-km domain for formaldehyde (HCHO) and acetaldehyde (ALD2) are also from GEOS-Chem, but others are either static or built based on scientific literatures and available field studies. A ten-day spin-up period from 12/22 to 12/31 2001 is used to minimize the influence of the ICONs for each simulation. More details regarding the model setups are referred to U.S. EPA (2008).

5.1.2 Evaluation Protocols and Observational Data

Currently the model performance evaluation for most CAPs and related variables such as O₃ and its precursors, PM_{2.5} and its components, and wet depositions of various species has been guided by U.S. EPA (U.S. EPA, 2007). However, there are no recommended performance goals or objectives for evaluating HAPs and the recommended statistics for O₃ or PM_{2.5} are inappropriate for air toxics. Both Seigneur et al. (2002) and

Morris et al. (2003) indicated that the model performance for HAPs modeling could be relatively poor due to higher uncertainties in toxics emissions than emissions of CAPs. In this work, an operational model performance evaluation for O₃, PM_{2.5} and its speciated components such as SO₄²⁻, NO₃⁻, NH₄⁺, EC, and OC, Hg wet deposition, and a selected set of HAPs has been conducted using available routine surface monitoring data and satellite column data (Table 5.1). The surface data include those from CASTNET, IMPROVE, STN, AIRS)-AQS, SEARCH, NADP, the Mercury Deposition Network (MDN), and the National Air Toxics Trends Stations (NATTS). A detailed description of most of these networks can be found in Eder and Yu (2006) and Y. Zhang et al. (2006a).

The satellite column data include the tropospheric CO columns from MOPITT (Deeter et al., 2003), the tropospheric NO₂ columns from GOME (Burrows et al., 1999) and the Scanning Imaging Absorption Spectrometer for Atmospheric Chartography (SCIAMACHY, DeSmedt et al., 2008), the tropospheric HCHO columns from GOME, the TORs from TOMS/SBUV (Fishman et al., 2003), and the AOD from MODIS (Remer et al., 2005).

The model performance has been examined using statistical metrics that follow the U.S. EPA (2005) and Y. Zhang et al. (2006a) and selected graphical techniques, which include the spatial plots, scatter plots, and time series plots. Several well-accepted statistical measures are selected including the mean bias (MB), correlation coefficient (R), the normalized mean bias (NMB), the normalized mean error (NME), and root mean square error (RMSE). The evaluation for surface predictions has been conducted primarily using the EPA's Atmospheric Model Evaluation Tool (AMET, Gilliam et al., 2005). AMET is a

software package developed by EPA that can perform the operational evaluation of complex models. There are two sets of toolkits from AMET: the meteorology toolkit and the air quality toolkit. AMET is being developed to be a comprehensive one-atmosphere model evaluation system, which will facilitate the integration of meteorology with air quality and air toxics model evaluation. The evaluation for column predictions has been conducted using the evaluation procedure as described in Chapter 3. Here we present a brief description of the procedure that is used to calculate column predictions in CMAQ. The column abundances of CO, NO₂, HCHO, and O₃ are calculated using both mass concentrations from CMAQ and meteorological/domain data (i.e., temperature, pressure, and layer thickness) from MM5 and converted into units of 10¹⁷ molecules cm⁻², 10¹⁵ molecules cm⁻², 10¹⁵ molecules cm⁻², and Dobson Unit (DU), respectively. CMAQ does not output AODs directly. Following the implementation method of Zhang et al. (2009a), AODs are estimated based on CMAQ PM_{2.5} predictions using an empirical equation of Chameides et al. (2002):

$$AOD_{\text{model}} = \sum_{i=1}^N (\sigma_{sp} + \sigma_{ap})_i \times \Delta z_i \quad (1)$$

where σ_{sp} is the scattering coefficient and σ_{ap} is the specific absorption coefficient (both in unit of m⁻¹), Δz_i is the layer thickness (in unit of m), and N is the total number of layers (14 for the 2002 CMAQ simulations).

5.2 Evaluation of Model Performance

5.2.1 Meteorological Variables

Before initiating air quality simulations, it is important to identify the biases and errors associated with meteorological modeling inputs. The MM5 model performance for

2002 MP modeling platform has been evaluated separately from this study by Kemball-Cool et al. (2005), Brewer et al. (2007), and Dolwick et al. (2007) using the combination approach of qualitative and quantitative analyses. These evaluations show that three sets of MM5 meteorological predictions over the three domains represent a reasonable approximation of the actual meteorology. The model captures large-scale synoptic patterns such as high-pressure domes and upper-level troughs. The surface “cold bias” temperature exists during the winter with an average of 2-3 °C, especially in January, from all three MM5 simulations, which may be due to the limitations of the PBL and land-surface schemes currently used in accurately simulating the air-land heat fluxes with the coarse grid resolution (Kemball-Cool et al., 2005). The effect is the largest at night, which could overestimate the stability in the lowest layers and have a significant impact on chemical predictions (Dolwick et al., 2007). MM5 is able to replicate the precipitation fairly accurately in spring, fall, and winter, but overestimates it in summer, likely due to the excessive convective cloud predicted by the model (Kemball-Cool et al., 2005). The model biases/errors for various variables over the Rocky Mountain and Great Lakes region are relatively larger than other regions due to complexity of terrains. Overall, the biases and errors associated with these meteorological simulations are generally within the range of past meteorological modeling results that have been used for air quality applications (U.S. EPA, 2008). A rigorous performance testing demonstrates that the dynamic and thermodynamic fields generated by MM5 are quite sufficient for the 2002 MP modeling platform (Dolwick et al., 2007).

5.2.2 Criteria Air Pollutants at the Surface

Because of known differences between networks in terms of sampling protocols and measurement procedures, the evaluation for surface chemical predictions has been conducted separately for individual network. For each network and pollutant, statistics are calculated for all sites in each domain (i.e., CONUS, EUS, and WUS) and also with separate breakouts of five sub-regions (i.e., Midwest, Northeast, Southeast, Central, and West of U.S.) over the CONUS domain for observed-predicted data pairs in monthly, seasonal, and annual averages. Since the CMAQ evaluation results for the 12km and 36 km grids are considerably similar and consistent. Here, we focus primarily on the CMAQ results from the 36 km simulation over CONUS unless stated otherwise.

5.2.2.1 Ozone

Figure 5.2a shows scatter plot of modeled and observed daily max 8-h O_3 with a cut off value of 40 ppb (i.e., data pairs containing observed concentrations less or equal to 40 ppb are not used in the analysis) for the O_3 season (i.e., May to September). The cut-off value is applied in order to examine model performance at levels above background concentrations (Russell and Dennis, 2000). To facilitate the comparison, the 1:1, 1.5:1, and 1:1.5 lines are drawn on the plot. As shown, CMAQ simulates max 8-h O_3 mixing ratios quite well with R, NMB, and NME of 0.7, 1.5%, and 14%, respectively. A vast majority of simulated max 8-h O_3 values are within a factor of 1.5 of observations. Figure 5.2b shows the box plot of 25% and 75% quartiles (shading regions) along with the median values for diurnal O_3 values during the entire O_3 season. The plot reflects the ability of CMAQ to represent the diurnal variation of O_3 values across the entire domain. As shown, there exists

a systematic overprediction of hourly O₃ by CMAQ especially during the nighttime. The median modeled O₃ values are much closer to observations between 10:00 and 19:00, which are the typical hours that make up the daily max 8-h O₃ during the O₃ season. These findings are consistent with previous studies (Eder and Yu, 2006; Appel et al., 2007). Although the capability of CMAQ in simulating nighttime O₃ has been improved with an updated parameterization of the minimum K_z since CMAQ v4.5 (see the CMAQ v4.5 release note at http://www.cmascenter.org/help/model_docs/cmaq/4.5/RELEASE_NOTES.txt), accurately simulating the evolution of nocturnal boundary layer remains difficult due to the limitation of PBL and land-surface schemes in current models and the use of a relatively coarse horizontal resolution and vertical resolution in lower portion of PBL (e.g., ~38 m in depth for surface layer in this work). As a consequence of an inaccurate representation of nocturnal PBL, nighttime surface NO_x emissions may be artificially diluted, which leads to an underestimation of modeled NO_x mixing ratios and thus an overprediction of O₃ mixing ratios due to insufficient titration of O₃ by NO_x (Mathur et al., 2005).

Figures 5.2c and 5.2d present the spatial distribution of NMBs and NMEs for maximum 8-h O₃ with a cutoff value of 40 ppb over the CONUS domain for the O₃ season in 2002. CMAQ shows a good performance to capture the spatial variation of max 8-h O₃ concentrations with NMBs of within ±10% and NMEs of less than 15% at majority (>80%) of AQS sites based on the suggested performance criteria by the U.S. EPA and other studies (Russell and Dennis, 2000; Morris et al., 2004; U.S. EPA, 2007). Slight overpredictions (with NMBs of < 10%) occur at most sites over the eastern U.S. and slight underpredictions (with NMBs of > -10%) occur over the western U.S. except for coastal regions. The plot of

NMBs also reveals several other interesting features. The most notable one is that CMAQ tends to moderately overpredict mixing ratios of O₃ along some coastal regions with NMBs generally range from 20 to 30% and sometimes > 30% along Pacific coast in California. This can be attributed to a poor representation of coastal boundary layers (i.e., model's boundary layer mixing cannot resolve the steep subgrid land-sea gradients) and the interaction with land/sea breezes (Gilliam et al., 2006; Yu et al., 2007). There are also several small clusters of overpredictions (with NMBs \geq 20%) in the Midwest and southeastern U.S. and a cluster of underpredictions (with NMBs \leq -20%) in some areas in southern California and Arizona. These large NMBs are likely due to the fact that the use of a coarse resolution of 36 km cannot present the elevated and/or complex terrains over those regions. The spatial distribution and magnitudes of NMEs are consistent with those of NMBs. The worse NMEs (>20%) are also found over coastal regions and over the aforementioned small clusters of inland areas with large NMBs.

Figures 5.2e and 5.2f show the MBs and RMSEs for daily max 8-h O₃ for the O₃ season binned for the range of observed O₃ values. As shown, CMAQ's capability to reproduce surface observations varies with O₃ levels. CMAQ tends to reproduce O₃ mixing ratios the best in the range of 40-60 ppb with MBs within 5 ppb and RMSEs within 10 ppb but significantly underpredicts high mixing ratios (> 80 ppb) and overpredicts low mixing ratios of O₃ (< 40 ppb) with absolute values of MB > 10 ppb and RMSEs > 10 ppb. We also find that those low mixing ratios typically coincide with non-conducive meteorological conditions (e.g., high cloud cover and precipitation and cool temperature). The overestimation of low observed mixing ratios of O₃ is due in part to the poor performance of

CMAQ in simulating the nighttime O_3 as discussed above. According to Yu et al. (2007), another reason is an insufficient titration of O_3 by NO at some AQS sites located in urban or suburban areas, resulting from the model's failure at a coarse grid resolution of 36 km in resolving urban plumes. The overestimation could also be due to the unrealistic vertical transport of excessive amounts of high O_3 from higher altitudes to the ground associated with downward entrainment in the CMAQ's convective cloud scheme over areas with cloud cover (Yu et al., 2010). When examining the statistics of max 8-h O_3 over the aforementioned sub-regions (see Table 5.2) in the O_3 season, CMAQ shows overall excellent performance with very small domain-wide NMBs of 1.7, 2.6, 2.7, 3.5, and -1.2% for northeast, southeast, Midwest, central, and west U.S., respectively. Although the discrepancies still exist for modeled and observed O_3 mixing ratios, the results in this study demonstrate a moderate to significant improvement as compared with previous studies (e.g., Eder and Yu, 2006; Tong et al., 2006; Appel et al., 2007; Smyth et al., 2009; Zhang et al., 2009a; Mao et al., 2010) because of several factors. First, a relatively new version of CMAQ v4.6 with the newest CB05 chemistry mechanism plus additional chloride reactions is used. Recent studies by Luecken et al. (2008) and Yu et al. (2010) showed that CB05 performs better in reproducing high O_3 mixing ratios especially in summer when compared with the Carbon Bond mechanism version IV (CBIV) and Statewide Air Pollution Research Center mechanism (SAPRC99) due to several updates in chemical species, reactions, and reaction rates. For example, CB05 includes several volatile organic compounds (VOCs) such as aldehydes with more than two carbons (ALDX) and additional acyl peroxy radicals (CXO_3) that can produce a greater conversion of NO to NO_2 . A study by Sarwar and Bhave (2007) reported that the

addition of chloride mechanism may improve O₃ predictions over several source regions such as Houston and New York-New Jersey areas where chlorine emissions and reactions may be important. Second, a new option of planetary boundary layer (PBL) scheme, ACM2, is available in CMAQ v4.6 and used in this study. ACM2 includes both eddy diffusion and nonlocal schemes from the original ACM, which enables ACM2 to better represent the rise and fall of the convective boundary layer. Appel et al. (2007) also compared O₃ performance of CMAQ v4.5 with CMAQ v4.6 both with CB05 and found a better overall performance for max 8-h O₃ by CMAQ v4.6, potentially due to the use of ACM2. Last, the emissions inventory used in this work is based on the NEI 2002 v3, which represents the most comprehensive emission inventory upon its release and are more accurate than those used in previous studies.

5.2.2.2 PM_{2.5} and its Compositions

Sulfate

Figures 5.3a and 5.3b show the spatial plots of NMBs for SO₄²⁻ over IMPROVE, STN and CASTNET sites for winter (Jan., Feb., and Dec.) and summer (Jun., Jul., and Aug.) 2002. In both winter and summer, CMAQ performs better over the eastern U.S. than the western U.S. with most of NMBs within $\pm 20\%$. This is especially true in summer when SO₄²⁻ contributes the most to total PM_{2.5} mass concentrations in the eastern U.S., likely as the results of a better representation of emissions of SO₂ and SO₄²⁻ in the eastern U.S. and the experience inherent in CMAQ and its predecessor (i.e., Regional Acid Deposition Model (RADM)) in simulating SO₄²⁻ more accurately over the eastern U.S. (U.S. EPA, 2005; Eder and Yu, 2006). The poor performance in the western U.S. can be attributed to difficulties of

the model in simulating more complex terrain in the western U.S. The worse performance over the western U.S. mainly occurs in California, Arizona, New Mexico, Utah, Colorado, and Kansas with underpredictions of SO_4^{2-} in summer (NMBs normally $< -30\%$) and overprediction of SO_4^{2-} in winter (NMBs normally $> 40\%$). CMAQ is also biased relatively high over the Pacific Northwest region with many sites having NMBs $> 30\%$ in both winter and summer. When comparing the modeled and observed SO_4^{2-} annually, most data pairs are within a factor of 1.5 reference line (figure not shown) with very high R values ranging from 0.90 (STN) to 0.96 (CASTNET).

Table 5.2 summarizes the overall seasonal statistical performance of CMAQ for all $\text{PM}_{2.5}$ species including SO_4^{2-} over different networks and sub-regions. The performance for SO_4^{2-} is the best among all $\text{PM}_{2.5}$ species, with domain-wide NMBs ranging from -0.9 (CASTNET) to 18.1% (IMPROVE) in winter, -11.2 (STN) to -3.1% (IMPROVE) in spring, -13.6 (IMPROVE) to -4.5% (STN) in summer, and -6.8 (STN) to -2.9% (IMPROVE) in fall. The NMEs are small to moderate ranging from 29.2 (CASTNET) to 50.0% (IMPROVE) in winter, 22.0 (CASTNET) to 35.7% (STN) in spring, 19.7 (CASTNET) to 35.5% (IMPROVE) in summer, and 20.2 (CASTNET) to 36.3% (IMPROVE) in fall. Consistent with the spatial plots NMBs and NMEs, the best overall statistics in terms of both NMBs and NMEs over northeastern and southeastern sub-regions, relatively better statistics over Midwest and central sub-regions, and the worst over western sub-region, especially over the IMPORVE sites, since most of which are located in the western U.S. There is no obvious evidence that CMAQ performs better for a certain network, although the NMEs are considerably smaller over CASTNET than the other two networks. As indicated by Eder and Yu (2006), the small

NMEs are mostly likely due to a longer sampling time by CASTNET (i.e., weekly integrated averages versus 24 h averages) and are not necessarily representative of improved performance. Contrary to the results from Tesch et al. (2006) and Appel et al. (2008), who found that CMAQ v4.4 underpredicted SO_4^{2-} in winter and spring and overpredicted it in summer and fall, our results show that CMAQ underestimates SO_4^{2-} in almost all the seasons (particularly in summer) and overestimates it over the IMPROVE sites in winter, which are more consistent with those studies of Appel et al. (2009) and Luo et al. (2009) that used CMAQ v4.6 and CMAQ v4.7. This discrepancy is likely due to the updates in both convective cloud module and aerosol dry deposition module in CMAQ v4.6. Appel et al. (2008) indicated that the use of ACM2-cloud scheme (in CMAQ v4.6 or later) over the RADM-cloud scheme (in CMAQ v4.4) might result in less aqueous production of SO_4^{2-} and the changes in aerosol dry deposition calculation in the new version of CMAQ might lead to higher dry deposition velocity and hence more SO_4^{2-} removal. Moreover, the CMAQ model bias in this study can be partially explained by the errors of MM5 in the predictions of precipitation and wet depositions. For example, MM5/CMAQ tends to overestimate domain-wide precipitation and wet deposition of SO_4^{2-} with NMBs of 42.5% and 13.1%, respectively, in summer and underestimate them with NMBs of -13.0% and -31.1%, respectively, in winter (figures not shown). Luo et al. (2009) further proved that the convective precipitating cloud fraction and cloud water contents have been overestimated by CMAQ v4.6, which leads to an excessive scavenging of SO_4^{2-} . After limiting the precipitating cloud fraction to 10 to 15%, they found no significant model biases.

Nitrate

Figures 5.3c and 5.3d show the spatial plots of NMBs for NO_3^- at the IMPROVE and STN sites for winter and summer 2002. In winter, CMAQ tends to overpredict NO_3^- concentrations in the eastern U.S. where NMBs often exceed 20% and can be up to 80-90% at some sites, and it tends to underpredict in most of the western U.S. where NMBs can be as low as -90%. In summer, underpredictions of NO_3^- occur over almost all the CONUS domain, where NMBs often range between -30% to -60% over Great Lakes and Midwest and can be lower than -80% over the western U.S. and southeastern U.S. A small cluster of overpredictions occurs over the New England area. When comparing the modeled and observed NO_3^- annually, most of data pairs fall outside the areas outlined with the factor of 1.5 reference lines (figure not shown) with R values ranging from 0.5 (STN) to 0.6 (IMPROVE). The relatively poor performance of CMAQ in simulating NO_3^- is not surprising and consistent with findings of other studies (e.g., Eder and Yu, 2006; Tesche et al., 2006), since NO_3^- is one of the most difficult compositions to predict due to its sensitivity to almost every physical and chemical process including emissions, atmospheric transport, gas-phase chemistry, gas/particle mass transfer, and depositions (Nolte et al., 2008). Despite the relatively poor CMAQ performance in the 2002 MP platform, some improvements of NO_3^- predictions (e.g., lower NMEs and higher R values) are found in this study, as compared with previous studies using older versions of CMAQ or the NEI.

As shown in Table 5.2, the CMAQ performance for NO_3^- is much worse than that for SO_4^{2-} . NMBs and NMEs are much larger. Domain-wide NMBs range from 3.6 (STN) to 54.7% (IMPROVE) in winter, 38.4 (STN) to 85.4% (IMPROVE) in spring, -36.8

(IMPROVE) to -27.0% (STN) in summer, and -4.5 (STN) to -50.7% (IMPROVE) in fall. Domain-wide NMEs range from 63.3 (STN) to 110.2% (IMPROVE) in winter, 88.5 (STN) to 139.9% (IMPROVE) in spring, 78.1 (STN) to 96.3% (IMPROVE) in summer, and 71.2 (STN) to 112.9% (IMPROVE) in fall. Note that NMBs at the STN sites are much lower in some seasons than those at the IMPROVE sites, although the NMEs from both networks are more comparable. The lower NMBs at the STN sites are the result of compensation of large overpredictions in the eastern U.S. and underpredictions in the western U.S. The model biases might also be partially associated with the uncertainties in NH₃ emissions, which are more rudimentary and poor temporally-distributed intra-annually, as compared to the much better developed and understood NO_x emissions (Morris et al., 2005). Model performance with respect to NO₃⁻ in this study suggests that NH₃ emissions based on the 2002 NEI v3 are probably too low for summer and too high for other seasons. The more accurate monthly-derived NH₃ emissions by Carnegie Mellon University NH₃ emission model were much higher in summer and lower in winter compared to the traditional NH₃ emission inventories (Pinder et al., 2006; Wu et al., 2008). Other important reasons include the high uncertainties in gas/particle partitioning simulated by ISORROPIA in CMAQ and the biases in the predictions of NO₃⁻ wet deposition fluxes. CMAQ tends to underestimate the NO₃⁻ wet deposition amounts throughout the whole year with NMBs of -23.2%, -25.7%, -42.8%, and -19.2% for winter, spring, summer, and fall, respectively. Finally, the large model biases and errors in NO₃⁻ predictions could also be due to the uncertainties in the measurements, especially in summer. In fact, both modeled and observed NO₃⁻ concentrations are very low in summer and the model biases might be comparable to the uncertainty level (roughly ±0.5

$\mu\text{g m}^{-3}$) of filter-based routine measurements (Karydis et al., 2007).

Ammonium

Figures 5.3e and 5.3f show the spatial plots of NMBs for NH_4^+ over STN and CASTNET sites for winter and summer 2002. Since NH_4^+ in the ambient atmosphere is generally present as $(\text{NH}_4)_2\text{SO}_4$ (or NH_4HSO_4) and NH_4NO_3 , the spatial pattern of NH_4^+ is more like the combined pattern of SO_4^{2-} and NO_3^- in winter when both $(\text{NH}_4)_2\text{SO}_4$ and NH_4NO_3 concentrations are high and more similar to that of SO_4^{2-} in summer when $(\text{NH}_4)_2\text{SO}_4$ is dominant. In winter, CMAQ overpredicts NH_4^+ concentrations in the eastern U.S. where NMBs often range from 20% to 60%. It underpredicts NH_4^+ concentrations in most of the western U.S., where NMBs range from -60% to -20%. In summer, CMAQ shows a better performance over space, with slight overpredictions of NH_4^+ over the eastern U.S. (with most NMBs of 0 to 40%) and slight underpredictions over the western U.S. (with most NMBs of -40% to -20%), because NH_4^+ is dominant by $(\text{NH}_4)_2\text{SO}_4$ and the performance of SO_4^{2-} in summer is much better than that of NO_3^- in winter. Table 5.2 shows a fairly good performance for NH_4^+ , which is slightly worse than SO_4^{2-} but better than NO_3^- . The domain-wide NMBs are 21.2% (STN) and 39.9% (CASTNET) in winter, 22.5% (STN) and 39.9% (CASTNET) in spring, -2.3% (STN) and -8.7% (CASTNET) in summer, and 2.8% (STN) and 16.7% (CASTNET) in fall. The domain-wide NMEs are 56.3% (STN) and 47.2% (CASTNET) in winter, 53.6% (STN) and 51.6% (CASTNET) in spring, 39.5% (STN) and 25.0% (CASTNET) in summer, and 47.7% (CASTNET) and 39.0% (IMPROVE) in fall. The statistics are consistent between STN and CASTNET, with domain-wide positive NMBs in most seasons except for summer over both networks. As discussed above, the uncertainty

associated with NH_3 emissions is indicative of the main reason for the model bias of NH_4^+ . Additionally, the underestimation of NH_4^+ wet depositions throughout the whole year (NMBs are -47.5%, -26.4%, -8.9%, and -22.2% for winter, spring, summer, and fall, respectively) can in part explain the overestimation of NH_4^+ in most seasons.

Organic and Elemental Carbon

Organic aerosol is a complex mixture of hundreds of organic compounds and is composed of primary organic aerosol (POA), anthropogenic secondary organic aerosol (SOA), and biogenic SOA in CMAQ, so the model performance of OC will largely depend on the accuracies of emission inventories, meteorological predictions, and model treatments in SOA formation. Differently, EC is normally directly emitted into the atmosphere from various sources such as diesel and gasoline-fueled mobile sources, meat cooking, as well as wild fires and its ambient concentration largely depend on accuracies in emission inventories, meteorological predictions, and removal processes. Figures 5.3g and 5.3h show the spatial plots of NMBs for OC at the IMPROVE and STN sites for winter and summer 2002. In winter, CMAQ has the tendency to overpredict OC over the western U.S., Midwest, and New England areas especially for the IMPROVE sites with most NMBs ranging from 30% to 70%. Underpredictions are also evident at most of the STN sites in the eastern U.S. and some sites along the California coast with NMBs normally $< -30\%$. While in summer, significant underpredictions are observed across the whole domain, particularly over the eastern U.S. with NMBs of generally $< -60\%$ and the worst NMBs normally occurring at the STN sites. The model seems to perform slightly better in winter (colder months) than summer (warmer months). As shown in Figures 5.3i and 5.3j, CMAQ moderately overpredicts EC in the

eastern U.S. with NMBs generally between 20% and 50% and underpredicts it in the western U.S. with NMBs between -50% and -20% in winter. This spatial pattern of EC is somehow opposite to that of OC, indicating some errors in the OC/EC split of measurements as discussed below. As compared with OC, much smaller degrees of underpredictions of EC are also observed over most of the domain in summer with NMBs generally between -50% and -10%. The R values at the IMPROVE and STN sites are only 0.5 and 0.3 for OC and 0.5 and 0.4 for EC, respectively, which are much lower than those for SO_4^{2-} , NO_3^- , and NH_4^+ .

The seemingly worse performance at the STN sites for OC is due to the fact that the measurements are not blank corrected for carbon on the background filter, which could add 20-40% to the observed OC concentrations (Rao et al., 2003). Because of that, the performance statistics of OC and EC are only summarized for the IMPORVE sites in Table 5.2. As shown, CMAQ appears to moderately underpredict OC in summer and overpredict it in winter with domain-wide NMBs of -41.7% and 45.3%, respectively, and slightly underpredict in both spring and fall with NMBs of -2.2% and -11.9%, respectively. The errors associated with OC are relatively high with domain-wide NMEs of 84.1%, 60.4%, 64.7%, and 54.2% for winter, spring, summer, and fall, respectively. On the other hand, the overall model performance for EC is much better than OC but with consistent seasonal trends of positive or negative biases over different sub-regions. The domain-wide NMBs range from -14.3% (summer) to 20.6% (winter) and NMEs range from 57.5% (fall) to 68.0% (winter). The model performance for OC and EC shown here is in somewhat similar to Tesche et al. (2006) and Appel et al. (2008), in which they also found that the largest underpredictions of OC and EC occur in the summer and fall. However, the overprediction

of OC and EC in winter is more consistent with Karydis et al. (2007). Since the major component of organic aerosols in winter is POA. Both POA and EC is mainly affected by emissions, vertical mixing and deposition. The overprediction of OC and EC in winter is believed to be more related to the poor representation of those processes. Lane et al. (2007) also reported the natural gas combustion and wood burning emissions from the NEI might be overestimated during winter over the northeastern U.S. Some other studies (e.g., Eder and Yu, 2006; Wiedinmyer et al., 2006) also indicated that the poor temporally-allocated wildfire emissions may contribute to the biases in OC and EC predictions. During the summer months when SOA concentrations are more comparable with those of POA, the model underpredictions for OC could also be attributed to the underpredictions of photochemically-produced SOA aside from the uncertainties in the emissions of POA and SOA precursors (Appel et al., 2008). This partly explains the worse model performance of OC, as compared with EC in summer. CMAQ v4.6 does not simulate SOA formation from the oxidation of several important precursors such as isoprene and sesquiterpenes, both of which may contribute substantially to the ambient OC concentrations (Morris et al., 2005; Zhang et al., 2007). In addition, the uncertainties associated with the measurement techniques of carbonaceous aerosols (e.g., OC and EC split) and the factor used to convert simulated organic matter (OM) to OC (i.e., OM:OC=1.4 used in this study versus 1.6-2.1 reported by Turpin and Lim (2001)) may also cause the discrepancies between simulations and observations.

PM_{2.5}

The accuracy in PM_{2.5} predictions in CMAQ is a composite of the accuracies in predictions of individual particulate species concentrations. Figures 5.3k and 5.3l show the spatial plots of NMBs for PM_{2.5} at the IMPROVE and STN sites for winter and summer 2002. CMAQ has a tendency of overpredictions of PM_{2.5} in winter and underpredictions in summer. In winter, the spatial variability of biases is more evident. The relatively high biases occur over the northeastern U.S., Great Lakes, and Midwest with NMBs generally over 50%. Slight overpredictions of PM_{2.5} also occur over the southeastern U.S. and Rocky Mountain areas with NMBs within 20%-50%. Conversely, a small clustered area of negative biases can be found stretching from California coast into Arizona with NMBs > -50%. The underprediction of PM_{2.5} in summer is more systematic with more than 95% of sites having negative biases. NMBs are typically larger (between -60% and -20%) in the western U.S. than in the eastern U.S. (> -40%).

When examining the monthly plots of average PM_{2.5} concentrations at the IMPROVE and STN sites in 2002 (Figures 5.4a and 5.4b), both CMAQ and observations show higher PM_{2.5} concentrations at the STN sites than the IMPROVE sites throughout the year because most of the IMPROVE sites are located in remote and rural areas and STN sites are located in more polluted urban areas. CMAQ underpredicts PM_{2.5} concentrations during the warmer months (i.e., April through September at the IMPROVE sites and May through August at the STN sites), but overpredicts during the cooler months. The above findings are consistent with those of Eder and Yu (2006) and Appel et al. (2008).

Figures 5.4c and 5.4d show the stacked bar charts of modeled and observed average

PM_{2.5} concentrations and the contributions of individual species concentrations (i.e., SO₄²⁻, NO₃⁻, NH₄⁺, total carbon (TC), and unspiciated PM_{2.5}) to the total PM_{2.5} concentration at the STN sites in both winter and summer. In winter, TC is the most abundant (33.2%) PM_{2.5} component, followed by NO₃⁻ (21.2%), SO₄²⁻ (19.8%), other unknown PM_{2.5} (14.3%) and NH₄⁺ (11.6%) from the STN observations. However, CMAQ predicts the highest other unknown PM_{2.5} (36.7%), which contributes to the most to the PM_{2.5} overprediction in winter. The agreement between predicted and observed PM_{2.5} concentrations without accounting for the contribution of other unknown PM_{2.5} would be considerably better with a slightly positive bias from CMAQ. In summer, both TC (34.2%) and SO₄²⁻ (29.9%) are the dominant PM_{2.5} component, following by other PM_{2.5} (21.2%), NH₄⁺ (9.9%), and NO₃⁻ (4.8%) from the STN observations. CMAQ predicts concentrations of SO₄²⁻, NH₄⁺, and other PM_{2.5} quite well, but significantly underpredicts TC and NO₃⁻. The reasons for this underprediction were discussed earlier in this section. It should be note that the comparison of the CMAQ and observed other unknown PM_{2.5} is challenging due to their different definitions. In CMAQ, the other unknown PM_{2.5} consists of the non-carbon atoms associated with OC, trace elements (e.g., Al, Si, Fe, etc), primary NH₄⁺ as well as other unidentified mass in the speciated profiles and assumed to be dry (Appel et al., 2008). While the observed other unknown PM_{2.5} is computed as the gravimetric mass minus the sum of all speciated components (e.g., SO₄²⁻, NO₃⁻, NH₄⁺, and TC) and is assumed to contain the trace elements, the non-carbon portion of OC and some mass from water (Rees et al., 2004; Frank 2006). Since the majority of the other unknown PM_{2.5} is primary aerosols, the model biases especially in winter are very likely due to errors in unspiciated primary emissions. Moreover,

the different treatment of primary NH_4^+ and aerosol water in CMAQ and the STN observations as mentioned above may contribute to the model biases displayed in the bar chart as well.

As shown in Table 5.2, both NMBs and NMEs are relatively low over most of sub-regions. Domain-wide NMBs range from -22.8% (summer) to 29% (winter) over the STN network and from -33.8% (summer) to 74.3% (winter) over the IMPORVE network. NMEs are generally lower than 50% at both STN and IMPROVE sites throughout the year except in winter. It also can be seen that NMBs and NMEs are consistently larger at the IMPROVE sites than the STN sites, indicating a systematic bias in model predictions at the rural sites versus urban sites. There are currently no universally-accepted or EPA-recommended quantitative performance criteria for $\text{PM}_{2.5}$. However, some specific model performance criteria have been recommended by other modeling studies (e.g., Seigneur, 2001; Morris et al., 2004; Boylan and Russel, 2006; Y. Zhang et al., 2006a). Generally $\pm 30\%$ for model biases and 50% for model errors can be considered as satisfactory performance and the values below or beyond them should be considered as excellent and poor performance, respectively. Overall the 2002 MP modeling platform demonstrates a good and satisfactory performance in predicting $\text{PM}_{2.5}$. It also confirms the findings from previous studies (e.g., Eder and Yu, 2006; Tesche et al., 2006; Appel et al., 2008) and provides comparable or even better performance because of the state-of-science treatments in the model as well as more accurate model inputs.

5.2.3 Hazardous Air Pollutants at the Surface

The evaluation and analysis of simulated HAPs will focus on Hg and some selected HAPs species such as HCHO, ALD2, and Benzene representing different levels of lifetime.

5.2.3.1 Mercury

No routine networks currently exist with measurements of ambient Hg concentrations and dry depositions over the U.S. MDN established by National Atmospheric Deposition Program is the only network that regularly monitors Hg wet deposition with most of its sites scattered throughout the remote areas in the U.S. and Canada. The model evaluation will thus focus on the comparison of modeled Hg wet deposition against the MDN measurements, which is considered to be sufficient to provide a general concept of model performance for Hg (Xu et al., 2000; Bullock and Brehme, 2002; Lin and Tao, 2003; Gbor et al., 2007). Only sites where data are available more than half the weeks in a season are utilized for the seasonal performance evaluation in this study. Figures 5.5a and 5.5b display the spatial variation of NMBs for Hg wet deposition against data from the MDN network for winter and summer 2002. As shown, most MDN sites are clustered in the eastern and Midwest U.S. In winter, NMBs are much more scattered with an overall overprediction (NMBs from 10% to 50%) occurring over the eastern U.S. and with some very high NMBs (>100%) occurring at several sites in both the western and eastern U.S. Some very low negative biases (NMBs > -20%) are observed in the eastern U.S. and moderate negative biases (NMBs of about -60%) also occur in the Midwest. However, the overall trend for Hg wet deposition in CMAQ is overprediction in winter. In summer, the Hg wet deposition is generally underpredicted at more than 80% of MDN sites, especially over the southern U.S. with NMBs of -70% to -10%.

When comparing the modeled and observed Hg wet deposition fluxes annually, more than half of data pairs are within the factor of 2 reference lines (figure not shown) with an R value of 0.45. As shown in Table 5.3 (due to the lack of the observations in the western and central U.S, only domain-wide statistics are shown for HAPs) and Figure 5.6a, CMAQ does reasonably well in simulating the monthly and seasonal Hg wet deposition. The domain-wide NMBs lie between -28.2% (summer) and 28.9% and NMEs lie between 66.9 (spring) and 84.0 (winter). The model performance is slightly better in spring and fall than in summer and winter.

The evaluation results of the present study are more in line with those from Gbor et al. (2007) and show an improvement over those reported by Bullock and Brehme (2002). The Hg wet depositions in Bullock and Brehme (2002) were significantly overpredicted for summer with an NMB of 60.2% and moderately overpredicted for spring with an NMB of 25.9%, compared to 12.4% and -28.2% for spring and summer, respectively, in this study. The performance for precipitation is very similar between the two studies. The improvement of model performance is thus more likely related to the science updates in the current MP version of CMAQ, in addition to those described in Bullock and Brehme (2002). These updates include 1) the modification of the products and reaction rates for reactions of Hg^0 with hydrogen peroxide (H_2O_2), O_3 , and hydroxyl radical (OH); 2) the explicit treatment of Hg^0 between the air and various underlying surfaces (i.e., the dry deposition velocity is no longer zero as assumed in the previous Hg module); 3) the consideration of recycling or re-emitted Hg^0 from the deposited Hg. These updates are made to reflect the up-to-date science published in the peer-reviewed literature (Bullock and Brehme, 2006). Despite the model

improvement, there still exist large discrepancies between CMAQ and MDN observations. The wet deposition of Hg is directly determined by the precipitation amount simulated by MM5 and the aqueous-phase concentrations of dissolved Hg(II) and absorbed PHg simulated by CMAQ. The model biases in Hg wet deposition predictions are thus determined by the errors in predicting those variables. However, as shown in the previous section, MM5 underpredicts precipitation in winter but overpredicts it in summer, which cannot help explain the overprediction of Hg wet deposition in winter and underprediction in summer. This means that the discrepancies between model and observations are more likely due to the predicted Hg(II) and PHg concentrations, which can be further attributed to the uncertainties in emission inputs, boundary conditions, and Hg chemistry treatments in the model. For example, as indicated by Gbor et al. (2007), most modeling studies on Hg in the U.S. have excluded a detailed treatment of Hg emissions from natural sources including vegetation, soil, and water. They estimated that the total natural mercury emission was 230 tons in 2002 based on their Hg natural emission model, while the anthropogenic emission was 126 tons based on the 1999 NEI. The total Hg emissions from the 2002 NEI are only 112 tons (the U.S. EPA 2002 NEI booklet) predominated by anthropogenic emissions. Although the natural Hg emissions based on a modified Biogenic Emission Inventory System (BEIS) model (Lin et al., 2005) are also included in the 2002 MP modeling platform, the estimation may still be too low, especially, since Lin et al. (2005) estimated that Hg emissions from vegetation ranged from 31 to 127 tons with the best estimation of 44 tons in 2001. This underestimation of natural Hg emissions is much more evident in the summer season during which meteorology, vegetation, and soil conditions favoring the generation of Hg emissions.

A recent study by Pongprueksa et al. (2008) showed that response of CMAQ to change of BCONs of Hg species, particularly Hg^0 , was strongly linear and they found an increase of 1 ng m^{-3} of Hg^0 in BCONs could result in an increase of 0.81 ng m^{-3} in the monthly average total Hg concentrations and 1270 ng m^{-2} in the monthly average total deposition. This indicates the uncertainties embedded in GEOS-Chem Hg simulation may contribute significantly to CMAQ predictions. Bullock et al. (2009) also showed that CMAQ-Hg with BCONs from another CTM gave better performance than GEOS-Chem. It is known that the majority of Hg wet deposition are attributable to dissolved Hg(II) (Selin and Jacob, 2008), thus an accurate estimation of their concentrations is essential for accurate Hg wet deposition predictions. Gardfeldt and Jonsson (2003) argued that Hg(II) reduction by HO_2 in aqueous-phase chemistry, which is the most important chemical removal pathway for Hg(II) in CMAQ, should not occur under ambient conditions. Lin et al. (2006) and Pongprueksa et al. (2008) tested this assumption by replacing the aqueous Hg(II)- HO_2 reduction in CMAQ by two other different reduction pathways separately. They found that those two new pathways generated more Hg wet deposition in summer and produced significantly better model agreement with the wet deposition measured by the MDN network.

5.2.3.2 Other Air Toxic Compounds

There are two groups of gaseous HAPs species treated in CMAQ-MP. The first one, including HCHO, ALD2, 1,3-butadiene, and acrolein, can be generated or destroyed and influence the concentrations of O_3 and radicals via their reactions with those oxidants. The second one, including the rest of species and serving as tracers, is only destroyed via chemical reactions with O_3 and radicals and does not alter the concentrations of those

oxidants. A modeling approach analogous to tracers in the gas phase is used for the aerosol-phase HAPs such as diesel PM, lead, and chromium. The emissions of primary components of those species are tracked. They are assumed to be chemically inert and only undergo microphysical and deposition processes that are similar to EC. In contrast, they do not affect the rates of those processes like EC due to their tracking function and they do not participate in cloud chemistry as well (see CMAQ release note, http://www.cmascenter.org/help/model_docs/cmaq/4.6/HAZARDOUS_AIR_POLLUTANT_S.txt). The approach taken above has its limitation. For example, Hutzell and Luecken (2008) indicated that the hexavalent and trivalent states of chromium mass exchange might occur through chemistry within cloud droplets. However, the kinetics for that process is not well understood currently and will only be considered for future model development.

We therefore select 6 representative species including 5 gases and one aerosol to assess the model performance of CMAQ-MP in predicting the HAPs. As shown in Figures 5.5c and 5.5d, CMAQ-MP tends to underpredict HCHO at most of the NATTS sites in both winter and summer. Similar to the MDN sites, most of NATTS sites are located in the eastern U.S. and the model performance evaluation may not be representative for the western U.S. However, there is a cluster of overestimation occurring over Minnesota and Wisconsin in winter with NMBs > 50%. The underpredictions are larger with NMBs of < -50% and as large as -80% in winter and smaller with NMBs of < -30% and as large as -50% in summer, indicating a slightly better model performance for HCHO in summer with respect to spatial patterns. As shown in Figures 5.5e and 5.5f, CMAQ-MP underpredicts ALD2 mixing ratios in winter while overpredicts in summer. The spatial variation of the NMBs for ALD2 in

winter is quite similar but with lower values, as compared to that of HCHO. NMBs generally range from -70% to -30%. The NMBs in summer range from 20% to 60% with some extreme values occurring over Tennessee and South Carolina. Figures 5.6b to 5.6f show the monthly concentrations between CMAQ and observations and Table 5.3 shows the seasonal statistics for HCHO, ALD2, benzene, 1,3-butadiene, acrolein, and particulate lead. The results show systematic underpredictions for most species except ALD2 throughout the year. No standard performance criteria are recommended by the U.S. EPA and literatures for HAPs modeling. According to those for PM_{2.5} used by most modeling studies, the overall model performance of the 2002 MP modeling platform is fairly good for HCHO and ALD2 with NMBs of -53.1% (spring) to -34.4% (winter) for HCHO and -11.8% (fall) to 21.9% (summer) for ALD2. The performance for benzene and particulate lead is satisfactory with NMBs of -42.4% (summer) to -54.7% (fall) for benzene and -40.1% (winter) to -59.6% (summer) for particulate lead. However, the model performance for 1,3-butadiene and acrolein is poor with NMBs generally < -75% and NMEs > 85%. The model performance for most species in this study is consistent and even better than that reported by Luecken et al. (2006). For example, in their study, NMBs were -52.0% (winter) and -40.0% (summer) for HCHO, -59.1% (winter) and -14.7% (summer) for ALD2, and -39.1% (winter) and -69.8% (summer) for benzene, respectively. Interestingly, the prediction of 1,3-butadiene in this study is worse than Luecken et al. (2006) with NMBs of ~-80% versus ~-55%. This is likely because that the CB05 mechanism generates more oxidants than SAPRC99 used by Luecken et al. (2006) and also includes chloride radicals, both of which will destroy more 1,3-butadiene and result in smaller concentrations.

Overall, the model performance for HAPs is not as good as that for CAPs and the model biases (mostly underpredictions) can be explained by the following reasons. First, the grid resolution used in this study may be too coarse to resolve the sub-grid phenomena (such as urban canopies and sub-grid plumes) frequently associated with many HAP species. For example, Logue et al. (2009) reported that most of air toxics compounds measured around Pittsburgh areas were characterized by short periods of elevated concentrations or plume events. Some local sources of emissions (e.g., formaldehyde) and the highly-reactive precursors (e.g., 1,3-butadiene with only a few hours of lifetime) may impact the monitors but not be reflected in the grid average model predictions (Luecken et al., 2006). Ching et al. (2004) and Hutzell et al. (2004) also found that CMAQ predictions of air toxics are generally better (and higher) with a horizontal grid resolution of 4 km than 36 km. Second, errors in emission estimations of HAPs may contribute significantly to model biases, especially for those chemically nonreactive species (e.g., benzene and various metal particles). As indicated by Hutzell and Luecken (2008), the uncertainties associated with HAPs emissions in 2002 NEI are generally larger than those for CAPs. Note that most of HAPs emissions in the 2002 NEI are derived from Toxics Release Inventory (TRI). De Marchi and Hamilton (2006) reported that the TRI underestimates lead emissions by as much as 50% and suggested that it may underestimate most other metal HAPs emissions since they normally share similar sources of emissions. Koehler and Spengler (2007) also believed that TRI tends to underestimate actual emissions of HAPs such as aromatic compounds. Luecken et al. (2006) argued that the underestimation of precursor emissions (e.g., isoprene) may contribute to the negative biases for HCHO and ALD2 in CMAQ. Third, the assumption in chemical

mechanism and aerosol module for HAPs in the current version of CMAQ-MP as described earlier in this section may play a role in the model underpredictions. In CB05, the rate of decay for most air toxic tracers is affected by OH and NO₃ and it is difficult to determine how well CB05 reproduces their concentrations due to the lack of observation data. In particular, CMAQ-MP performs poorly for those short-live and highly active species (e.g., 1,3-butadiene and acrolein), further investigation of the reactions associated with those species is warranted. Finally, the errors from measurements such as sample handling, accuracy of analytical standards, and a lack of site density may also contribute to the model biases, but impacts these factors are believed to be smaller as compared to other reasons (Pratt et al., 2004).

5.2.4 Column Variables

5.2.4.1 Column Mass of Gases

The model performance of the 2002 MP modeling platform above surface is further examined by evaluating seasonal CMAQ column predictions against available satellite measurements over both 36 km CONUS and 12 km EUS domains. The satellite measurements can provide substantial additional information with more complete spatial coverage and can also represent better the scale characteristics of model outputs that are averaged over a grid cell. The satellite dataset used in this study are all level-3 monthly-averaged data with various resolutions (i.e., 1° × 1.25° for TOMS/SBUV TOR, 1° × 1° for MOPITT CO column, 0.25° × 0.25° for GOME and SCIAMACHY NO₂ column, 0.5° × 0.5° for GOME HCHO column, and 1° × 1° for MODIS AOD). The satellite data with different resolutions are mapped to the Lambert conformal projection used in CMAQ using the bi-

linear interpolation of the NCAR command language and the CMAQ model outputs are also processed and averaged at the same time of satellite overpasses in order to facilitate the comparison.

Figure 5.7 shows the observed and simulated seasonal mean TORs over 36 km CONUS and 12 km EUS domains in 2002. The simulated TORs from both CMAQ 36 km and 12 km simulations show consistent spatial patterns and magnitudes. Both TOMS/SBUV and CMAQ TORs show some similarities with respect to spatial patterns in all seasons. The observed highest TORs occurred over the Northeastern, Midwest, and Pacific coastal areas and the lowest TORs occurred over elevated terrains such as areas around Rocky Mountains in the U.S. However, CMAQ fails to capture the observed seasonal variation by TOMS/SBUV (i.e., simulated maximum and minimum TORs occur in spring and fall, respectively, but those observed ones occur in summer and spring, respectively). This discrepancy might be due to the boundary conditions for O₃ used in CMAQ, especially in the upper layers, which make the greatest contribution to TORs (Douglass et al., 2003; Zhang et al., 2009a). Tang et al. (2009) also found that the choice of boundary conditions can affect O₃ predictions throughout the domain, particularly at higher altitudes. It might be worthwhile to further investigate the predictions of GEOS-Chem in future study, which provides the boundary conditions for CMAQ in those upper layers. The observed and simulated seasonal mean TORs over the whole CONUS domain range from 29.2 to 41.8 DU and 32.0 to 37.9 DU, respectively. The simulated TORs in this study are relatively small compared to those of the 2001 36 km CONUS simulation from Zhang et al. (2009a) due to different BCONs used in the upper layers, but both studies show very similar seasonal

variations. In terms of statistic performance, CMAQ simulates TORs the best in fall and the worst in winter. As shown in Table 5.4, CMAQ tends to overpredict TORs in winter and spring with NMBs of 18.0% and 6.4% and underpredict TORs in summer and fall with NMBs of -18.1% and -3.0%. CMAQ also better captures the spatial distribution of TORs in summer and fall with R values of 0.64 and 0.56, respectively, than in winter and spring with R values of only 0.3 and 0.26. Overall, CMAQ shows certain abilities to simulate TORs moderately well with some inconsistencies against TOMS/SBUV data. In addition to the issue related to boundary conditions mentioned above, other possible factors may be responsible for those discrepancies, including the uncertainties in both CMAQ model treatments and the satellite retrieval algorithms. As pointed out by Tong and Mauzerall (2006), the assumption of zero flux at the top layer of the model and the exclusion of the contribution of stratosphere-troposphere exchange (STE) of O₃ limited the capability of CMAQ to reproduce O₃ mixing ratios in the upper troposphere. Since TORs only represent about 10% of the total O₃ columns in the atmosphere, they are very sensitive to errors in both retrievals of the total O₃ column from TOMS and the stratospheric O₃ column from SBUV (Fishman et al., 2005). One of the most important uncertainties in TOMS/SBUV data lies in the definition of tropopause. Stajner et al. (2008) indicated that the differences of 1-2 km in tropopause altitudes can yield differences of 10-20% in tropospheric O₃ columns (TOCs). They compared TOCs from four different definitions of tropopause. One of those tropopauses was determined from the lapse rate in the NECP/NCAR reanalysis, which is also used by TOMS/SBUV data. They found that the differences of TOCs from different tropopause definitions could be up to ~10 DU in summer and ~3-4 DU in winter over the U.S.

Figure 5.8 shows the observed and simulated seasonal mean tropospheric CO columns over the 36 km CONUS and 12 km EUS domains in 2002. Both MOPITT and CMAQ show high CO columns in winter and spring, especially over the CO source regions, notably the northeastern U.S., Great Lakes, and California, although the MOPITT CO column peaks in Spring and that from CMAQ peaks in winter. Both observed and simulated CO columns are also low over elevated altitude terrains (i.e., Rocky Mountains), which is similar to the TOR results. There are also observed elevated CO columns from MOPITT over the northeastern Pacific coastal region throughout the whole year and with maximum values in spring, which is attributed to the long-range transport of CO (Jaffe et al. 2003, Heald et al., 2006, Wang et al., 2009a). CMAQ is able to capture the spatial pattern of high CO columns over the coastal area, partly resulted from the better performance of CO from GEOS-Chem, which provides the boundary conditions of CO (Heald et al., 2006). Nevertheless, CMAQ underpredicts CO columns throughout the whole year with NMBs of -22.2%, -23.6%, -18.8%, and -8.9% for spring, summer, fall, and winter, respectively (as shown in Table 5.4). Mean CMAQ and MOPITT CO columns are better correlated in fall and summer with R values of 0.76 and 0.62, respectively. The seasonal variation of 2002 CMAQ CO columns is very similar to that of 2001 CMAQ simulation from Zhang et al. (2009a), but with lower amounts, which is associated with the lower CO emissions used in this study. Overall, the results presented in Figure 5.8 and in Table 5.4 indicate that CMAQ can reasonably capture the pattern of the MOPITT observations. Several previous studies (e.g., Heald et al., 2003; Chen et al., 2009; Pfister et al., 2010) pointed out that the regional emissions, more specifically biomass burning emissions, could contribute significantly to

elevated CO levels. The uncertainties in CO emissions used in this study therefore could potentially be a major source of errors. The seasonal CO emissions in CMAQ have been closely examined (figures not shown) and it is found that the CO emissions are the highest in winter, which accordingly contributes to the peak of simulated CO columns in winter. On the other hand, the MOPITT CO observation (peaks in spring) shows that the CO emissions over CONUS, particularly in spring, might be too low and can be further verified by sensitivities studies in the future. Other possible uncertainties such as boundary conditions and MOPITT retrieval methods may also contribute to the discrepancies between model and satellite. For example, Heald et al. (2006) indicated that the model bias in the vertical structure of CO (equivalent with boundary conditions or profile) could be an important source of model vs. MOPITT discrepancies. Emmons et al. (2004, 2009) also showed positive biases (19%) of version 3 MOPITT retrievals over continents, as compared to oceans, and the bias may have been increasing over time.

Figure 5.9 shows the observed and simulated seasonal mean tropospheric NO₂ columns over the 36 km CONUS and 12 km EUS domains in 2002. The spatial distribution and seasonal changes of GOME NO₂ columns are generally well reproduced by CMAQ, with larger NO₂ column amounts shown in winter than in other seasons and in the eastern U.S. than in the western U.S. Both GOME and CMAQ show high NO₂ columns over the industrialized and metropolitan areas, in particular, over the Boston/New York City/Philadelphia areas, Great Lakes, Ohio Valley area, and Los Angeles area throughout the whole year. Those areas are correlated very well with NO_x emission source regions (figures not shown), which provides the rationale for many studies that used GOME NO₂ columns as

the constraints for emission inventories of NO_x (Martin et al., 2003). The NO_2 columns over industrial source regions are the lowest in the summer due to a rapid loss by the reaction of NO_2 with OH. The high winter NO_2 columns are likely resulted from a combined effect of a decreased loss of NO_2 via its reaction with OH, reduced vertical transport from PBL to higher altitudes, and slightly increased emissions as compared to the summer (Velders et al., 2001). CMAQ are well correlated with the GOME measurements throughout the whole year with R values of 0.74 to 0.85. CMAQ at 36 km slightly underpredicts the NO_2 columns with NMBs of -7.5% and -4.5% for spring and summer, respectively and moderately overpredicts them with NMBs of 20.1% and 29.1% for fall and winter, respectively (Table 5.4). The larger discrepancies in fall and winter suggest that there might be some errors in the NO_x emission inventory for those seasons. NO_2 column is also compared against the SCIAMACHY measurement for the period when satellite data are available (Wang et al., 2009b). The performance of CMAQ against SCIAMACHY is very similar to GOME, however SCIAMACHY data show greater spatial details than GOME, due to their higher grid resolution. Overall, the model performance for NO_2 column is better than other column variables in this study. When compared with other similar studies (e.g., Ma et al., 2006; Uno et al., 2007; Shi et al., 2008; Han et al., 2009; Herron-Thorpe et al., 2010), this study also shows more satisfactory results that might be attribute to the refined emission inventory and better model treatments. Despite the overall good performance, there are still some discrepancies between GOME and CMAQ, which can be attributed to both errors in model inputs and treatments and satellite measurements and retrievals. For example, there might be overestimations of NO_x emissions in some seasons as discussed above. There might also be

missing sources of NO_x emissions such as lightning emissions, which could be important in spring and summer. Estimations from other studies show that the percentage of NO_x produced by lightning ranges from 7% to 16% of the total (Lee et al., 1997; Beirle et al., 2004) and the resulted NO₂ columns can go up to $0.5-2.0 \times 10^{15}$ molecules cm⁻² over the southern U.S., the Gulf of Mexico, and western North Atlantic in May (Choi et al., 2008). Also as discussed in Vijayaraghavan et al. (2009) and Zhang et al. (2009a), the plume-in-grid treatment in CMAQ for large U.S. power plants can result in improved column NO₂ performance in summer, which can be explored in future study. Boersma et al. (2004) and some other studies (e.g., Richter and Burrows, 2002; Martin et al., 2003; van Noije et al., 2006) also showed that different NO₂ column retrieval approaches may lead to $\pm 5 \times 10^{14} - 1 \times 10^{15}$ molecules cm⁻² for additive error and $\pm 35\% - 60\%$ for relative error over polluted areas, particularly in winter. It is also worth noting that unlike TORs, the tropospheric NO₂ columns are insensitive to the tropopause definition due to that the contributions to NO₂ columns from the upper troposphere and lower stratosphere are negligibly small as compared to those from lower troposphere, especially over polluted regions (Noije et al., 2006). This may partly explain the better performance of this study, since CMAQ typically gives more accurate predictions at lower altitudes.

Figure 5.10 shows the observed and simulated seasonal mean tropospheric HCHO columns over the 36 km CONUS and 12 km EUS domains in 2002. Both GOME and CMAQ present strong seasonal variations of HCHO columns with values of about a factor of two higher in summer than in winter. GOME measurements show high HCHO columns over the southeastern U.S., particularly in summer, which is well captured by CMAQ despite

some overpredictions. The spatial and temporal variability of HCHO columns over the southeastern U.S. in the model correlates clearly with biogenic and biomass burning emissions (figures not shown here) and is believed to be largely driven by oxidation of biogenic VOCs (e.g., isoprene and terpene; Palmer et al., 2003; Stavrou et al., 2009). As shown in Table 5.4, overprediction of HCHO columns from CMAQ occurs in all seasons except for winter. The NMBs are 20.7%, 39.4%, 22.3%, and -24.9% for spring, summer, fall, and winter, respectively. R values range from 0.37 to 0.65. Part of the discrepancies between GOME and CMAQ could be due to the relatively high yield of HCHO from isoprene and terpene in the CB05 chemical mechanism, particularly in warm seasons and uncertainties in the emission inventory, particularly for biogenic emissions. More importantly, according to De Smedt et al. (2008) and Stavrou et al. (2009), the GOME HCHO columns retrieved by Belgian Institute for Space Aeronomy (BIRA)/Royal Netherlands Meteorological Institute (KNMI) used in this study are about 4×10^{15} molecules cm^{-2} (by 30%) lower in summer over the eastern U.S. and about 2×10^{15} molecules cm^{-2} higher in winter over the U.S. than another set of GOME columns retrieved by Harvard University (Chance et al., 2000), which used trace gas profiles from GEOS-Chem model and a different approach to calculate air mass factor. This indicates that the satellite retrievals from Harvard University may provide a better representative of HCHO columns in the eastern U.S. The uncertainties imbedded in the satellite retrievals are worth the further examination.

5.2.4.2 AOD

Figure 5.11 shows observed and simulated seasonal mean AODs over the 36 km CONUS and 12 km EUS domains in 2002. Both MODIS and CMAQ AODs show consistent seasonal variations with the highest values in summer and the lowest in winter. They, however, display quite different spatial distributions over the CONUS domain with the most noticeable differences occurring in the western U.S. There is a persistently high level of AODs that is up to 0.6 in summer and spring over the northwestern U.S., western U.S., and northern Mexico observed by MODIS in 2002. Contrastingly, CMAQ AODs are much lower (by a factor of 3-4) over those regions with only up to about 0.15 in summer. In addition, CMAQ does not reproduce elevated AODs (with values of up to 0.3) over Pacific and off the Pacific coast observed by MODIS in spring as the results of trans-Pacific transport of Asian air pollutants and dust storms. CMAQ does predict the enhanced AODs in summer over the eastern U.S. observed by MODIS although they are lower by a factor of two than MODIS. Statistically, CMAQ underpredicts AODs for all seasons with NMBs of -44.6% to -17.0%. The above findings are consistent with those of Roy et al. (2007) and Zhang et al. (2009a). Several possible reasons may explain the the discrepancies between MODIS and CMAQ AODs. First, the lack of model treatment of mineral dust in CMAQ may lead to the underprediction of AODs over the arid areas of the western U.S. According to Heald et al. (2006), the contribution of mineral dust to the springtime AODs could be as high as that of other anthropogenic pollutants. Second, the inaccurate predictions of $PM_{2.5}$ concentrations, particularly the underprediction of SO_4^{2-} and OC (as shown in Section 5.2.2.2) over the southeastern U.S. can contribute significantly to the underestimate of AOD in the

eastern U.S. An analysis of species-wise AODs estimated by CMAQ (figures not shown here) show that SO_4^{2-} and OC can contribute to more than 50% of the total AOD in summer. Third, there are uncertainties in boundary conditions of $\text{PM}_{2.5}$ and its components. The AODs derived from CMAQ $\text{PM}_{2.5}$ concentration are highly related to the vertical profiles of $\text{PM}_{2.5}$ species. Kaufman et al. (2001) derived the background AODs to be 0.052 at 500 nm over the Pacific Ocean by using Aerosol Robotic network (AERONET) data. However, the averaged CMAQ AODs over the Pacific Ocean in this work are only from 0.015 to 0.039 in different seasons. This reflects that the boundary conditions for $\text{PM}_{2.5}$ species might be too low from GEOS-Chem. Fourth, uncertainties exist in the empirical equations and the associated parameters for the AOD calculation. For example, the equations used in this study do not explicitly consider the contribution of NH_4^+ . They also completely exclude the other fine-mode inorganic aerosols and coarse-mode aerosols (e.g., soils and sea salts). Moreover, the hygroscopic growth factor (i.e., $f(\text{RH})$) is assumed to be a constant value, which may also cause errors in the AOD estimation. A set of modified empirical equations are being developed and will be applied in the future work to improve the model-derived AODs (Wang et al., 2011). Finally, just like other satellite data, there are limitations and uncertainties in the MODIS data used in this work. For example, according to Chu et al. (2002) and Remer et al. (2005), the uncertainty of MODIS monthly AODs (denoted as τ) can be up to $\pm 0.05 \pm 0.15\tau$ over land because of clouds and surface reflectance. MODIS AOD retrievals are typically less accurate over land than over ocean (Ichoku et al., 2005). More recently, Drury et al. (2008) found that there are some errors in the surface reflectance estimates in MODIS operational AOD products (which are used in this study), which can lead to high

biases of AODs especially over the western and central U.S. The results (Figure 6 in Drury et al., 2008) by using their improved AOD retrieval algorithm showed more consistent pattern as our CMAQ AODs in summer.

5.3 Process Analysis

Process analysis is a diagnostic tool that quantifies the contributions of individual physical/chemical processes or chemical reactions to the formation/destruction of chemical species (Jeffries and Tonnesen, 1994). Two process analysis approaches are embedded in CMAQ and they are integrated process rate (IPR) analysis and integrated reaction rate (IRR) analysis. In CMAQ, the time-rate changes in chemical species concentrations in a single grid cell are governed by the following partial differential equation:

$$\begin{aligned} \frac{\partial C_i}{\partial t} = & - \left(u \frac{\partial C_i}{\partial x} + v \frac{\partial C_i}{\partial y} + w \frac{\partial C_i}{\partial z} \right) + \left(\frac{\partial}{\partial x} \left(K_x \frac{\partial C_i}{\partial x} \right) + \frac{\partial}{\partial y} \left(K_y \frac{\partial C_i}{\partial y} \right) + \frac{\partial}{\partial z} \left(K_z \frac{\partial C_i}{\partial z} \right) \right) \\ & + \left(P_{chem,i} - L_{chem,i} \right) + E_i + \left(\frac{\partial C_i}{\partial t} \right)_{dry} + \left(\frac{\partial C_i}{\partial t} \right)_{cloud} \end{aligned} \quad (1)$$

where $\frac{\partial C_i}{\partial t}$ is the change of concentrations of species I with the time; u, v, and w are the velocity components in the x, y, and z directions, respectively; K_x , K_y , and K_z are turbulent diffusivities; the first two terms represent the advection and diffusion of species i in x, y, and z directions; $P_{chem,i}$ and $L_{chem,i}$ are the chemical production and loss rates for either gas or aerosol species; E_i is the emission rates; the last two terms are rates of change of species concentrations due to dry deposition and cloud processes. IPRs assess the net effects of each atmospheric process simulated in CMAQ while IRRs calculate the rates of change of species concentration due to individual gas-phase reactions and track the chemical transformation

pathways. Both IPRs and IRRs have been used for investigating various issues such as O₃ chemistry and transport (Jang et al., 1995a, b; Zhang et al., 2005, 2009b; Huang et al., 2005; O'Neill and Lamb, 2005; Yu et al., 2008; X.-H. Liu et al., 2010; Liu et al., 2011), climate impacts on O₃ and aerosols (Hogrefe et al., 2005), regional and long range transport of air pollutants (Wang et al., 2009a; Zhang et al., 2009b), and controlling processes/process budgets of different air pollutants (Kang et al., 2003; Yu et al., 2008; Liu et al., 2011). In this section, the relative contributions of controlling processes to the formation and destruction of the selected CAPs and HAPs species are quantified through IPR analysis and the seasonal photochemical characteristics are examined through IRR analysis for January (representing winter) and July (representing summer) 2002.

5.3.1 IPR Analysis

The original outputs of IPRs are combined to represent several major processes including horizontal transport (sum of horizontal advection and diffusion), vertical transport (sum of vertical advection and diffusion), gas-phase chemistry, aerosol processes (the net effect of gas-to-particle mass transfer and coagulation), emissions, dry deposition, and cloud processes (the net effect of cloud attenuation of photolytic rates, convective and non-convective mixing and scavenging by clouds, aqueous-phase chemistry, and wet deposition). The hourly IPRs due to different processes in units of ppb h⁻¹ for gases or μg m⁻³ h⁻¹ for aerosols are integrated first to generate daily mass changes for each species over each column grid cell in the PBL (from surface to ~2.5km). The accumulative monthly-mean daily mass changes in units of mole day⁻¹ for gases or gram day⁻¹ for aerosols over different sub-regions are then generated by averaging the values over all grid cells within a certain sub-region

during the one month period. The process contribution can be either positive or negative, indicating build-up or consumption, respectively, of a species concentration due to a specific process.

Figure 5.12 depicts the process budgets for selected CAPs species including NO_x , O_3 , NO_3^- , and $\text{PM}_{2.5}$ in PBL over different sub-regions in January and July 2002. The process budgets for NO_x in both months show very similar variation with major contribution coming from emissions and major removal by chemistry. The contribution from transport seems to be higher in winter, indicating the higher wind speed in cold season. The emission rates for NO_x are the highest over Midwest and the lowest over the western U.S. in both months. The removal rate of NO_x due to gas-phase chemistry is comparable between winter and summer, due to different reasons. In winter, the removal of NO_x is mainly caused by the strong titration of O_3 , but in summer, NO_x is mainly removed by radicals. Contrast to NO_x , the processes contributed to O_3 show a strong seasonality, with much higher formation of O_3 from gas-phase chemistry over all sub-regions in summer than in winter. In summer, the highest chemistry production over Midwest is consistent with the highest precursor emissions (e.g., NO_x). The vertical transport and dry deposition are two major removal processes for O_3 over all sub-regions. In winter, the contribution from chemistry is much weaker, as expected. The horizontal/vertical transport instead plays more important role in the O_3 budgets. The high values of O_3 build-up from vertical transport and consumption from horizontal transport over the western U.S. indicate the persistent period of high pressure system locating over the western U.S. in January 2002 that transports more O_3 vertically from the free troposphere to the PBL and horizontally out of western U.S. The opposite vertical transport for O_3 over the

western U.S. in summer indicates the dominant low pressure system. For NO_3^- , the aerosol process is the dominant contributor over most sub-regions in winter. While in summer the higher temperature prevents HNO_3 from condensing onto the existing particle surface to form NO_3^- , although the HNO_3 concentrations are higher. In particular, over the central and western U.S., aerosol process removes significant amount of NO_3^- via evaporation and desorption. Besides the aerosol process, horizontal/vertical transport and cloud processes over most sub-regions in winter and vertical transport over the central/western U.S. in summer also play important roles in the NO_3 budget. The processes contributed to $\text{PM}_{2.5}$ also show a strong seasonality. The overall emissions are comparable between two months with higher emission contributions over the northeastern, southeastern, and Midwest U.S. in winter and higher emission contributions over central and western U.S. in summer. The removal of $\text{PM}_{2.5}$ due to dry deposition is higher in summer than winter. The changes of $\text{PM}_{2.5}$ due to other processes are complicated over different sub-regions in both months. For example, the aerosol process tends to remove $\text{PM}_{2.5}$ over the northeastern U.S. and southeastern U.S., where ocean grid cells are included in IPR calculation in winter because a negative contribution to aerosol process of particle-phase chloride (figure not shown) due to the fact that the reaction $\text{NaCl(s)} + \text{HNO}_3(\text{g}) \rightarrow \text{NaNO}_3(\text{s}) + \text{HCl}(\text{g})$ is favorable in winter. The negative budget of $\text{PM}_{2.5}$ due to aerosol processes over the western U.S. in summer is mainly due to the loss of NO_3^- and SOA (figures not shown), both of which have relatively low precursor emissions and high removal rates due to gas-particle equilibrium favoring their volatility to the gas phase over that region. As for most of other species, horizontal/vertical transport also plays an important role in the change of $\text{PM}_{2.5}$ concentrations. The

horizontal/vertical transports for different pollutants do not always play the same role (i.e., increase or decrease) for different pollutants indicating the mismatch of timing with high level concentrations for different air pollutants with wind fields.

Figure 5.13 depicts the process budgets for selected HAPs species Hg(II), PHg, HCHO, and particulate lead in PBL over different sub-regions in January and July 2002. The gas-phase chemistry, emission, and horizontal/vertical transports (except the horizontal transport in the Midwest and west U.S. and the vertical transport in the Central U.S.) dominate the production of Hg(II) and dry deposition and cloud processes dominate the removal of Hg(II) over most sub-regions in both months, but the magnitude of IPR for each process has a strong seasonality. For example, the IPRs of chemistry are much higher in summer because of higher oxidant levels. The IPR of dry deposition is comparable to that of cloud processes in both months, indicating the wet deposition may also contribute significantly to the removal of Hg(II). The signs of IPRs for horizontal/vertical transports are more diverse in winter than summer, indicating a much different wind field pattern in some regions in winter. The IPRs of emissions for PHg also indicate that the major sources of Hg are located in the northeastern and Midwest U.S. The IPRs for PHg also show a strong seasonality, especially for aerosol and cloud processes and to a lesser extent for horizontal and vertical transports. The aerosol process contributes to the formation of PHg and the cloud process contributes to the removal. The contributions from both processes are much higher in summer due to the higher concentrations of oxidants. The remaining processes also play some roles in the PHg budgets to a lesser extent. The IPRs for HCHO show a strong seasonality with much higher contributions in summer than winter. Both emission and

chemistry contribute to the formation of HCHO. The IPRs for chemistry, however, are about 5 to 10 times higher over different sub-regions in summer than winter, resulting from much higher direct and precursor emissions and rates of formation from precursors due to a stronger oxidation capability. The vertical transport, dry deposition, and cloud processes are the major processes to remove HCHO from the atmosphere. Unlike other HAPs, the seasonality for particulate lead is not evident. Emission is the major or only source for the build-up of lead over almost all sub-regions, indicating that the uncertainties in emission inventory might contribute significantly to model biases as discussed in the previous section (see Table 5.3). Cloud processes act as the major removal process of particulate lead followed by horizontal transport, vertical transport, and dry deposition. The contribution from aerosol processes is zero due to the assumption of chemical inertia of lead in CMAQ. The vertical transport for particulate lead and PHg plays different role indicates the long-range transport of PHg is more important than particulate lead.

5.3.2 IRR Analysis

CB05 used in this study include 219 reactions, which include 156 reactions from base CB05 mechanism, 21 reactions for chlorine chemistry, 38 reactions for gas-phase HAPs, and 4 reactions for gas-phase Hg. The IRRs of those reactions are grouped into 43 products according to the reactions for radical initiation, propagation, production, and termination (see Table 1, Zhang et al., 2009b for some of the products). Figure 5.14 shows the monthly mean spatial distributions of two of those products including OH reacted with anthropogenic VOCs (AVOCs), and OH reacted with biogenic VOCs (BVOCs) over the surface layer in January and July 2002. As shown in Figures 5.14a and 5.14b, the reaction rates of OH with both

AVOCs and BVOCs are much higher in summer indicating the higher potential of O₃ formation. OH reaction rates with AVOCs are significant over metropolitan and industry areas, especially in New England, Midwest, and California coast in summer. OH reaction rates with BVOCs are generally significant in the southeastern U.S. and south California where vegetation coverage is denser and BVOC emissions are higher.

Figure 5.15 shows the monthly-mean spatial distributions of photochemical indicators of surface layer $P_{\text{H}_2\text{O}_2}/P_{\text{HNO}_3}$ and column HCHO/NO₂ predicted by CMAQ and column HCHO/NO₂ observed by GOME satellite in January and July 2002. As reported by Zhang et al. (2009b), several photochemical indicators have been proposed in the past in order to determine the NO_x- or VOC-limited O₃ chemistry in the regional modeling studies (e.g., Sillman, 1995; Tonnesen and Dennis, 2000; Hammer et al., 2002; Sillman and He, 2002; Martin et al., 2004). The ratio between the production rates of H₂O₂ and HNO₃ ($P_{\text{H}_2\text{O}_2}/P_{\text{HNO}_3}$) has been widely used in chemical indicator analysis due to its robust theoretical background (Sillman, 1995; Tonnesen and Dennis, 2000). $P_{\text{H}_2\text{O}_2}/P_{\text{HNO}_3}$ less than 0.2 typically indicates a VOC-limited O₃ chemistry and the larger value indicates the NO_x-limited O₃ chemistry (Zhang et al., 2009b). As shown in Figure 5.15a, during winter, most regions over U.S. except for some areas over the western U.S. have VOC-limited O₃ chemistry due to high NO_x and low BVOC emissions. By contrast, while the major cities and industry areas remain VOC-limited chemistry, all other areas (mostly rural and remote areas) change to NO_x-limited O₃ chemistry in summer. The results shown here are overall consistent with those reported by Zhang et al. (2009b) and Liu et al. (2011). In order to verify the robustness of $P_{\text{H}_2\text{O}_2}/P_{\text{HNO}_3}$ as a photochemical indicator, we also calculate the column ratio of HCHO/NO₂,

another indicator recommended by Martin et al. (2004). The rationale to use two column species to indicate the surface photochemistry is due to that the bulk of their columns are within the lower mixed layer over polluted regions and the columns are closely related to VOC and NO_x emissions (Martin et al., 2004; Duncan et al., 2009). Another reason is that there are space-based observations of both tropospheric HCHO and NO₂ and the modeled ratio of HCHO/NO₂ can be further examined by large-scale and long time period of satellite observations. The transition value for HCHO/NO₂ originally used by Martin et al. (2004) was 1, but Duncan et al. (2009) suggested values of 1.2-2.2. As shown in Figures 5.15b and 15c, the spatial pattern of VOC- vs. NO_x-limited areas indicated by HCHO/NO₂ predicted by CMAQ is very similar to that of P_{H₂O₂}/P_{HNO₃} in both months, if a transition value of 1.5 is used. When compared with satellite observations, CMAQ demonstrates a promising accuracy in reproducing the spatial variation of column HCHO/NO₂, indicating that both P_{H₂O₂}/P_{HNO₃} and HCHO/NO₂ are robust indicators and can be used as a scientific basis for the regulation of precursor emission reductions in order to reduce the ambient O₃ levels.

REFERENCES

- Appel, K. W., A. B. Gilliland, G. Sarwar, and R. C. Gilliam (2007), Evaluation of the community multiscale air quality (CMAQ) model version 4.5: Sensitivities impacting model performance; Part I – Ozone, *Atmos. Environ.*, *41*, 9603-9615.
- Appel, K. W., P. V. Bhave, A. B. Gilliland, G. Sarwar, and S. J. Roselle (2008), Evaluation of community multiscale air quality (CMAQ) model version 4.5: Sensitivities impacting model performance; Part II – particulate matter, *Atmos. Environ.*, *42*, 6057-6066.
- Aulinger, A., V. Matthias, and M. Quante (2007), Introducing a partitioning mechanism for PAHs into the community multiscale air quality modeling system and its application to simulating the transport of benzo(a)pyrene over Europe, *J. Appl. Meteor. Climatol.*, *46*, 1718-1730.
- Beirle, S., U. Platt, M. Wenig, and T. Wagner (2004), NO_x production by lightning estimated with GOME, *Adv. Space Res.*, *34*, 793-797.
- Betts, A. K., and M. J. Miller (1993), The Betts-Miller scheme, Chapter in *The representation of cumulus convection in numerical models of the atmosphere*, Eds. K.A. Emanuel and D.J. Raymond, American Meteorological Society.
- Binkowski, F. S., and S. J. Roselle (2003), Models-3 community multiscale air quality (CMAQ) model aerosol component, 1. Model description, *J. Geophys. Res.*, *108*, 4183, doi:10.1029/2001JD001409.
- Boersma, K. F., H. J. Eskes, and E. J. Brinksma (2004), Error analysis for tropospheric NO₂ retrieval from space, *J. Geophys. Res.*, *109*, D04311, doi:10.1029/2003JD003962.

- Boylan, J. W., and A. G. Russell (2006), PM and light extinction model performance metrics, goals, and criteria for three-dimensional air quality models, *Atmos. Environ.*, *40*, 4946-4959.
- Brewer J., P. Dolwick, and R. Gilliam (2007), Regional and local scale evaluation of MM5 meteorological fields for various air quality modeling applications, presentation at the 87th Annual American Meteorological Society Annual Meeting, San Antonio, TX, January 15-18.
- Bullock, O. R., and K. A. Brehme (2002), Atmospheric mercury simulation with CMAQ model: formulation description and analysis of wet deposition results, *Atmos. Environ.*, *36*, 2135-2146.
- Bullock, O. R., and K. A. Brehme (2006), Atmospheric mercury simulation with CMAQ version 4.5.1, presentation at the 5th annual CMAS conference, Chapel Hill, NC, October 16-18.
- Bullock, O. R., et al. (2009), An analysis of simulated wet deposition of mercury from the North American Mercury Model Intercomparison Study, *J. Geophys. Res.*, *114*, D08301, doi:10.1029/2008JD011224.
- Burrows, J. P., et al. (1999), The Global Ozone Monitoring Experiment (GOME): Mission concept and first scientific results, *J. Atmos. Sci.*, *56*, 151-175.
- Byun, D. W., and K. L. Schere (2006), Review of the governing equations, computational algorithms, and other components of the models-3 Community Multi-scale Air Quality (CMAQ) modeling system, *Appl. Mech. Rev.*, *59*, 51-77.

- Chance, K. V., P. I. Palmer, R. J. D. Spurr, R. V. Martin, T. P. Kurosu, and D. J. Jacob (2000), Satellite observations of formaldehyde over North America from GOME, *Geophys. Res. Lett.*, *27*, 3461-3464.
- Chameides, W. L., C. Luo, R. Salor, D. Streets, Y. Huang, M. Bergin, and F. Giorgi (2002), Correlation between model-calculated anthropogenic aerosols and satellite-derived cloud optical depths: Indication of indirect effect? *J. Geophys. Res.*, *107*(D10), 4085, doi:10.1029/2000JD00208.
- Chang, J. S., R. A. Brost, I. S. A. Isaksen, S. Madronich, P. Middleton, W. R. Stockwell, and C. J. Walcek (1987), A three-dimensional Eulerian acid deposition model: physical concepts and formulation, *J. Geophys. Res.*, *92*, 14681-14700.
- Chen, D., Y. Wang, M. B. McElroy, K. He., R. M. Yantosca, and P. Le Sager (2009), Regional CO pollution and export in China simulated by the high-resolution nested-grid GEOS-Chem model, *Atmos. Chem. Phys.*, *9*, 3825-3839.
- Ching, J., T. Pierce, T. Palma, and W. Hutzell (2004), Application of fine scale air toxics modeling with CMAQ and HAPEM5, presentation at the 3rd Annual CMAS Conference, Chapel Hill, NC, October 18-20.
- Choi, Y., Y. Wang, T. Zeng, D. Cunnold, E.-S. Yang, R. Martin, K. Chance, V. Thouret, and E. Edgerton (2008), Springtime transitions of NO₂, CO, and O₃ over North America: Model evaluation and analysis, *J. Geophys. Res.*, *113*, D20311, doi:10.1029/2007JD009632.

- Chu, D. A., Y. J. Kaufman, C. Ichoku, L. A. Remer, D. Tanre, and B. N. Holben (2002), Validation of MODIS aerosol optical depth retrieval over land, *Geophys. Res. Lett.*, 29(12), 1671, doi:10.1029/2001GL013205.
- Cook, R., et al. (2007), Impact of underestimating the effects of cold temperature on motor vehicle start emissions of air toxics in the United States, *J. Air & Waste Manage. Assoc.*, 57, 1469-1479.
- Deeter, M. N., et al. (2003), Operational carbon monoxide retrieval algorithm and selected results for the MOPITT instrument, *J. Geophys. Res.*, 108(D14), 4399, doi:10.1029/2002JD003186.
- De Marchi, S., and J. T. Hamilton (2006), Assessing the accuracy of self reported data: An evaluation of the toxics release inventory, *J. Risk Uncertain*, 32, 57-76.
- De Smedt, I., J.-F. Müller, T. Stavrakou, R. Van derA, H. Eskes, and M. Van Roozendael (2008), Twelve years of global observation of formaldehyde in the troposphere using GOME and SCIAMACHY sensors, *Atmos. Chem. Phys.*, 8, 4947-4963.
- Dolwick, P, R. Gilliam, L. Reynolds, and A. Huffman (2007), Regional and local-scale evaluation of 2002 MM5 meteorological fields for various air Quality modeling applications, presentation at 6th Annual CMAS Conference, Chapel Hill, NC, October 1-3.
- Douglass, A. R., M. R. Schoeberl, R. B. Rood, and S. Pawson (2003), Evaluation of transport in the lower tropical stratosphere in a global chemistry and transport model, *J. Geophys. Res.*, 108(D9), 4259, doi:10.1029/2002JD002696.

- Drury, E., D. J. Jacob, J. Wang, R. J. D. Spurr, and K. Chance (2008), Improved algorithm for MODIS satellite retrievals of aerosol optical depths over western North America, *J. Geophys. Res.*, *113*, D16204, doi:10.1029/2007JD009573.
- Dudhia, J. (1989), Numerical study of convection observed during the winter monsoon experiment using a mesoscale two-dimensional model. *J. Atmos. Sci.*, *46*, 3077-3107.
- Duncan, B., Y. Yoshida, C. Retscher, K. Pickering, and E. Celarier (2009), The sensitivity of U.S. surface ozone formation to NO_x and VOCs as viewed from space, presentation at 8th Annual CMAS Conference, Chapel Hill, NC, October 19-21.
- Eder, B., and S. Yu (2006), A performance evaluation of the 2004 release of Models-3 CMAQ, *Atmos. Environ.*, *40*, 4811-4824.
- Emmons, L. K., et al. (2004), Validation of Measurements of Pollution in the Troposphere (MOPITT) CO retrievals with aircraft in situ profiles, *J. Geophys. Res.*, *109*, D03309, doi:10.1029/2003JD004101.
- Emmons, L. K., D. P. Edwards, M. N. Deeter, J. C. Gille, T. Campos, P. Nedelec, P. Novelli, and G. Sachse (2009), Measurements of Pollution In The Troposphere (MOPITT) validation through 2006, *Atmos. Chem. Phys.*, *9*, 1795-1803.
- Fishman, J., A. E. Wozniak, and J. K. Creilson (2003), Global distribution of tropospheric ozone from satellite measurements using the empirically corrected tropospheric ozone residual technique: Identification of the regional aspects of air pollution, *Atmos. Chem. Phys.*, *3*, 893-907.

- Frank, N. H. (2006), Retained nitrate, hydrated sulfates, carbonaceous mass in federal reference method PM_{2.5} for six eastern U.S. cities, *J. Air & Waste Manage. Assoc.*, *56*, 500-511.
- Gardfeldt, K., and M. Jonsson (2003), Is bimolecular reduction of Hg(II) complexes possible in aqueous systems of environmental importance, *J. Phys. Chem. A*, *107*, 4478-4482.
- Gbor, P. K., D. Wen, F. Meng, F. Yang, and J. J. Sloan (2007), Modeling of mercury emission, transport and deposition in North America, *Atmos. Environ.*, *41*, 1135-1149.
- Gilliam, R. C., W. Appel, and S. Phillips (2005), The Atmospheric Model Evaluation Tool (AMET): Meteorology module, presentation at 4th Annual CMAS Conference, Chapel Hill, NC, September 26-28.
- Gilliam, R., C. Hogrefe, and S. T. Rao (2006), New methods for evaluating meteorological models used in air quality applications, *Atmos. Environ.*, *40*, 5073-5086.
- Grell, G., J. Dudhia, and D. Stauffer (1994), A description of the fifth-generation Penn State/NCAR Mesoscale model (MM5) NCAR Tech. Note NCAR/TN-398+STR, National Center for Atmospheric Research, Boulder, Colorado.
- Hammer, M.-U., B. Vogel, and H. Vogel (2002), Findings on H₂O₂ /HNO₃ as an indicator of ozone sensitivity in Baden-Württemberg, Berlin-Brandenburg, and the Po valley based on numerical simulations, *J. Geophys. Res.*, *107*(D22), 8190, doi:10.1029/2000JD000211.
- Han, K. M., et al. (2009), Investigation of NO_x emissions and NO_x-related chemistry in East Asia using CMAQ-predicted and GOME-derived NO₂ columns, *Atmos. Chem. Phys.* *9*, 1017-1036.

- Heald, C. L., et al. (2003), Asian outflow and trans-Pacific transport of carbon monoxide and ozone pollution: An integrated satellite, aircraft, and model perspective, *J. Geophys. Res.*, *108*(D24), 4804, doi:10.1029/2003JD003507.
- Heald, C. L., D. J. Jacob, R. J. Park, B. Alexander, T. D. Fairlie, and R. M. Yantosca (2006), Transpacific transport of Asian anthropogenic aerosols and its impact on surface air quality in the United States, *J. Geophys. Res.*, *111*, D14310, doi:10.1029/2005JD006847.
- Herron-Thorpe, F. L., B. K. Lamb, G. H. Mount, and J. K. Vaughan (2010), Evaluation of a regional air quality forecast model for tropospheric NO₂ columns using the OMI/Aura satellite tropospheric NO₂ product, *Atmos. Chem. Phys.*, *10*, 8839-8854.
- Hogrefe, C., B. Lynn, C. Rosenzweig, R. Goldberg, K. Civerolo, J.-Y. Ku, J. Rosenthal, K. Knowlton, and P. L. Kinney (2005), presentation at the 4th Annual CMAS Conference, Chapel Hill, NC, September 26-28.
- Huang, J.-P., J. C. H. Fung, A. K. H. Lau, and Y. Qin (2005), Numerical simulation and process analysis of typhoon-related ozone episodes in Hong Kong, *J. Geophys. Res.*, *110*, D05301, doi:10.1029/2004JD004914.
- Hutzell, W. T., D. J. Luecken, and J. Ching (2004), Simulating urban air toxics over continental and urban scales, presentation at the 3rd Annual CMAS Conference, Chapel Hill, NC, October 18-20.
- Hutzell, W. T., G. Pouliot, and D. J. Luecken (2006), Changes to the chemical mechanisms for hazardous air pollutants in CMAQ version 4.6, presentation at the 5th annual CMAS conference, Chapel Hill, NC, October 16-18.

- Hutzell, W. T., and D. J. Luecken (2008), Fate and transport of emissions for several trace metals over the United States, *Sci. Total Environ.*, 396, 164-179.
- Ichoku, C., L. A. Remer, and T. F. Eck (2005), Quantitative evaluation and intercomparison of morning and afternoon Moderate Resolution Imaging Spectroradiometer (MODIS) aerosol measurements from Terra and Aqua, *J. Geophys. Res.*, 110, D10S03, doi:10.1029/2004JD004987.
- Jaffe, D. A., J. Snow, and O. Cooper (2003), The 2001 Asian dust events: Transport and impact on surface aerosol concentrations in the U.S., *Eos*, 84(46), 501-516.
- Jeffries, H. E., and S. Tonnesen (1994), A comparison of two photochemical reaction mechanisms using mass balance and process analysis, *Atmos. Environ.*, 28(18), 2991-3003.
- Jang, J.-C. C., H. E. Jeffries, D. Byun, and J. E. Pleim (1995a), Sensitivity of ozone to model grid resolution—I. Application of high-resolution regional acid deposition model, *Atmos. Environ.*, 29(21), 3085-3100.
- Jang, J.-C. C., H. E. Jeffries, D. Byun, and J. E. Pleim (1995b), Sensitivity of ozone to model grid resolution—II. Detailed process analysis for ozone chemistry, *Atmos. Environ.*, 29(21), 3101-3114.
- Kain, J. S. (2003), The Kain-Fritsch convective parameterization: An update, *J. of Appl. Meteor.*, 43, 170-181.

- Kang, D., V. P. Aneja, R. Mathur, and J. D. Ray (2003), Nonmethane hydrocarbons and ozone in three rural southeast United States national parks: A model sensitivity analysis and comparison to measurements, *J. Geophys. Res.*, *108*(D19), 4604, doi:10.1029/2002JD003054.
- Karydis, V. A., A. P. Tsimpidi, and S. N. Pandis (2007), Evaluation of a three-dimensional chemical transport model (PMCAMx) in the eastern United States for all four seasons, *J. Geophys. Res.*, *112*, D14211, doi:10.1029/2006JD007890.
- Kaufman, Y. J., A. Smirnov, B. N. Holben, and O. Dubovik (2001), Baseline maritime aerosol: Methodology to derive the optical thickness and scattering properties, *Geophys. Res. Lett.*, *28*, 3251-3254.
- Kelly, T., R. Mukund, C. Spicer, and A. Pollack (1994), Concentrations and transformations of hazardous air pollutants, *Environ. Sci. Technol.*, *28*, 378A-387A.
- Kemball-Cook, S., Y. Jia, C. Emery, R. Morris, Z. Wang, and G. Tonnesen (2004), 2002 annual MM5 simulation to support WRAP CMAQ visibility modeling for the section 308 SIP/TIP – MM5 sensitivity simulations to identify a more optimal MM5 configuration for simulating meteorology in the western United States, Western Regional Air Partnership, Regional Modeling Center, December 10. (http://pah.cert.ucr.edu/aqm/308/reports/mm5/MM5SensitivityRevRep_Dec_10_2004.pdf)
- Kemball-Cook, S., Y. Jia, C. Emery, R. Morris, Z. Wang, and G. Tonnesen (2005), Annual 2002 MM5 meteorological modeling to support regional haze modeling of the western United States, prepared for the Western Regional Air Partnership (WRAP), Denver, CO, March.

- Lane, T. E., R. W. Pinder, M. Shrivastava, A. J. Robinson, and S. N. Pandis (2007), Source contributions to primary organic aerosol; Comparison of the results of a source-resolved model and the Chemical Mass Balance approach, *Atmos. Environ.*, *41*, 3758-3776.
- Lee, D. S., et al. (1997), Estimations of global NO_x emissions and their uncertainties, *Atmos. Environ.*, *31*, 1735-1749.
- Lin, X., and Y. Tao (2003), A numerical modeling study on regional mercury budget for eastern North America, *Atmos. Chem. Phys.*, *3*, 535-548.
- Lin, C.J., S. E. Lindberg, T. C. Ho, and C. Jang (2005), Development of a processor in BEIS3 for estimating vegetative mercury emission in the continental United States, *Atmos. Environ.*, *38*, 7529-7540.
- Lin, C.J., P. Pongprueksa, S. E. Lindberg, S. O. Pehkonen, D. Byun, and C. Jang (2006), Scientific uncertainties in atmospheric mercury models I: Model science evaluation, *Atmos. Environ.*, *40*, 2911-2928.
- Liu, X.-H., Y. Zhang, J. Xing, Q. Zhang, K. Wang, D. G. Streets, C. J. Jang, W.-X. Wang, and J.-M. Hao (2010), Understanding of regional air pollution over China using CMAQ: Part II. Process analysis and ozone sensitivity to precursor emissions, *Atmos. Environ.*, *44*(20), 3719-3727.
- Liu, P., Y. Zhang, S. Yu, and K. Schere (2011), Use of a process analysis tool for diagnostic study on fine particulate matter predictions in the U.S.—Part II: Analyses and sensitivity simulations, *Atmos. Pollution Res.*, *2*, 61-67.

- Logue, J. M., K. E. Huff-Hartz, A. T. Lamb, N. M. Donahue, and A. L. Robinson (2009), High time-resolved measurements of organic air toxics in different source regimes, *Atmos. Environ.*, *43*, 6205-6217.
- Luecken, D. J., and A. J. Cimorelli (2008), Codependencies of reactive air toxic and criteria pollutants on emission reductions, *J. Air & Waste Manage. Assoc.*, *58*, 693-701.
- Luecken, D. J., W. T. Hutzell, and G. L. Gipson (2006), Development and analysis of air quality modeling simulations for hazardous air pollutants, *Atmos. Environ.*, *40*, 5087-5096.
- Luecken, D. J., S. Phillips, G. Sarwar, and C. Jang (2008), Effects of using the CB05 vs. SAPRC99 vs. CB4 chemical mechanism on model predictions: Ozone and gas-phase photochemical precursor concentrations, *Atmos. Environ.*, *42*, 5805-5820.
- Luo, C., Y. Wang, S. Mueller, and E. Knipping (2009), Evaluation of sulfate simulations using CMAQ version 4.6, presentation at the 8th Annual CMAS Conference, Chapel Hill, NC, October 19-21.
- Ma, J., A. Richter, J. P. Burrows, H. Nüß, and J. A. van Aardenne (2006), Comparison of model-simulated tropospheric NO₂ over China with GOME-satellite data, *Atmos. Environ.*, *40*, 593-604.
- Mao, H., M. Chen, J. D. Hegarty, R. W. Talbot, J. P. Koermer, A. M. Thompson, and M. A. Avery (2010), A comprehensive evaluation of seasonal simulations of ozone in the northeastern US during summers of 2001–2005, *Atmos. Chem. Phys.*, *10*, 9-27.

- Martin, R. V., D. J. Jacob, K. Chance, T. P. Kurosu, P. I. Palmer, and M. J. Evans (2003), Global inventory of nitrogen oxide emissions constrained by space-based observations of NO₂ columns, *J. Geophys. Res.*, *108*(D17), 4537, doi:10.1029/2003JD003453.
- Martin, R. V., A. M. Fiore, and A. Van Donkelaar (2004), Space-based diagnosis of surface ozone sensitivity to anthropogenic emissions, *Geophys. Res. Lett.*, *31*, L06120, doi:10.1029/2004GL019416.
- Mather, R et al. (2005), Multiscale air quality simulation platform: Initial applications and performance for tropospheric ozone and particulate matter, *J. Geophys. Res.*, *110*, D13308, doi:10.1029/2004JD004918.
- Matthias, V., A. Aulinger, and M. Quante (2008), Adapting CMAQ to investigate air quality pollution in North Sea coastal regions, *Env. Mod. and. Sof.*, *23*, 356-368.
- McCarthy, M. C., H. R. Hafner, and S. A. Montzka (2006), Background concentrations of 18 air toxics for North America, *J. Air & Waste Manage. Assoc.*, *56*, 3-11.
- Mlawer, E. J., S. J. Taubman, P. D. Brown, M. J. Iacono, and S. A. Clough (1997), Radiative transfer for inhomogeneous atmospheres: RRTM, a validated correlated-k model for the longwave. *J. Geophys. Res.*, *102*, 16,663-16,682.
- Morris R. E., S Lau, and G. Yarwood (2003), Development and application of an advanced air toxics hybrid photochemical grid modeling system, presentation at 96th Annual Conference and Exhibition of the A&WMA, San Diego, California, June.
- Morris, R. E., B. Koo, D. McNally, T. W. Tesche, and G. Tonnesen (2004), Application of multiple models to simulation fine particulate in the southeastern US, National RPO Modeling Meeting, Denver, CO, May 25-26.

- Morris, R. E., D. E. McNally, T. W. Tesche, G. Tonnesen, J. W. Boylan, and P. Brewer (2005), Preliminary evaluation of the Community Multiscale Air Quality Model for 2002 over the southeastern United States, *J. Air & Waste Manage. Assoc.*, *55*, 1694-1708.
- Nolte, C. G., P. V. Bhave, J. R. Arnold, R. L. Dennis, K. M. Zhang, and A. S. Wexler (2008), Modeling urban and regional aerosols—Application of the CMAQ-UCD Aerosol Model to Tampa, a coastal urban site, *Atmos. Environ.*, *42*, 3179-3191.
- O'Neill, S. M., and B. K. Lamb (2005), Intercomparison of the Community Multiscale Air Quality Model and CALGRID using process analysis, *Environ. Sci. Technol.*, *39*, 5742-5753.
- Palmer, P. I., D. J. Jacob, A. M. Fiore, R. V. Martin, K. Chance, and T. P. Kurosu (2003), Mapping isoprene emissions over North America using formaldehyde column observations from space, *J. Geophys. Res.*, *108*(D6), 4180, doi:10.1029/2002JD002153.
- Phillips, S., K. Wang, C. Jang, N. Possiel, M. Strum, and T. Fox (2008), Evaluation of 2002 multi-pollutant platform: Air toxics, ozone, and particulate matter, presentation at the 7th Annual CMAS Conference, Chapel Hill, NC, October 6-8, 2008.
- Pfister, G. G., L. K. Emmons, D. P. Edwards, A. Aerllano, G. Sachse, and T. Campos (2010), Variability of springtime transpacific pollution transport during 2000–2006: the INTEX-B mission in the context of previous years, *Atmos. Chem. Phys.* *10*, 1345-1359.
- Pinder, R. W., P. J. Adams, S. N. Pandis, and A. B. Gilliland (2006), Temporally resolved ammonia emission inventories: Current estimates, evaluation tools, and measurement needs, *J. Geophys. Res.*, *111*, D16310, doi:10.1029/2005JD006603.

- Pleim, J. E., and J. S. Chang (1992), A nonlocal closure-model for vertical mixing in the convective boundary-layer, *Atmos. Environ.*, 26, 965-981.
- Pleim, J. E., and A. Xiu (2003), Development of a land surface model. Part II: Data assimilation. *J. Appl. Meteor.*, 42, 1811-1822.
- Pongprueksa, P., C. J. Lin, S. E. Lindberg, C. Jang, T. Braverman, O. R. Bullock, T. C. Ho, and H. Chu (2008), Scientific uncertainties in atmospheric mercury models III: Boundary and initial conditions, model grid resolution, and Hg(II) reduction mechanism, *Atmos. Environ.*, 42, 1828-1845.
- Pratt, G. C., Y. Chun, D. Bock, J. L. Adgate, G. Ramachandran, T. H. Stock, M. Morandi, and K. Sexton (2004), Comparing air dispersion model predictions with measured concentrations of VOCs in urban communities, *Environ. Sci. Technol.*, 38, 1949-1959.
- Rao, V., N. Frank, A. Rush, and F. Dimmick (2003), Chemical speciation of PM_{2.5} in urban and rural areas in national air quality and emissions trends report.
(<http://www.epa.gov/air/airtrends/aqtrnd03>)
- Rees, S. L., A. L. Robinson, A. Khlystov, C. O. Stanier, and S. N. Pandis (2004), Mass balance closure and the Federal Reference Method for PM_{2.5} in Pittsburgh, Pennsylvania, *Atmos. Environ.*, 38, 3305-3318.
- Reisner, J., R. T. Bruintjes, and R. M. Rasmussen (1993), Preliminary comparisons between MM5 NCAR/Penn State model generated icing forecasts and observations. In: Preprints, the 5th International Conference on Aviation Weather Systems, Vienna, VA, August 2-6, 5pp.

- Reisner, J., R. M. Rasmussen, and R. T. Bruintjes (1998), Explicit forecasting of supercooled liquid water in winter storms using the MM5 mesoscale model. *Q. J. R. Meteorol. Soc.* *124B*, 1071-1107.
- Remer, L. A, et al. (2005), The MODIS aerosol algorithm, products, and validation, *J. Atmos. Sci.*, *62*(4), 947-973.
- Richter, A., and J. P. Burrows (2002), Tropospheric NO₂ from GOME measurements, *Adv. Space Res.*, *29*, 1673-1683.
- Roselle, R., D. J. Luecken, W. T. Hutzell, O. R. Bullock, G. Sarwar, and K. L. Schere (2007), Development of a multipollutant version of the Community Multiscale Air Quality (CMAQ) modeling system, presentation at the 6th annual CMAQ conference, Chapel Hill, NC, October 1-3.
- Rosenbaum, A. S., D. A. Axelrad, T. J. Woodruff, Y. H. Wei, M. P. Ligocki, and J. P. Cohen (1999), National estimates of outdoor air toxics concentrations, *J. Air & Waste Manage. Assoc.*, *49*, 1138-1152.
- Roy, B., R. Mathur, A. B. Gilliland, and S. C. Howard (2007), A comparison of CMAQ-based aerosol properties with IMPROVE, MODIS, and AERONET data, *J. Geophys. Res.*, *112*, D14301, doi:10.1029/2006JD008085.
- Russell, A. G., and R. Dennis (200), NARSTO critical review of photochemical models and modeling, *Atmos. Environ.*, *34*, 2283-2324.
- Sarwar, G., and P. V. Bhave (2007), Modeling the effect of chlorine emissions on ozone levels over the eastern United States, *J. Appl. Meteor. Climatol.*, *46*, 1009-1019.

- Sarwar, G., D. Luecken, G. Yarwood, G. Whitten, and W. P. L. Carter (2008), Impact of an updated carbon bond mechanism on predictions from the Community Multiscale Air Quality modeling system: Preliminary assessment, *J. Appl. Meteor. Climatol.*, *47*, 3-14.
- Scheffe, R., B. Hubbell, T. Fox, V. Rao, and W. Pennell (2007), The Rationale for a multipollutant, multimedia air quality management framework, *EM*, May, 14-20.
- Shi, C. H. J. S. Fernando, Z. Wang, X. An, and Q. Wu (2008), Tropospheric NO₂ columns over east central China: Comparisons between SCIAMACHY measurements and nested CMAQ simulations, *Atmos. Environ.*, *42*, 7165-7173.
- Seigneur, C. (2001), Current status of air quality models for particulate matter, *J. Air Waste Manage. Assoc.*, *51*, 1508-1521.
- Seigneur, C., K. Lohman, and B. Pun (2002), Critical review of air toxics modeling current status and key Issues, CRC A-42-Phase I. Prepared for Coordinating Research Council, Inc., Alpharetta, GA. September.
- Selin, N. E., and D. J. Jacob (2008), Seasonal and spatial patterns of mercury wet deposition in the United States: Constraints on the contribution from North American anthropogenic sources, *Atmos. Environ.*, *42*, 5193-5204.
- Sillman, S. (1995), The use of NO_y, H₂O₂, and HNO₃ as indicators for ozone-NO_x-hydrocarbon sensitivity in urban locations, *J. Geophys. Res.*, *100*, 4175-4188.
- Sillman, S., and D. He (2002), Some theoretical results concerning O₃-NO_x-VOC chemistry and NO_x-VOC indicators, *J. Geophys. Res.*, *107*, 10.1029/2001JD001123.

- Smyth, S. C., W. Jiang, H. Roth, M. D. Moran, P. A. Makar, F. Yang, V. S. Bouchet, and H. Landry (2009), A comparative performance evaluation of the AURAMS and CMAQ air-quality modeling systems, *Atmos. Environ.*, *43*, 1059-1070.
- Stajner, I., et al. (2008), Assimilated ozone from EOS-Aura: Evaluation of the tropopause region and tropospheric columns, *J. Geophys. Res.*, *113*, D16S32, doi:10.1029/2007JD008863.
- Stavrakou T., J.-F. Müller, I. De Smedt, M. Van Roozendael, G. R. van der Werf, L. Giglio, and A. Guenther (2009), Evaluating the performance of pyrogenic and biogenic emission inventories against one decade of space-based formaldehyde columns, *Atmos. Chem. Phys.*, *9*, 1037-1060.
- Stockwell, W. R., P. Middleton, and J. S. Chang (1990), The second generation regional acid deposition model chemical mechanism for regional air quality modeling, *J. Geophys. Res.*, *95*(D10), 16343-16367, 10.1029/90JD00461.
- Tang, Y., et al. (2009), The impact of chemical lateral boundary conditions on CMAQ predictions of tropospheric ozone over the continental United States, *Environ. Fluid Mech.*, *9*, 43-58.
- Tesche, T. W., R. Morris, G. Tonnesen, D. McNally, J. Boylan, and P. Brewer (2006), CMAQ/CAMx annual 2002 performance valuation over the eastern US, *Atmos. Environ.*, *40*, 4906-4919.
- Tonnesen, G. S., and R. L. Dennis (2000), Analysis of radical propagation efficiency to assess ozone sensitivity to hydrocarbons and NO_x 1. Local indicators of instantaneous odd oxygen production sensitivity, *J. Geophys. Res.*, *105*, 9213-9225.

- Tong, D. Q., and D. L. Mauzerall (2006), Spatial variability of summertime tropospheric ozone over the continental United States: Implications of an evaluation of the CMAQ model, *Atmos. Environ.*, *40*, 3041-3056.
- Turpin, B. J., and H. J. Lim (2001), Species contributions to PM_{2.5} mass concentrations: revisiting common assumptions for estimating organic mass, *Aerosol Sci. Technol.* *35*, 602-610.
- U.S. EPA (2005), Technical support document for the Clean Air Interstate Rule: Air quality modeling, Office of Air Quality Planning and Standards, Research Triangle Park, NC, Docket No. OAR-2005-0053-2151.
- U.S. EPA (2007), Guidance on the use of models and other analyses for demonstrating attainment of air quality goals for ozone, PM_{2.5}, and regional haze, the U.S. Environmental Protection Agency, Research Triangle Park, NC, EPA-454/B-07-002.
- U.S. EPA (2008), Air quality modeling platform for the ozone national ambient air quality standard final rule regulatory impact analysis, Office of Air Quality Planning and Standards, Research Triangle Park, NC (EPA-454/R-08-003).
- Uno I., et al. (2007), Systematic analysis of interannual and seasonal variations of model-simulated tropospheric NO₂ in Asia and comparison with GOME-satellite data, *Atmos. Chem. Phys.*, *7*, 1671-1681.
- Van Noije, T. P. C., et al. (2006), Multi-model ensemble simulations of tropospheric NO₂ compared with GOME retrievals for the year 2000, *Atmos. Chem. Phys.*, *6*, 2943-2979.
- Velders, G. J. M., C. Granier, R. W. Portmann, K. Pfeilsticker, M. Wenig, T. Wagner, U. Platt, A. Richter, and J. P. Burrows (2001), Global tropospheric NO₂ column

distributions: Comparing the three-dimensional model calculations with GOME measurements, *J. Geophys. Res.*, *106*(D12), 12,643-12,666.

Vijayaraghavan, K., Y. Zhang, C. Seigneur, P. Karamchandani, and H. E. Snell (2009), Export of reactive nitrogen from coal-fired power plants in the USA: Estimates from a plume-in-grid modeling study, *J. Geophys. Res.*, *114*, D04308, doi:10.1029/2008JD010432.

Wang, K., Y. Zhang, C. Jang, S. Phillips, and B. Wang (2009a), Modeling intercontinental air pollution transport over the trans-Pacific Region in 2001 using community multiscale air quality (CMAQ) model, *J. Geophys. Res.*, *114*, D04307, doi:10.1029/2008JD010807.

Wang, K., S. Phillips, C. Jang, Y. Zhang, N. Possiel, and T. Fox (2009b), Evaluation of 2002 multi-pollutant modeling platform using satellite measurements, presentation at the 8th Annual CMAS Conference, Chapel Hill, NC, October 19-21.

Wang, K., and Y. Zhang (2010), Development of an online dust module in CMAQ and its application to simulate the trans-Pacific transport of Asian dust, presentation at the International Symposium on Asian Dust/Aerosol and its Impact on Global Climate Change, Shanghai, China, August 8-10.

Wang, K., Y. Zhang, A. Nenes, and C. Fountoukis (2011), Implementation of dust emission and heterogeneous chemistry into the Community Multiscale Air Quality Model and an initial application to April 2001 Asian dust storm episode, manuscript in preparation.

- Wiedinmyer, C., B. Quayle, C. Geron, A. Belote, D. McKenzie, X. Zhang, S. O'Neill, and K. Klos Wynne (2006), Estimating emissions from fires in North America for air quality modeling, *Atmos. Environ.*, *40*, 3419-3432.
- Wu, S.-Y., S. Krishnan, Y. Zhang, and V. Aneja (2008), Modeling atmospheric transport and fate of ammonia in North Carolina, Part I: Evaluation of meteorological and chemical predictions, *Atmos. Environ.*, *42*, 3419-3436.
- Xiu, A., and J. E. Pleim (2001), Development of a land surface model, Part I: Application in a mesoscale meteorological model, *J. Appl. Meteor.*, *40*, 192-209.
- Xu, X., X. Yang, D. R. Miller, J. J. Helble, and R. J. Carley (2000), A regional scale modeling study of atmospheric transport and transformation of mercury. I. Model development and evaluation, *Atmos. Environ.*, *34*, 4933-4944.
- Yantosca, B. (2004), GEOS-CHEMv7-01-02 user's guide, Atmospheric Chemistry Modeling Group, Harvard University, Cambridge, MA, October 15.
- Yarwood, G., S. Rao, M. Yocke, and G. Z. Whitten (2005), Updates to the carbon bond mechanism: CB05, Report to the U. S. Environmental Protection Agency, RT-04-00675.
- Yu, S., R. Mathur, K. Schere, D. Kang, J. Pleim, and T. L. Otte (2007), A detailed evaluation of the Eta-CMAQ forecast model performance for O₃, its related precursors, and meteorological parameters during the 2004 ICARTT study, *J. Geophys. Res.*, *112*, D12S14, doi:10.1029/2006JD007715.
- Yu, S., R. Mathur, K. Schere, D. Kang, J. Pleim, J. Young, D. Tong, G. Pouliot, S. A. McKeen, and S. T. Rao (2008), Evaluation of real-time PM_{2.5} forecasts and process

analysis for PM_{2.5} formation over the eastern United States using the Eta-CMAQ forecast model during the 2004 ICARTT study, *J. Geophys. Res.*, *113*, D06204, doi:10.1029/2007JD009226.

Yu, S., R. Mathur, G. Sarwar, D. Kwang, D. Tong, G. Pouliot, and J. Pleim (2010), Eta-CMAQ air quality forecasts for O₃ and related species using three different photochemical mechanisms (CB4, CB05, SAPRC-99): comparisons with measurements during the 2004 ICARTT study, *Atmos. Chem. Phys.*, *10*, 3001-3025.

Zhang, M., et al. (2003), Large-scale structure of trace gas and aerosol distributions over the western Pacific Ocean during the Transport and Chemical Evolution Over the Pacific (TRACE-P) experiment, *J. Geophys. Res.*, *108*(D21), 8820, doi:10.1029/2002JD002946.

Zhang, M., I. Uno, R. Zhang, Z. Han, Z. Wang, and Y. Pu (2006), Evaluation of the Models-3 Community Multi-scale Air Quality (CMAQ) modeling system with observations obtained during the TRACE-P experiment: Comparison of ozone and its related species, *Atmos. Environ.*, *40*, 4874-4882.

Zhang, Y., B. Pun, S.-Y. Wu, K. Vijayaraghavan, and C. Seigneur (2004), Application and evaluation of two air quality models for particulate matter for a Southeastern U.S. episode, *J. Air & Waste Manage. Assoc.*, *54*, 1478-1493.

Zhang, Y., K. Vijayaraghavan, and C. Seigneur (2005), Evaluation of three probing techniques in a three-dimensional air quality model, *J. Geophys. Res.*, *110*, D02305, doi:10.1029/2004JD005248.

- Zhang, Y., P. Liu, B. Pun, and C. Seigneur (2006a), A comprehensive performance evaluation of MM5-CMAQ for the Summer 1999 Southern Oxidants Study episode- Part I: Evaluation protocols, databases, and meteorological predictions, *Atmos. Environ.*, *40*, 4825-4838.
- Zhang, Y., P. Liu, A. Queen, C. Misenis, B. Pun, and C. Seigneur (2006b), A comprehensive performance evaluation of MM5-CMAQ for the Summer 1999 Southern Oxidants Study episode-Part II: Gas and aerosol predictions, *Atmos. Environ.*, *40*, 4839-4855.
- Zhang, Y., P. Liu, B. Pun, and C. Seigneur (2006c), A comprehensive performance evaluation of MM5-CMAQ for the Summer 1999 Southern Oxidants Study episode- Part III: Diagnostic and mechanistic evaluations, *Atmos. Environ.*, *40*, 4856-4873.
- Zhang, Y., J.-P. Huang, D. K. Henze, and J. H. Seinfeld (2007), Role of isoprene in secondary organic aerosol formation on a regional scale, *J. Geophys. Res.*, *112*, D20207, doi:10.1029/2007JD008675.
- Zhang, Y., K. Vijayaraghavan, X.-Y. Wen, H. E. Snell, and M. Z. Jacobson (2009a), Probing into regional O₃ and PM pollution in the U.S., Part I: A 1-year CMAQ simulation and evaluation using surface and satellite data, *J. Geophys. Res.* *114*, D22304, doi:10.1029/2009JD011898.
- Zhang, Y., X.-Y. Wen, K. Wang, K. Vijayaraghavan, and M. Z. Jacobson (2009b), Probing into regional O₃ and PM pollution in the U.S., Part II: An examination of formation mechanisms through a process analysis technique and sensitivity study, *J. Geophys. Res.* *114*, D22305, doi:10.1029/2009JD011900.

Table 5.1. Summary of observational databases used in the model evaluation.

| Database ^a | | Variables/Species | Data Frequency | Number of Sites |
|-----------------------|----------|---|--------------------------|-----------------|
| <i>Surface</i> | | | | |
| GAS | AIRS-AQS | O ₃ | Hourly | ~1000 |
| PM | CASTNET | SO ₄ ²⁻ , NH ₄ ⁺ | Weekly average | ~80 |
| PM | IMPROVE | PM _{2.5} , SO ₄ ²⁻ , NO ₃ ⁻ , EC, OC | 1 in 3 days; 24h average | ~100 |
| PM | STN | PM _{2.5} , SO ₄ ²⁻ , NO ₃ ⁻ , NH ₄ ⁺ , EC, OC | 1 in 3 days; 24h average | ~60 |
| PM | NADP | Wet deposition of SO ₄ ²⁻ , NO ₃ ⁻ , NH ₄ ⁺ | Weekly total | ~220 |
| Hg | MDN | Wet deposition of Hg | Weekly total | ~100 |
| Toxics | NATTS | Various air toxics and metals | 24h average | <100 |
| <i>Satellite</i> | | | | |
| GOME | | Column NO ₂ /HCHO | Monthly average | N/A |
| SCIAMACHY | | Column NO ₂ | Monthly average | N/A |
| MODIS | | AOD | Monthly average | N/A |
| MOPITT | | Column CO | Monthly average | N/A |
| TOMS/SBUV | | TOR | Monthly average | N/A |

^aAIRS-AQS, Aerometric Information Retrieval System-Air Quality Subsystem; CASTNET, Clean Air Status and Trends Network; GOME, Global Ozone Monitoring Experiment; IMPROVE, Interagency Monitoring of Protected Visual Environments; MDN, Mercury Deposition Network; MODIS, Moderate Resolution Imaging Spectroradiometer; MOPITT, Measurements of Pollution in the Troposphere; NADP, National Acid Deposition Program; NATTS, National Air Toxics Trends Stations; SCIAMACHY, Scanning Imaging Absorption Spectrometer for Atmospheric Chartography; STN, Speciated Trends Network; TOMS/SBUV, Total Ozone Mapping Spectrometer and the Solar Backscattered Ultraviolet.

Table 5.2. Seasonal-mean model performance statistics for criteria air pollutants over CONUS and sub-regions in 2002¹.

| Variables | Network | Sub-regions | Winter | | Spring | | Summer | | Fall | |
|------------------------------|----------|-------------|----------|----------|---------|---------|---------|---------|---------|---------|
| | | | NMB* (%) | NME* (%) | NMB (%) | NME (%) | NMB (%) | NME (%) | NMB (%) | NME (%) |
| Max 8-h O ₃ | AIRS-AQS | CONUS | | | | | 1.5 | 14.0 | | |
| | | Northeast | | | | | 2.7 | 13.2 | | |
| | | Southeast | | | | | 1.7 | 14.2 | | |
| | | Midwest | | | | | 2.6 | 13.0 | | |
| | | Central | | | | | 3.5 | 13.0 | | |
| | | West | | | | | -1.2 | 15.5 | | |
| PM _{2.5} Total Mass | STN | CONUS | 29.0 | 59.5 | 12.3 | 48.3 | -22.8 | 34.4 | 2.4 | 41.5 |
| | | Northeast | 38.6 | 49.7 | 38.4 | 57.6 | -9.1 | 25.4 | 15.0 | 30.3 |
| | | Southeast | 71.8 | 74.7 | 35.6 | 49.8 | -17.7 | 33.2 | 26.6 | 43.4 |
| | | Midwest | 21.0 | 46.8 | -2.0 | 36.0 | -29.6 | 33.7 | -8.3 | 32.7 |
| | | Central | 48.8 | 65.4 | -3.5 | 50.1 | -24.1 | 37.8 | 18.3 | 46.7 |
| | | West | -19.6 | 57.3 | 4.1 | 54.8 | -33.4 | 42.6 | -28.2 | 50.9 |
| | IMPROVE | CONUS | 74.3 | 94.0 | 5.6 | 53.7 | -33.8 | 48.0 | 11.4 | 50.9 |
| | | Northeast | 65.7 | 70.8 | 47.2 | 64.7 | -24.2 | 32.5 | 29.5 | 46.7 |
| | | Southeast | 143.9 | 146.9 | 47.4 | 61.0 | -28.0 | 38.7 | 42.3 | 57.6 |
| | | Midwest | 47.6 | 66.5 | -1.8 | 43.3 | -33.5 | 39.9 | 9.2 | 42.1 |
| | | Central | 53.4 | 73.6 | -19.1 | 52.3 | -46.1 | 47.9 | 16.0 | 54.1 |
| | | West | 57.0 | 89.3 | -5.7 | 54.5 | -33.7 | 57.3 | -1.5 | 51.5 |

Table 5.2. (Continued)

| Variables | Network | Sub-regions | Winter | | Spring | | Summer | | Fall | |
|---|---------|-------------|--------|------|--------|------|--------|------|-------|------|
| | | | NMB | NME | NMB | NME | NMB | NME | NMB | NME |
| Sulfate (SO ₄ ²⁻) | STN | CONUS | -5.1 | 38.1 | -11.2 | 35.7 | -4.5 | 32.7 | -6.8 | 36.2 |
| | | Northeast | 3.4 | 40.9 | 2.1 | 37.7 | 10.0 | 30.2 | -6.2 | 31.3 |
| | | Southeast | 0.7 | 32.4 | 0.5 | 36.1 | 1.4 | 29.7 | -4.5 | 28.4 |
| | | Midwest | -14.5 | 34.3 | -16.0 | 31.1 | -3.0 | 31.1 | -6.8 | 34.7 |
| | | Central | 1.5 | 41.6 | -24.7 | 38.5 | -12.9 | 35.3 | 4.0 | 43.8 |
| | | West | -24.4 | 52.2 | -16.7 | 41.6 | -42.1 | 49.6 | -38.8 | 49.2 |
| | IMPROVE | CONUS | 18.1 | 50.0 | -3.1 | 35.0 | -13.6 | 35.5 | -2.9 | 36.3 |
| | | Northeast | 1.9 | 43.3 | -4.4 | 29.1 | -2.5 | 29.9 | 0.9 | 28.3 |
| | | Southeast | 6.3 | 35.4 | 1.5 | 31.1 | -9.5 | 30.8 | -4.2 | 27.4 |
| | | Midwest | 2.2 | 36.9 | -8.6 | 31.1 | -6.7 | 35.9 | 3.9 | 39.2 |
| | | Central | 4.8 | 41.7 | -24.8 | 35.7 | -26.2 | 35.3 | -8.0 | 36.9 |
| | | West | 64.3 | 89.8 | 8.8 | 43.2 | -19.8 | 42.2 | -6.5 | 42.1 |
| | CASTNET | CONUS | -0.9 | 29.2 | -10.3 | 22.0 | -9.7 | 19.7 | -4.3 | 20.2 |
| | | Northeast | -8.3 | 29.8 | -7.7 | 18.9 | -4.8 | 16.0 | -5.9 | 16.3 |
| | | Southeast | 0.0 | 24.4 | -2.6 | 17.3 | -9.3 | 16.7 | -1.8 | 15.7 |
| | | Midwest | -2.0 | 27.3 | -14.5 | 22.3 | -6.8 | 19.8 | -1.5 | 22.2 |
| | | Central | -7.2 | 24.4 | -35.2 | 35.8 | -24.1 | 27.3 | -18.9 | 24.0 |
| | | West | 46.2 | 65.2 | -7.8 | 32.0 | -35.2 | 40.7 | -12.7 | 35.8 |

Table 5.2. (Continued)

| Variables | Network | Sub-regions | Winter | | Spring | | Summer | | Fall | |
|---|---------|-------------|--------|-------|--------|-------|--------|-------|-------|-------|
| | | | NMB | NME | NMB | NME | NMB | NME | NMB | NME |
| Nitrate (NO ₃ ⁻) | STN | CONUS | 3.6 | 63.3 | 38.4 | 88.5 | -27.0 | 78.1 | -4.5 | 71.2 |
| | | Northeast | 16.6 | 46.2 | 79.4 | 104.9 | 20.1 | 89.9 | 23.2 | 48.2 |
| | | Southeast | 50.4 | 67.1 | 61.5 | 92.3 | 5.1 | 84.5 | 50.8 | 91.0 |
| | | Midwest | 37.0 | 90.9 | 44.5 | 116.0 | -57.5 | 76.2 | -4.3 | 78.5 |
| | | Central | 12.0 | 42.5 | 46.8 | 70.0 | -8.1 | 73.8 | 39.4 | 65.2 |
| | | West | -49.5 | 68.1 | -22.0 | 68.5 | -64.7 | 69.3 | -54.3 | 72.7 |
| | IMPROVE | CONUS | 54.7 | 110.2 | 85.4 | 139.9 | -36.8 | 96.3 | 50.7 | 112.9 |
| | | Northeast | 28.6 | 59.0 | 168.0 | 194.5 | -6.4 | 96.1 | 56.6 | 75.6 |
| | | Southeast | 181.9 | 192.5 | 196.6 | 221.0 | 26.2 | 128.2 | 160.0 | 191.7 |
| | | Midwest | 65.0 | 117.5 | 92.8 | 161.1 | -37.3 | 96.4 | 76.1 | 146.1 |
| | | Central | 29.5 | 74.1 | 58.8 | 116.1 | -65.2 | 82.9 | 61.7 | 96.5 |
| | | West | 3.5 | 95.2 | 38.6 | 103.9 | -47.3 | 92.2 | 11.4 | 98.4 |
| Ammonium (NH ₄ ⁺) | STN | CONUS | 21.2 | 56.3 | 22.5 | 53.6 | -2.3 | 39.5 | 2.8 | 47.7 |
| | | Northeast | 25.6 | 42.5 | 52.9 | 71.7 | 19.6 | 38.7 | 14.0 | 35.8 |
| | | Southeast | 44.5 | 51.8 | 30.0 | 49.1 | 3.4 | 37.9 | 22.6 | 44.0 |
| | | Midwest | 33.8 | 59.3 | 16.9 | 44.2 | -0.1 | 34.7 | -1.4 | 39.9 |
| | | Central | 43.4 | 62.5 | 11.0 | 47.0 | -5.0 | 37.3 | 23.9 | 53.1 |
| | | West | -33.8 | 64.6 | -0.8 | 65.9 | -42.2 | 56.2 | -42.0 | 65.5 |
| | CASTNET | CONUS | 39.9 | 47.2 | 39.9 | 51.6 | -8.7 | 25.0 | 16.7 | 39.0 |
| | | Northeast | 16.8 | 23.5 | 63.6 | 65.7 | 6.6 | 20.6 | 26.8 | 32.9 |
| | | Southeast | 84.6 | 84.8 | 54.0 | 56.8 | -8.6 | 24.1 | 26.7 | 45.9 |
| | | Midwest | 32.8 | 42.3 | 15.9 | 36.4 | -16.6 | 25.6 | 3.9 | 35.2 |
| | | Central | 41.4 | 53.8 | 7.0 | 39.9 | -8.4 | 22.7 | 18.4 | 38.2 |
| | | West | 45.5 | 76.4 | 28.8 | 50.9 | -27.3 | 43.9 | -0.4 | 53.1 |

Table 5.2. (Continued)

| Variables | Network | Sub-regions | Winter | | Spring | | Summer | | Fall | |
|-----------------------|---------|-------------|--------|-------|--------|------|--------|------|-------|------|
| | | | NMB | NME | NMB | NME | NMB | NME | NMB | NME |
| Elemental Carbon (EC) | IMPROVE | CONUS | 20.6 | 68.0 | -3.8 | 58.7 | -14.3 | 64.6 | -7.2 | 57.6 |
| | | Northeast | 21.3 | 40.9 | -11.9 | 32.4 | -40.0 | 43.0 | -7.1 | 33.8 |
| | | Southeast | 69.1 | 82.1 | 23.7 | 48.8 | -30.3 | 49.9 | 9.7 | 46.5 |
| | | Midwest | -3.0 | 42.8 | -21.0 | 41.3 | -43.2 | 48.1 | -24.4 | 39.0 |
| | | Central | 3.8 | 51.0 | -33.4 | 39.4 | -43.5 | 49.5 | -2.0 | 47.6 |
| | | West | 9.1 | 78.9 | 28.6 | 79.3 | 4.9 | 77.9 | -8.5 | 71.1 |
| Organic Carbon (OC) | IMPROVE | CONUS | 45.3 | 84.1 | -2.2 | 60.4 | -41.7 | 64.7 | -11.9 | 54.2 |
| | | Northeast | 25.0 | 53.6 | -20.8 | 41.8 | -68.5 | 68.9 | -36.3 | 41.9 |
| | | Southeast | 115.1 | 128.1 | 31.1 | 53.2 | -61.2 | 65.8 | 17.9 | 46.3 |
| | | Midwest | 3.2 | 47.6 | -32.9 | 55.3 | -67.9 | 68.5 | -34.9 | 46.4 |
| | | Central | 11.7 | 57.1 | -46.0 | 55.7 | -71.0 | 71.4 | -31.5 | 50.2 |
| | | West | 42.4 | 90.3 | 13.7 | 67.8 | -25.7 | 62.5 | -8.1 | 59.1 |

¹ Winter: Jan., Feb., and Dec.; Spring: Mar., Apr., and May; Summer: Jun., Jul., and Aug, for other species and May to Sep. for O₃; Fall: Sep., Oct., and Nov.

*NMB: Normalized mean bias; NME: Normalized mean error.

Table 5.3. Seasonal-mean model performance statistics for selected hazardous air pollutants over CONUS in 2002.

| Variables | Network | Winter | | Spring | | Summer | | Fall | |
|---------------------|---------|----------|----------|---------|---------|---------|---------|---------|---------|
| | | NMB* (%) | NME* (%) | NMB (%) | NME (%) | NMB (%) | NME (%) | NMB (%) | NME (%) |
| Mercury (Hg) | MDN | 28.9 | 84.0 | 12.4 | 66.9 | -28.2 | 68.3 | -11.7 | 70.5 |
| Formaldehyde (HCHO) | NATTS | -34.4 | 65.7 | -53.1 | 66.2 | -42.6 | 52.7 | -40.0 | 57.0 |
| Acetaldehyde (ALD2) | NATTS | -24.1 | 50.0 | -15.9 | 54.7 | 21.9 | 75.1 | -11.8 | 66.1 |
| Benzene | NATTS | -47.8 | 69.6 | -46.8 | 65.5 | -42.4 | 60.6 | -54.7 | 65.8 |
| 1,3-Butadiene | NATTS | -71.3 | 87.4 | -78.4 | 89.6 | -83.6 | 89.2 | -80.0 | 86.8 |
| Acrolein | NATTS | -89.4 | 89.4 | -92.7 | 92.7 | -95.1 | 95.2 | -94.6 | 94.6 |
| Particulate Lead | NATTS | -40.1 | 65.4 | -57.6 | 70.1 | -59.6 | 72.6 | -56.2 | 68.4 |

*NMB: Normalized mean bias; NME: Normalized mean error.

Table 5.4. Seasonal-mean performance statistics for column predictions over the 36 km CONUS domain in 2002¹.

| Season | Attributes ² | TOR | CO Column | NO ₂ Column | HCHO Column | AOD |
|--------|-------------------------|-------|-----------|------------------------|-------------|-------|
| Spring | Data Number | 13710 | 16471 | 11920 | 10081 | 13446 |
| | Mean Obs. | 35.6 | 21.0 | 2.1 | 3.2 | 0.19 |
| | Mean Pred. | 37.9 | 16.3 | 2.0 | 3.9 | 0.11 |
| | Correlation | 0.26 | 0.55 | 0.85 | 0.45 | 0.13 |
| | NMB (%) | 6.4 | -22.2 | -7.5 | 20.7 | -43.2 |
| | NME (%) | 11.5 | 22.7 | 34.3 | 47.7 | 49.5 |
| Summer | Data Number | 13710 | 16576 | 15243 | 15448 | 16574 |
| | Mean Obs. | 41.8 | 18.4 | 1.5 | 4.9 | 0.21 |
| | Mean Pred. | 34.2 | 14.1 | 1.4 | 6.9 | 0.12 |
| | Correlation | 0.64 | 0.62 | 0.74 | 0.65 | 0.59 |
| | NMB (%) | -18.1 | -23.6 | -4.5 | 39.4 | -44.6 |
| | NME (%) | 18.1 | 24.3 | 38.1 | 48.8 | 44.9 |
| Fall | Data Number | 13710 | 16570 | 12794 | 13065 | 14691 |
| | Mean Obs. | 33.0 | 19.3 | 1.9 | 3.5 | 0.11 |
| | Mean Pred. | 32.0 | 15.6 | 2.3 | 4.3 | 0.09 |
| | Correlation | 0.56 | 0.76 | 0.78 | 0.48 | 0.01 |
| | NMB (%) | -3.0 | -18.8 | 20.1 | 22.3 | -17.0 |
| | NME (%) | 7.2 | 19.1 | 51.3 | 45.3 | 48.5 |
| Winter | Data Number | 13710 | 16287 | 11278 | 12386 | 12416 |
| | Mean Obs. | 29.2 | 19.1 | 2.7 | 3.7 | 0.11 |
| | Mean Pred. | 34.4 | 17.4 | 3.4 | 2.8 | 0.06 |
| | Correlation | 0.3 | 0.46 | 0.80 | 0.37 | 0.18 |
| | NMB (%) | 18.0 | -8.9 | 29.1 | -24.9 | -39.9 |
| | NME (%) | 18.3 | 13.9 | 52.4 | 41.7 | 53.1 |

¹The units for TOR, CO, NO₂, and HCHO columns are DU, 10¹⁷ molecules cm⁻², 10¹⁵ molecules cm⁻², and 10¹⁵ molecules cm⁻², respectively.

²NMB-normalized mean bias; NME-normalized mean error.

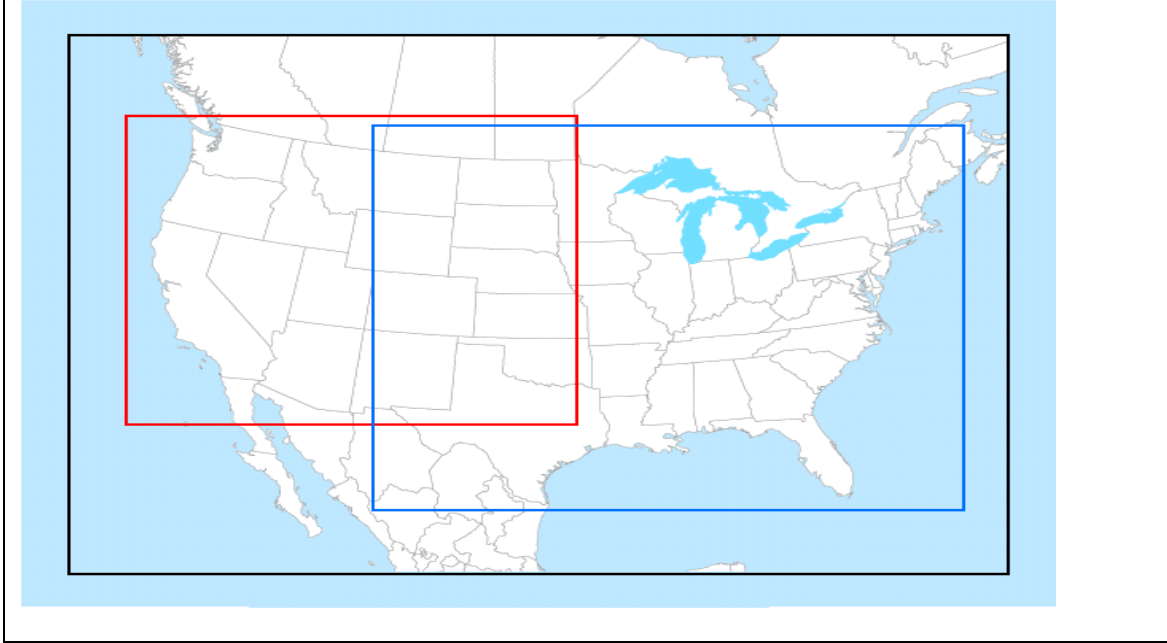


Figure 5.1. The CMAQ modeling domain map (the black box denotes the 36-km continental U.S. modeling domain; the red box denotes the 12-km western U.S. domain; and the blue box is the 12-km eastern U.S. domain; adopted from U.S. EPA, 2008).

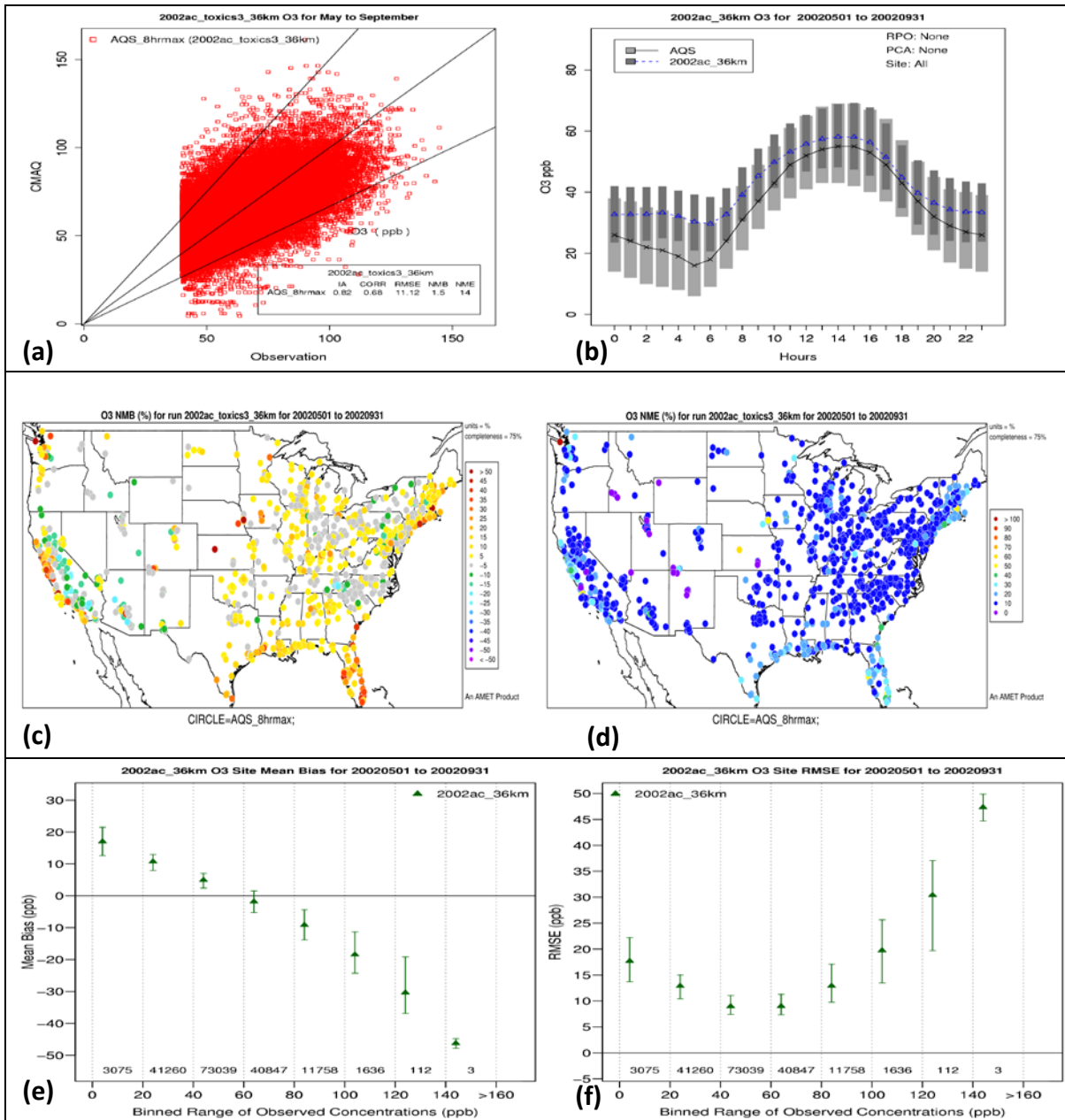
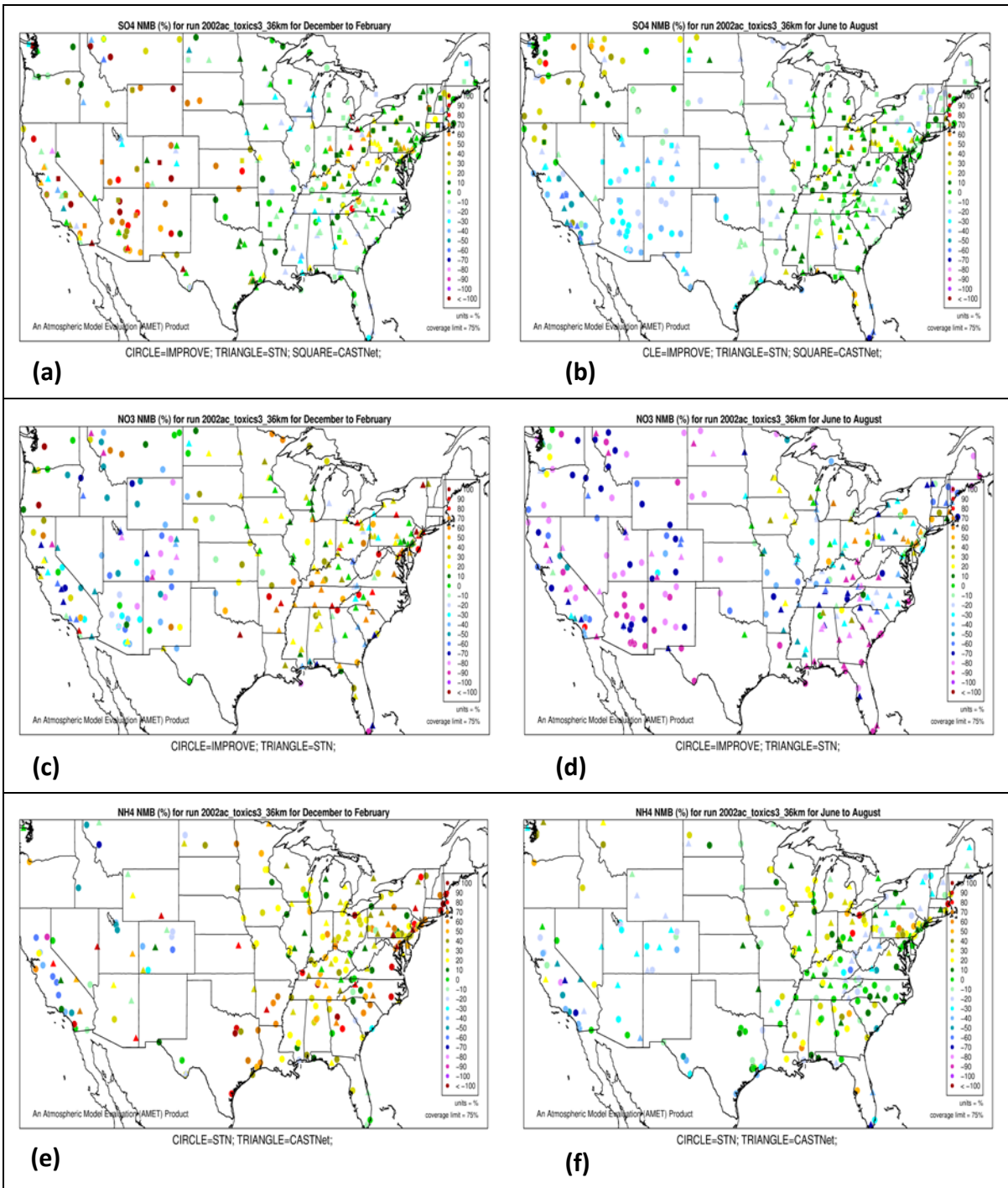
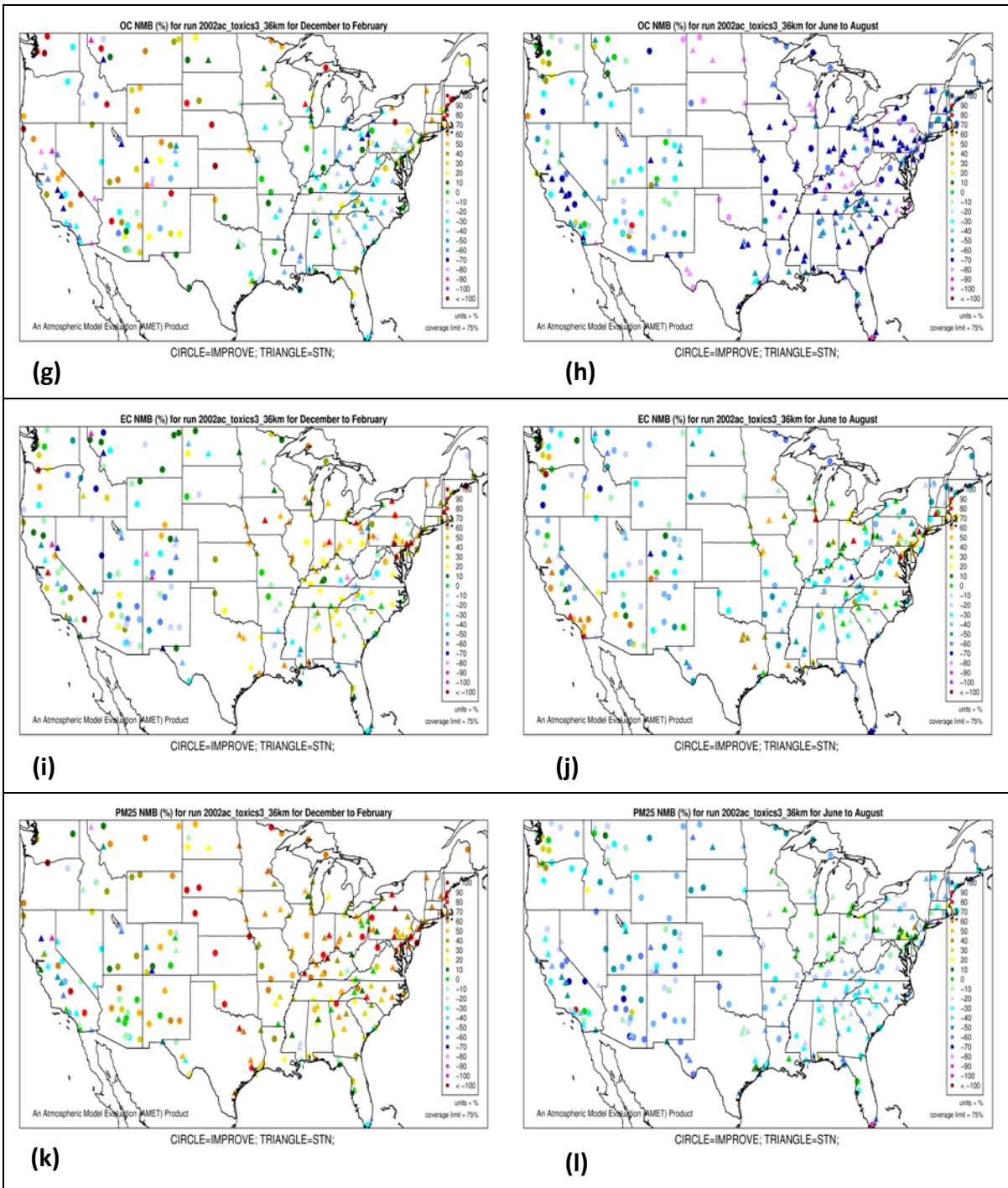


Figure 5.2. Comparison of the modeled and observed O₃ concentrations at the AIRS-AQS monitoring sites for O₃ season (i.e., from May to September) in 2002. (a) Scatter plot of daily maximum 8-h O₃ with cut off value of 40 ppb (the 1:1, 1.5:1 and 1:1.5 lines are shown for reference); (b) box plot of diurnal variation of median (the cross symbol denotes AQS and the triangle symbol denotes CMAQ) and inter-quartile ranges (light shading denotes AQS and dark shading denotes CMAQ) for hourly average O₃; Spatial distributions of (c) NMB and (d) NME for daily maximum 8-h O₃; (e) Median and inter-quartile range of MB binned by observation concentration of daily maximum 8-h O₃. The number of model/observation pairs for each bin is also shown; (f) The same as (e), but for RMSE.

Figure 5.3. Spatial plots of NMBs for SO_4^{2-} (a and b), NO_3^- (c and d), and NH_4^+ (e and f), OC (g and h), EC (i and j), and $\text{PM}_{2.5}$ (k and l) for winter (left panel) and summer (right panel) 2002.





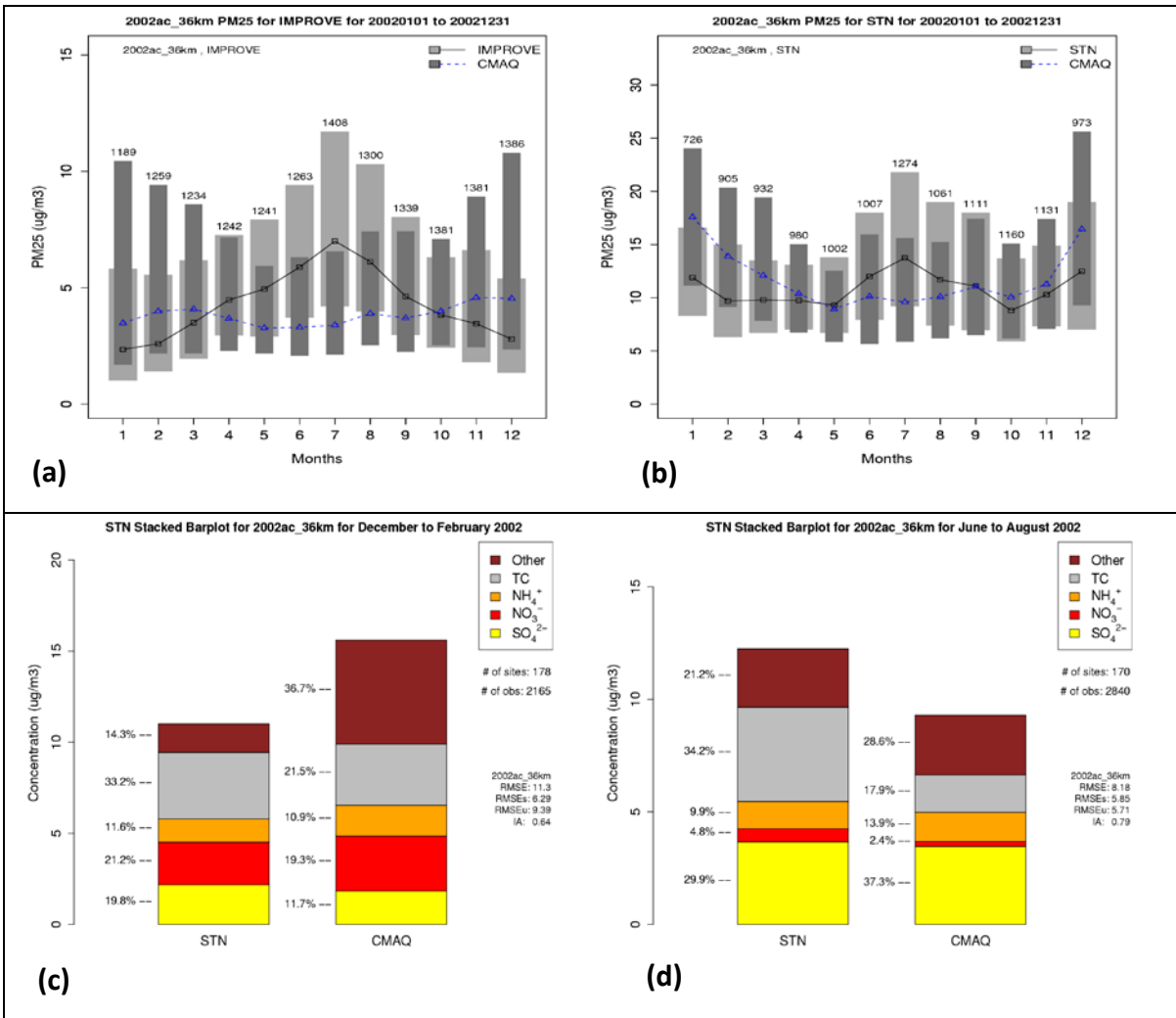


Figure 5.4. Comparison of the modeled and observed PM_{2.5} concentrations at the IMPROVE and STN monitoring sites in 2002. Monthly box plot for total PM_{2.5} concentrations with 25% and 75% quartiles and median values over (a) IMPROVE sites and (b) STN sites in 2002 (triangle and dark shading denote CMAQ, square and light shading denote observations, and numbers over each bar represents the numbers of observations); Stacked bar charts of total PM_{2.5} mass and its components over STN sites for (c) winter and (d) summer in 2002. The percent of each species contributed to the total PM_{2.5} is included.

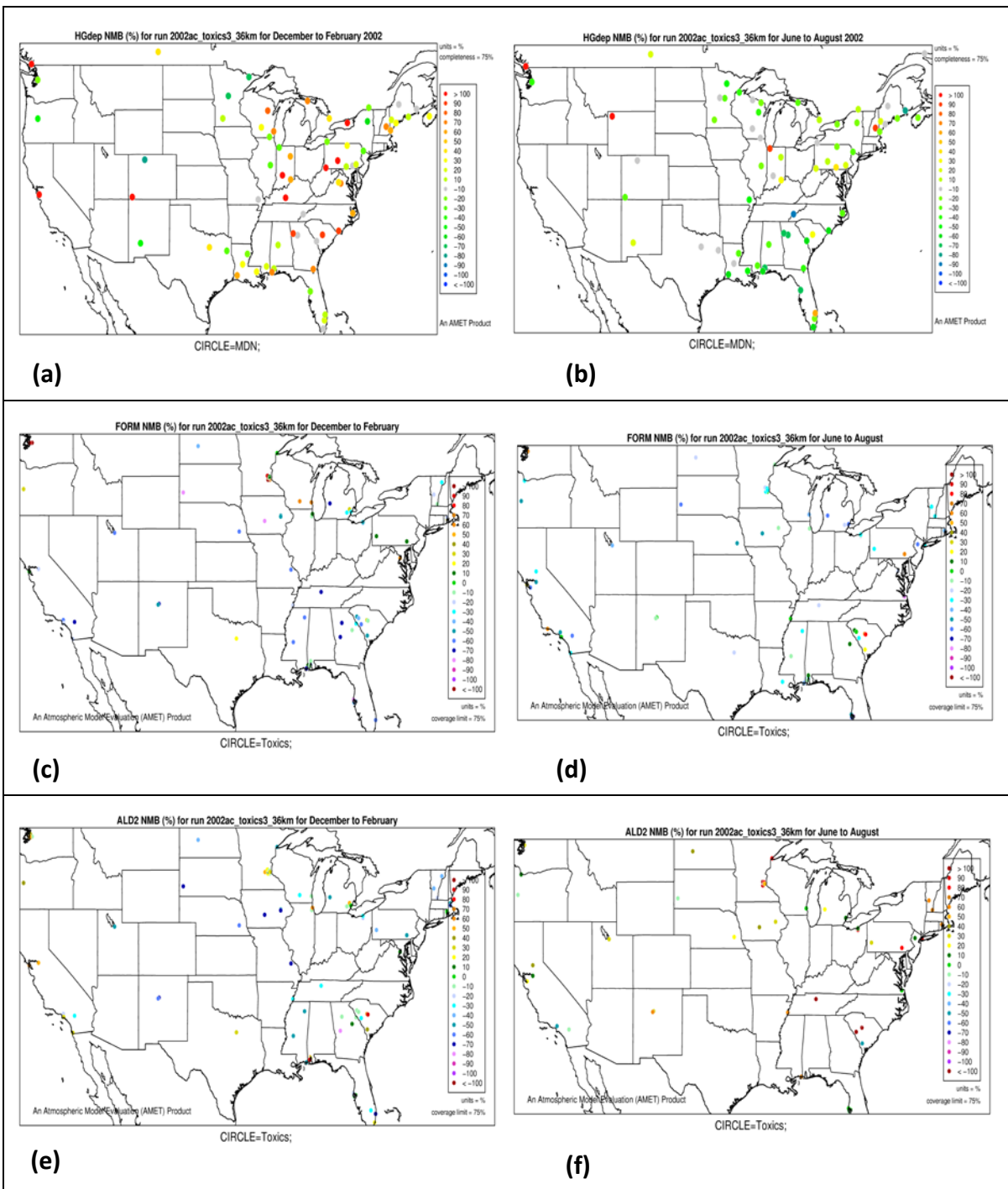


Figure 5.5. Spatial plots of NMBs for Hg wet deposition (top), formaldehyde (middle), and acetaldehyde (bottom) for winter (left panel) and summer (right panel) 2002.

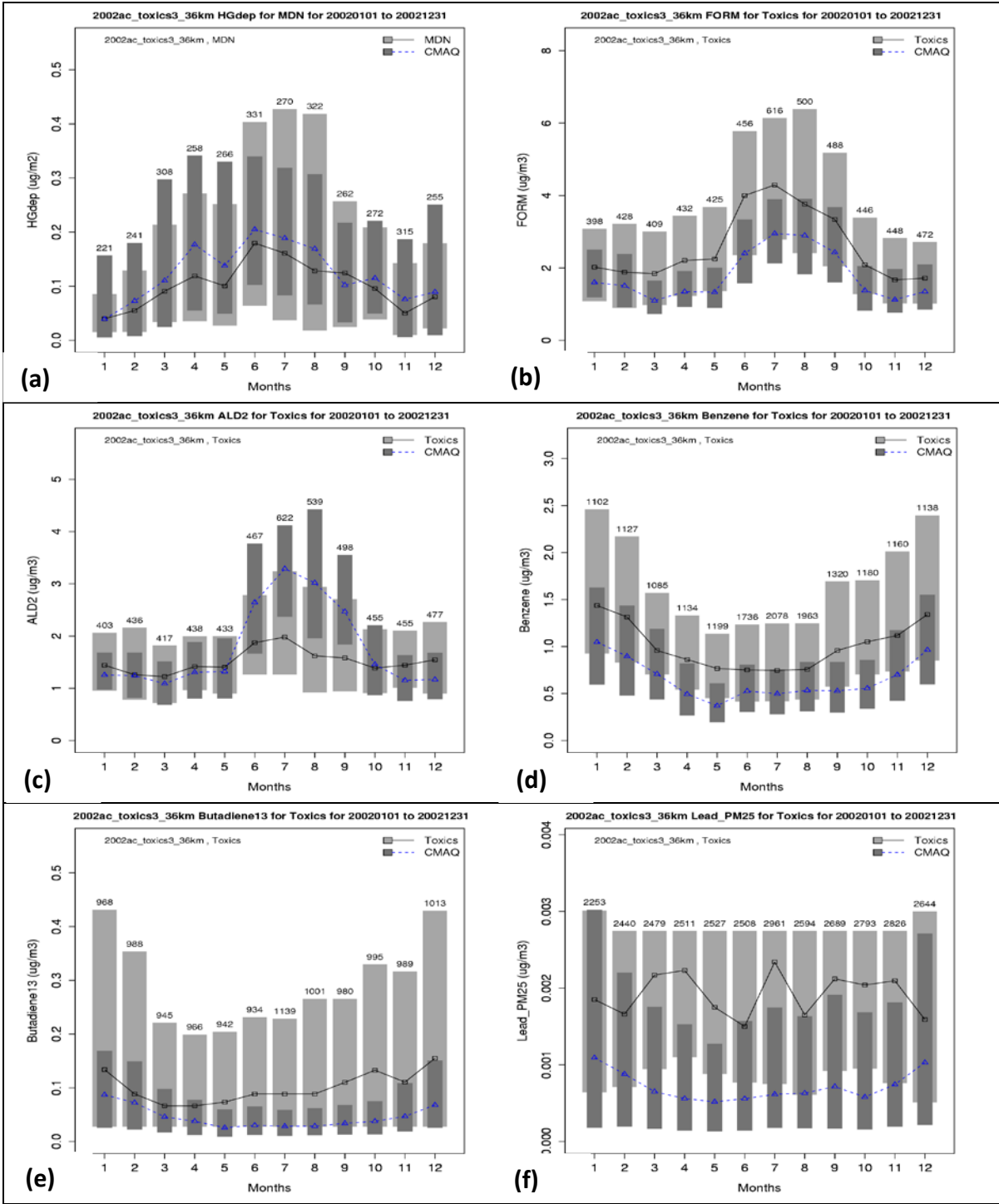


Figure 5.6. Monthly box plot for (a) Hg wet deposition, (b) HCHO, (c) ALD2, (d) benzene, (e) butadiene_13, and (f) particulate lead with 25% and 75% quartiles and median values in 2002 (triangle and dark shading denote CMAQ, square and light shading denote observations, and numbers over each bar represents the numbers of observations).

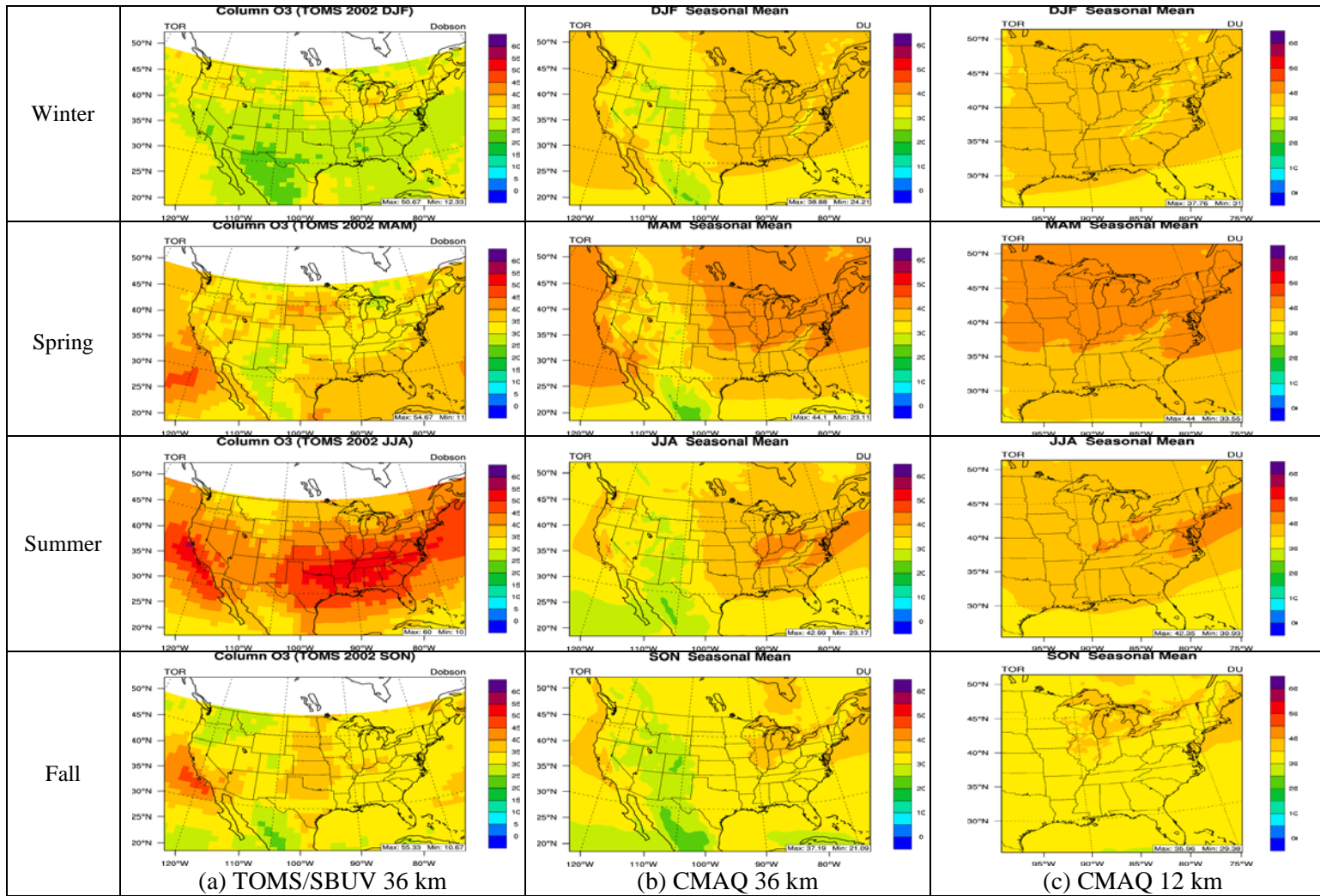


Figure 5.7. Spatial distributions of seasonal TOR from TOMS/SBVU and CMAQ over the 36-km CONUS domain and 12-km EUS for 2002.

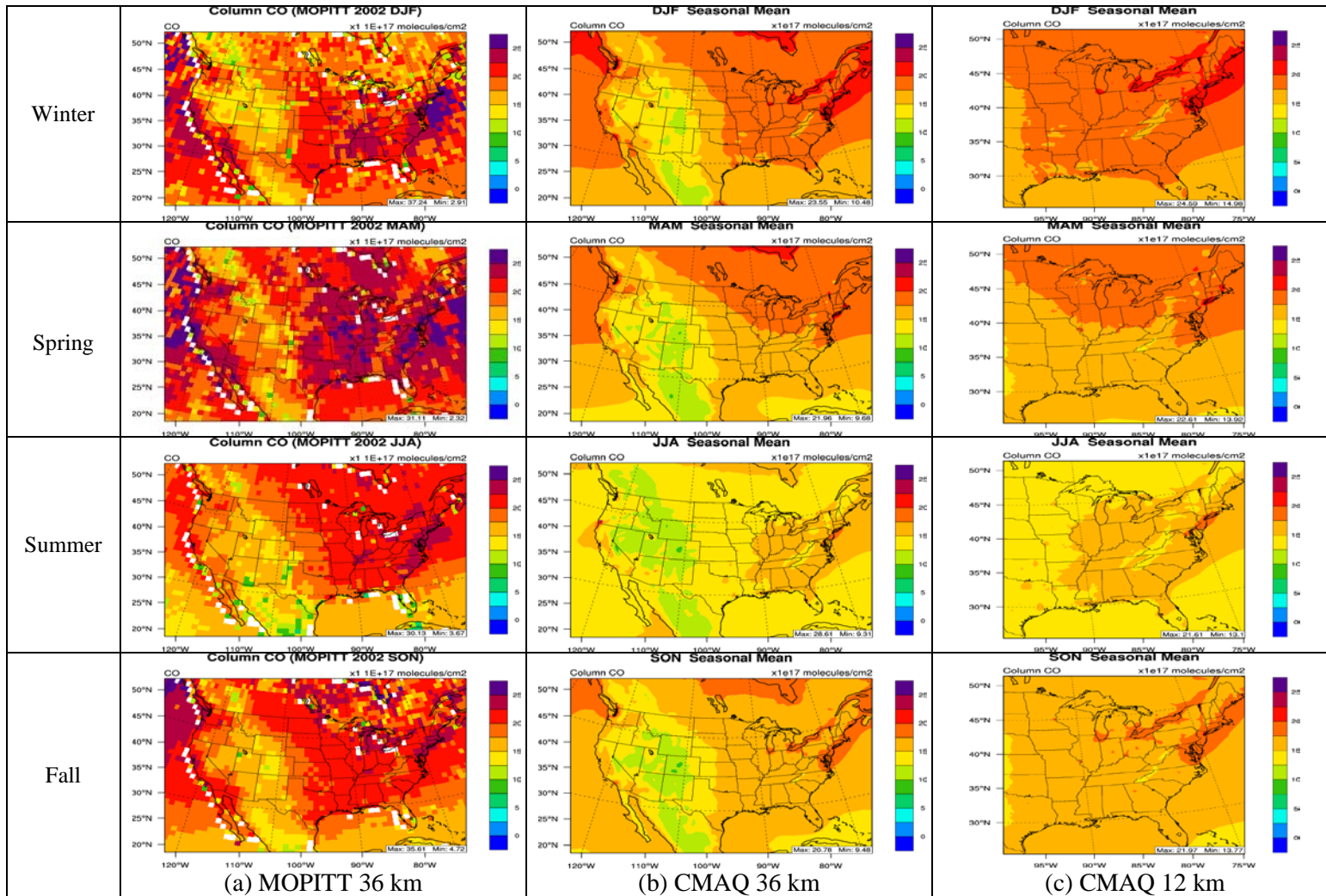


Figure 5.8. Spatial distributions of seasonal tropospheric CO columns from MOPITT and CMAQ over the 36-km CONUS domain and 12-km EUS for 2002.

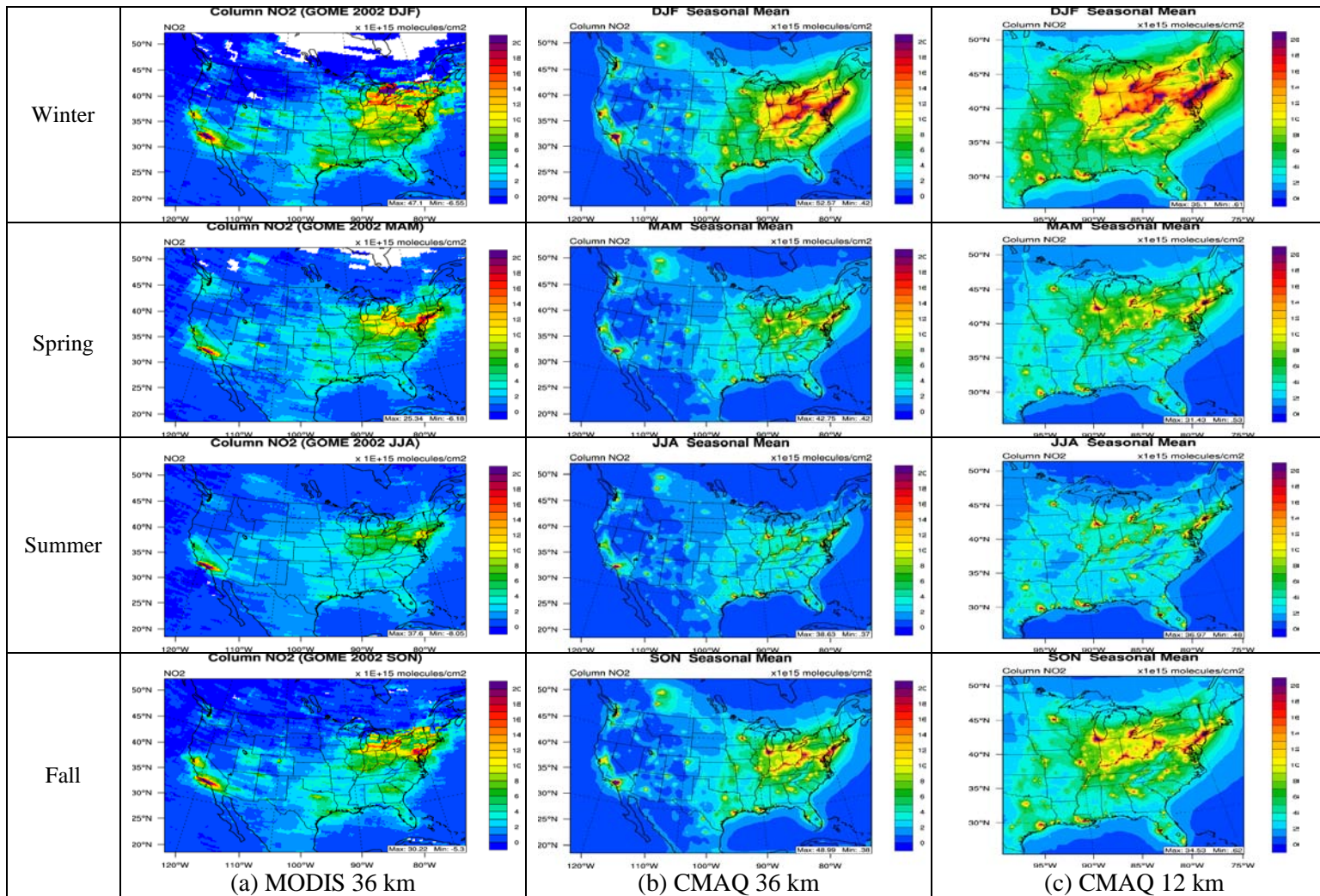


Figure 5.9. Spatial distributions of seasonal tropospheric NO₂ columns from GOME and CMAQ over the 36-km CONUS domain and 12-km EUS for 2002.

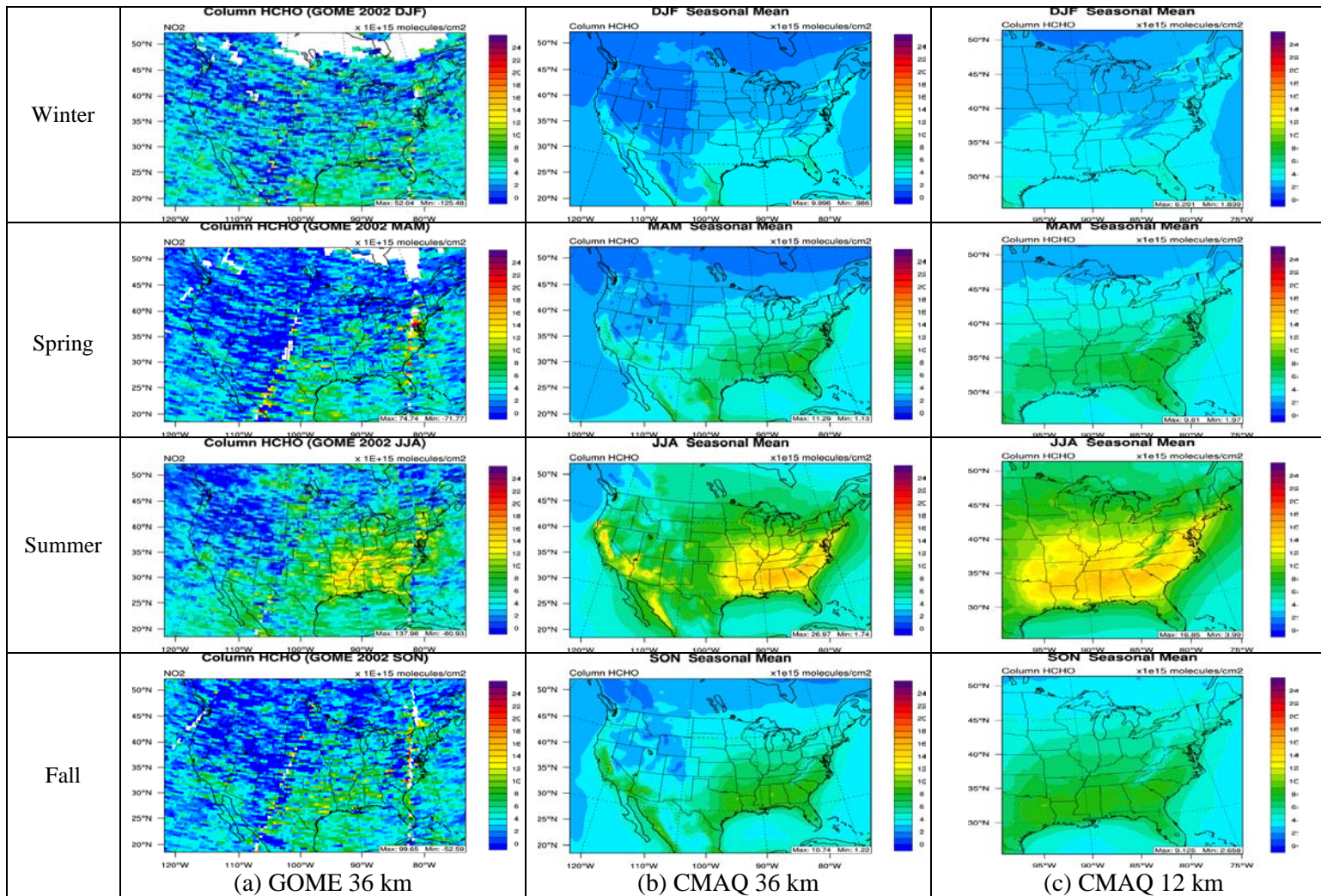


Figure 5.10. Spatial distributions of seasonal tropospheric HCHO columns from GOME and CMAQ over the 36-km CONUS domain and 12-km EUS for 2002.

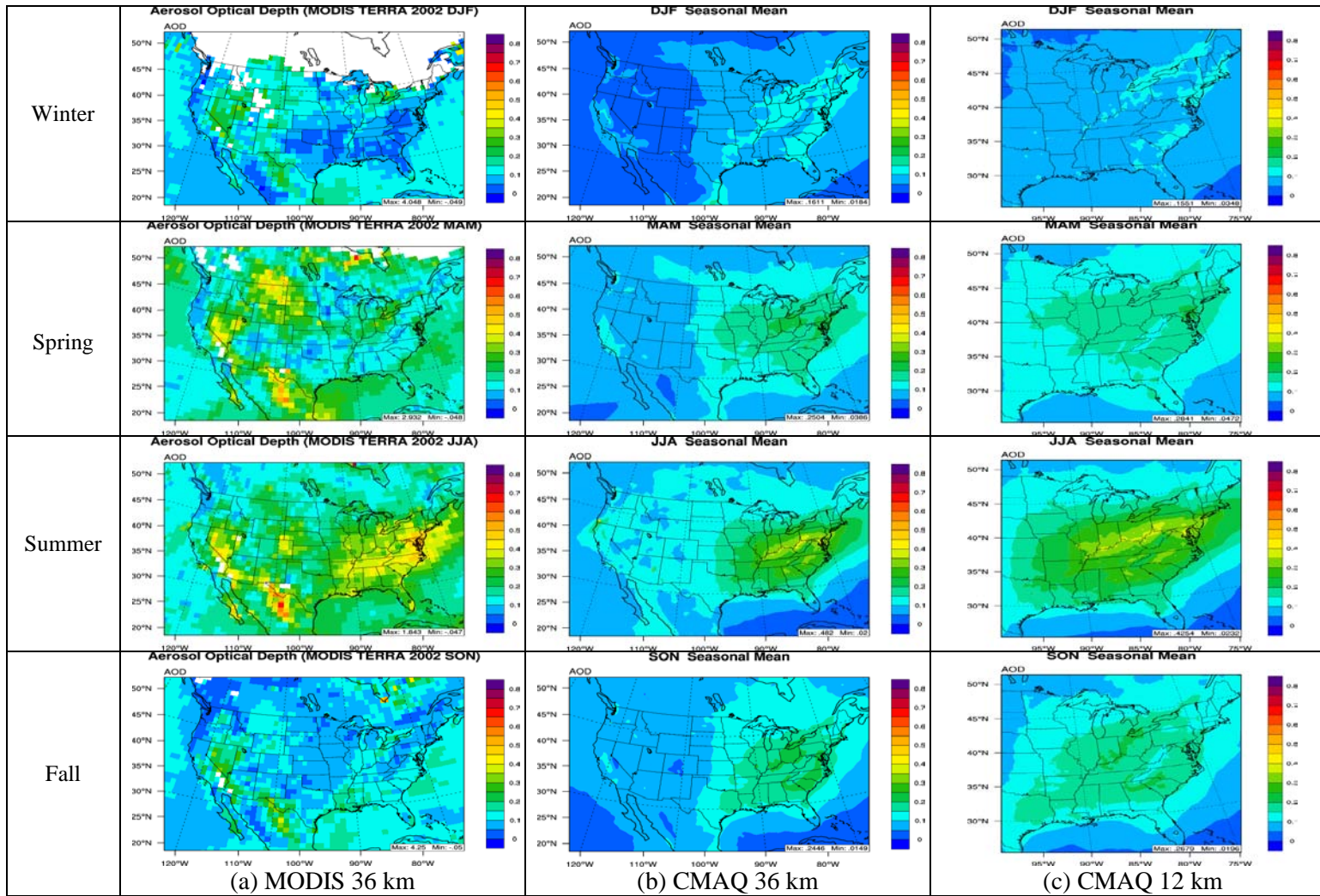


Figure 5.11. Spatial distributions of seasonal AODs from MODIS and CMAQ over the 36-km CONUS domain and 12-km EUS for 2002.

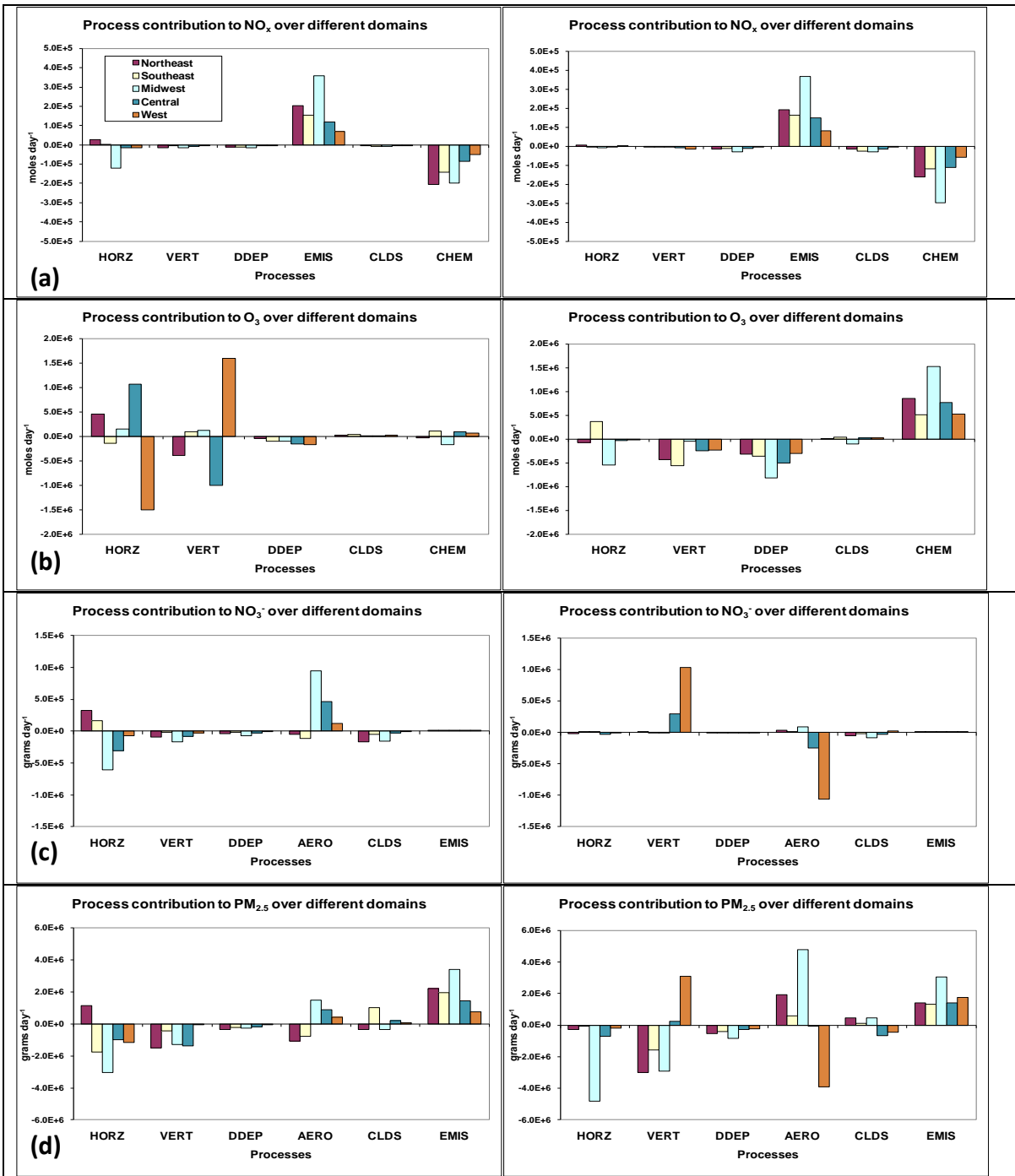


Figure 5.12. The monthly mean contributions of individual processes to the changes of selected criteria air pollutants (a) NO_x (b) O₃, (c) NO₃⁻, and (d) PM_{2.5} over different sub-regions in January (left panel) and July (right panel) 2002.

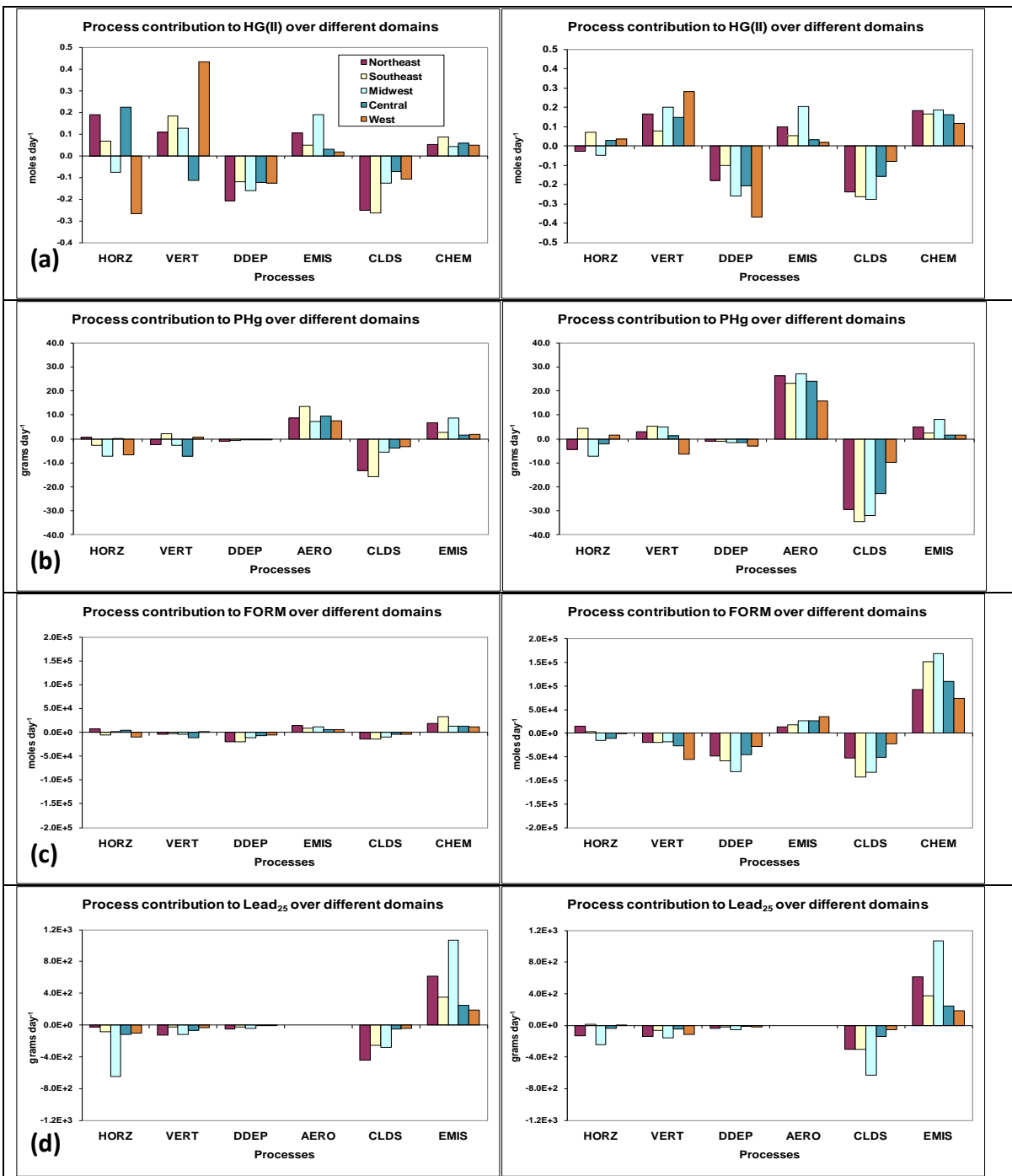


Figure 5.13. The monthly mean contributions of individual processes to the changes of selected hazardous air pollutants (a) Hg(II) (b) PHg, (c) formaldehyde, and (d) particulate lead over different sub-regions in January (left panel) and July (right panel) 2002.

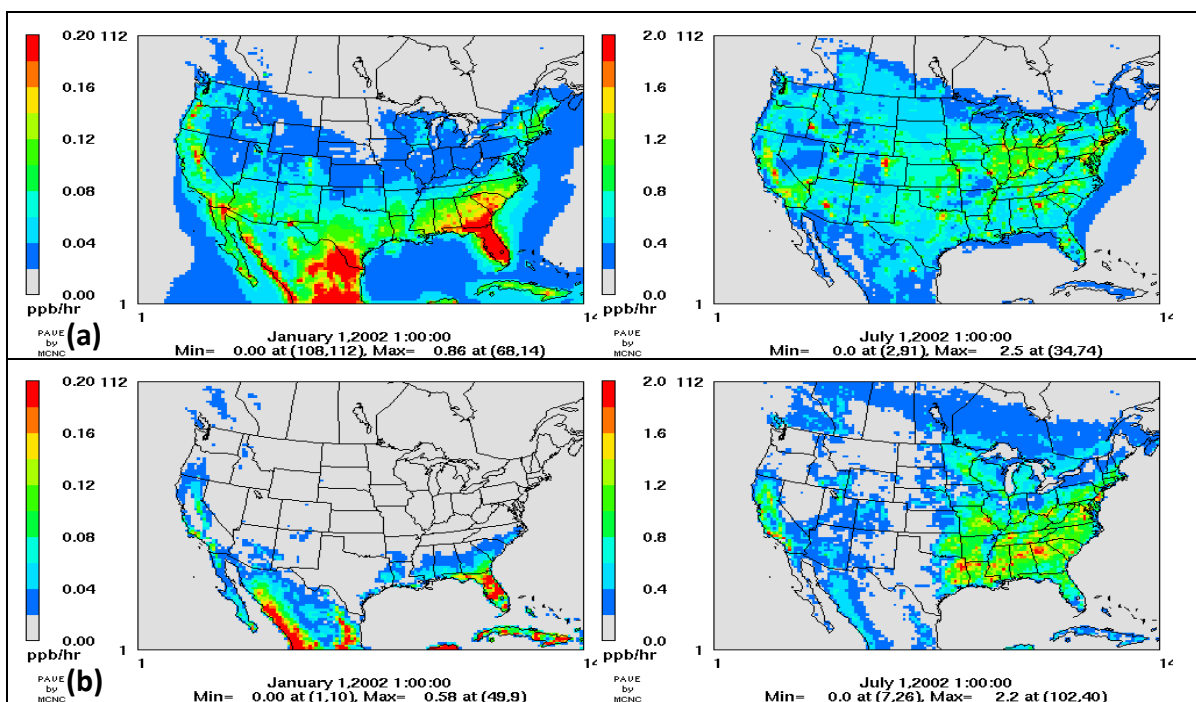


Figure 5.14. The monthly-mean spatial distributions of (a) OH reacted with anthropogenic VOCs and (b) OH reacted with biogenic VOCs in the first layer in January (left panel) and July (right panel) 2002.

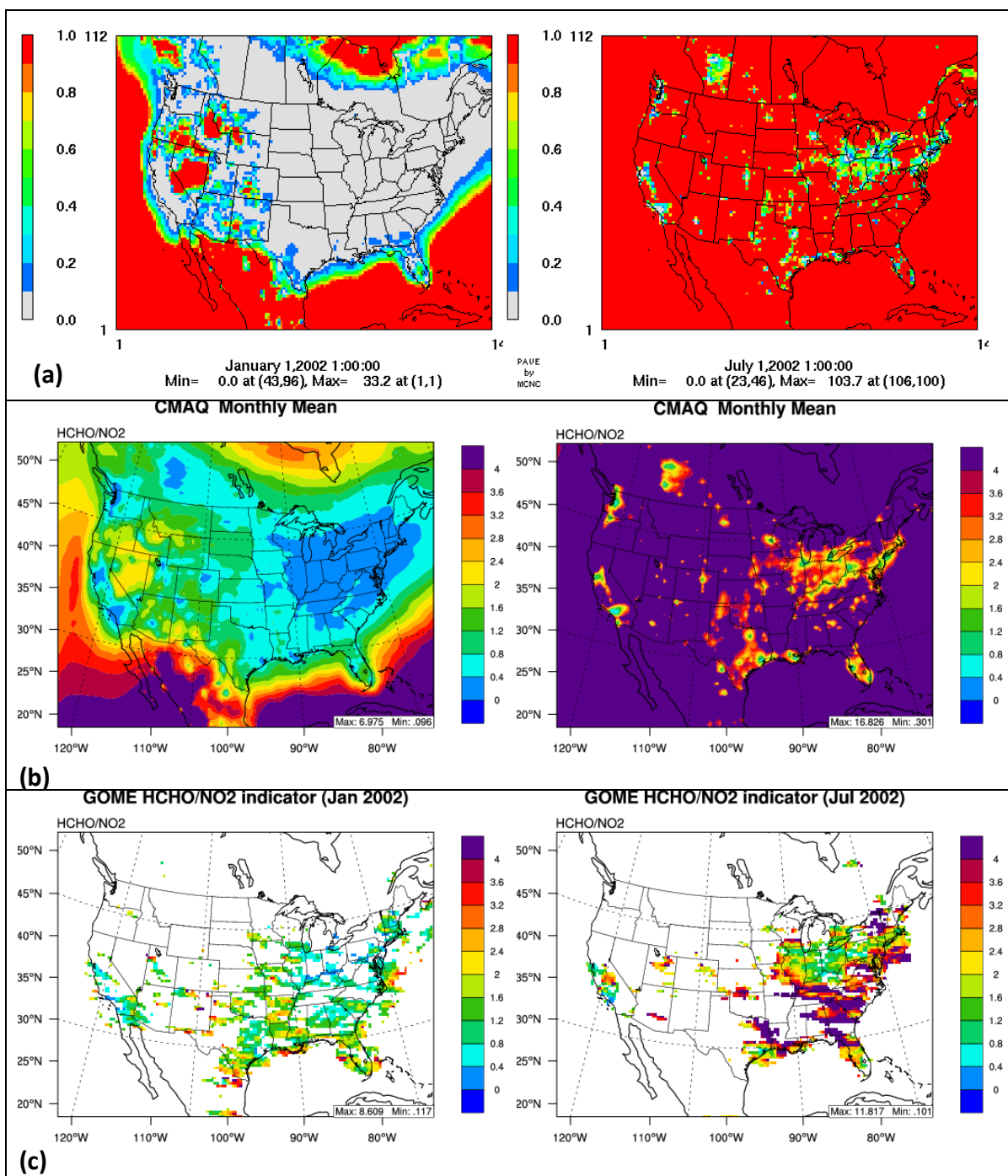


Figure 5.15. The monthly-mean spatial distributions of photochemical indicators of (a) surface layer $P_{H_2O_2}/P_{HNO_3}$ and (b) column HCHO/NO₂ predicted by CMAQ and (c) column HCHO/NO₂ observed by GOME satellite in January (left panel) and July (right panel) 2002.

CHAPTER 6. SUMMARY

6.1 Summary

The U.S. EPA's CMAQ modeling system provides the capability in modeling the complex ambient atmosphere over a broad range of multiple temporal and spatial scales of multiple-pollutant interactions. In this work, the CMAQ modeling system is further developed, applied, and evaluated via several specific studies in order to demonstrate and improve its "one atmosphere" analysis capability.

The CMAQ model with its embedded process analysis tool is first applied to the trans-Pacific domain to further investigate the magnitude, mechanism, and impacts of Asian pollution export following the previous ICAP studies. The four-month (i.e., January, April, July, and October 2001) baseline and the one-month (i.e., April 2001) sensitivity simulations without Asian anthropogenic emissions are conducted with a 108-km horizontal grid spacing over the trans-Pacific region. Model evaluation is conducted for both meteorological and chemical predictions for MM5/CMAQ simulations. Overall, MM5 gives a reasonably good performance over U.S. and China, considering a relatively coarse grid resolution used. The model performs much better in terms of T2 and RH2 (or QV2) in July than January but underpredicts precipitation to a relatively large extent for all four months. Seasonal analysis shows a cold bias for surface temperatures, especially during winter and spring. Several reasons might result in this cold bias, which include the slow response of deep soil temperature to synoptic-scale air temperature changes, inaccurate air-land heat fluxes simulated by the current land-surface and radiation schemes, and the incapability of the simulation in capturing fine-scale meteorological phenomena at a coarse grid resolution.

Evaluation of chemical predictions of CMAQ in the U.S. shows a relatively good performance for max 1-hr and max 8-hr O₃, especially in July with NMBs of -0.7%, -12.1%, and 4.3% for AIRS-AQS, CASTNET, and SEARCH, respectively. There is a large overprediction of total PM_{2.5} concentrations, especially in January. This can be attributed to several possible reasons including the overestimated emissions of SO₂ (~30%) and NO_x (~10%) used in this study, underpredicted precipitation, and cold biases in temperature predictions. Evaluation over East Asia shows a systematic underprediction for most air pollutants in this region, which is highly related to the uncertainties of emission inventories over Asia in this study. The underpredictions of PM₁₀ and SPM over East Asia are also due to the poor capability of CMAQ to simulate coarse PM. In addition to aforementioned factors, the use of a coarse grid resolution, which cannot capture the complex local terrain and small-scale atmospheric processes, contributes to the biases in both meteorological and chemical predictions.

Aircraft data and satellite observations are also used to evaluate model performance in capturing vertical profiles of pollutants and chemical concentrations in upper layers. CMAQ underpredicts AODs throughout all four months. Possible reasons include the high values of MODIS data over the land, the uncertainties associated with the AOD calculation, the exclusion of the contributions of coarse particles (e.g., sea salt and dust) to AODs in CMAQ, and the impacts of the boundary conditions of PM_{2.5}. Tropospheric NO₂ and CO column abundances are reproduced well in CMAQ. Some discrepancies exist between TORs from TOMS/SBUV and CMAQ, which are most likely resulted from the uncertainties of boundary O₃ values from GEOS-CHEM in upper layers.

The analyses of transport mechanisms show that there are mainly two pathways for trans-Pacific transport, i.e., a relatively-strong export for CO, O₃, PM_{2.5}, SO₄²⁻ at the mid-latitude in the PBL and the strongest export for most of other species such as O₃, PAN, HCHO, and NO₃⁻ at 25-45° N in the LFT, which have also been reported by previous field and modeling studies. The analyses of IPRs further quantitatively confirm that vertical transport in the PBL of East Asia and the U.S. and horizontal transport in both the PBL and LFT of the Pacific Ocean play a very important role in the export of O₃ and PM_{2.5} from the source regions (e.g., East Asia). Asian pollution export can contribute to an enhancement of ~0.1 Gmoles or ~0.31 Gmoles of O₃ and ~0.5 Gg or ~4.1 Gg of PM_{2.5} per day in the PBL of U.S. during dust storm season based on two different calculations. Such an enhancement can lead to increased background concentrations of O₃ and SO₄²⁻ in the western U.S. by ~1 ppb (~2.5%) and 0.4 μg m⁻³ (~20%) in monthly average, and up to 2.5 ppb and 1.0 μg m⁻³ in daily average, respectively. Among all anthropogenic aerosol species, SO₄²⁻ and NH₄⁺ are dominant, with enhancements of 20% and 18%, respectively for the western U.S., during the trans-Pacific transport.

The CMAQ modeling system is then further developed by incorporating two dust emission flux schemes and nine dust-related heterogeneous reactions to investigate the role of dust particles in affecting chemical predictions in CMAQ. In addition, three crustal species associated with dust particles are also added into the model and the default thermodynamic equilibrium module is updated to ISORROPIA II to examine the impact of crustal species on the inorganic gas/particle partitioning through the thermodynamic equilibrium. This newly-developed dust version of CMAQ model is applied to April 2001

over the same trans-Pacific domain as the first part of this thesis work to improve the capability of model in predicting dust storms. The meteorological fields predicted by WRF v3.2 are first evaluated against available observation data. WRF generally predicts both T2 and RH2 (or Q2) well and moderately overpredicts wind speed. WRF predicts precipitation relatively poor as compared to other variables which may have impacts on chemical predictions via scavenging and wet deposition. Overall, the meteorological predictions by WRF are consistent with other meteorological models such as MM5 that were used to provide meteorological inputs for air quality studies. The model evaluation of chemical variables indicates that this dust version of CMAQ can reproduce those variables pretty well. The model performance for PM₁₀ and AOD is greatly improved as compared with default CMAQ v4.7 and the study conducted in Chapter 3 and by Wang et al. (2009) using the old version of CMAQ v4.4 in the same episode due to the updates in aerosol treatments. Overall, although there exist uncertainties in our results, the present work demonstrates the promising ability of CMAQ in capturing dust emissions and the physical/chemical processes associated with dust particles and gives us confidence in applying this dust version of CMAQ for further research studies and improving the predictions of CMAQ in arid and semiarid areas.

We estimate the total dust emission produced by CMAQ to be ~ 111.4 and 110.9 Tg from Zender and Westphal schemes for April 2001, which is in line with previous studies and may represent a conservative estimation of dust emissions, considering the large uncertainties in the dust emission estimations from different models. The model produces the highest dust emissions from Taklimakan desert and Gobi desert over China and Mongolia and fewer emissions from the western India, the southwest and Great Plains over U.S., and Sonoran

desert of Mexico, which is consistent with previous studies. CMAQ also captures the dust outbreak event during April 4-14. The monthly-mean surface concentration of dust predicted by CMAQ can reach more than $80 \mu\text{g m}^{-3}$ for fine-mode and more than $200 \mu\text{g m}^{-3}$ for coarse-mode dust, respectively over source regions and reach $5\text{-}30 \mu\text{g m}^{-3}$ for both fine dust and coarse dust over the down-wind areas such as eastern China, Japan, northeastern India, Midwest U.S. The long-range transport can build up the surface concentrations of dust to almost $2 \mu\text{g m}^{-3}$ over the remote regions such as the eastern Pacific and eastern U.S.

Six full month sensitivity simulations have been conducted in order to investigate the dust influences on the spatial distribution of various gaseous and aerosol species. The results show that the inclusion of crustal species affects the volatile species (e.g., NH_3 , NH_4^+ , HNO_3 , and NO_3^-) to a greater extent than others (e.g., SO_4^{2-}). The concentration of $\text{PM}_{2.5}$ over the eastern Asia is reduced due to the combined effect of crustal species on reducing NO_3^- and NH_4^+ . The heterogeneous uptakes on dust particles have much greater impacts on the gaseous species. The heterogeneous chemistry tends to decrease the mixing ratios of O_3 by up to 4 ppb ($\sim 9\%$) over the dust source regions and reduce SO_2 concentration by up to 0.3 ppb ($\sim 5\%$) over the polluted areas and up to 0.05 ppb ($\sim 30\%$) over the dust source regions. Different from other species, the mixing ratio of NO_x is increased throughout the domain due to the renoxification effect considered in the model. The decrease of HNO_3 is not evident, indicating a compensation effect of the decrease of HNO_3 by heterogeneous chemistry and the increase of HNO_3 by evaporation of NO_3^- particles caused by the increase of SO_4^{2-} concentrations. On the other hand, the heterogeneous uptakes play more important role on SO_4^{2-} formation than other aerosol species. The examination of dust impacts at higher

altitudes indicate that the long-range transport of dust may play an important role in affecting both gaseous and aerosol species in the remote areas.

Finally, a comprehensive evaluation and analysis of several full year simulations over 36/12 km contiguous U.S. domains using MP version of CMAQ is presented to demonstrate the capability of CMAQ in predicting the multiple-pollutant air quality. Model evaluation is performed by comparing simulated concentrations of O₃, PM_{2.5}, and its components, precursors O₃ and PM_{2.5}, and major air toxics as well as the Hg deposition with the measurements collected from ground-based monitoring networks and satellites. Our results show that CMAQ simulates well the spatial and seasonal variation of O₃, especially during the O₃ season with a vast majority of simulated max 8-h O₃ falling within a factor of 1.5 of the observations and NMBs within ±10% at most AQS sites. CMAQ tends to reproduce O₃ mixing ratios the best in the range of 40-60 ppb. Compared with previous studies, these results demonstrate the moderate to great improvement in O₃ predictions, because of several factors including the newest CB05 gas-phase chemistry mechanism with chloride related reactions, a new PBL scheme ACM2, and new emission inventories. Model performance for PM_{2.5} and its components is satisfactory or marginally-satisfactory. CMAQ predicts SO₄²⁻ the best among all PM_{2.5} components with domain-wide NMBs typically within ±20% over different networks. The prediction of SO₄²⁻ is better over the eastern U.S. than the western U.S. Our results show a small improvement compared with previous studies, which is likely due to updates in both convective cloud module and aerosol dry deposition module in CMAQ. CMAQ predicts NH₄⁺ and EC relatively well. CMAQ shows better performance of NH₄⁺ in summer due to the fact that NH₄⁺ is dominated by (NH₄)₂SO₄ and the performance of SO₄²⁻

in summer is much better than that of NO_3^- in winter. The uncertainty associated with NH_3 emissions is found to be indicative of the main reason for the model bias of NH_4^+ . CMAQ moderately overpredicts EC in winter and underpredicts it in summer. Different from OC, EC is directly emitted into the atmosphere and its ambient concentrations depend largely on emission inventories. The performance for NO_3^- and OC is relatively poor. CMAQ performance in the 2002 MP platform actually shows some improvements of NO_3^- predictions in terms of statistics as compared with earlier studies. Unlike EC, OC is determined by both aerosol processes and emissions. OC underpredictions are much worse than those of EC, particularly in summer when SOA concentrations are more comparable with those of POA. This is because of underpredictions of photochemically-produced SOA, in addition to uncertainties in the emissions of POA and SOA precursors in summer. CMAQ shows a satisfactory performance in predicting $\text{PM}_{2.5}$ that is comparable to or even better than previous studies due to several model updates, although it overpredicts $\text{PM}_{2.5}$ in winter mainly due to overpredictions in concentrations of other unknown $\text{PM}_{2.5}$, and underpredicts it in summer mainly due to underpredictions in OC concentrations. The domain-wide NMBs for $\text{PM}_{2.5}$ are relatively low, likely due to a compensation of positive and negative biases of $\text{PM}_{2.5}$ species.

The overall model performance for HAPs is worse than CAPs due to several reasons. For example, the emission inventory for HAPs is not as accurate as that of CAPs, the model treatments for HAPs species are not as robust and complete as those for CAPs, and there is a lack of routine measurements of HAPs. However, CMAQ does reasonably well in simulating seasonal Hg wet deposition, with consistent or even better performance, as

compared with previous studies because of several model updates. The model performance is slightly better in spring and fall than in summer and winter. The evaluation results for selected air toxics show a systematic underprediction for most species except for ALD2 throughout the year due to several reasons, including the coarse grid resolution that cannot resolve the high-level plume event, the underestimation of emissions for most of HAPs and the simplified assumption of HAPs chemistry in current CMAQ-MP. The overall model performance in the 2002 MP modeling platform is fairly good for HCHO and ALD2, moderately good for benzene and particulate lead, and very poor for 1,3-butadiene and acrolein.

The spatial distribution and seasonal variations of GOME NO₂ columns are generally well reproduced by CMAQ, with higher NO₂ columns over the industrialized and metropolitan areas. CMAQ predictions are well correlated with GOME measurements throughout the whole year with R values ranging from 0.74 to 0.85. CMAQ reasonably captures the spatial pattern of the MOPITT CO observations, especially the high CO columns over the source regions, although it underpredicts those throughout the whole year with seasonally-mean NMBs of -22.2% to -8.9%. Both TOMS/SBUV and CMAQ TORs show some similarities with respect to spatial patterns in all seasons. However, CMAQ fails to capture the observed seasonal variations, with maximum and minimum TORs occurring in spring and fall, respectively, for CMAQ but in summer and spring for TOMS/SBUV, respectively. This discrepancy might be due to uncertainties in the upper boundary conditions for O₃ used in CMAQ. Overpredictions of HCHO columns from CMAQ occur in all seasons except for winter. MODIS and CMAQ AODs display much different spatial

distributions over CONUS and CMAQ underpredicts AODs for all seasons. Several possible reasons for model biases in column predictions are identified. These include inaccurate seasonal allocation and underestimation of emissions, inaccurate boundary conditions at higher altitudes, lack of model treatments such as mineral dust or plume-in-grid process, as well as limitations and errors in satellite data retrievals.

The seasonal photochemical characteristics and controlling processes to the formation and destruction of key pollutants are also examined through process analysis. As illustrated in this study, the predictions of CAPs and HAPs from the 2002 MP 36-km and 12-km simulations are within the range or better than those reported in several recent EPA applications. This attests its scientific capability in assessing O₃ and PM_{2.5} as well as air toxics for the purposes of the NAAQS Final Rule. The model evaluation also identifies several key areas for potential model improvements and thus provides guidance for sensitivity studies, further model development and improvement efforts, and directions in the future research.

6.2 Limitations and Future Work

This work demonstrates the “one atmosphere” analysis capability of the CMAQ modeling system in modeling the complex ambient atmosphere with multiple temporal and spatial scales of multiple-pollutant interactions. A comprehensive model evaluation in this work reveals several systematic trends in model biases and errors that need to be addressed to further improve CMAQ’s skills in reproducing ambient air quality. The model biases associated with uncertainties in photochemical mechanism, aerosol chemical/physical treatments, emission inventories, and meteorological variables are identified. The sensitivity

simulations by modifying model inputs and improving model treatments are warranted and should be included in the future work.

Other limitations of this work lie in the model development of dust treatments. The dust treatments in this work include several simplified assumptions. For example, the crustal species are prescribed uniformly throughout the modeling domain. The spatially-varied concentrations should be considered once such information becomes available. The seasonal variations of vegetation coverage are not considered for dust emission calculation in this study, which could be important over some semi-arid areas. As discussed in Chapter 4, the uptake coefficient of chemical species on the surface of dust has high uncertainties and may depend on the ambient conditions (e.g., temperature and relative humidity). Those factors should be considered for future model development when more robust treatments are available.